



HAL
open science

Fracture of dual-crosslink dynamic hydrogels : from molecular interactions to fracture energy

Louis Debertrand

► **To cite this version:**

Louis Debertrand. Fracture of dual-crosslink dynamic hydrogels: from molecular interactions to fracture energy. Polymers. Université Paris sciences et lettres, 2020. English. NNT : 2020UPSLS027 . tel-03163056

HAL Id: tel-03163056

<https://pastel.hal.science/tel-03163056>

Submitted on 9 Mar 2021

HAL is a multi-disciplinary open access archive for the deposit and dissemination of scientific research documents, whether they are published or not. The documents may come from teaching and research institutions in France or abroad, or from public or private research centers.

L'archive ouverte pluridisciplinaire **HAL**, est destinée au dépôt et à la diffusion de documents scientifiques de niveau recherche, publiés ou non, émanant des établissements d'enseignement et de recherche français ou étrangers, des laboratoires publics ou privés.



THÈSE DE DOCTORAT

DE L'UNIVERSITÉ PSL

Préparée à l'Ecole Supérieure de Physique et de Chimie
Industrielles de la ville de Paris (ESPCI Paris)

**Fracture of dual-crosslink dynamic hydrogels: from
molecular interactions to fracture energy**

**Rupture d'hydrogels dynamiques à double réticulation :
des interactions moléculaires à l'énergie de rupture**

Soutenue par

Louis DEBERTRAND

Le 09 Décembre 2020

Ecole doctorale n° 397

**Physique et chimie des
matériaux**

Spécialité

Chimie des matériaux

Composition du jury :

Min-Hui, LI Directrice de Recherche, CNRS / Chimie ParisTech	<i>Présidente</i>
Laurence, RAMOS Directrice de Recherche, CNRS / Université de Montpellier	<i>Rapporteur</i>
Evelyne, VAN RUYMBEKE Professeure, Université Catholique de Louvain	<i>Rapporteur</i>
Sebastian, SEIFFERT Professeur, Johannes Gutenberg Universität - Mainz	<i>Examineur</i>
Kees, STORM Professeur, Eindhoven University of Technology	<i>Examineur</i>
Costantino, CRETON Directeur de recherche, CNRS / ESPCI Paris	<i>Directeur de thèse</i>
Tetsuharu, NARITA Chargé de recherches, CNRS / ESPCI Paris	<i>Directeur de thèse</i>

Table of contents

Table of contents	iii
General Introduction	1
Chapter 1: From polymer physics to the toughening of hydrogels	7
1.1. Polymer network physics	10
1.2. Fracture of soft matter	14
1.2.1. “Bulk” vision of fracture	14
1.2.2. Molecular vision.....	16
1.3. Reinforcement of hydrogels	17
1.3.1. Homogeneous networks	17
1.3.2. Introducing an energy dissipation mechanism	19
1.4. Using dynamic coordination crosslinks.....	22
1.4.1. Transient networks with versatile dynamics	22
1.4.2. Toughened gels	28
1.5. Objectives of this project.....	34
Chapter 2: Preparation and microstructure of a dual-crosslink hydrogel	39
2.1. Gel synthesis	42
2.1.1. Synthesis of the P(AAm-co-VIm) chemical gel.....	42
2.1.2. Synthesis of the P(AAm-co-VIm)/Ni ²⁺ dual crosslink gels	43
2.2. Absorption of Ni ²⁺ ions	46
2.2.1. Absorption kinetics of Ni ²⁺ ions.....	46
2.2.2. Influence of [NaCl]	47
2.2.3. Absorption isotherms – influence of [Ni ²⁺].....	48
2.3. Stress-free dynamics – study by dynamic light scattering (DLS)	51
2.3.1. Dynamic Light Scattering – Principles and protocol	51
2.3.2. Results for a bare chemical gel.....	53
2.3.3. Results for a “One-pot” dual-crosslink gel.....	55
2.3.4. Conclusions	62
2.4. Linear mechanical behavior at small deformations.....	64
2.4.1. Rheology of a chemical gel.....	64
2.4.2. Rheology of a “One-Pot” dual-crosslink hydrogel.....	66
2.4.3. Comparing “One-pot” and “Diffusion” dual-crosslink hydrogels.	68

2.4.4. Fitting with fractional model.....	69
2.4.5. Relaxation experiments	72
2.4.6. Conclusions	73
2.5. Small-Angle X-Ray scattering experiments.....	73
2.5.1. SAXS – Principle and protocol	73
2.5.2. Qualitative analysis	76
2.5.3. Attempt at quantitative analysis	79
2.5.4. Conclusions from X-ray scattering.....	85
2.6. Conclusion on microstructure and dynamics	85
Chapter 3 : Large deformations of a dual-crosslink hydrogels with Ni²⁺ ions	89
3.1. Standard uniaxial tensile tests: continuous loading.....	92
3.1.1. Comparison of “One-pot” and “Diffusion” gels with [Ni ²⁺] = 100 mmol/L	92
3.1.2. Continuous loading.....	93
3.1.3. Discussion	99
3.2. Cyclic testing.....	101
3.2.1. Influence of stretch and stretch-rate	101
3.2.2. Damage during cycles?	105
3.3. Relaxation.....	109
3.4. Fracture of Ni ²⁺ dual-crosslink hydrogels.....	113
3.4.1. Single-notch fracture under continuous stretching.....	113
3.4.2. Delayed fracture of “pure-shear” samples.....	115
3.5. Conclusions and discussions	120
Chapter 4: Dual-crosslink hydrogels with fast dynamics	125
4.1. Preparation	129
4.1.1. Cu ²⁺ dual-crosslink hydrogel	129
4.1.2. Zn ²⁺ dual-crosslink hydrogels.....	130
4.1.3. Absorption isotherms	130
4.2. Rheology	131
4.2.1. Cu ²⁺ and Zn ²⁺ dual-crosslink hydrogels	131
4.2.2. Zn ²⁺ dual-crosslink hydrogel – “One-pot” vs. “Diffusion”	132
4.3. Small-angle X-Ray scattering	133
4.3.1. General observations	133
4.3.2. Fitting	134

4.3.3. Scattered intensity normalization method	135
4.3.4. Normalized results – comparison between Ni ²⁺ and Zn ²⁺ dual-crosslink hydrogels	137
4.3.5. Conclusions	139
4.4. Large deformations.....	139
4.4.1. “One-Pot” vs “Diffusion” Zn ²⁺ hydrogels	140
4.4.2. Tensile tests on Zn ²⁺ and Cu ²⁺ dual-crosslink hydrogels	140
4.5. Cyclic tests	145
4.5.1. Influence of stretch-rate and stretch	145
4.5.2. Damage during cycles?	147
4.6. Fracture of a fast dual-crosslink hydrogel	150
4.6.1. Single-notch fracture under continuous stretching.....	150
4.6.2. Delayed fracture of “pure-shear” samples of Zn ²⁺ dual-crosslinked hydrogel	152
4.7. Conclusions	154
Chapter 5: Slowing down the dynamics	159
5.1. P(AAm-co-VIm) – Hg ²⁺ hydrogels.....	162
5.1.1. Preparation and absorption isotherms	162
5.1.2. Linear rheology	163
5.1.3. Small angle X-Ray scattering.....	164
5.1.4. Tensile tests	165
5.1.5. Conclusions on P(AAm-co-VIm)-Hg ²⁺ dual-crosslink hydrogel.....	166
5.2. Synthesis of P(AAm-co-tPy) hydrogels	166
5.3. Rheology of the P(AAm-co-tPy) chemical hydrogel	167
5.4. Incorporation of physical bonds	168
5.5. Rheology of the slow Terpyridine-Zn ²⁺ hydrogel.....	169
5.6. Behavior in large deformations	170
5.6.1. Tensile tests	170
5.6.2. Cycles	172
5.6.3. Fracture – Single notch test	174
5.7. Discussion and conclusions.....	177
Chapter 6: One bond to rule them all.....	181
6.1. Linear rheology	184
6.2. Large deformations.....	186
6.2.1. Tensile tests.....	186

6.2.2. Cyclic	191
6.3. General remarks on the results in large deformations	194
6.4. Fracture.....	195
6.4.1. Single edge notch	195
6.4.2. Delayed fracture of pure shear samples.....	199
6.5. On the dynamic behavior of the dual-crosslink network.....	201
Chapter 7: Mapping the damage in dual-crosslink hydrogels with mechanophores	207
7.1. Mechanophores in hydrogels.....	211
7.2. A hydrosoluble dioxetane derivative to obtain time-resolved fracture information.....	213
7.2.1. Synthesis of the mechanophore and the hydrogel	214
7.2.2. Results and discussion.....	215
7.3. Anthracene Diels-Alder adduct as a crosslinker.....	216
7.3.1. Synthesis of the mechanophore	217
7.3.2. Synthesis of the chemical network with mechanophore	218
7.3.3. Mechanical properties of the dual-crosslinked hydrogel with mechanophores.....	220
7.3.4. Imaging the fracture front.....	222
7.4. Conclusion and perspectives	229
General conclusion	235
Annexes	245

Résumé en français

Rupture d'hydrogels dynamiques à double réticulation : des interactions moléculaires à l'énergie de rupture

Les hydrogels sont une classe importante de matériaux, grâce à leurs propriétés très particulières : composés en grande partie d'eau, ils sont particulièrement mous mais ne s'écoulent pas sous leur poids, conservant une intégrité mécanique comme n'importe quel solide. Enormément d'exemples d'hydrogels peuvent être trouvés dans la nature : les concombres en sont un très bon exemple, mais le corps humain est aussi composé de différents hydrogels (muscles, tendons, organes, tous sont solides et composés en très grande partie d'eau). Les hydrogels de synthèse trouvent leur place dans notre vie de tous les jours, des applications ayant été développées dans beaucoup d'industries. On les utilise dans les couches (pour leur capacité à absorber de l'eau), en tant que lentilles de contact (pour leurs propriétés mécaniques et leur capacité à contenir une solution aqueuse), en tant que cosmétiques... Plus récemment, la recherche s'est orientée vers l'utilisation d'hydrogels dans un contexte biomédical : comme les lentilles de contact l'ont montré, ils sont particulièrement bien adaptés au corps humain et peuvent être utilisés en tant que cartilages artificiel par exemple. Ces applications nécessitent cependant une certaine ténacité et rigidité, et l'hydrogel synthétique classique est plutôt fragile. En d'autres termes, l'énergie maximale qu'on peut lui apporter est faible.

1. Présentation du projet

Au cours de ce projet, nous avons voulu renforcer un hydrogel et comprendre les mécanismes moléculaires menant à ce renforcement. Pour cela, nous avons synthétisé un matériau purement élastique, sans aucun mécanisme de dissipation d'énergie interne. Nous y avons introduit des liaisons non-covalentes, sous la forme de complexes de coordination entre des ions métalliques libres présents dans la solution, et des ligands présents sur la chaîne de polymère. La réaction de complexation étant réversible, ces liaisons sont constamment en équilibre entre un état « ouvert » (où l'ion métallique est sous forme de mono-complexe, avec un seul ligand) et un état « fermé » (où l'ion métallique est sous forme de bi-complexe, avec deux ligands). Le passage d'un état à un autre se fait au bout d'un certain temps, déterminé par la cinétique du complexe que l'on a choisi.

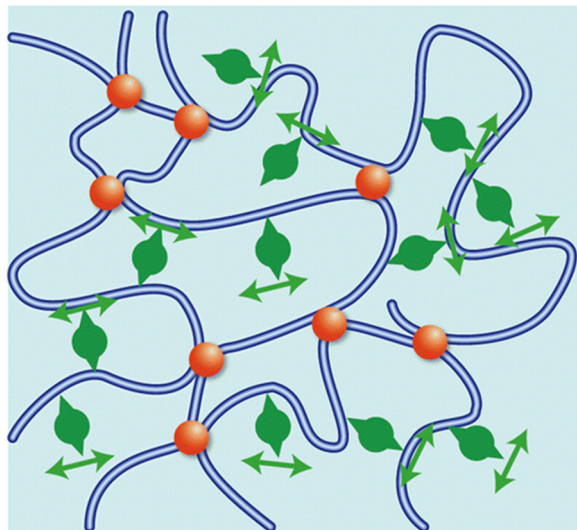


Figure 1.1 : Réseau de chaînes de polymères, réticulées chimiquement (en rouge) et physiquement (en vert).

Cela nous permet de définir un temps durant lequel la liaison est fermée, durant laquelle elle existe. On parle alors de « temps de vie » de la liaison. Ce temps de vie est fini ; par opposition aux liaisons

covalentes chimiques, qui ont un temps de vie infini, nous appellerons donc ces liaisons des « liaisons physiques ».

Cette liaison physique permettra au réseau de dissiper de l'énergie, sous forme d'entropie. Lorsqu'on étire le matériau, on étire les chaînes entre deux points de réticulation ; si l'un de ces points est une liaison physique, elle va s'ouvrir au bout de son temps de vie. Cela permettra alors à la chaîne de relaxer vers son état le plus stable, dissipant toute l'énergie qui y avait été stocké. Un intérêt de cette stratégie est qu'elle dépend de la vitesse à laquelle on sollicite ces chaînes de polymères : si on les déforme rapidement, la liaison physique n'aura pas le temps de s'ouvrir au cours de la déformation. Elle ne pourra donc pas dissiper d'énergie, et le matériau devrait être rigide et fragile. Si au contraire on déforme ces matériaux trop lentement, les liaisons physiques seront invisibles à l'échelle de la déformation. Elles ne participeront pas à la dissipation d'énergie, et le matériau devrait être mou et fragile.

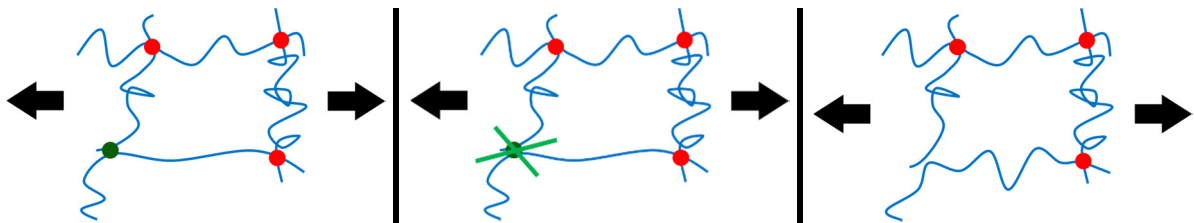


Figure 1.2 : Principe de la dissipation d'énergie par relaxation des chaînes dans le réseau lors de l'ouverture d'une liaison physique

Tout l'intérêt de la chimie particulière que l'on a choisie réside dans le fait que ce temps de vie de la liaison physique est déterminé par la nature du complexe que l'on utilise : en changeant l'ion métallique ou le ligand utilisé, on change la cinétique de complexation et donc le temps de vie de la liaison.

Dans la suite, nous allons étudier la microstructure et les propriétés mécaniques de ces hydrogels à double réticulation. L'hydrogel sans ions métalliques, nommé « gel chimique », sera utilisé comme référence.

2. Etude de la microstructure d'un hydrogel à double réticulation

Nous avons d'abord étudié la structure de ces hydrogels à double réticulation, pour ensuite essayer de la relier à leurs propriétés mécaniques. Pour cela, nous avons d'abord étudié l'absorption d'ions métalliques par l'hydrogel chimique de base, pour connaître l'état d'équilibre des ions métalliques dans le réseau. Le gel chimique est placé dans une solution d'ions métalliques à concentration connue. La Figure 2.1 présente la quantité d'ions métalliques absorbés, en fonction de la concentration en ions de la solution diffusante à la fin de la diffusion.

Cette expérience montre clairement qu'un état d'équilibre est atteint pour les ions cuivre et nickel lorsque l'hydrogel contient un ion métallique pour deux ligands (ce qui confirme que les ions métalliques peuvent former des liaisons physiques). Pour les ions zinc, l'état d'équilibre semble être d'abord à un ion pour 4 ligands ; puis, avec assez d'ions dans la solution diffusante, on atteint le même état que les ions cuivre et nickel.

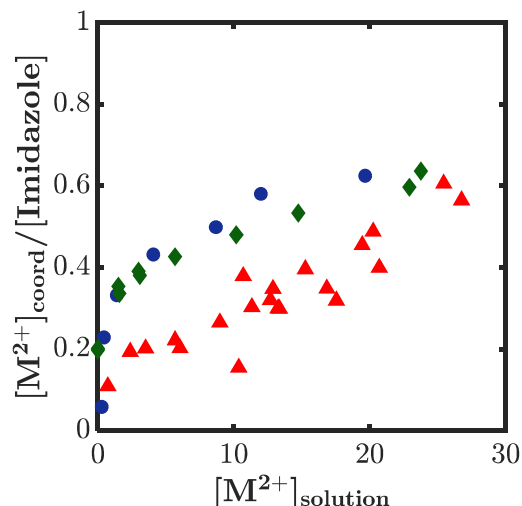


Figure 2.1 : Isothermes d'absorption pour les ions Cuivre (cercles bleus), Zinc (triangles rouges) et Nickel (losanges verts)

Nous avons ensuite réalisé plusieurs expériences de diffusion dynamique de la lumière (DLS) et de rhéologie.

La première méthode consiste à envoyer un laser au travers de l'hydrogel, et de mesurer les fluctuations de la lumière diffusée par l'échantillon. En mesurant ces fluctuations, il est possible de remonter aux mouvements des chaînes de polymères dans le réseau, et plus particulièrement aux temps caractéristiques de ces mouvements.

Là où nous attendions un seul temps caractéristique, liée au temps de vie de la liaison physique, nous en avons découvert deux. Ces deux temps ont été confirmés par des mesures de rhéologie sur les mêmes échantillons (voir Figure 2.2).

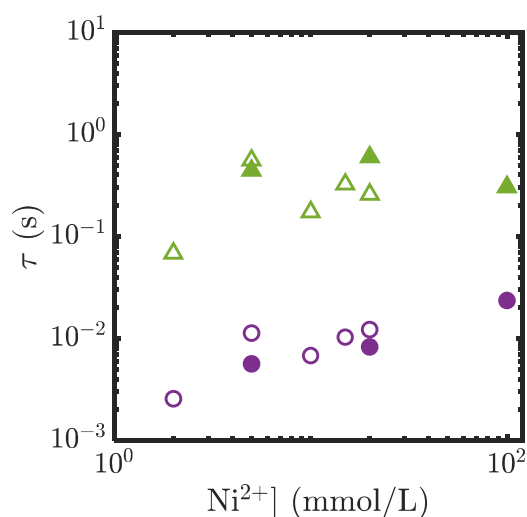


Figure 2.2 : Temps caractéristiques mesurés en DLS (points creux) et en rhéologie (points pleins).

Les deux échelles de temps que nous mesurons dans ces expériences peuvent être reliées à des distances caractéristiques différentes, autour de 3 et 16 nm, suggérant une organisation particulière de notre hydrogel à double réticulation. Nous avons donc réalisé des expériences de diffusion de rayons X sur

ces hydrogels, pour étudier l'organisation des chaînes de polymère à l'échelle nanométrique. Ces mesures ont confirmé les deux distances caractéristiques que nous avons mesurées en rhéologie et DLS.

L'ensemble de ces résultats suggère que les liaisons physiques à l'intérieur des hydrogels s'organisent plutôt sous forme d'agrégats, ce qui n'était pas inattendu. Comme nous le verrons, ces agrégats auront une forte influence sur les propriétés du matériau aux très grandes déformations. Ils possèdent en effet, par définition, un temps caractéristique bien plus long que la liaison physique seule.

3. Evolution des propriétés mécaniques avec le temps caractéristique et la vitesse de déformation

Nous avons ensuite voulu étudier les propriétés mécaniques de ces hydrogels à double réticulation, et les comparer à celles du gel chimique référence. Pour cela, nous avons réalisé des essais de traction sur ces matériaux. Un résultat typique d'une telle expérience est présenté en Figure 3.1.

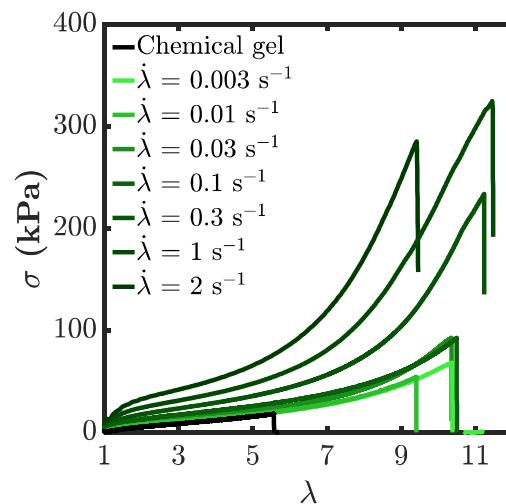


Figure 3.1 : Contrainte en fonction de la déformation appliquée ($\lambda = \text{longueur} / \text{longueur initiale}$), pour des hydrogels à double réticulation avec des ions nickel, déformés à différentes vitesses de traction relatives.

On observe ici que le comportement du matériau dépend de la vitesse à laquelle il est déformé. Le module d'Young par exemple (la pente des courbes à l'origine), qui caractérise la rigidité du matériau, augmente avec la vitesse de traction. Cette augmentation est simplement liée au fait que plus on déforme vite nos matériaux, moins on laisse aux liaisons physiques le temps de s'ouvrir. Et donc, moins on laisse aux chaînes de polymère le temps de relaxer, et dissiper les contraintes qu'on leur impose. Les contraintes internes au matériau augmentent donc plus vite, et celui-ci a l'air plus rigide.

On mesure aussi un durcissement du matériau aux très larges déformations, qui dépend de la vitesse de traction. On observe là l'influence des agrégats de liaisons physiques, qui ont un temps de vie beaucoup plus long que la liaison physique seule.

Nous montrons finalement que dans ce système, le paramètre qui contrôle les propriétés du matériau est en fait la vitesse de déformation par rapport aux temps de vie de la liaison physique. Ainsi, diminuer la vitesse de déformation est équivalent à augmenter le temps de vie de la liaison. C'est ce que représente la Figure 3.2.

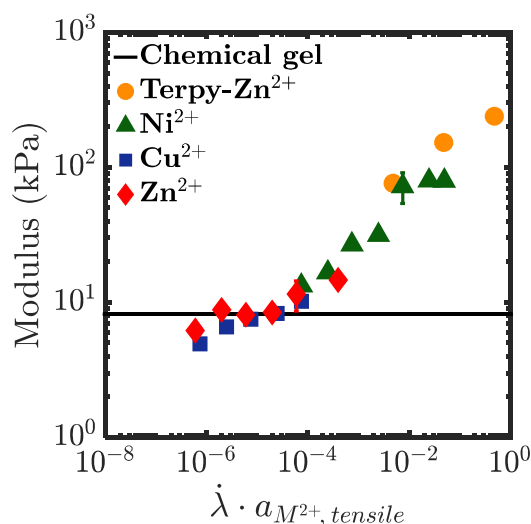


Figure 3.2 : Module élastique d'hydrogels à double réticulation, en fonction de la vitesse de déformation normalisée par le temps de vie de la liaison.

4. Mécanophores et perspectives

Au cours de ce projet, nous avons aussi tenté d'intégrer dans le réseau un « mécanophore », une molécule qui devient fluorescente lorsqu'elle casse. Ceci nous permettrait de cartographier l'endommagement dans le matériau au cours d'une déformation, ou lors de la propagation d'une fracture.

Les premiers résultats sont encourageants, montrant clairement une zone de dissipation autour de la tête de fracture lorsqu'elle se propage, et donneront certainement lieu à plus de travail à ce sujet.

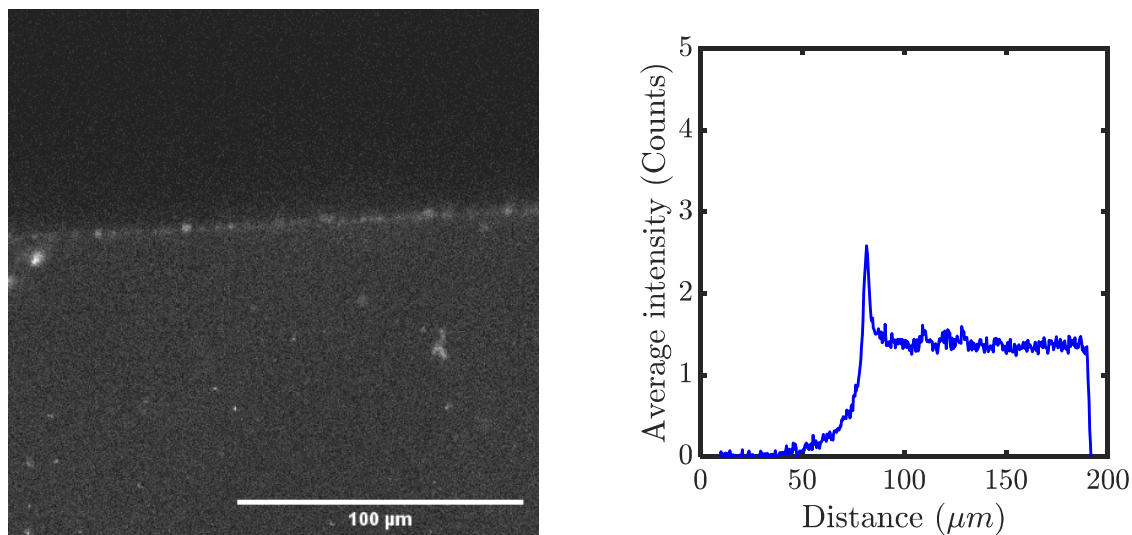


Figure 4.1 : Gauche : Front de fissure d'un hydrogel à double réticulation avec des ions Zn^{2+} , déformé à une vitesse $\dot{\lambda} = 2 \text{ s}^{-1}$. Droite : Intensité de fluorescence moyennée, en fonction de la distance, issue de l'image de gauche.

5. Conclusions

On a montré que le paramètre principal de nos hydrogels à double réticulation est simplement le temps de vie de la liaison physique qu'on introduit dans le matériau. Ce résultat n'était pas inattendu, mais est ici clairement établi dans des hydrogels pour la première fois. Un résultat inattendu est par contre l'influence très forte des agrégats de liaisons physiques, qui modifient très fortement les propriétés du matériau à grandes déformations et lors de la propagation d'une fissure.

Nous avons finalement montré la possibilité d'utiliser des mécanophores comme marqueurs de la rupture moléculaire dans un hydrogel lors de la déformation de cet hydrogel, ou lors de la propagation d'une fissure dans ce matériau.

Remerciements

Remerciements

Je voudrais tout d'abord remercier les personnes qui ont accepté de juger mon travail, pour leur temps et pour l'intérêt qu'ils ont montré à mon sujet : Min-Hui Li, Sebastian Seiffert, Kees Storm, ainsi que les rapporteurs de mon manuscrit Laurence Ramos et Evelyne van Ruymbeke. J'ai beaucoup apprécié les discussions qu'on a eues au cours de (et même avant) ma soutenance.

Je tiens aussi évidemment à remercier mes deux encadrants de thèse, Costantino Creton et Tetsuharu Narita. D'abord pour m'avoir donné la chance de travailler sur ce sujet, que je trouvais passionnant au début et qui m'a passionné tout du long. Ensuite, pour ce que vous m'avez apporté pendant ces 3 ans. Nos échanges ont toujours été constructifs, et j'ai énormément appris avec vous. Ma thèse s'est très bien passée (en tout cas, de mon point de vue !) et c'est en grande partie grâce à notre bonne entente et à votre disponibilité.

Cette thèse, je ne l'ai évidemment pas faite tout seul. Au cours de ces trois ans et quelque, j'ai pu collaborer et échanger avec bon nombre de personnes. Il est bien sûr compliqué de citer tout le monde, mais quelques-uns ont été d'une aide précieuse. Gabriel Sanoja, merci pour ton aide incomparable et une année de tentatives et expériences infructueuses, ainsi que pour ta curiosité, ta bonne humeur et tout ce qui fait que j'ai énormément apprécié de travailler avec toi. Jean Comtet, merci pour ton aide incomparable dans l'observation de la fluorescence d'hydrogels avec mécanophores : je te dois une très grande partie de mon dernier chapitre, et ce n'est pas rien ! Et enfin, last but not least, Xavier Morelle, merci pour ton aide incomparable dans l'étude de la mécanique de mes matériaux – les deux années à travailler ensemble ont été particulièrement profitables et agréables. Je voudrais aussi remercier tous les membres du laboratoire SIMM avec qui j'ai pu échanger, de près ou de loin. Vous êtes bien trop nombreux pour que je vous cite tous. Merci Mohamed pour les analyses footballistiques du lundi matin, merci à Ludo et Alex, merci Guylaine, Armand, Bruno, Freddy,...

J'ai aussi eu la chance de pouvoir encadrer une stagiaire, et ça a été pour moi une expérience géniale. Merci beaucoup Ippolyti, pour toute ton aide. Certes tes gels n'ont pas fonctionné comme prévu, mais tu as su prouver clairement et précisément pourquoi il ne fallait pas les utiliser ! J'ai beaucoup apprécié travailler avec toi.

Ces 3 années auraient été très différentes sans les doctorants et post-docs du labo qui les ont rythmées. J'ai eu la chance de vivre cette thèse dans une ambiance incroyable et je pense que ça a été crucial pour la réussite de ma thèse, donc merci à vous tous. J'ai même pu me faire d'excellents amis, qui ont été d'incroyables soutiens. Merci Guillaume, Gabo, Christophe, Pierre, Julie, Sandrine, Mélanie, Gaele, Claire, Paul, Nassim, ... Vous voyez, vous êtes trop nombreux !

Merci aux incroyables Maxime et Jules, mes collègues d'escalade, de brassage (et buvage) de bière, de jeux de société, de tout en fait. Je sais que je peux toujours compter sur vous, quelle que soit la distance.

Enfin, merci à ma famille. Je n'ai pas vraiment les mots pour dire l'immensité de ce que vous m'apportez, mais rien de tout ce que j'ai réalisé n'aurait été possible sans vous.

A bientôt à Clermont-Ferrand !

General Introduction

Hydrogels are networks of crosslinked polymers swollen in water. They are an important class of soft matter, thanks to their liquid-like and solid-like properties. Many examples of hydrogels can be found in nature, including in living beings (whether a cucumber or a human being). Synthetic hydrogels find their place in our everyday life, and numerous applications in various industries have been developed. Their capacity to absorb and diffuse water and solutes has been extensively studied for applications such as contact lenses, diapers, cosmetics or plasters. More recently, research has focused on the use of natural and synthetic hydrogels in a biomedical context. Indeed, their high water content and their soft-solid behavior makes them particularly suited to the use inside a human body. Their ability for reversible deformation is attractive for applications as artificial cartilage or ligaments. However, for these applications requiring a certain mechanical toughness and stiffness of the material, the classical synthetic hydrogels reach their limit, being usually fragile materials.

There are two intrinsic properties of the classical hydrogels that causes their mechanical fragility. The first is the heterogeneity of the crosslinking. A classical hydrogel made of chemically crosslinked polymer chains has in general the heterogeneous crosslinking density, creating defects in the network. Upon deformation, stress concentrations on certain chains can occur, which weakens the hydrogel. The second is the lack of energy dissipation mechanism in such a network. When stretched, all the energy brought to the network is stored as mechanical energy in the polymer chain. Since the material is swollen in a low viscosity solvent (water), none (or at best a negligible part) of this applied energy is dissipated by the usual mechanisms one can find in elastomers, such as chain friction. The catastrophic failure of polymer chains will occur upon reaching a critical energy level, which in this case is quite low.

The strategies explored nowadays to reinforce hydrogels have been based on these two limitations of hydrogels, either by homogenizing the network structure (or the stress) or by introducing energy dissipation mechanisms into it. In these two strategies, two particularly interesting pioneering works can be cited. Ito et al. [1] have developed a type of topological crosslinks able to ‘slide’ along the polymer chains (so-called ‘slide-ring hydrogels’). This particular bond allows the homogenization of the stress during its deformation, which makes it particularly deformable in the absence of notch. Gong et al. [2], working on the other strategy, have developed a ‘double-network hydrogel’, consisting of a first highly-crosslinked network which is interpenetrated by a second loosely crosslinked network. The first network gives the hydrogel a high stiffness, and acts as a sacrificial network that dissipates energy by irreversibly breaking during stretching. After its breaking, the second network maintains the mechanical integrity of the material. The properties of this double-network hydrogel are then much better than that of each network taken apart.

However, the toughness of this double-network hydrogel, while particularly high, is based on an irreversible mechanism – the breaking of the first sacrificial network. Once this network is broken, the properties of the virgin material are irremediably lost. Suo [3] et al. have circumvented this issue by using a physically crosslinked alginate as a first sacrificial network. This network is reversibly crosslinked by ionic interactions between the alginate and calcium ions placed in the solution. Upon stretching, the physical bonds of alginate ‘unzip’ in the characteristic deformation of such an alginate network, dissipating energy. The material is able to recover part of its original properties after being stretched below its critical stretch, but this recovery is still quite slow owing to the slow dynamic of the alginate- Ca^{2+} ‘egg box’ bond.

In our laboratory, K. Mayumi and J. Zhao [4,5] have worked on a single chemically crosslinked network, having also a large amount of physical bonds which act as sacrificial bonds. Based on a chemically crosslinked network of poly(vinyl alcohol), physically crosslinked by borate ions, this ‘dual-crosslink’ hydrogel has shown good mechanical and fracture-resistance properties. In particular, these properties were found to depend on the rate at which the material was deformed. A characteristic frequency of the material was found, defined by the frequency at which the physical bonds break and the chains relax. If deformed at rates much higher than this frequency, the material became brittle. At those rates, the physical bonds did not have time to break and dissipate energy before the network reached a critical energy level and broke. On the contrary, at low rates, its extensibility and resistance to fracture increased because of the energy dissipated by the physical crosslinks.

The work on the PVA-borax dual-crosslink hydrogels raised the question of the evolution of the material behavior with the rate at which it is deformed, and in particular what happens at even lower rates. These rates being inaccessible in a laboratory (owing to the time-length of the experiments), Zhao et al. [5] developed a new type of dual-crosslink hydrogel with which they would be able to modify the characteristic dynamics of the network. These gels are based on a copolymer of acrylamide and vinylimidazole. The latter play the role of ligand, and create coordination complexes with the metallic ions. The coordination complexes then serve as reversible physical bonds, whose dynamics can be changed by simply changing the ion. The dynamic of the network could then be tuned. These new materials showed some first insights into the mechanisms taking place at low stretch-rate, but also showed some limitations (in particular in their preparation method). Hence, some open questions remain:

- Is it possible to prepare those dual-crosslink hydrogels with any metal ion, allowing to access to a wide range of dynamics? Is the microstructure of these materials the same for each ion used?
- Is it possible to identify a general behavior for the dual-crosslink hydrogel over this wide range of dynamics, dependent only on the ion used? Can the properties in rheology, large strains or fracture of these materials be predicted just by knowing the dynamics of the network?
- How does a fracture propagate in such a dynamic network? Is this propagation characteristic of the deformation rate? Does it evolve with the dynamics of the network?

To bring some answers to these questions, the present manuscript is composed of 7 chapters.

The first chapter is a review of the present literature on hydrogels, some proposed mechanisms on how to reinforce them, and a state of the art review of dynamic hydrogels and their resistance to fracture.

Chapter 2 presents the preparation of a standard dual-crosslink hydrogel. We will investigate its dynamics by two different methods and try to build a picture of its microstructure.

In Chapter 3, we will characterize and analyze the mechanical properties in large deformations of this dual-crosslink hydrogel and its properties of fracture resistance as a function of the deformation rate.

In Chapter 4, we will extend the methodology of chapter 3 by simply changing the metallic ion used, to modify the dynamics and the mechanical properties of the dual-crosslink hydrogels.

Fracture of dual-crosslink dynamic hydrogels: from molecular interactions to fracture energy

In Chapter 5, we will investigate the mechanical and fracture properties of a dual-crosslink hydrogel with even slower dynamics than the first dual-crosslink hydrogel, by changing the ligand instead of the metallic ion.

In Chapter 6, we will try to unify the results from the three different types of dual-crosslink hydrogels, by representing our key data as a function of the Weissenberg number, a product of the stretch-rate by a characteristic time of the material.

Finally, in Chapter 7, we will show some first results on the introduction of mechanophores into the chemical network of the dual-crosslink hydrogel. Two different mechanophores will be tried.

References

1. Ito, K. Novel Cross-Linking Concept of Polymer Network: Synthesis, Structure, and Properties of Slide-Ring Gels with Freely Movable Junctions. *Polymer Journal* 39, 489–499 (2007).
2. Gong, J. P., Katsuyama, Y., Kurokawa, T. & Osada, Y. Double-Network Hydrogels with Extremely High Mechanical Strength. *Adv. Mater.* 15, 1155–1158 (2003).
3. Suo, Z. et al. Highly stretchable and tough hydrogels. *Nature* 489, 133–136 (2012).
4. Mayumi, K., Guo, J., Narita, T., Hui, C. Y. & Creton, C. Fracture of dual crosslink gels with permanent and transient crosslinks. *Extreme Mechanics Letters* 6, 52–59 (2016).
5. Zhao, J. Structure et propriétés des hydrogels à réticulation chimique et physique. (PSL Research University, 2018).

Chapter 1

From polymer physics to the toughening of hydrogels

1. From polymer physics to the toughening of hydrogels

Table of contents

1.1. Polymer network physics	10
1.2. Fracture of soft matter	14
1.2.1. “Bulk” vision of fracture	14
1.2.2. Molecular vision.....	16
1.3. Reinforcement of hydrogels	17
1.3.1. Homogeneous networks	17
1.3.2. Introducing an energy dissipation mechanism	19
1.4. Using dynamic coordination crosslinks	22
1.4.1. Transient networks with versatile dynamics	22
1.4.2. Toughened gels.....	28
1.5. Objectives of this project	34
References	36

1. From polymer physics to the toughening of hydrogels

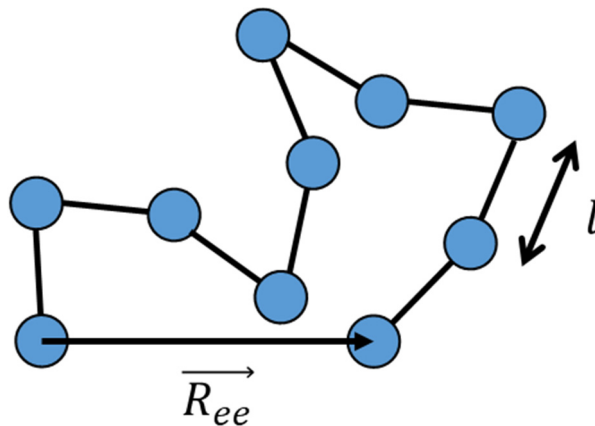
Polymeric materials are used in a large variety of applications, in particular because of their interesting and easily tunable mechanical properties. By playing on the molecular composition of the polymer, on its supramolecular architecture and on its microstructure, it is possible to reach a large array of properties. The challenge in this process is to relate the molecular properties of the polymer, what chemistry imposes, to the macroscopic (mechanical, electrical, optical...) properties of the material.

In this chapter, we will detail first the physics of an isolated chain of polymer and, from this basis, try to understand the mechanical behavior of a network of polymer chains. We will then study the fracture of a soft material, and review some methods of toughening soft matter (elastomers or hydrogels). Finally, we will focus on a specific strategy to toughen materials: the use of a transient and reversible crosslink.

1.1. Polymer network physics

In this part, the models presented to understand the behavior of polymeric networks have been taken from a reference textbook from Colby and Rubinstein [1].

a. Physics of an isolated polymer chain



Scheme 1.1: Representation of a polymer chain containing $N = 10$ monomers, with a bond length l .

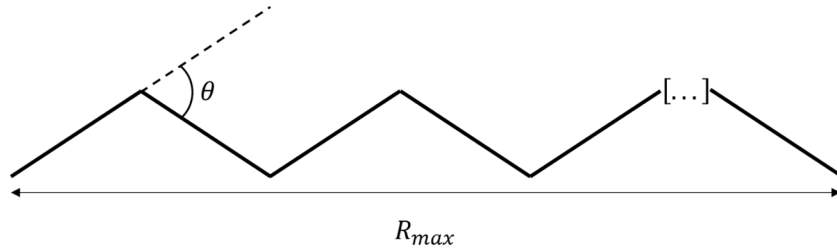
A polymer chain can be defined as an assembly of N bonds, each of them of length l . If all the monomers are perfectly aligned, the maximal length of the chain will be

$$R_c = N \times l \quad \text{Eq. 1.1}$$

This length, called contour length, represents the maximal length of the chain. In practice, each bond i is at an angle θ with the next bond $i + 1$, a valence angle that is defined by quantum physics.

$$R_{max} = N \times l \times \cos\left(\frac{\theta}{2}\right) \quad \text{Eq. 1.2}$$

For a carbon-carbon bond with an sp^3 hybridization state, which composes the backbone of the chain of many usual polymers, $\theta = 109.5^\circ$ and $R_{max} = 0.82 \times R_c$.



Scheme 1.2: Representation of the maximum size of a polymer chain R_{max} and the valence angle θ between bonds

In reality, a relevant characteristic length of this chain is the average end-to-end distance, which represents the average size of the polymer chain at thermodynamic equilibrium. Maximizing the conformational entropy imposes the polymer chain to be a random walk of monomers, in the ideal case where the chain is made of independently linked and randomly oriented segments, this distance is given by:

$$\langle R_{ee}^2 \rangle = N \times l \quad \text{Eq. 1.3}$$

In real chains, the segments are not randomly oriented. The characteristic ratio C_∞ accounts for this correlation. It is a material parameter, dependent on the material used, and corresponds to the rigidity (or flexibility) of the bonds:

$$R_0^2 = \langle R_{ee}^2 \rangle = C_\infty \times N \times l \quad \text{Eq. 1.4}$$

The polymer chain can then be extended, in theory up to its maximal length R_{max} , by applying a force on one end of the chain. When applying such a force, the chain unfolds and changes in conformation, which implies a low energy cost. This low energy cost explains why polymeric materials are easier to deform than crystalline materials, where deformation implies breaking of bonds.

The mechanical characterization of a single polymer chain has been carried out using an AFM tip. In particular, Oesterhelt *et al.* studied a poly(ethylene glycol) polymer chain [2]. In Figure 1.1, two different regimes can be seen:

- At first, while the force value is low, the chain is unfolding. The response is not specific of the properties of the monomer, but of the statistics of the chain itself. The main drive for the force here is the loss of entropy that one induces when extending a chain – the loss of accessible conformations increases the entropy of the system, and the polymer chain tends to go back to its initial conformation. Force-displacement plot is linear;
- When reaching a critical deformation, dependent on the length of the chain, the force increases steeply. The chain has reached its extended state, so further elongation implies the distortion of the bonds of the chain (decrease of the valence angle θ). This regime is enthalpy-controlled, and depends mainly on the properties of the bonds.

At a certain level of elongation, the energy stored in the polymer chain (area under the force-displacement curve) reaches a critical level, dependent on the nature of the monomers: the chain breaks.

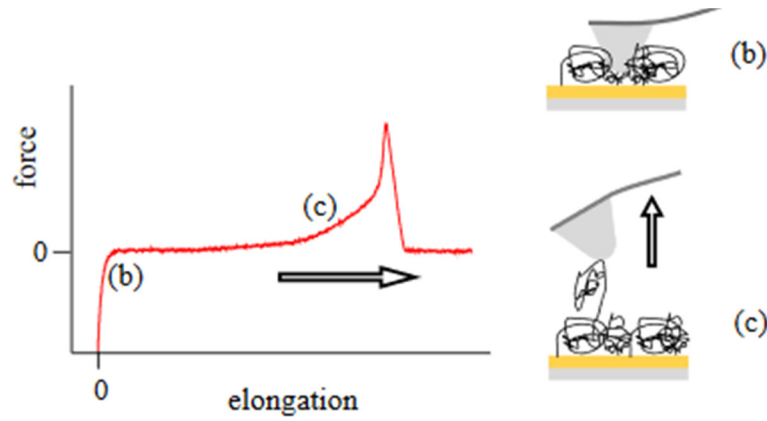


Figure 1.1: Schematic of a single molecule force spectroscopy experiment. Upon retraction of the cantilever the polymer chain is stretched while force and elongation are recorded. Figure reprinted from [2].

b. Rubber elasticity of a network

The physics of polymer networks derives from the physics of isolated chains. However, in this particular case, one needs to consider how the different polymer chains interact with each other, whether by chemical covalent bonds or physical interactions.

In the case of “standard” hydrogels, covalently crosslinked networks swollen in water, the only interaction between the different polymer chains is through the chemical crosslinks. There is no physical interaction between the chains, friction is negligible.

To describe the mechanical properties of such a network, Kuhn, Wall and Flory [3] developed an affine model. The main assumption of this model is that the relative deformation of each strand of the network is the same as the macroscopic deformation of the material. As long as there is no bond breakage, any deformation applied to this material is reversible, because of the entropic elasticity of the strands.

A strand of this network, with an initial end-to-end vector $\vec{R}_0(R_{x,0}, R_{y,0}, R_{z,0})$ is deformed to $\vec{R}(R_x, R_y, R_z)$. We can define the stretches λ_i , stretches of the chain in the three directions (x, y, z) such as:

$$\begin{aligned} R_x &= \lambda_x R_{x,0} \\ R_y &= \lambda_y R_{y,0} \\ R_z &= \lambda_z R_{z,0} \end{aligned} \tag{Eq. 1.5}$$

The strain energy density applied to this network to stretch it is then

$$W = \frac{\nu_x k_b T}{2} (\lambda_x^2 + \lambda_y^2 + \lambda_z^2 - 3) \tag{Eq. 1.6}$$

With k_b the Boltzmann constant, T the temperature and ν_x the number density of elastic strands in the network. Considering the material to be incompressible (which is largely the case in polymers), we have $\lambda_x \lambda_y \lambda_z = 1$. In the case of uniaxial tension in the x direction, at a stretch λ , we have $\lambda_x = \lambda$ and $\lambda_y = \lambda_z = 1/\sqrt{\lambda}$.

The value of the nominal stress can then be predicted from deriving the energy density function W relatively to the uniaxial stretch λ , giving:

$$\sigma_N = \nu_x k_b T \left(\lambda - \frac{1}{\lambda^2} \right) \quad \text{Eq. 1.7}$$

$G = \nu_x k_b T$ is then the shear modulus of the material. This modulus may also be defined as

$$G = \frac{k_b T}{\xi^3} \quad \text{Eq. 1.8}$$

With ξ the mesh size of the network (which gives an estimate of the average end-to-end distance of the polymer strands in the network). The shear modulus is also linked to the materials Young's modulus by

$$E = G \times 2(1 + \nu) \quad \text{Eq. 1.9}$$

Where ν is Poisson's ratio. In our case, where we considered an incompressible material, $\nu \approx 0.5$ which gives $E = 3G$.

c. Limitations – no elasticity

The affine model supposes that $\sigma_N/(\lambda - \lambda^{-2})$ is a constant, only dependent on the crosslinking density of the material ν_x . This might not always be the case. Mooney and Rivlin [4,5] developed an empirical approach to describe the effect of chain entanglement on the mechanical properties of a network, using the following expression:

$$\sigma_{reduced} = \frac{\sigma_N}{\lambda - 1/\lambda^2} = 2C_1 + \frac{2C_2}{\lambda} \quad \text{Eq. 1.10}$$

This non-linear modification catches well the decrease of $\sigma_N/(\lambda - \lambda^{-2})$ with increasing strain in uniaxial tension, linked to the entanglements in the network.

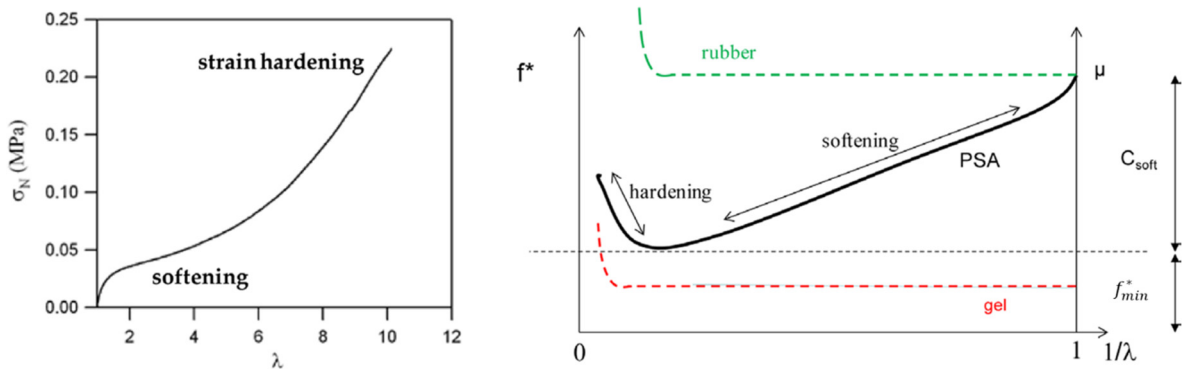


Figure 1.2: (a) Typical nominal stress versus uniaxial stretch plot for a PSA and (b) Mooney representation of the same data as a function of $1/\lambda$ and comparison with an elastic gel and an elastic rubber. Figure reprinted from [6].

However, this linear dependence of the reduced stress with $1/\lambda$ is rarely seen. In usual pressure-sensitive adhesives for example, as described by Creton and Ciccotti [6], the Mooney stress decreases (not necessarily linearly) with increasing λ (decreasing $1/\lambda$) until a certain stretch, after which it increases (Figure 1.2, from [6]). This behavior is typical of those materials, with a first visco-elastic softening followed by a strain-hardening behavior when the polymer chains in the network reach a critical level of stretch.

1. From polymer physics to the toughening of hydrogels

With this kind of behavior, it is possible to extract three common values:

- f_{min}^* , the minimal value that the reduced stress reaches. In an experiment realized infinitely slowly, with no visco-elastic behavior, one would find the elastic modulus μ to be equal to f_{min}^* . However, f_{min}^* is usually dependent on the stretch-rate (experiments are never realized infinitely slowly);
- λ_{SH} , the value of stretch of onset of strain-hardening. This stretch is related to the finite extensibility of the crosslinked polymer chains (and hence to f_{min}^*) by $\lambda_{SH} \approx (\rho RT / f_{min}^*)^{1/2}$;
- $C_{soft} = \mu - f_{min}^*$, which is characteristic of the softening process due to the different visco-elastic relaxations taking place in the material during the stretching.

These three parameters will depend on the stretch-rate in a visco-elastic material, or in a network with entanglements.

1.2. Fracture of soft matter

1.2.1. “Bulk” vision of fracture

a. Linear elastic fracture mechanics

The study of fracture consists in determining how much mechanical energy a material needs to propagate a crack. This fracture energy is generally noted Γ . In order to simplify this study, a major assumption is that the behavior of the bulk of the material remains linearly elastic everywhere, except in a small region around the tip of the crack – which is the basis of the Linear Elastic Fracture Mechanics (LEFM).

During the propagation of a crack, two new surfaces are created. The so-called “strain energy release rate” is defined as the change in total mechanical energy W_m with a change in crack area \mathcal{A} .

$$G = \frac{dW_m}{d\mathcal{A}} \quad \text{Eq. 1.11}$$

Griffith [6] stated that a crack from a pre-existing defect would propagate in the material when this strain energy release rate G reaches a critical value G_c . In theory, this energy corresponds to the energy needed to create two new surfaces of the material, also called Dupré energy of adhesion. The crack will only propagate when there is enough energy to create these two new surfaces. In practice, this critical value G_c , also noted Γ , includes two components. The first is this energy needed to create two new surfaces of the material. The second component is the energy dissipation linked to the propagation.

Irwin [8] expanded this model by studying the stress concentration at the tip of a crack, expressing a singularity at the tip of the crack in the form of an inverse square root dependence of σ on the distance to the crack tip:

$$\sigma(r) \sim \frac{K}{\sqrt{r}} \quad \text{Eq. 1.12}$$

where K (in $Pa \cdot m^{1/2}$) is called the stress intensity factor. Here, the crack propagates when $K \geq K_c$, with K_c a material property called material toughness. In LEFM, $K \geq K_c$ and $G \geq \Gamma$ are equivalent parameters.

However, these results are valid in the case of the LEFM, which is not a suitable tool to describe soft materials such as elastomers or hydrogels. In those cases, the propagation of a crack is very different from what happens in a brittle material, where only the bonds near the tip of the crack break. The energy needed to propagate a crack is dissipated by:

- Bond breakage to propagate the crack;
- Possible visco-elastic or plastic deformations in the bulk of the material, which decrease the energy available to propagate the crack;
- Blunting of the crack tip. Elastomers and gels being very soft, the deformations at the crack tip can reach very high values, leading to a removal of the stress concentrations in this region;
- Visco-elastic or plastic dissipation in a region around the crack tip, that are not beneficial to the crack propagation.

The fracture energy Γ takes then into account all these sources of energy dissipation, including the breaking of bonds for propagation of the fracture [6].

b. Greensmith approximation

The measurement of the fracture energy has been extensively studied in the literature, and some reliable experimental protocols have been developed. The general idea is always the same: pre-notching a sample, and stretching it until it breaks.

Based on a series of experiments with different notch lengths, Greensmith [9] proposed a simple empirical expression to quantify the strain energy release rate for neo-Hookean elastomers, in a single-edge notch test:

$$\mathcal{G}(\lambda) = \frac{6cW(\lambda)}{\sqrt{\lambda}} \quad \text{Eq. 1.13}$$

With c the length of the initial notch, and W the strain energy density defined as $W = \int \sigma d\lambda$, calculated from the stress-stretch curves of an un-notched sample. When λ reaches a critical stretch λ_c , the crack starts to propagate. Γ is computed from this value λ_c , such as:

$$\Gamma = \mathcal{G}(\lambda_c) = \frac{6cW(\lambda_c)}{\sqrt{\lambda_c}} \quad \text{Eq. 1.14}$$

In the case of a pure-shear geometry, where the height H of the sample is lower than its width L , supposing we have $c < H$, the strain energy release rate can be written as

$$\mathcal{G}(\lambda) = W(\lambda) \times H \quad \text{Eq. 1.15}$$

As mentioned earlier, in the case of non-elastic materials, $W(\lambda)$ will also take into account the energy dissipated by the bulk of the material during loading. This energy is not available for fracture propagation, and should not be taken into account in the computation of Γ . To solve this, it is possible to calculate $W(\lambda_c)$ not by integrating the loading curve of an un-notched sample up to λ_c , but by integrating the unloading curve of the same sample. The unloading curve gives an idea of the recovered energy after the test, hence shows the energy that was available in the material at λ_c . This way, it is possible to compute Γ_{local} , the fracture energy that does not take into account the mechanisms happening in the bulk of the material.

1. From polymer physics to the toughening of hydrogels

To account for the dissipative mechanisms happening close to the crack tip, Gent and Schultz, in 1972 [10], proposed to define Γ as the sum of two contributions:

- Γ_0 , the intrinsic fracture energy of the material if there were no dissipative mechanisms;
- $f(v, T)$, a function dependent on the stretch rate v and the temperature T , that characterizes the linear viscoelastic dissipation in front of the crack tip during propagation.

The fracture energy is then given by [11]

$$\Gamma = \Gamma_0(1 + f(v, T)) \quad \text{Eq. 1.16}$$

This approach was first developed for adhesion problematics, but also applied to fracture tests later on. Persson estimated the contribution $f(v, T)$ from the linear viscoelastic properties of the material. However, this contribution does not take into account the non-linear processes happening during crack propagation (cavitation, chain pullout, bond breaking...). Those processes cannot yet be calculated theoretically.

Γ_0 , on the other hand, has been estimated quite successfully by Lake and Thomas as we will now see.

1.2.2. Molecular vision

In order to compute the intrinsic fracture energy of an elastic material Γ_0 , Lake and Thomas [12] studied materials at temperatures and stretches where the viscoelasticity could be neglected. To be able to compute and predict accurately this Γ_0 , they decided to take a “bottom-up” approach by considering the molecular mechanics taking place when a crack propagates.

Let us consider a notched material under tension. The propagation of this notch requires the breaking of all the chains in front of the crack, in the plane normal to the tension direction. Each C-C bond of these chains carries an energy U , determined by the level of stretch at which they are. Once this energy reaches a critical level U_b , one of the bonds of the chain will break; this will allow the chain to release its stored energy in all bonds, moving back to an un-stretched conformation. Lake and Thomas proposed that this energy U_b would simply be the bond energy (around 350 kJ/mol for a carbon-carbon bond). The fracture energy Γ_0 would then be, with no source of dissipation:

$$\Gamma_0 = 2N_x U_b \Sigma \quad \text{Eq. 1.17}$$

Where N_x is the average number of C-C bonds between two crosslinks and Σ is the areal density of chains in the fracture plane.

A recent article from Craig and coworkers [13] suggests that the average energy per bond needed to break a chain is much lower than the energy of the carbon-carbon bond, around 60 kJ/mol instead. Indeed, the previous assumptions from Lake and Thomas neglected the stochastic nature of bond scission and the fact that the application of a the force on the chains during the deformation, increases the probability to break the bond so that at realistic strain rates the most probable energy stores at breakage is 60 kJ/mol. This Lake and Thomas theory has been used for 50 years because although it is unrealistic in terms of localization of fracture in a plane it predicts the correct scaling with N_x and the right order of magnitude in Γ [6].

1.3. Reinforcement of hydrogels

Hydrogels, polymeric networks swollen in water, are interesting materials, with various potential applications. However, the use of conventional chemically crosslinked hydrogels is limited due to their poor mechanical properties. Being neither stiff nor tough, it is then no surprise that the improvement of their mechanical properties has been intensively studied.

The low resistance to fracture of hydrogels comes from two main considerations:

- A heterogeneity of the network, linked to the polymerization process. This leads to the existence of weaknesses and defects in the network, where fractures can nucleate;
- The absence of energy dissipation inside the hydrogel. As seen before, a mechanism of energy dissipation is a good way to increase the fracture energy of a material. Conventional hydrogels, show none of the friction between chains that can be observed in elastomers, thus having no inherent mechanism to dissipate mechanical energy.

Several strategies have been developed, following these two main trends: increasing the homogeneity of the material, or incorporating dissipative mechanisms inside the hydrogel.

1.3.1. Homogeneous networks

a. Creating a “perfect” network

Sakai et al. [14] developed a homogeneous hydrogel, with a well-defined mesh size and a minimal number of imperfections. To do so, they used tetra-PEG, a four arms star-shaped macro-monomer, terminated with either amine (TAPEG) or NHS-glutarate (TNPEG) functions. The polymerization process is simply a reaction between the amines and the glutarate functions. This ensures a very small distribution of mesh sizes inside the hydrogel, and a good consequent homogeneity.

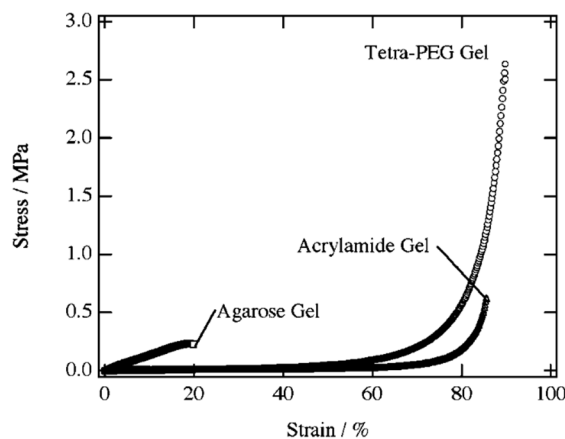


Figure 1.3: Stress-strain curves of agarose gel (squares), acrylamide gels (triangles) and tetra-PEG gel (circles). Figure reprinted from [14].

The obtained hydrogels had a high compression stress at break and high extensibility in traction (up to 12 times its initial size). The very regular structure of this network prevents the early nucleation of a crack inside the hydrogel, which explains its high extensibility and stress at break. However, this material is not intrinsically tough: once a crack appears, it propagates very fast. The measured fracture energy is in good agreement with the Lake-Thomas theory.

1. From polymer physics to the toughening of hydrogels

b. Are homogeneous networks the best solution?

Recent work from Yamaguchi et al. [15] on model sparse elastic networks suggests that, contrary to what has been said just before, the existence of heterogeneities in the chain lengths contributes to the introduction of sacrificial bonds in the network. This delays the final rupture of the material, as shown in Figure 1.4. In this work, they created a chain length heterogeneity such as half of the chains are $2\delta L$ longer than the other half, L being the mean chain length of the network. It is clear on the figure that, when increasing the heterogeneity of the network, one creates energy dissipation mechanisms that prevent the complete breaking of the network.

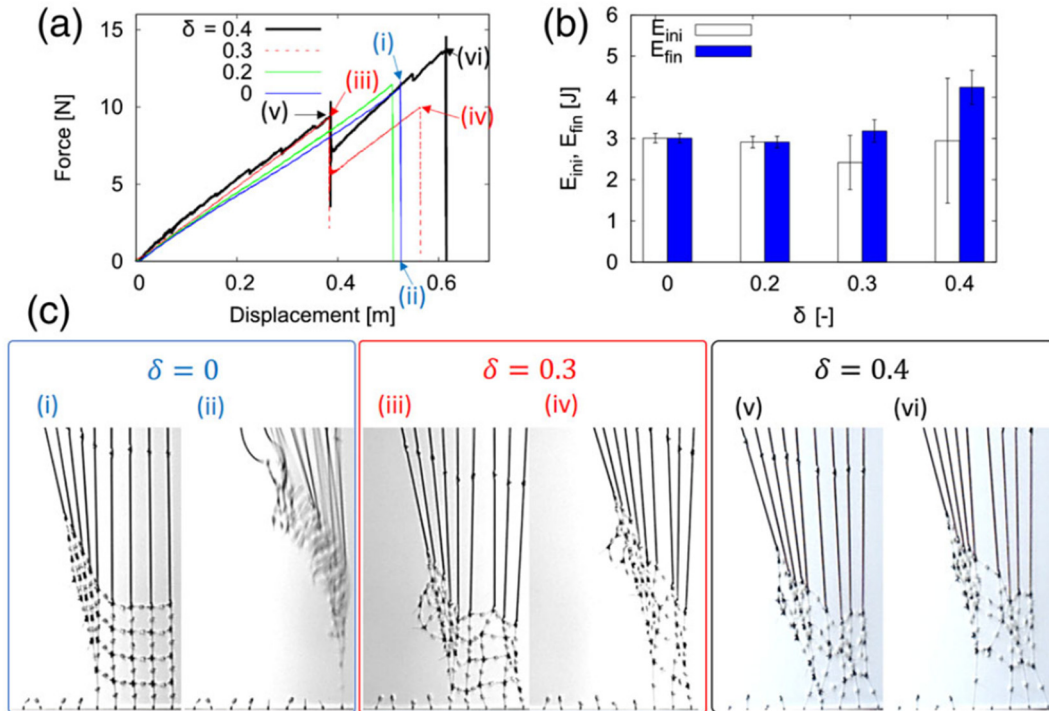


Figure 1.4: Fracture behavior for samples with different degrees of link length heterogeneity δ . (a) Force-displacement curves, (b) fracture energies at initial break and final rupture, and (c) snapshots of the deformations, where numbers (i)–(vi) correspond to those shown in Figure 1.4(a). Figure reprinted from [15].

This study also demonstrates that increasing the functionality of the crosslinker increases the toughness of the material. It consequently implies the possibility of an optimization of the network, maybe giving better performances than the “simple” tetra-PEG network previously presented.

c. Creating a perfect network is very challenging – how about erasing the imperfections?

Okumura and Ito, in 2001, [16-20] first developed what they called topological hydrogels, or polyrotaxane gels: instead of using fixed crosslinking points between the polymer chains, they introduced a moving crosslink. The crosslink acts as a pulley, and is able to homogenize the tension along the chains of the network.

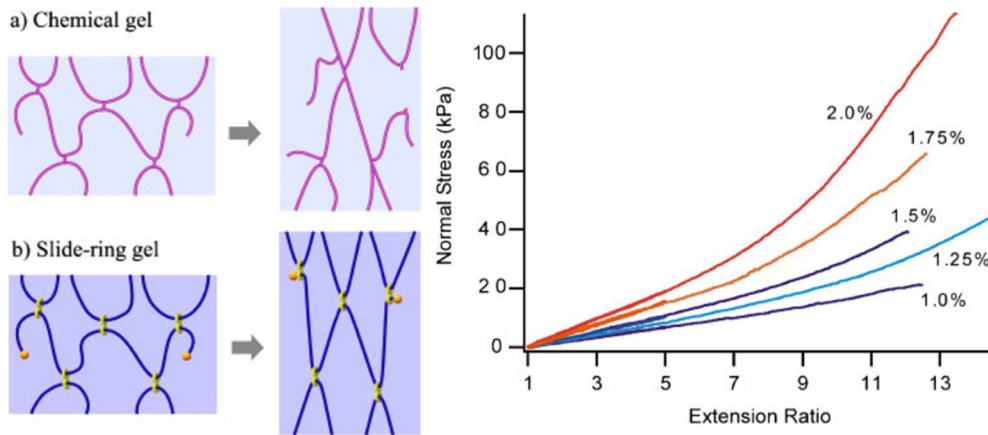


Figure 1.5: Left: Schematic comparison between chemical and slide-ring gels. Right: Stress-strain curve of the slide-ring gel with different concentrations of cross-linker. Figure reprinted from [18].

These gels show some resistance to fracture propagation, linked to the dynamic movement of those slide-rings when a fracture propagates.

1.3.2. Introducing an energy dissipation mechanism

a. Double network hydrogels

One example of dissipation mechanism is given by the “double-network” hydrogels developed by Gong and coworkers, in 2003 [21,22]. This material is based on inter-penetrated networks, with a first network of highly crosslinked polyelectrolytes poly(2-acrylamido-2-methylpropane sulfonic acid) which is diluted and stretched, and a second network of a concentrated and loosely crosslinked neutral polyacrylamide. In large deformations, the first network acts as a sacrificial network: being more stretched than the second network, it is the one storing the more energy during deformation. When it breaks, all the energy it was bearing is dissipated. The deformable second network keeps the integrity of the material by preventing the correlated fracture propagation in the first network. None of the mechanisms involved are of viscoelastic nature, which makes the material a strain-rate independent soft and tough hydrogel.

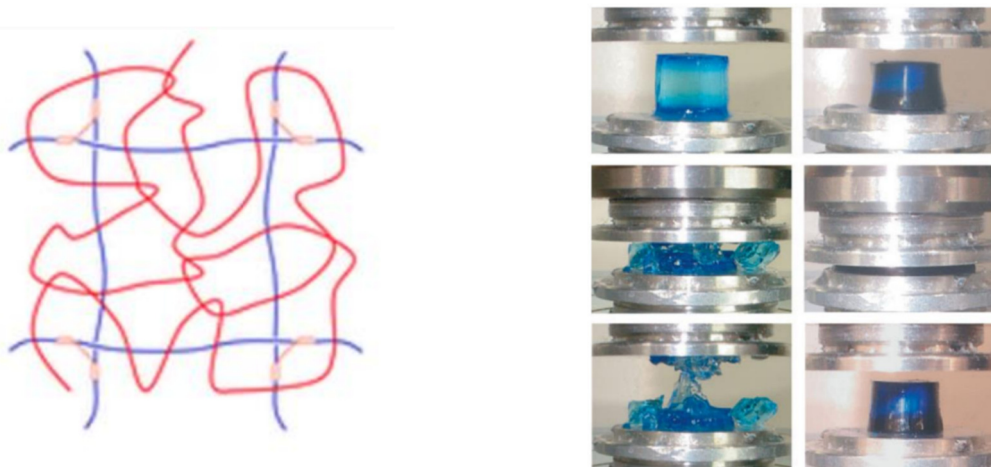


Figure 1.6: Left: Schematic representation of a double network hydrogel. Right: Mechanical resistance of a double network hydrogel under compression, compared to its fragile single network counterpart. Figure reprinted from [21].

1. From polymer physics to the toughening of hydrogels

This sequential synthesis method has been successfully applied to elastomers, with double, triple and quadruple networks [23]. Millereau et al. [24] showed that the mechanical properties of the so-called “multiple network” elastomers are directly dependent on the swelling (and thus the pre-stretch) of the first sacrificial network, and not on the number of networks used. Figure 1.7 shows very well this phenomenon: by normalizing the stress with the dilution of the filler network, and shifting the stretch by the initial elongation of this same network, it is possible to obtain a master curve of the behavior of a multiple network elastomer, independent on the number of networks used (1, 2, 3 or 4 here).

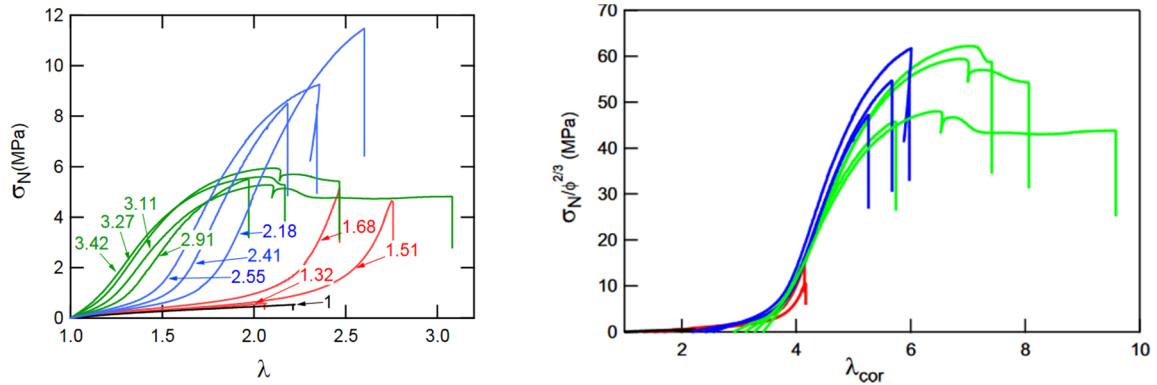


Figure 1.7: Left: Nominal stress as a function of the stretch for a single (black), double (red), triple (blue) and quadruple (green) network elastomer. The numbers represent the elongation of the filler network. Right: Nominal stress renormalized by the concentration of the filler network, versus the elongation of the filler network. Figure reprinted from [24].

b. Composite hydrogels

The double network previously presented can be seen as composite materials, composed of a soft matrix filled with a hard and brittle network. ‘Classical’ composite hydrogels have been developed in the literature, with excellent fracture resistance properties. For example, silica nanoparticles have been introduced in a poly(N,N-dimethylacrylamide) network [25,26]. By increasing the amount of nanoparticles, it is possible to increase dramatically the stiffness, strength and the toughness of the material.

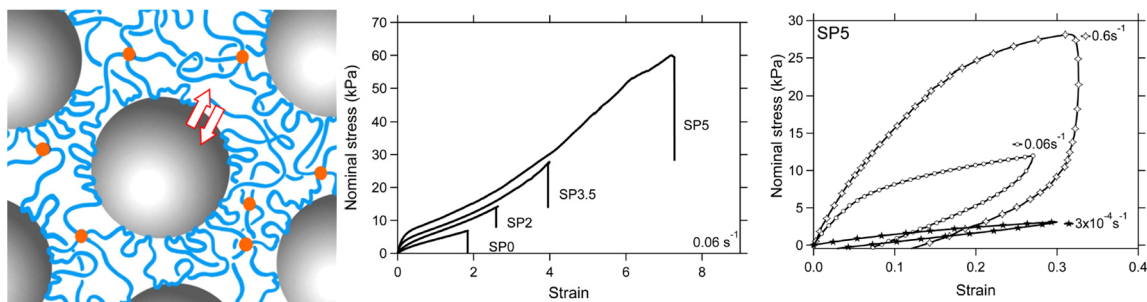


Figure 1.8: Left: Schematic representation of hybrid hydrogels combining covalent crosslinks (orange) and physical interactions sketched by polymer chains absorbed onto the surface of silica nanoparticles. Center: Strain rate effect on hysteresis of hybrid hydrogels. Right: Tensile stress-strain curves with for hydrogels with different silica contents. Figure reprinted from [25].

In this loosely crosslinked hydrogel, the polymer chains are adsorbed on the surface of the silica nanoparticles. This adsorption process is reversible and consequently possesses a definite dynamic of sorption and desorption. The resulting hydrogels show then a clear visco-elastic behavior, with energy

dissipation and recovery processes. When stretching the hydrogel, this reversible bonding of the polymer on the surface of the nanoparticle will provoke energy dissipation, toughening the hydrogel.

c. Ionically crosslinked

Another mechanism of dissipation used in the literature is based on ionic interactions between a polyelectrolyte, and oppositely charged ions in the solution. This creates dynamic physical bonds. The mechanism of energy dissipation is reversible here, and the material can be self-healing.

A well-known example of this particular bond is the PAAm/Alginate network developed by Suo and coworkers [27]. The polyacrylamide network is covalently crosslinked, and serves as a ‘frame’ of the material, onto which is branched a secondary, physically crosslinked network of alginate and Ca^{2+} ions (Figure 1.9). This second network forms a special “zip” structure by physical ionic bonds, which is the key point of the reinforcing mechanism. The unzipping of the crosslinks causes a dissipation of energy, which is reversible by “re-zipping”. The stretch-at-break of such a hydrogel can reach 21 (Figure 1.10), with fracture energies up to 3000 J/m^2 .

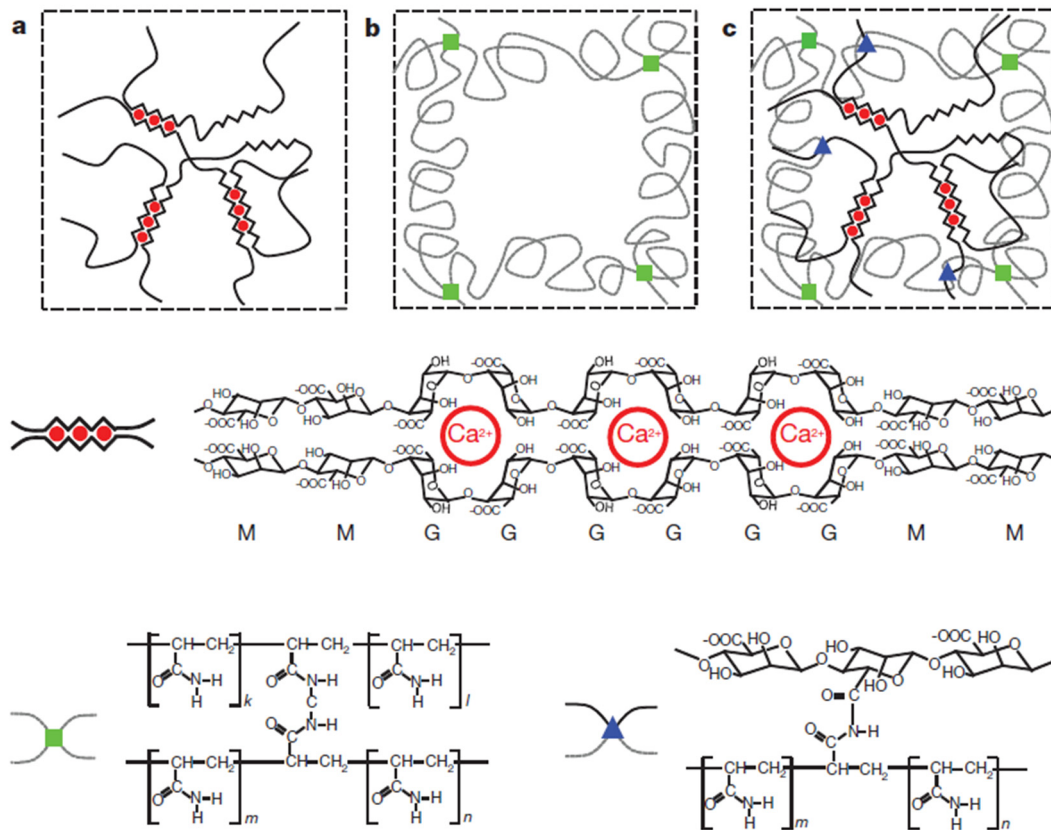


Figure 1.9: Schematics of three types of hydrogel. **a**, In an alginate gel, the G blocks on different polymer chains form ionic crosslinks through Ca^{2+} (red circles). **b**, In a polyacrylamide gel, the polymer chains form covalent crosslinks through N,N-methylenebisacrylamide (MBAA; green squares). **c**, In an alginate–polyacrylamide hybrid gel, the two types of polymer network are intertwined, and joined by covalent crosslinks (blue triangles) between amine groups on polyacrylamide chains and carboxyl groups on alginate chains. Figure reprinted from [27].

1. From polymer physics to the toughening of hydrogels

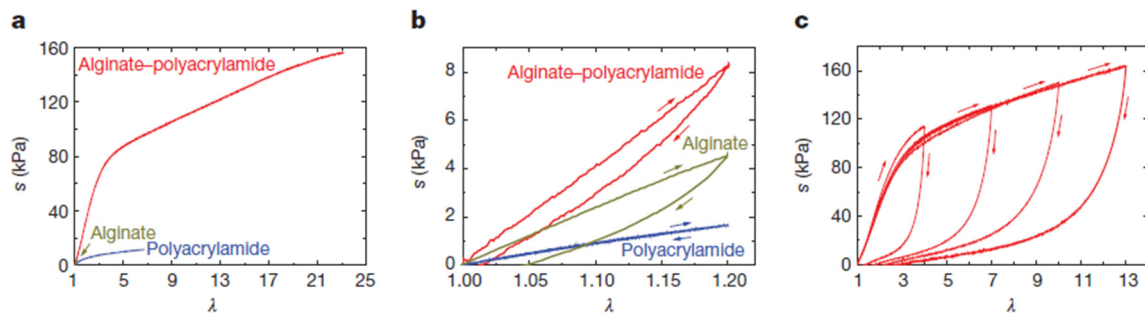


Figure 1.10: Mechanical tests under various conditions. *a*, Stress–stretch curves of the three types of gel, each stretched to rupture. The nominal stress, s , is defined as the force applied on the deformed gel, divided by the cross-sectional area of the undeformed gel. *b*, The gels were each loaded to a stretch of 1.2, just below the value that would rupture the alginate gel, and were then unloaded. *c*, Samples of the hybrid gel were subjected to a cycle of loading and unloading of varying maximum stretch. Figure reprinted from [27].

1.4. Using dynamic coordination crosslinks

Coordination complexes have been widely used in the literature as a very versatile physical bond, as we will now see. Its dynamic is simply controlled by the kinetics of association and dissociation of the coordination complex.

These coordination crosslinks are found in nature, particularly in the mussel byssus (the organ with which the mussel attaches to a surface), where catechol functions create coordination crosslinks with Fe^{3+} ions, which reinforces the byssus. Holten-Andersen *et al.* [28] have shown that this bond can be integrated in a synthetic model polymer solution, creating a viscoelastic solution with high energy dissipation and a characteristic dynamic. This idea has been applied to multiple types of complexes, in polymer solutions and polymer networks.

1.4.1. Transient networks with versatile dynamics

a. ‘Simple’ model transient networks

Histidine, an amino acid, has been widely used as a physical crosslinker for its ligand role. In particular, Grindy *et al.* [29,30] showed the versatility of this ligand by grafting it at the end of the arms of a tetra-PEG network. These PEG-histidine monomers are then mixed with a solution of metal ions, creating physical coordination crosslinks. The dynamics of the network is simply controlled by the ratio of metallic ion to histidine.

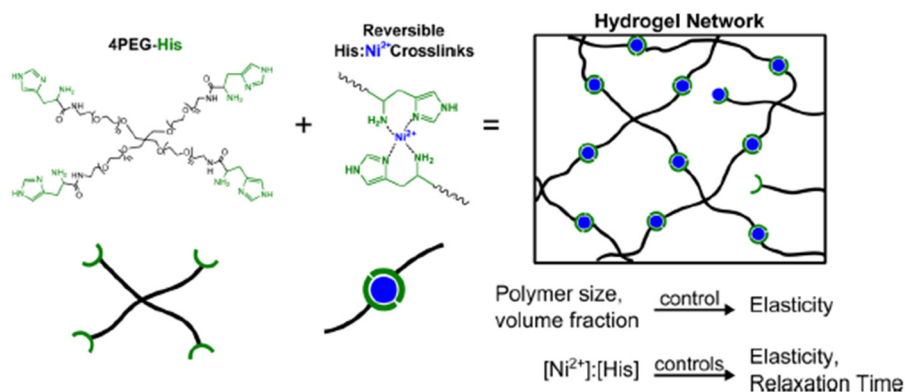


Figure 1.11: The model system is composed of 4-arm poly(ethylene glycol); the end of each arm is functionalized with an N-terminal histidine residue (4PEG-His). The hydrogels are synthesized by mixing a pH 7.4-buffered 4PEG-His solution with aqueous Ni^{2+} ions. Figure reprinted from [29].

By changing the metallic ion, the behavior of the network changes, depending on the stability of the ion used. Figure 1.12 shows the storage and loss moduli of these networks with two different metal ions, Ni^{2+} and Zn^{2+} , in varied quantities. The storage modulus increases with the frequency, as is expected for a dynamic network. More interestingly, when looking at the loss modulus, two frequencies are found and the intensity of each contribution follows the concentration in its metal ion (the fast contribution being related to Zn^{2+} , the slow to Ni^{2+}).

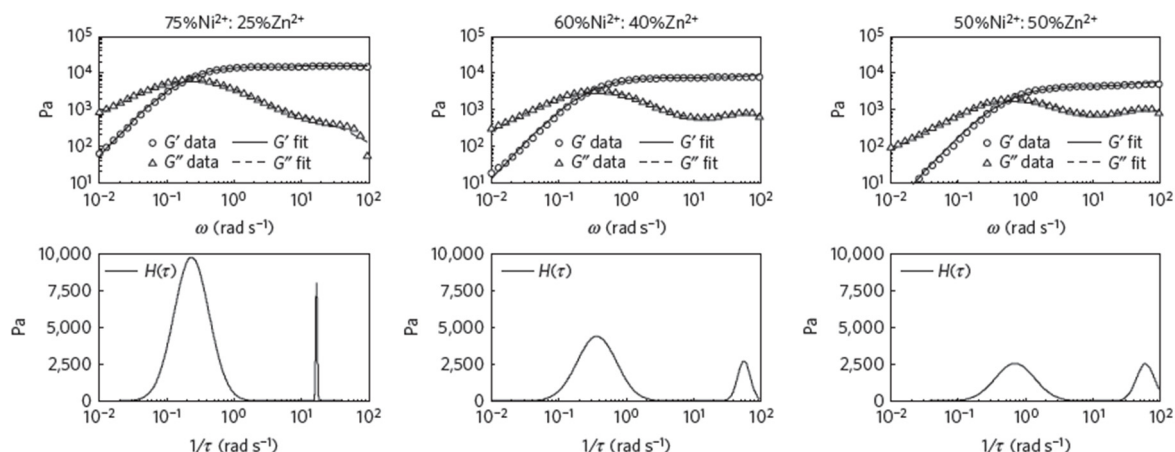


Figure 1.12: By varying the relative amounts of Ni^{2+} and Zn^{2+} , it is possible to control the active crosslinks within the hybrid gel network and thereby modulate the relative magnitudes of their corresponding energy dissipation modes. The moduli are fitted with a relaxation spectra $H(\tau)$, as seen in the lower part of each figure. Figure reprinted from [30].

Another example of ligand is terpyridine. This ligand creates much more stable bonds than the histidine ligand, and its properties have been widely studied in the literature [31]. Its complexes with ions such as Ru^{2+} [32], Zn^{2+} or Co^{2+} [33] have been used successfully as physical crosslinker in networks and hydrogels.

For example, Rossow and Seiffert [34] developed a network made of 4-arms star-shaped PEG, end-capped with terpyridine, with metallic ions in the solution. This network is very similar to the one previously mentioned, but allows for the study of a different range of dynamics, as exhibited on Figure 1.13. The loss modulus G'' shows a peak around the characteristic frequency of bond dissociation. This peak is shifted when the ion is changed. The storage modulus G' increases up to a plateau at high

1. From polymer physics to the toughening of hydrogels

frequencies, which value depends on the number of physical bonds introduced in the network. At low frequencies compared to the characteristic frequency of the physical bond, the material behaves as a solution and flows. This demonstrates the existence of two limit behaviors:

- at low frequencies compared to the dissociation frequency of the physical bond, the physical crosslinks break, and the network viscously flows;
- at high frequencies compared to the dissociation frequency of the physical bond, the physical crosslinks are closed and behave similarly than permanent crosslinks and the network behaves as an elastic solid.

The characteristic relaxation time of the hydrogel is directly defined by the dissociation kinetics of the M^{2+} -terpyridine bond.

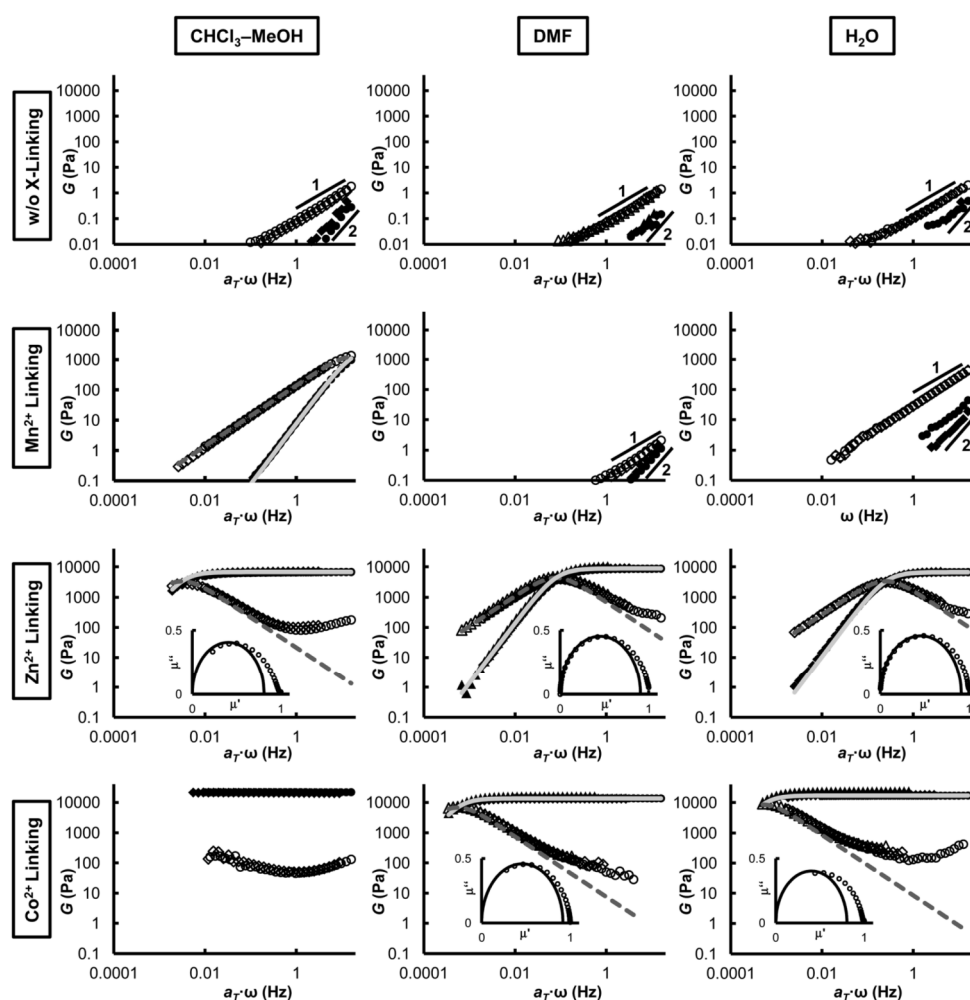


Figure 1.13: Rheology data of 200 g/L semidilute solutions and supramolecular gels of tetra-arm PEG-terpyridine that can transiently associate through different metal ions such as Mn^{2+} , Zn^{2+} , or Co^{2+} , as denoted by the left-side labeling, in chloroform–methanol (1:1), DMF, or water, as denoted by the top labeling. All plots show the elastic (full symbols, G') and viscous (open symbols, G'') parts of the complex shear modulus, G , as a function of the test frequency, ω . Figure reprinted from [34].

The study of this structure by DLS also shows a potential clustering of physical bonds, an unexpected heterogeneity that tends to stiffen the network.

b. Combination of coordination bonds with other bonds, to enhance the properties of the material

The physical bonds made of coordination complexes with terpyridine ligands have also been integrated in a chemically crosslinked network, using 4-arms star-shaped PEGs and linear PEGs with pendent terpyridine moieties, as shown on Figure 1.14 [35].

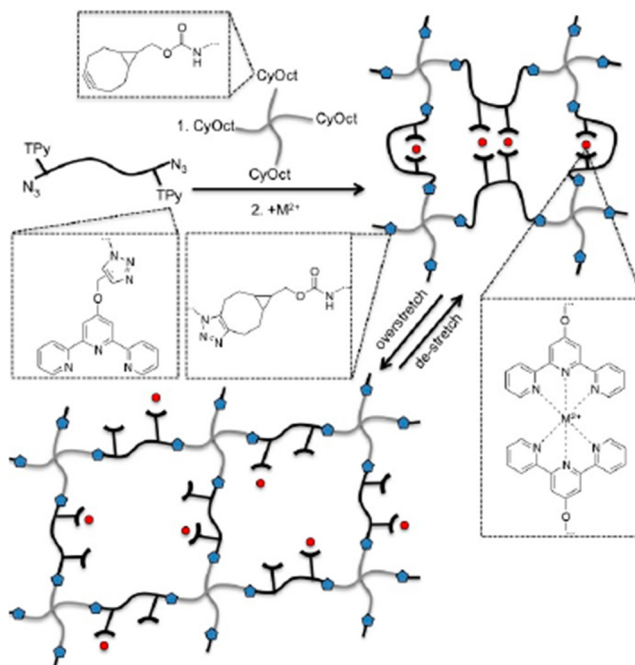


Figure 1.14: this purpose, linear poly(ethylene glycol) (PEG) is functionalized with both azide (N₃) and terpyridine (TPy) moieties at each end, and tetra-arm PEG is functionalized with cyclooctynes (CyOct) capped to each arm. Gelation occurs by strain-promoted azide–alkyne cycloaddition forming triazole-linking units sketched as blue pentagons in the schematic. Addition of metal(II) ions, sketched as red circles in the schematic, leads to formation of physical crosslinks. Figure reprinted from [35].

When adding chemical crosslinks into such a network, one prevents the polymer chains from flowing. Hence, the behavior at comparatively low frequencies of the network changes. It does not behave as a flowing polymer solution, but as a purely elastic chemical network, with no physical bonds. Those physical bonds are still invisible at these low frequencies.

In Figure 1.15 [36,37], the authors have used the same chemical network with a variety of metal ions, showing how the dynamics of the network change. Ni²⁺ and Co²⁺ create physical bonds with slow dynamics and hydrogels that behave as highly crosslinked elastic gels at the frequencies observed. Mn²⁺ creates bonds with fast dynamics, and the bonds are invisible at the frequencies observed – the storage and loss moduli of such a gel are almost identical to the moduli of the equivalent chemical gel. Only hydrogels with Zn²⁺ ions show a clear dynamic behavior, with a peak of loss modulus around 20 rad/s.

1. From polymer physics to the toughening of hydrogels

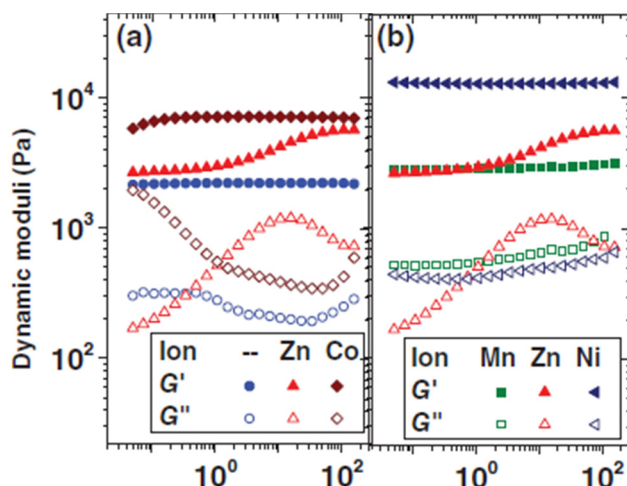


Figure 1.15: Dynamic moduli of the dually crosslinked networks in presence of different metal ions at a representative temperature of 25°C. Figure reprinted from [36].

Brassine et al. [38,39] developed a somewhat less conventional combination of coordination bonds and hydrophobic sticker associations. The hydrogel they prepared possesses two very distinct relaxations (Figure 1.16). The faster relaxation corresponds to the dissociation of the micro-domains of hydrophobic stickers, and its characteristic dissociation time (or strain) can be shifted by changing the length of the hydrophobic stickers. The slower dissociation is related to the terpyridine- M^{2+} complexes, and can be shifted by changing the metallic ion. A very interesting conclusion of this study is that both dynamics are completely independent from one another. Each can be selectively tuned by well-chosen external stimuli (adding an organic solvent for the hydrophobic dynamic, changing the pH for the coordination dynamic).

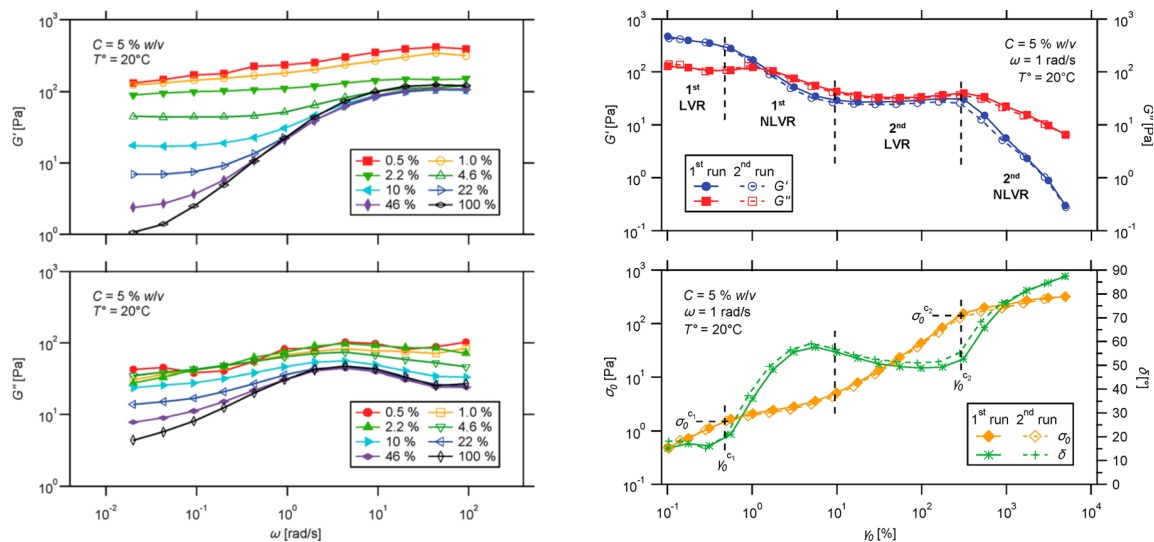


Figure 1.16: *Left*: Evolution of elastic and viscous moduli of a supramolecular hydrogel prepared from the PS27-*b*-PNIPAAm235-*tpy* copolymer and Ni(II) ions, in frequency sweep at different strain amplitudes. *Right*: Amplitude strain sweeps on a supramolecular hydrogel prepared from the PS27-*b*-PNIPAAm235-*tpy* copolymer and Ni(II) ions: first run under increasing strain, second run under decreasing strain. Figure reprinted from [39].

Zhugue et al. [40] successfully applied this terpyridine- M^{2+} coordination bond to a system of entangled polymers (linear and star polymers with 4 arms). In the same way as with the hydrophobic interactions in a hydrogel, the physical bonds are here slower than the dynamics brought by the entanglements of

polymers. They delay the flow of polymer chains to even lower frequencies (Figure 1.17). The dynamics of the entanglements is otherwise unmodified by the presence of these physical bonds.

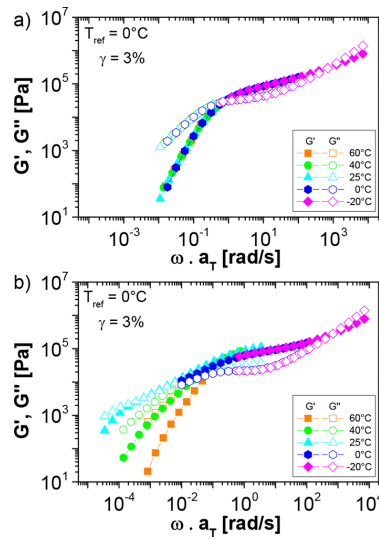


Figure 1.17: G' and G'' master curves for (a) entangled linear PnBA-tpy₂ (reference) and (b) linear entangled PnBA-tpy₂ + Co(II) at $T_{ref} = 0^\circ\text{C}$. The color of experimental curves indicates the temperature at which frequency sweeps in the linear regime are performed. Figure reprinted from [40].

c. Towards the formulation we will use in this project

Ozaki et al. [41] have studied a solution of poly(acrylamide-co-vinylimidazole), physically crosslinked with Ni^{2+} ions, by DLS, rheology and microrheology. The results show three different dynamics in the network:

- a fast dynamics, linked to the collective fluctuations of the polymer chains in the solution;
- an intermediate dynamics, linked to the macroscopic stress relaxation due to the dissociation of the physical crosslinks;
- a slow dynamics, attributed to the terminal flow of the polymer chains.

The intermediate dynamics characterizes the evolution of the lifetime of the physical bond with Ni^{2+} ions concentration, this time the lifetime of a ‘physical strand’ in the network. The strand becomes shorter when the concentration in physical crosslinks increase, and therefore its lifetime increases (Rubinstein and Semenov [42]).

In this manuscript, we will study a formulation very close to this one.

1. From polymer physics to the toughening of hydrogels

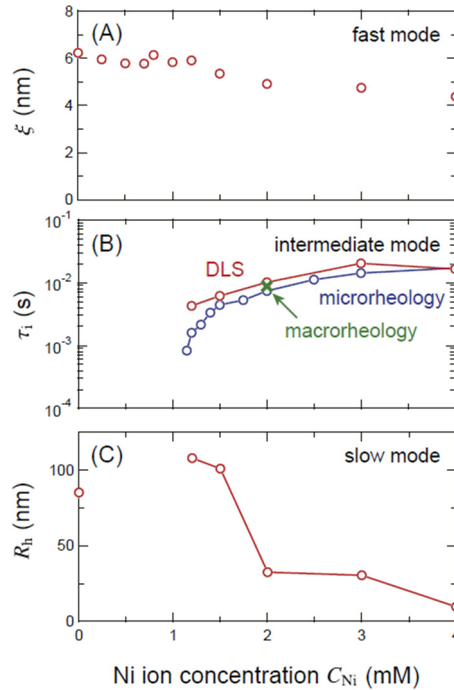


Figure 1.18 (A) Correlation length ξ estimated from the fast mode as a function of Ni ion concentration. (B) Relaxation time τ_i of the intermediate mode in the postgel regime ($1:1\text{mM} < C_{Ni}$). Relaxation times obtained by macrorheology (green) and microrheology (blue) are also plotted. (C) Hydrodynamic radius R_h estimated from the slow mode. Figure reprinted from [41].

1.4.2. Toughened gels

As previously mentioned, the strategy of using physical bonds made by interactions with cations has been widely explored in the literature. Ionic bonds between a negatively charged polymer and a positively charged ion or coordination complex are quite easy to introduce, and give a good mechanical reinforcement of the material.

Mayumi et al. [43,44] have demonstrated that a hydrogel made of chemically crosslinked poly(vinyl alcohol) chains shows a drastic increase in toughness when physical bonds (in the form of borate ions) are incorporated in the network. This hydrogel clearly exhibits a dynamic behavior in linear rheology, as shown in Figure 1.19, just as the hydrogels we have seen before. The dynamics of this gel is controlled by the dynamic covalent bond of the borate-diol reaction. The behavior of this gel at large deformations in uniaxial tensile tests is also shown in the same figure. The Young's modulus estimated from the initial slope of the stress stretch curves increases clearly with the stretch-rate, just as the storage modulus does in rheology. The stretch at break, on the contrary, decreases with the stretch-rate. From a critical stretch $\lambda_c = 5.5$ at a stretch-rate $\dot{\lambda} = 0.0001\text{ s}^{-1}$, the gel reaches only $\lambda_c = 1.5$ at $\dot{\lambda} = 0.9\text{ s}^{-1}$.

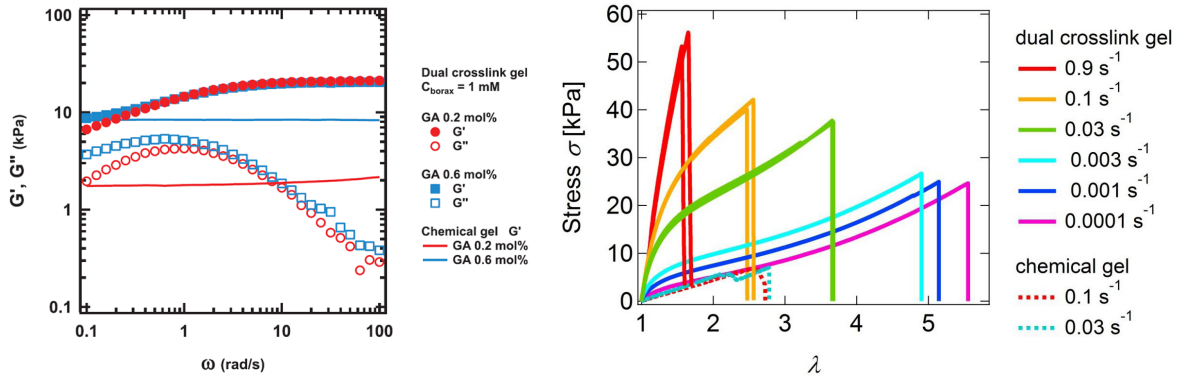


Figure 1.19: Left: Storage and loss moduli for two different compositions of a PVA-Borax hydrogel, with concentrations in chemical crosslinker of 0.2 or 0.6 mol%. Right: Stress versus stretch curves for un-notched chemical gels and dual-crosslink gels at different stretch rates, with crosslinker concentration of 0.2 mol%. Figure reprinted from [43].

This fragilization of the material can also be observed when looking at the energy needed to propagate a fracture in the material, which is the value Γ computed using Eq. 1.14. It decreases clearly with the stretch-rate, as seen on the left part of Figure 1.20. However, as previously mentioned, the formula is only valid for elastic materials, with no viscoelasticity. It has been applied to various polymeric materials displaying a viscoelastic behavior, but it is possible to refine it using a value Γ_{local} computed by taking into account the energy dissipated in the bulk of the material during loading. This dissipated energy is not available for the propagation of the crack, which makes Γ_{local} a more realistic measurement of the fracture energy.

As can be seen in Figure 1.20, Γ_{local} decreases until it reaches the same value as the pure chemical gel. At those high stretch-rates compared to the characteristic lifetime of the physical bond measured in rheology, the physical bonds behave as permanent bonds, and do not dissipate any energy. The energy needed to propagate the crack decreases then drastically.

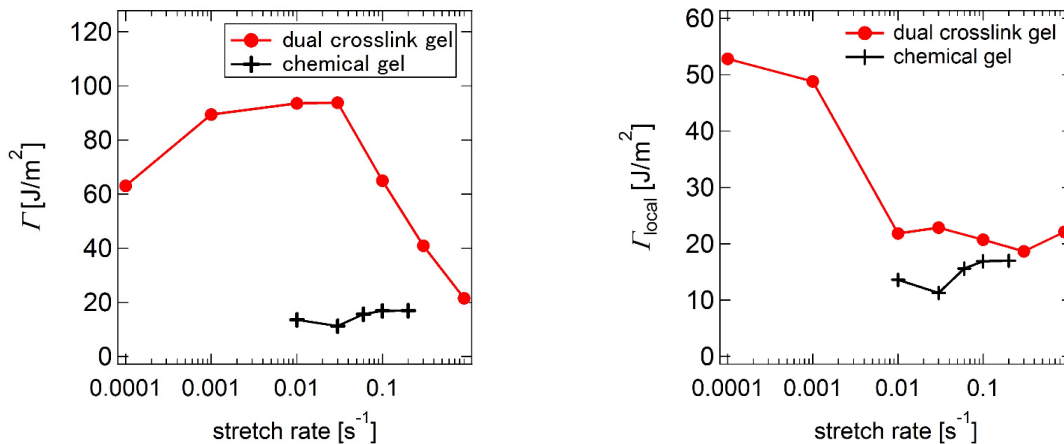


Figure 1.20: Fracture energy Γ (left) and true fracture energy Γ_{local} (right) as a function of the stretch-rate, for the dual-crosslink hydrogel (red) and the corresponding chemical gel (black). Figure reprinted from [43].

Craig and coworkers [45-47] realized some interesting studies on chemically crosslinked organogels, swollen in DMSO, with physical crosslinks by palladium and platinum-based pincers, with varying lifetimes. They show that incorporating the physical crosslinks in the material increases the strain-at-

1. From polymer physics to the toughening of hydrogels

break of the organogel only if the physical crosslink is fast enough (Figure 1.21). The slowest physical crosslinker increases the Young's modulus of the hydrogel, but decreases its strain at break. The other pincers, which create bonds with faster dynamics, have no visible influence on the mechanical properties of the organogel except for the increase in deformability. The strain at break increases, even with transient crosslinks that neither store nor dissipate measurable macroscopic stress in the network (under the conditions tested).

They suggest that the timescale of crack propagation is much more critical to fracture than the timescale of deformation, and that the fast physical bonds might help dilute the stresses in the network, hence avoiding stress concentrations that usually provoke the fracture of the material. A crucial conclusion of these works is that the mean lifetime of the physical bond controls the energy dissipation inside the dual-crosslink organogel.

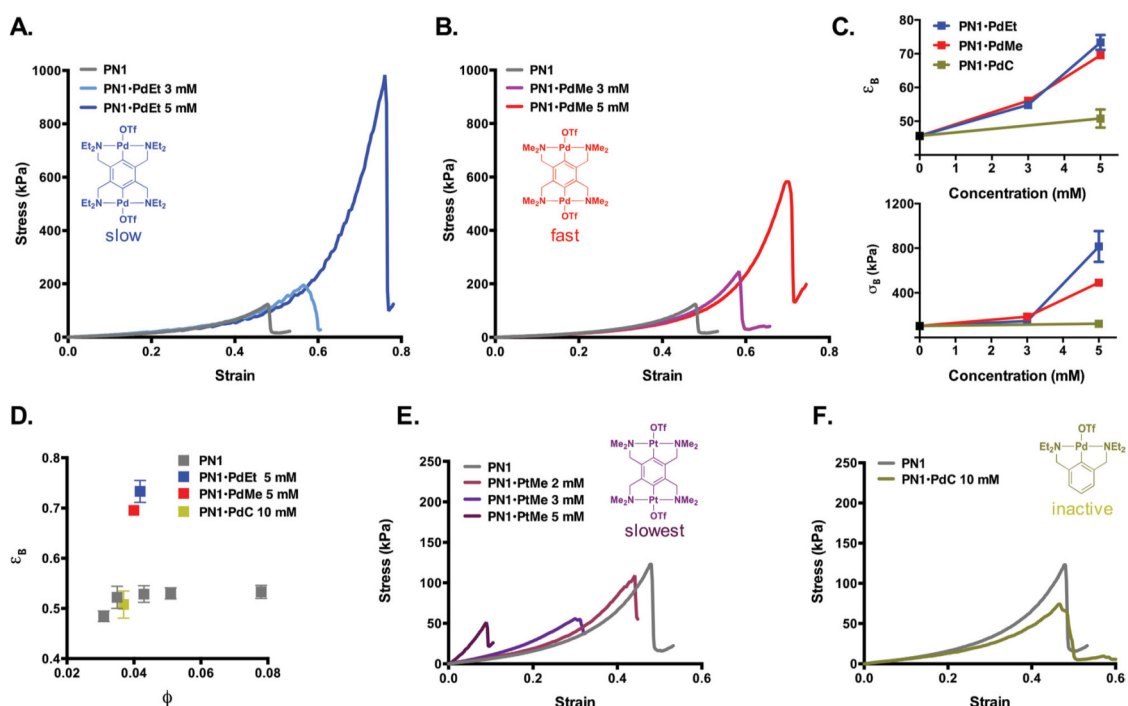


Figure 1.21: Compression testing of covalent (PNI) and hybrid (PNI·Pd) organogels: (a,b) Representative stress-strain behavior of PNI (grey), PNI·PdEt (blue), and PNI·PdMe (red) as a function of pincer concentration. (c) Monotonic increases in ϵ_B and σ_B of PNI network with increasing pincer concentration. (d) Strain at break (ϵ_B) vs. polymer volume fraction (ϕ) showing only minimal change in properties of PNI due to differential swelling. Error bars denote SEM, $n = 5$. (e) Stress-strain behavior of PNI·PtMe gels bearing the slowest dissociating cross-links. In contrast to the more transient pincers, samples become increasingly brittle with increased PtMe concentration. (f) Representative stress-strain curve showing the effect of added mechanically inactive control pincer PdC. Loading rate = $80 \mu\text{m}\cdot\text{s}^{-1}$, $T = 25^\circ\text{C}$. Figure reprinted from [47].

This range of fast dynamics has also been studied by J. Zhao during her PhD [48-50], on dual-crosslink hydrogels with transient coordination bonds. In this work, two dual-crosslink hydrogels with different dynamics were studied at a range of stretch-rates. It was shown that the resistance to fracture of those hydrogels increased with stretch-rate, contrary to what was observed for PVA-Borax dual crosslink hydrogels (Figure 1.22).

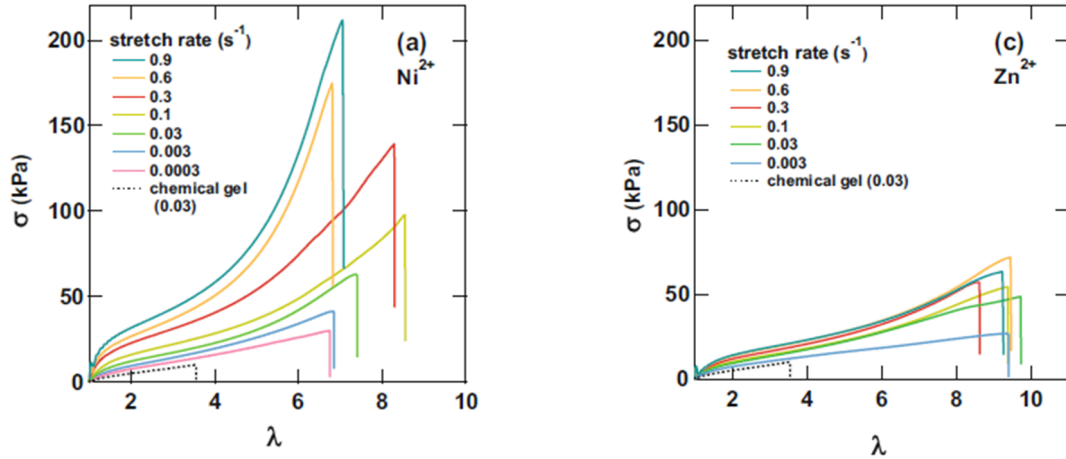


Figure 1.22: Stress-strain curves of P(AAm-co-VIm) dual crosslink gels with $[Ni^{2+}] = 100 \text{ mM}$ (left), $[Zn^{2+}] = 100 \text{ mM}$ (right). Figure reprinted from [48].

This difference in behavior was simply explained by the difference in the dissociation rate of the physical crosslinks. Each of the physical bonds studied has a characteristic dissociation rate, based on the chemistry involved in the bond. As Craig and coworkers mentioned, this dissociation rate (or lifetime of the physical bond) controls the energy dissipation inside the hydrogel. At stretch-rates lower than this characteristic dissociation frequency, the energy dissipation increases with the stretch-rate and the fracture resistance properties increase in turn. On the contrary, at stretch-rates higher than the characteristic dissociation rate of the physical bond, the energy dissipation decreases with the stretch-rate and the fracture resistance decreases. Figure 1.23 shows this idea, with the fracture energy Γ plotted as a function of the Weissenberg number $\lambda\tau_R$, with τ_R the lifetime of the physical bond measured in rheological experiments. The Weissenberg number represents the relative stretch-rate at which the experiment is done, compared to the characteristic dynamics of the physical bond measured in linear rheology. They observe an increase of the fracture properties with stretch-rate at low Weissenberg number, followed by a decrease when $\lambda\tau_R > 10^{-2}$.

However, the superposition is not clear at these intermediate Weissenberg number. The fracture energy of the Ni^{2+} dual-crosslink hydrogel does not seem to decrease or even reach a plateau, whereas for the PVA-borax dual-crosslink hydrogel it decreases sharply.

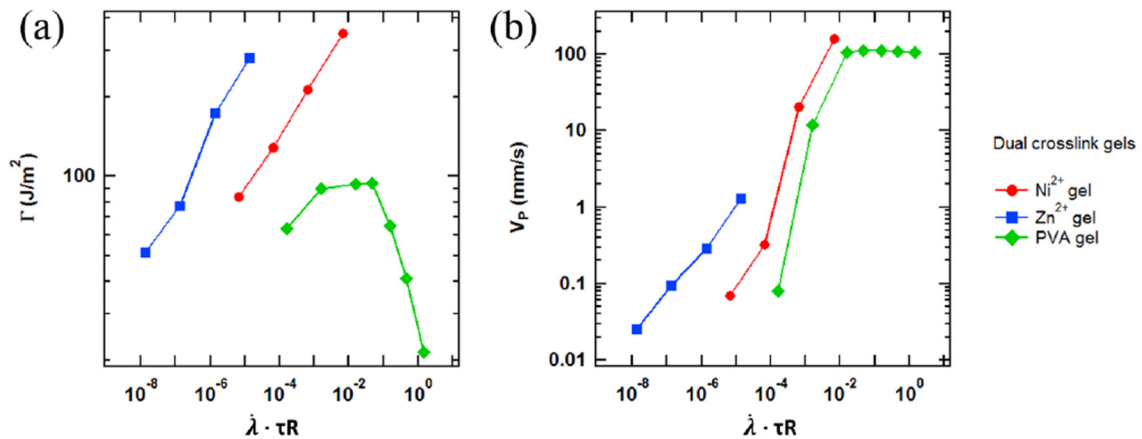


Figure 1.23: Fracture energy Γ (a) and crack propagation velocity V_P (b) as a function of $\lambda\tau_R$, for Ni^{2+} (red), Zn^{2+} (blue), and PVA-borax (green) dual crosslink gels. Figure reprinted from [48].

1. From polymer physics to the toughening of hydrogels

Even more recently, Zheng et al. [51,52] prepared a purely physically crosslinked hydrogel, with coordination bonds by acrylic acid moieties and Fe^{3+} ions. The properties of this hydrogel are very interesting, with a clear influence of the loading rate confirming the visco-elasticity of the material. The fracture energy Γ particularly shows a clear peak at a loading rate around 60 mm/min, corresponding to a relaxation time of ~ 5 s. However, this peak does not correspond to the frequency at which $\tan(\delta)$ of the material, measured in rheology, reaches a maximum. The authors explain this by the fact that the loading rate V_d/H they apply is different from the effective loading rate $V_d/\lambda H$. The material being stretched, the effective stretch-rate decreases during the experiment. Another explanation may be that during stretching, large stresses are applied to those physical crosslinks. This decreases the energy barrier to overcome in order to open the bond, and makes the lifetime of the physical bond shorter.

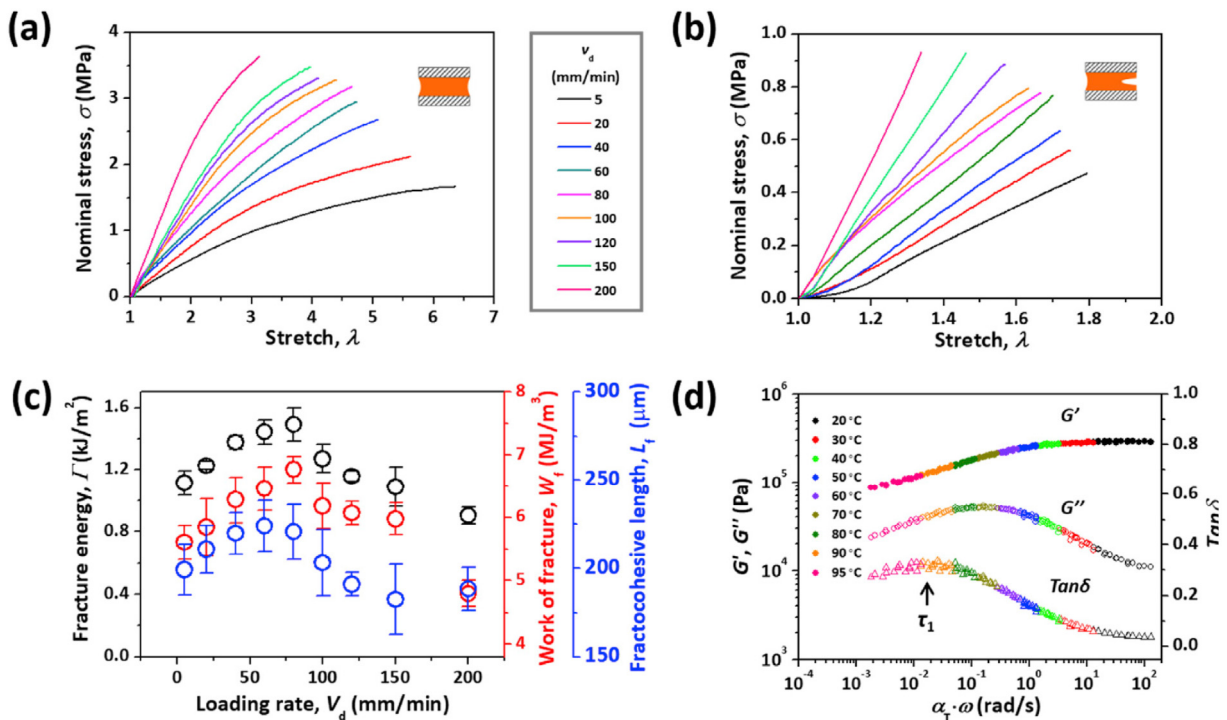


Figure 1.24 Nominal stress-stretch curves of (a) uncut and (b) cut gel samples with different loading rates, V_d . (c) Corresponding mechanical properties. $f_{AAc} = 10$ mol%; $c_0 \approx 5$ mm; $H = 5$ mm; $a_0 = 35$ mm. (d) Constructed master curves of storage modulus G' , loss modulus G'' and loss factor $\tan(\delta)$ of Fe^{3+} coordinated $P(\text{AAc-co-AAm})$ hydrogel ($f_{AAc} = 10$ mol%) via time-temperature superposition. Reference temperature $T_0 = 30$ °C. Figure reprinted from [52].

Finally, Chen et al. [54] recently studied a large range of dynamics of elastomers by tuning their Kuhn segment relaxation time, noted τ_0 . This was done very simply by varying the structure and composition of the acrylate monomers used for polymerization. In these materials, the dynamics are controlled by the entanglements of the network.

They observed a universal ductile-brittle transition of those elastomers with the criterion $\dot{\epsilon}\tau_0 = 0.1$ s $^{-1}$, regardless of the structure of the elastomer. The elastomers exhibit a peak in fracture energy at that criterion, followed by a clear decrease of properties when increasing the strain-rate. This transition is associated with the rubber-glass transition of the elastomers. It is interesting to note that, in this study, the authors showed that the relaxation time to take into account to create these master curves shown in Figure 1.25 was not the Rouse relaxation time τ_e but the Kuhn relaxation time $\tau_0 = \tau_e/N_e^2$ with N_e the number of Kuhn segments between entanglements.

The observation time at which the material exhibits the best fracture performances is 10 times larger than the Kuhn segment relaxation time, and 100 times lower than what can be extracted from the peak of $\tan(\delta)$.

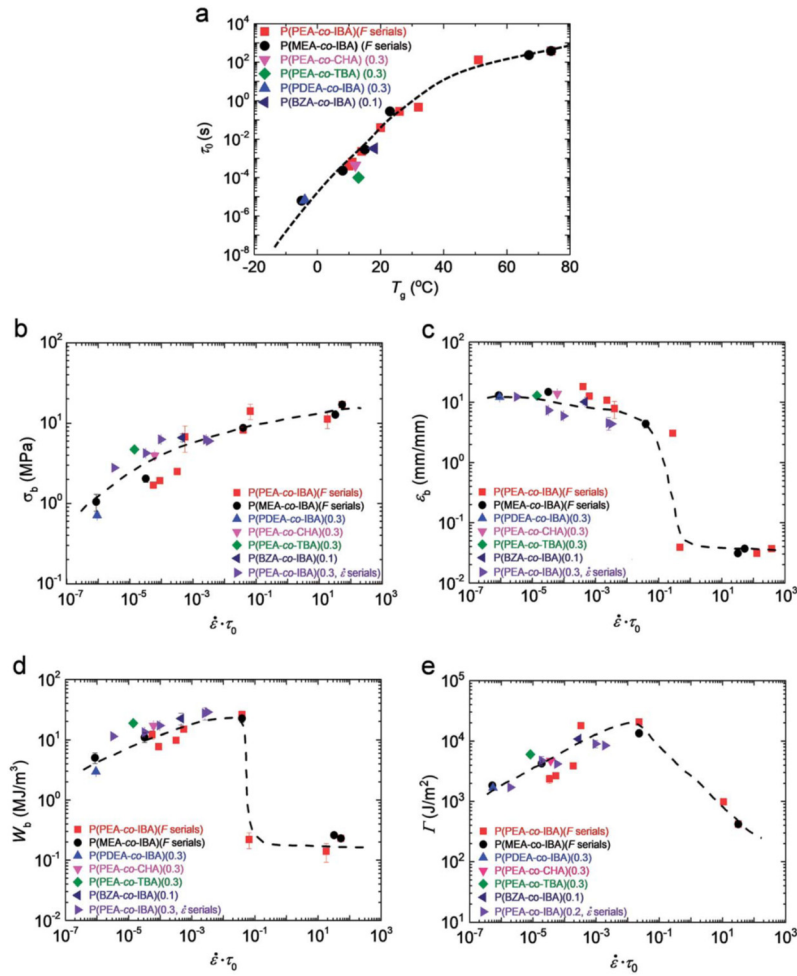


Figure 1.25: (a) Logarithmic plot of τ_0 and T_g . The dotted lines are a guide for the eye. (b–e) Master curves of mechanical performance versus $\dot{\epsilon} \cdot \tau_0$. (b) Fracture stress σ_b ; (c) fracture strain ϵ_b ; and (d) work of extension to fracture W_b , from the tensile test; (e) fracture energy Γ from the single-edge notch test. In all the graphs, different colors of the data plots show different compositions of elastomers. Figure reprinted from [54].

1.5. Objectives of this project

Different promising approaches have been developed in the literature to increase the mechanical properties of hydrogels. In particular, the introduction of transient physical crosslinks, with a finite lifetime, in a chemically crosslinked network, gives tougher materials, with properties that depend strongly on the lifetime of this physical bond. The work of this project will focus on the dual-crosslink hydrogels based on coordination complexes developed by J. Zhao [48-50]. Those hydrogels present some limitations in their preparation that we will have to overcome first, before studying their properties further. Hence, the objectives of this PhD project are multiple:

- To develop a new and more versatile strategy to prepare in a repeatable manner those dual-crosslink hydrogels, with tunable dynamics of the physical crosslinks. The characteristic time of the physical bonds will be tuned by changing the metallic ion, and it should not ideally modify the other properties of the network. We will explore a wide range of characteristic lifetimes (three groups, fast, slow and intermediate will be tested);
- To study the evolution of the mechanical properties of this dual-crosslink hydrogel with a wide range of deformation rates, and with the change in dynamics brought by changing the metallic ion;
- To examine the hypothesis of universality of the linear and nonlinear mechanical properties in terms of the Weissenberg number, the product of the deformation rate and the characteristic relaxation time of the dual crosslink hydrogels. By changing both deformation rate and characteristic time, the accessible range for the Weissenberg number is large;
- To investigate the fracture properties of the dual crosslink gels in a broad range of Weissenberg numbers. We will correlate the properties in fracture with the viscoelastic energy dissipation within the material;
- To explain the molecular mechanism of toughening of a chemical network by transient bonds. In particular, we will closely examine the fracture mechanics at low stretch rates and/or with fast dynamics, corresponding to the conditions where the dual crosslink gels are supposed to exhibit no visible energy dissipation but still an increase in toughness;
- Finally, to verify these molecular mechanisms, by incorporating mechanophores in the network. These molecules (that will be described later in this manuscript) emit a light or become fluorescent upon breaking, which allows a mapping of the damage inside the material. This mapping should allow us to understand how physical bonds prevent chemical bond breakage in the material.

We will try to answer these questions in this manuscript, which is organized in seven Chapters.

After this introductory Chapter 1, we will describe in Chapter 2 the preparation of a standard dual-crosslink hydrogel with Ni^{2+} ions. We will study its dynamics by two different methods and try to build a picture of its microstructure.

Fracture of dual-crosslink dynamic hydrogels: from molecular interactions to fracture energy

In Chapter 3, we will study the mechanical properties in large deformations of this Ni²⁺ dual-crosslink hydrogel and its properties of fracture resistance as a function of the deformation rate.

In Chapter 4, we will show that by simply changing the metallic ion used, the dynamics and the mechanical properties of the dual-crosslink hydrogel can be modified. Using Zn²⁺ or Cu²⁺ ions, we will create dual-crosslink hydrogels with faster dynamics. These hydrogels will prove to be softer and more fragile than the Ni²⁺ dual-crosslink hydrogel.

In Chapter 5, we will investigate the mechanical and fracture properties of a dual-crosslink hydrogel with even slower dynamics than the Ni²⁺ dual-crosslink hydrogel, by changing the ligand instead of the metallic ion.

In Chapter 6, we will try to unify the results from the three different types of dual-crosslink hydrogels, by observing our data as a function of the Weissenberg number, multiplication of the stretch-rate by the lifetime of the physical bond we introduced.

Finally, in Chapter 7, we will show some first results on the introduction of mechanophores into the chemical network of the dual-crosslink hydrogel. Two different mechanophores will be tested.

References

1. Rubinstein, M. & Colby, R. H. *Polymer Physics*. (Oxford University Press, 2003).
2. Oesterhelt, F., Rief, M. & Gaub, H. E. Single molecule force spectroscopy by AFM indicates helical structure of poly(ethylene-glycol) in water. *New J. Phys.* 1, 6–6 (1999).
3. Treloar, L. R. G. *The Physics of Rubber Elasticity*. (Oxford University Press, USA, 1975).
4. Mooney, M. A Theory of Large Elastic Deformation. *Journal of Applied Physics* 11, 582–592 (1940).
5. Rivlin, R. S. Large elastic deformations of isotropic materials. *Philosophical Transactions of the Royal Society of London. Series A, Mathematical and Physical Sciences* 240, 459–490 (1948).
6. Creton, C. & Ciccotti, M. Fracture and adhesion of soft materials: a review. *Reports on Progress in Physics* 79, 046601 (2016).
7. Griffith, A. A. The phenomena of rupture and flow in solids. *Philosophical Transactions of the Royal Society of London. Series A, Containing Papers of a Mathematical or Physical Character* 221, 163–198 (1921).
8. G. R. Irwin, Analysis of Stresses and Strains near the End of a Crack Traversing a Plate. *Journal of Applied Mechanics* 24, 351-369 (1957).
9. Greensmith, H. W. Rupture of rubber. X. The change in stored energy on making a small cut in a test piece held in simple extension. *Journal of Applied Polymer Science* 7, 993–1002 (1963).
10. A. N. Gent, J. Schultz, Effect of Wetting Liquids on the Strength of Adhesion of Viscoelastic Material. *The Journal of Adhesion* 3, 281-294 (1972).
11. A. N. Gent, Adhesion and Strength of Viscoelastic Solids. Is There a Relationship between Adhesion and Bulk Properties? *Langmuir* 12, 4492-4496 (1996).
12. Lake, G. J. & Thomas, A. G. The strength of highly elastic materials. *Proceedings of the Royal Society of London. Series A. Mathematical and Physical Sciences* 300, 108–119 (1967).
13. Wang, S., Panyukov, S., Rubinstein, M. & Craig, S. L. Quantitative Adjustment to the Molecular Energy Parameter in the Lake–Thomas Theory of Polymer Fracture Energy. *Macromolecules* 52, 2772–2777 (2019).
14. Sakai, T. et al. Design and Fabrication of a High-Strength Hydrogel with Ideally Homogeneous Network Structure from Tetrahedron-like Macromonomers. *Macromolecules* 41, 5379–5384 (2008).
15. Yamaguchi, T., Onoue, Y. & Sawae, Y. Topology and Toughening of Sparse Elastic Networks. *Phys. Rev. Lett.* 124, 068002 (2020).
16. Okumura, Y. & Ito, K. The Polyrotaxane Gel: A Topological Gel by Figure-of-Eight Cross-links. *Advanced Materials* 13, 485–487 (2001).
17. Ito, K. Novel Cross-Linking Concept of Polymer Network: Synthesis, Structure, and Properties of Slide-Ring Gels with Freely Movable Junctions. *Polymer Journal* 39, 489–499 (2007).
18. Mayumi, K. & Ito, K. Structure and dynamics of polyrotaxane and slide-ring materials. *Polymer* 51, 959–967 (2010).
19. Mayumi, K., Tezuka, M., Bando, A. & Ito, K. Mechanics of slide-ring gels: novel entropic elasticity of a topological network formed by ring and string. *Soft Matter* 8, 8179 (2012).
20. Liu, C., Kadono, H., Yokoyama, H., Mayumi, K. & Ito, K. Crack propagation resistance of slide-ring gels. *Polymer* 181, 121782 (2019).

21. Gong, J. P., Katsuyama, Y., Kurokawa, T. & Osada, Y. Double-Network Hydrogels with Extremely High Mechanical Strength. *Adv. Mater.* 15, 1155–1158 (2003).
22. Gong, J. P. Why are double network hydrogels so tough? *Soft Matter* 6, 2583–2590 (2010).
23. Ducrot, E., Chen, Y., Bulters, M., Sijbesma, R. P. & Creton, C. Toughening Elastomers with Sacrificial Bonds and Watching Them Break. *Science* 344, 186–189 (2014).
24. Millereau, P. et al. Mechanics of elastomeric molecular composites. *PNAS* 115, 9110–9115 (2018).
25. Lin, W.-C., Fan, W., Marcellan, A., Hourdet, D. & Creton, C. Large Strain and Fracture Properties of Poly(dimethylacrylamide)/Silica Hybrid Hydrogels. *Macromolecules* 43, 2554–2563 (2010).
26. Rose, S., Dizeux, A., Narita, T., Hourdet, D. & Marcellan, A. Time Dependence of Dissipative and Recovery Processes in Nanohybrid Hydrogels. *Macromolecules* 46, 4095–4104 (2013).
27. Suo, Z. et al. Highly stretchable and tough hydrogels. *Nature* 489, 133–136 (2012).
28. Holten-Andersen, N. et al. pH-induced metal-ligand cross-links inspired by mussel yield self-healing polymer networks with near-covalent elastic moduli. *PNAS* 108, 2651–2655 (2011).
29. Grindy, S. C. et al. Control of hierarchical polymer mechanics with bioinspired metal-coordination dynamics. *Nature Materials* 14, 1210 (2015).
30. Grindy, S. C., Lenz, M. & Holten-Andersen, N. Engineering Elasticity and Relaxation Time in Metal-Coordinate Cross-Linked Hydrogels. *Macromolecules* 49, 8306–8312 (2016).
31. Schubert, U. S. & Eschbaumer, C. Macromolecules Containing Bipyridine and Terpyridine Metal Complexes: Towards Metallosupramolecular Polymers. *Angewandte Chemie International Edition* 41, 2892–2926 (2002).
32. Aamer, K. A. & Tew, G. N. Supramolecular Polymers Containing Terpyridine–Metal Complexes in the Side Chain. *Macromolecules* 40, 2737–2744 (2007).
33. Xu, X., Jerca, F. A., Jerca, V. V. & Hoogenboom, R. Self-Healing and Moldable Poly(2-isopropenyl-2-oxazoline) Supramolecular Hydrogels Based on a Transient Metal Coordination Network. *Macromolecules* (2020) doi:10.1021/acs.macromol.0c01242.
34. Rossow, T. & Seiffert, S. Supramolecular polymer gels with potential model-network structure. *Polymer Chemistry* 5, 3018 (2014).
35. Czarnecki, S., Rossow, T. & Seiffert, S. Hybrid Polymer-Network Hydrogels with Tunable Mechanical Response. *Polymers* 8, 82 (2016).
36. Ahmadi, M. & Seiffert, S. Dynamic Model Metallo-Supramolecular Dual-Network Hydrogels with Independently Tunable Network Crosslinks. *Journal of Polymer Science* 58, 330–342 (2020).
37. Ahmadi, M. & Seiffert, S. Thermodynamic control over energy dissipation modes in dual-network hydrogels based on metal–ligand coordination. *Soft Matter* 16, 2332–2341 (2020).
38. Brassinne, J., Cadix, A., Wilson, J. & van Ruymbeke, E. Dissociating sticker dynamics from chain relaxation in supramolecular polymer networks—The importance of free partner! *Journal of Rheology* 61, 1123–1134 (2017).
39. Brassinne, J., Gohy, J.-F. & Fustin, C.-A. Orthogonal Control of the Dynamics of Supramolecular Gels from Heterotelechelic Associating Polymers. *ACS Macro Lett.* 5, 1364–1368 (2016).

1. From polymer physics to the toughening of hydrogels

40. Zhuge, F., Brassinne, J., Fustin, C.-A., van Ruymbeke, E. & Gohy, J.-F. Synthesis and Rheology of Bulk Metallo-Supramolecular Polymers from Telechelic Entangled Precursors. *Macromolecules* 50, 5165–5175 (2017).
41. Ozaki, H., Indei, T., Koga, T. & Narita, T. Physical gelation of supramolecular hydrogels cross-linked by metal-ligand interactions: Dynamic light scattering and microrheological studies. *Polymer* 128, 363–372 (2017).
42. Rubinstein, M. & Semenov, A. N. Thermoreversible gelation in solutions of associating polymers. 2. Linear dynamics. *Macromolecules* 31, 1386–1397 (1998).
43. Mayumi, K., Guo, J., Narita, T., Hui, C. Y. & Creton, C. Fracture of dual crosslink gels with permanent and transient crosslinks. *Extreme Mechanics Letters* 6, 52–59 (2016).
44. Mayumi, K., Marcellan, A., Ducouret, G., Creton, C. & Narita, T. Stress–Strain Relationship of Highly Stretchable Dual Cross-Link Gels: Separability of Strain and Time Effect. *ACS Macro Lett.* 2, 1065–1068 (2013).
45. Yount, W. C., Loveless, D. M. & Craig, S. L. Strong Means Slow: Dynamic Contributions to the Bulk Mechanical Properties of Supramolecular Networks. *Angewandte Chemie International Edition* 44, 2746–2748 (2005).
46. Yount, W. C., Loveless, D. M. & Craig, S. L. Small-Molecule Dynamics and Mechanisms Underlying the Macroscopic Mechanical Properties of Coordinatively Cross-Linked Polymer Networks. *J. Am. Chem. Soc.* 127, 14488–14496 (2005).
47. Kean, Z. S. et al. Increasing the Maximum Achievable Strain of a Covalent Polymer Gel Through the Addition of Mechanically Invisible Cross-Links. *Advanced Materials* 26, 6013–6018 (2014).
48. Zhao, J. Structure et propriétés des hydrogels à réticulation chimique et physique. (PSL Research University, 2018).
49. Zhao, J., Mayumi, K., Creton, C. & Narita, T. Rheological properties of tough hydrogels based on an associating polymer with permanent and transient crosslinks: Effects of crosslinking density. *Journal of Rheology* 61, 1371–1383 (2017).
50. Zhao, J., Narita, T. & Creton, C. Dual Crosslink Hydrogels with Metal-Ligand Coordination Bonds: Tunable Dynamics and Mechanics Under Large Deformation. in *Self-Healing and Self-Recovering Hydrogels* (Springer International Publishing, 2020).
51. Zheng, S. Y. et al. Metal-Coordination Complexes Mediated Physical Hydrogels with High Toughness, Stick–Slip Tearing Behavior, and Good Processability. *Macromolecules* 49, 9637–9646 (2016).
52. Zheng, S. Y. et al. Fracture of tough and stiff metallosupramolecular hydrogels. *Materials Today Physics* 13, 100202 (2020).
53. Li, X., Yang, Q., Zhao, Y., Long, S. & Zheng, J. Dual physically crosslinked double network hydrogels with high toughness and self-healing properties. *Soft Matter* 13, 911–920 (2017).
54. Chen, L. et al. Facile synthesis of novel elastomers with tunable dynamics for toughness, self-healing and adhesion. *J. Mater. Chem. A* 7, 17334–17344 (2019).

Chapter 2

Preparation and microstructure of a dual-crosslink hydrogel

2. Preparation and microstructure of a dual-crosslink hydrogel

2. Preparation and microstructure of a dual-crosslink hydrogel

Table of contents

2.1. Gel synthesis.....	42
2.1.1. Synthesis of the P(AAm-co-VIm) chemical gel.....	42
2.1.2. Synthesis of the P(AAm-co-VIm)/M ²⁺ dual crosslink gels.....	43
2.2. Absorption of Ni²⁺ ions.....	46
2.2.1. Absorption kinetics of Ni ²⁺ ions.....	46
2.2.2. Influence of [NaCl]	47
2.2.3. Absorption isotherms – influence of [M ²⁺]	48
2.3. Stress-free dynamics – study by dynamic light scattering (DLS)	51
2.3.1. Dynamic Light Scattering – Principles and protocol.....	51
2.3.2. Results for a bare chemical gel.....	53
2.3.3. Results for a “One-pot” dual-crosslink gel.....	55
2.3.4. Conclusions	62
2.4. Linear mechanical behavior at small deformations	64
2.4.1. Rheology of a chemical gel	64
2.4.2. Rheology of a “One-Pot” dual-crosslink hydrogel.....	66
2.4.3. Comparing “One-pot” and “Diffusion” dual-crosslink hydrogels.....	68
2.4.4. Fitting with fractional model.....	69
2.4.5. Relaxation experiments	72
2.4.6. Conclusions	73
2.5. Small-Angle X-Ray scattering experiments	73
2.5.1. SAXS – Principle and protocol	73
2.5.2. Qualitative analysis	76
2.5.3. Attempt at quantitative analysis	79
2.5.4. Conclusions from X-ray scattering.....	85
2.6. Conclusion on microstructure and dynamics	85
References	87

2. Preparation and microstructure of a dual-crosslink hydrogel

Our objective is to incorporate, in an elastic material, a dynamic dissipative mechanism to toughen an otherwise fragile hydrogel. This mechanism of dissipation being dynamic, the energy dissipation inside the hydrogel should vary with the frequency or the stretch-rate at which it is being deformed. As a dissipative mechanism, we have chosen to introduce physical bonds in the form of coordination crosslinks. The polymer backbone will incorporate ligand moieties, and the solution of the hydrogel will contain metallic cations. Those ions will create coordination complexes with the ligands on the chains, thus creating physical crosslinks on the hydrogel. This technique should allow us to easily tune the dynamics of our dual-crosslink hydrogel, simply by changing the metal cation.

In this chapter, we will present a study of the preparation and microstructure of such a hydrogel, with Nickel(II) ions. We will first detail the synthesis of the hydrogel, and two methods of incorporation of the physical bonds: a “One-pot” method where the ions are incorporated before the synthesis of the polymer network, and a “Diffusion” method where they are incorporated afterwards.

This “Diffusion” method relying on the absorption of ions by the hydrogel, a study of the kinetics of this absorption will be conducted. To understand the dynamics of the dual-crosslink hydrogel, we will then present a set of dynamic light scattering measurements, to investigate the existence of characteristic relaxation times in our material. These relaxation times will be also measured in linear rheology, at small deformations. To complete the study of the microstructure of the hydrogel, a short series of X-Ray scattering experiments will be presented, to investigate the possible existence of characteristic length scales in our material.

2.1. Gel synthesis

2.1.1. Synthesis of the P(AAm-co-VIm) chemical gel

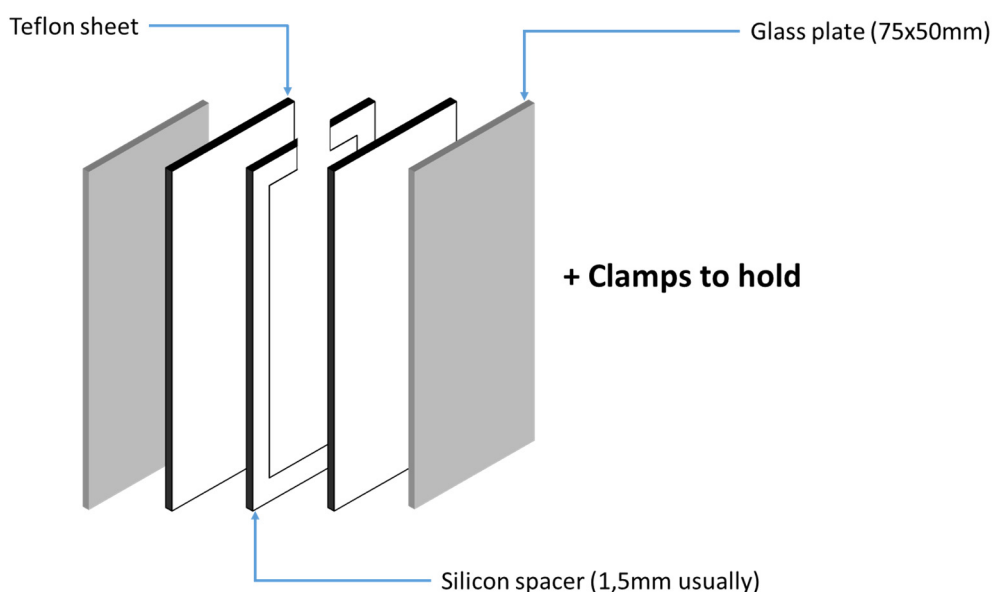
The synthesis of the P(AAm-co-VIm) chemical gel was performed by a conventional free radical polymerization. The polymer backbone, a copolymer of acrylamide (AAm) and vinyl-imidazole (VIm), was chemically crosslinked by methylene bis-acrylamide (MBA). As polymerization initiator, a redox couple, potassium peroxydisulfate (KPS) and N,N,N',N'-tetramethylethylenediamine (TEMED), was used. The composition of the copolymer is presented on Table 2.1.

The synthesis was done under inert atmosphere, to avoid O₂ scavenging free radicals during polymerization. To do this, a solution of monomers in water, a solution of KPS in water and TEMED were degassed with N₂ during at least 30 minutes and then introduced in a glovebox with a controlled atmosphere (N₂, with at most 2 ppm of O₂). There, the three solutions were mixed with the right ratios, and the resulting solution was poured in a mold, schematically shown in Scheme 2.1.

The mold was left in the glovebox overnight to carry out the polymerization/gelation. The chemical gel in as prepared condition was then ready to be used.

Table 2.1: Concentrations of each component for the standard chemical gel. *Percentage for water is a weight percentage

	Molar mass (g/mol)	Specific gravity (g/mL)	Objective (mol %)	Concentration (mol/L)
AAm	71.1	-	90 %	1.8
VIm	94.1	1.039	10 %	0.2
MBA	154.2	-	0.15 %	0.003
KPS	270.3	-	0.30 %	0.006
TEMED	116.2	0.775	1 %	0.02
Water	-	-	85.11 %*	-



Scheme 2.1: Mold used to synthesize chemical gels

2.1.2. Synthesis of the P(AAm-co-VIm)/M²⁺ dual crosslink gels

The synthesis of dual crosslink gels having simultaneously chemical crosslinks and physical crosslinks by coordination bonds of metallic (M²⁺) ions with imidazole was performed by the following two methods:

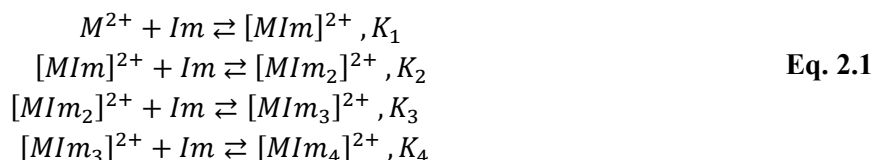
“One-Pot” method: in the preparation of the chemical gel, metallic ions were added to the monomer solution and the free radical polymerization was done in the presence of the ions;

“Diffusion” method: the chemical gel was prepared, then the physical crosslinks were incorporated, by immersing the chemical gel in a solution of M²⁺ ions and letting them diffuse inside the gel and complex with the imidazole moieties.

a. Cations used

In this chapter, we will mainly use Ni²⁺ ions. Imidazole ligands will complex with these ions following the reactions:

2. Preparation and microstructure of a dual-crosslink hydrogel



The different K_i are the stability constants of each of these reactions. Each of these reactions being at equilibrium, it possesses kinetic constants of dissociation and association noted k_{diss} and k_{ass} , which will be of interest in the future. The values of the different constants found in the literature are listed in Table 2.2.

Table 2.2: Stability constant of Imidazole- Ni^{2+} complexes, and corresponding association and dissociation kinetic constants for the dissociation of one imidazole from a $[NiIm_2]^{2+}$ complex [1,2].

Metal ion	$\log(K_1)$	$\log(K_2)$	$\log(K_3)$	$\log(K_4)$	k_{ass} ($M^{-1}.s^{-1}$)	k_{diss} (s^{-1})
Ni^{2+}	3.03	2.51	2.01	1.47	4.3×10^3	8.9

b. "One-pot" synthesis

Here, we mix the metallic ions with the stock solution of monomers. The concentrations of each component are shown on Table 2.3. For the $NiCl_2$, that we used here, concentrations ranging from 5 mmol/L to 100 mmol/L, corresponding to 0.25 to 5 mol% of physical crosslinks were used.

Table 2.3: Concentrations of each component in "one-pot" synthesis. *Percentage for water is a weight percentage

	Molar mass (g/mol)	Specific gravity (g/mL)	Objective (mol %)	Concentration (mol/L)
AAm	71.1	-	90 %	1.8
VIm	94.1	1.039	10 %	0.2
MBA	154.2	-	0.15 %	0.003
NiCl₂	129.6	-	0.25 – 5 %	0.005 – 0.1
KPS	270.3	-	0.30 %	0.006
TEMED	116.2	0.775	1 %	0.02
Water	-	-	85.11 %*	-

This first method presents the advantage of being very simple and allows a good control of the amount of physical crosslinks incorporated in the material as well as of the polymer concentration. However, it has been shown by Jingwen Zhao during her PhD that the presence of metallic cations in the solution can influence the polymerization:

- In the presence of Ni^{2+} ions, some black particles will appear during the polymerization. We suspect them to be NiO_2 particles, created by a redox reaction by KPS. They are unstable in water and disappear overnight;
- In the presence of Zn^{2+} ions, the hydrogel becomes white and opaque during the polymerization. This does not disappear afterwards;
- In the presence of Cu^{2+} ions, the solution does not polymerize.

c. “Diffusion” method

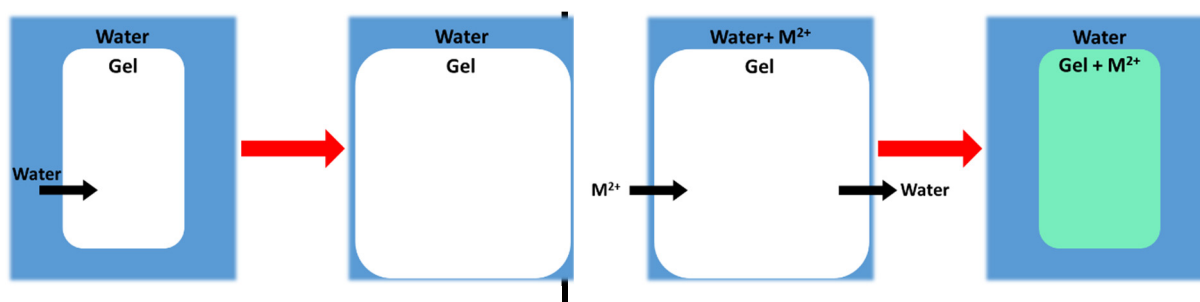
i. *General comments*

With the “Diffusion” method, three steps were required. First, the chemical gel was prepared as described above. Then the chemical gel was washed from any trace of non-reacted monomers, by placing the gel in at least three baths of distilled water for at least 24 hours. At this step, the chemical gel swelled up to its equilibrium swelling in water (around 6.5 times its initial weight, corresponding to a weight percentage in water of around 97.5%) due to the very low chemical crosslinking ratio. Finally, after washing, the swollen gel was placed in a solution of NiCl_2 to incorporate the physical bonds: those ions diffused from the solution phase to the gel. Once in the gel, they formed complex with the imidazole ligands. Due to the complexation, the concentration of the metallic ions in the gel becomes higher than the low initial concentrations of ions in the solution.

It should be noted that, in order to investigate accurately the effects of the physical crosslinks on the mechanical properties and dynamics of the gel, by comparing it the corresponding chemical gel, the polymer concentration should be the same. Contrary to the gels prepared by the “One-Pot” method, the gels prepared by the “Diffusion” method are at equilibrium swelling, and the polymer concentration depends on the crosslinking ratio. We evaluated more precisely the swelling of the dual crosslink gels with three factors:

- the enthalpy of mixing of the chemical network in water, inducing swelling;
- the amount of added physical crosslinks, inducing deswelling;
- the osmotic pressure of the counter ions (Cl^-) coming with the metallic ions introducing charges, linked to the difference of concentration in charges between the gel and the diffusing solution, inducing swelling.

With the composition shown in Table 2.3, the obtained dual crosslink gel swelled as the osmotic pressure was dominant. The obtained dual crosslink gel behaved as polyelectrolyte hydrogel with a high swelling (>99 w% of water). In order to deswell the gel by screening the electrostatic effect, and to bring the dual-crosslink gel back to its initial swelling ratio of the reference “as prepared” chemical gel (14.89% of polymer, in weight, in the gel), we added sodium chloride (NaCl) in the diffusing solution. These preparation steps are schematically illustrated in Scheme 2.2.



Scheme 2.2: Washing and incorporation of physical bonds in a chemical gel

This second method ensures that the chemical network is not affected by the presence of a metallic cation during the polymerization, and makes it possible to use some metallic cations (like Cu_{2+}) that inhibit the polymerization..

2. Preparation and microstructure of a dual-crosslink hydrogel

ii. Protocol

The details of the incorporation by diffusion are given here. The washed chemical gel was placed in the solution of NiCl_2 of desired concentration, containing a fixed amount of NaCl . The volume of the solution was set equal to 20 times the volume of the gel. Ni^{2+} ions being sensitive to pH (precipitating at pH 7), the pH of the diffusing solution was set at 6.5 with an HCl solution before each experiment.

We define the swelling ratio of the gel as:

$$w_r = \frac{\text{weight at equilibrium (after diffusion)}}{\text{weight as prepared (after synthesis)}} \quad \text{Eq. 2.2}$$

The concentration of NaCl was beforehand determined by tuning the swelling ratio of the dual crosslink gel at different NaCl concentrations, the value of $[\text{NaCl}]$ giving $w_r = 1$ was found 107 mmol/L for $[\text{Ni}^{2+}] = 100$ mmol/L.

2.2. Absorption of Ni^{2+} ions

The process of incorporating the physical bonds by the “diffusion” method requires a quantitative study of the absorption of those ions by the hydrogel. Here, we show first a kinetic study of the absorption by the chemical hydrogel, estimating the equilibration time. Then the absorption isotherm is measured to evaluate the amount of the uptake in metallic ions, which will be needed for all the mechanical studies that will be shown later. Finally, we will study the potential influence of NaCl on the absorption of Ni^{2+} ions.

2.2.1. Absorption kinetics of Ni^{2+} ions

Let us first analyze the kinetics of absorption of the Ni^{2+} ion by the chemical gel. For this, three solutions were made at an initial concentration $[\text{Ni}^{2+}] = 12$ mmol/L and the concentration change of free nickel ions in the solution was monitored as a function of time by using the UV-visible spectrometer (absorption of Ni^{2+} in water at 395 nm). The results are plotted in Figure 2.1.

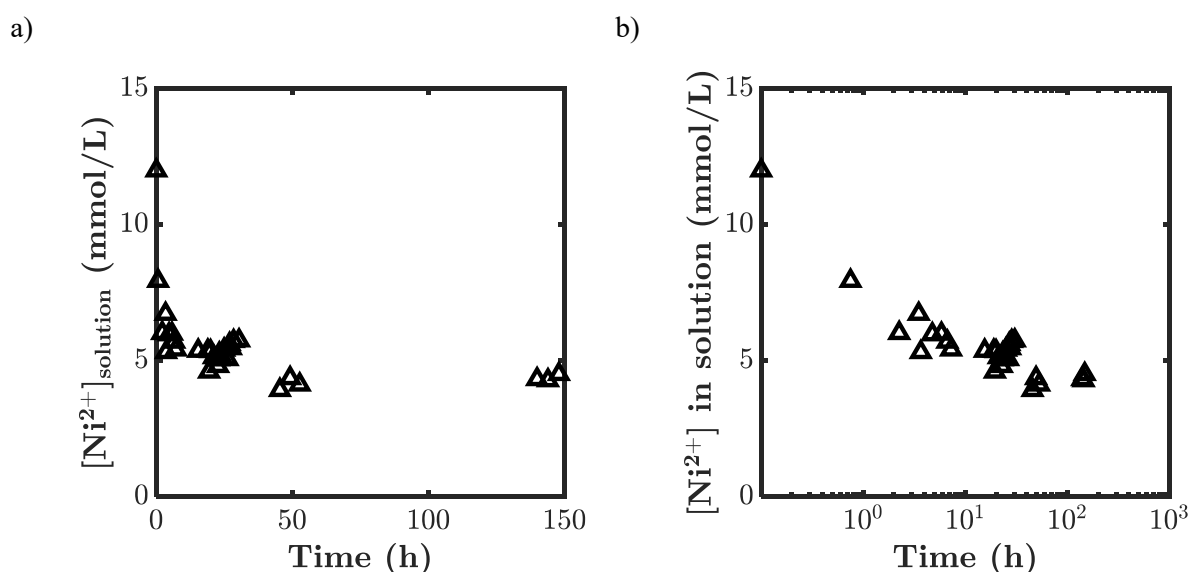


Figure 2.1: Ion concentration $[\text{Ni}^{2+}]$, in mmol/L, in the diffusing solution as a function of time in a) linear scale; b) logarithmic scale

We see very clearly in these figures that the Ni^{2+} concentration in solution decreased with time to reach at an equilibrium state at around 50 hours of diffusion. This result means that for this system, an equilibration time of two days was sufficient. To ensure that we are indeed at equilibrium, every diffusion experiment will be carried out for three days. One can roughly estimate the order of magnitude of the diffusion coefficient: the equilibration time t is in the order of $\sim L^2/D$, where L is half of the thickness of the gel sheet, 0.75 mm, and D the diffusion coefficient. With $t \sim 50$ (h), we found $D \sim 10^{-12} \text{ m}^2/\text{s}$, which is much lower than the diffusion coefficient of the ion in water and in a swollen gel (of the order of $10^{-9} \text{ m}^2/\text{s}$ [3]). This is due to the absorption: the ions bound to the polymer chains do not diffuse further inside the gel, decreasing the concentration of the mobile ions in the gel.

2.2.2. Influence of [NaCl]

There is no evidence in the literature of a coordination complex between Na^+ ions and Imidazole ligands; however, the change in ionic strength might change the equilibrium of the diffusion-complexation reaction in the polyelectrolyte network. To confirm the absence of effects of the salt, we carried out diffusion experiments with a fixed initial concentration in nickel ($[\text{Ni}^{2+}] = 5 \text{ mmol/L}$), and with varied NaCl concentration. The results are plotted in Figure 2.2. We found from Figure 2.2a) that the equilibrium concentration of the solution in Ni^{2+} (and hence the amount of Ni^{2+} absorbed by the gel) was independent of the amount of NaCl used. The swelling ratio w_r showed a pronounced NaCl concentration dependence: as seen in Figure 2.2 (right), it increased at the very low NaCl concentration, then decreased to level off at about $w_r = 1$.

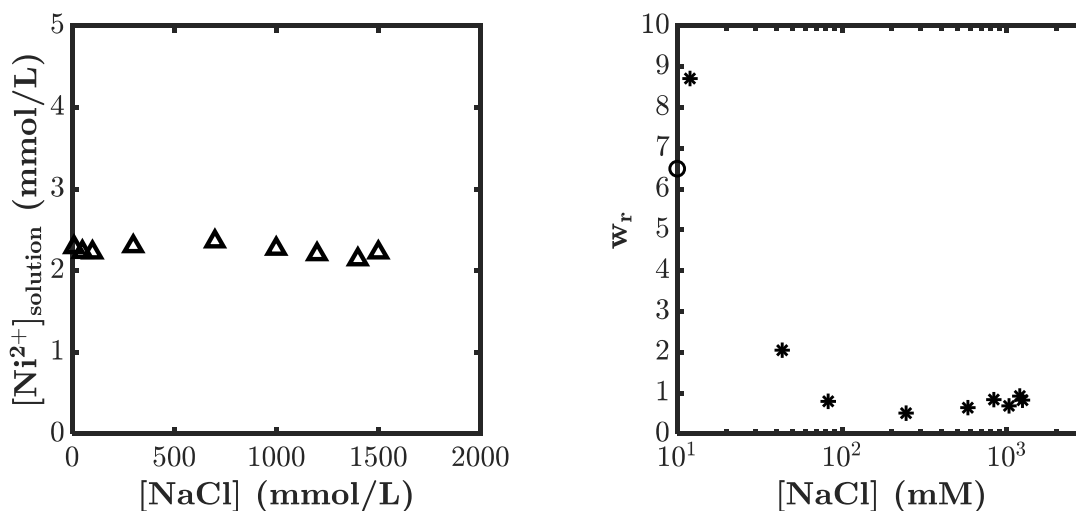


Figure 2.2: *Left:* Ion concentration $[\text{Ni}^{2+}]$, in mmol/L, in the diffusing solution as a function of salt concentration $[\text{NaCl}]$. *Right:* Swelling as a function of salt concentration $[\text{NaCl}]$. The open circle at $[\text{NaCl}] = 1 \text{ Mm}$ represents the swelling ratio of the chemical gel in distilled water, with no ions in solution.

It is then possible to study the evolution of the swelling ratio as a function of salt concentration with different initial concentrations in NiCl_2 of the diffusing solution, as shown in Figure 2.3.

2. Preparation and microstructure of a dual-crosslink hydrogel

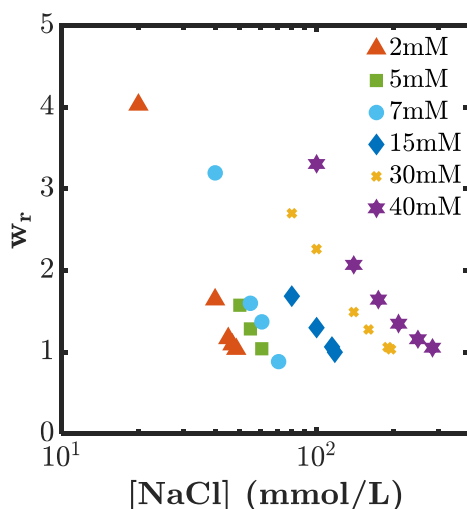


Figure 2.3: Swelling ratio w_r of the dual-crosslinked hydrogel for different initial concentrations in NiCl_2 , versus the salt concentration $[\text{NaCl}]$ of the solution

For each of these Ni^{2+} concentrations, we determined a NaCl concentration to reach a value $w_r = 1$ for the swelling ratio. This means that we can use any of these “optimized” dual-crosslink hydrogels and compare their properties to those of the bare chemical gel, since their weight percentage of polymer in the hydrogel (or the swelling ratio) is always the same.

2.2.3. Absorption isotherms – influence of $[\text{M}^{2+}]$

a. Composition of a “Diffusion” dual-crosslink hydrogel

Imidazole ligands and Nickel(II) ions can form coordination complexes with one, two, three or four ligands for one chelating ion, each of these reactions having its own thermodynamic stability constant (see Eq. 2.1).

Within the dual-crosslinked hydrogel where the ligands are on the polymer network, possible coordination number are unclear. In order to define the majoritarian family of complexes in our gels, we realized a binding isotherm of nickel ions into the P(AAm-co-VIm) chemical gel. Samples of chemical gel were placed in solutions of Ni^{2+} at various concentrations and the quantity of nickel ions absorbed by the gel were estimated by measuring the decrease in the concentration in the solution phase. All solutions had a concentration in salt $[\text{NaCl}]$ such as, for the dual-crosslinked gel obtained after diffusion, $w_r = 1$.

After three days of equilibration, the concentration of coordinated nickel ions $[\text{Ni}^{2+}]_{\text{coord}}$ was computed thanks to the protocol shown in Annex I. The results are plotted in Figure 2.4. In this figure, we plotted the absorption isotherm, the molar ratio of Ni^{2+} ions absorbed by the gel to imidazole as a function of the concentration of free Ni^{2+} ions in the solution. We took into account the equilibrium, in the gel, between bound and free Ni^{2+} (see Annex). The results plotted here show only the bound (or coordinated) Ni^{2+} ions.

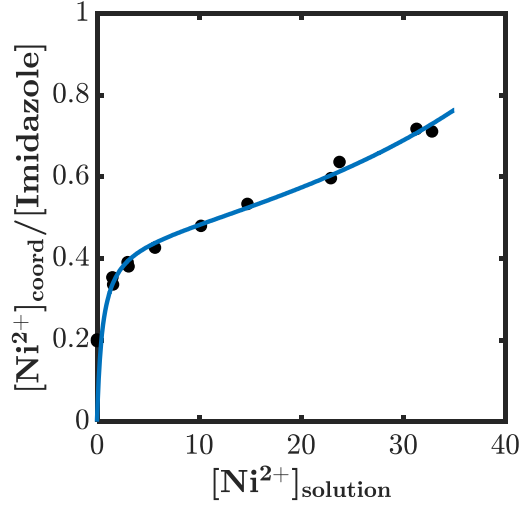


Figure 2.4: Concentration of complexed Ni^{2+} ions, divided by the concentration of Imidazole moieties, as a function of the concentration of Ni^{2+} cations in the diffusing solution. All concentrations are at equilibrium. Circles are the data points, blue line is a guide for the eye.

Within the studied concentration range, the amount of absorbed ions increased with free Ni^{2+} concentration, while the concentration dependence was rather complex. At concentrations lower than 10 mmol/L, the ratio $[Ni^{2+}]_{coord}/[Imidazole]$ approached 0.5, suggesting that the majority of Ni^{2+} had a coordination number of 2 (imidazoles per Ni^{2+}) and that the physical crosslinks had a functionality $f = 4$. The $[Ni^{2+}]_{coord}/[Imidazole]$ ratio continued to increase with increasing Ni^{2+} concentration, suggesting that complexes with a coordination number of 1 could form at higher concentrations of free Ni^{2+} .

This result suggests that in the dual-crosslink hydrogel a mixture of complexes with coordination numbers 1 and 2 are formed in majority, and only the latter form physical crosslinks between polymer chains. We estimated the real quantity of $[NiIm_2]^{2+}$ complexes in the hydrogel, by solving the system of equations:

$$[Ni^{2+}]_1 = k_1 \cdot [Ni^{2+}]_{free} \cdot [Im]_{free} \quad \text{Eq. 2.3}$$

$$[Ni^{2+}]_2 = k_2 \cdot [Ni^{2+}]_1 \cdot [Im]_{free} \quad \text{Eq. 2.4}$$

$$[Im]_{free} = [Im]_0 - [Ni^{2+}]_1 - 2 * [Ni^{2+}]_2 \quad \text{Eq. 2.5}$$

where $[Ni^{2+}]_1$ is the concentration in $[NiIm]^{2+}$ complexes, $[Ni^{2+}]_2$ is the concentration in $[NiIm_2]^{2+}$ complexes, $[Im]_0$ is the initial concentration in imidazole ligands and $[Im]_{free}$ is the concentration free imidazole ligand available for binding. k_1 and k_2 are binding constants. Using k_1 , k_2 and $[Im]_0$ as fit parameters, we obtained the results shown in Figure 2.5. Note that $[Im]_0$ needed to be a fitting parameter, as it can be lower than the concentration in the feed (200 mmol/L) since the reactivity of imidazole during the polymerization is unknown; also, the protonation of imidazole competitively decreases the binding efficiency of the Ni^{2+} , making the imidazole less available for complexation. The fitting curve well captured the trends, and we found $k_1 = 0.13 \text{ L/mol}$, $k_2 = 0.031 \text{ L/mol}$ and $[Im]_0 = 0.17 \text{ mol/L}$. This last result implies that about 83% of the imidazole ligands were available or integrated in the network during polymerization.

2. Preparation and microstructure of a dual-crosslink hydrogel

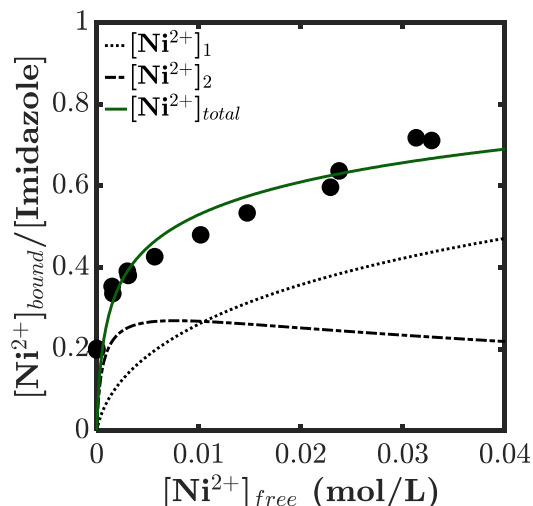


Figure 2.5: Concentration of mono- and bis-complexes of Ni^{2+} ions and imidazole ligands, as a function of the free Ni^{2+} ion concentration, in a dual-crosslink hydrogel. Circles are the data from Figure 2.4, dotted line is the concentration in $[\text{NiIm}_2]^{2+}$ computed from Eq. 2.4, pointed line is the concentration in $[\text{NiIm}]^{2+}$ computed from Eq. 2.3 and green line is the total concentration of complexed Ni^{2+} ions.

b. Diffusion results applied to “One-pot” dual-crosslink hydrogel

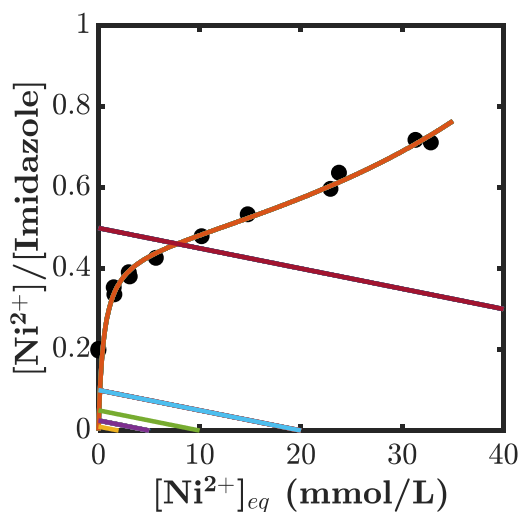


Figure 2.6: Computation method of the concentrations of free and complexed Ni^{2+} ions in a gel. Circles and orange line are the data from Figure 2.4. Colored parallel lines are the guides used to compute the concentration in complexed Ni^{2+} ion in the “One-pot” dual-crosslink hydrogel, with feed concentrations $[\text{Ni}^{2+}] = 2, 5, 10, 20$ and 100 mmol/L (see text below for more details).

Supposing the same binding equilibrium in the “one-pot” dual-crosslink gel than in the “diffusion” one, we estimated the free and bound ion concentration in the “one-pot” gel. These equilibrium concentrations were determined thanks to the crossover point of the binding isotherm and the straight line connecting zero binding to total binding (the slope is determined from the volume ratio of the gel to the solution, 0.05 here), as shown on Figure 2.6. The results are shown in Table 2.4. They indicate that for the concentrations lower than 20 mmol/L, almost all the ions in the system were bound, thus the

concentration of Ni^{2+} in coordination complexes was proportional to the initial concentration in the solution. For the gel with 100 mmol/L, 86 % of the Ni^{2+} ions were bound. Using the curves from Figure 2.5, we could also compute the concentration of Ni^{2+} ions creating bi-complexes with two imidazole ligands, the only ions potentially creating physical crosslinks between the polymer chains.

Table 2.4: Complexation state of the different "One-pot" hydrogels

$[\text{Ni}^{2+}]$ initial (mmol/L)	$[\text{Ni}^{2+}]$ free (mmol/L)	$[\text{Ni}^{2+}]$ complexed (mmol/L)	$[\text{Ni}^{2+}]$ crosslinking (mmol/L)
2	0	2	1.7
5	0	5	4.2
10	0.02	9.98	8.3
20	0.09	19.91	16.3
100	14.23	85.77	39.5

2.3. Stress-free dynamics – study by dynamic light scattering (DLS)

Now that we understand how the metallic ions complex with the imidazole ligands in the gel, we want to characterize the dynamics of this dual-crosslinked hydrogel. In order to do so, we realized dynamic light scattering (DLS) experiments on dual-crosslink gels with nickel ions. Since the samples for this experiment need to be polymerized in a test tube, the "Diffusion" method is not usable here. We will study a Ni^{2+} hydrogel prepared by the "One-pot" method, but we will show later that, in the case of Ni^{2+} , there is no real difference between the hydrogels obtained with both methods. Zn^{2+} and Cu^{2+} hydrogels cannot be studied with this experiment.

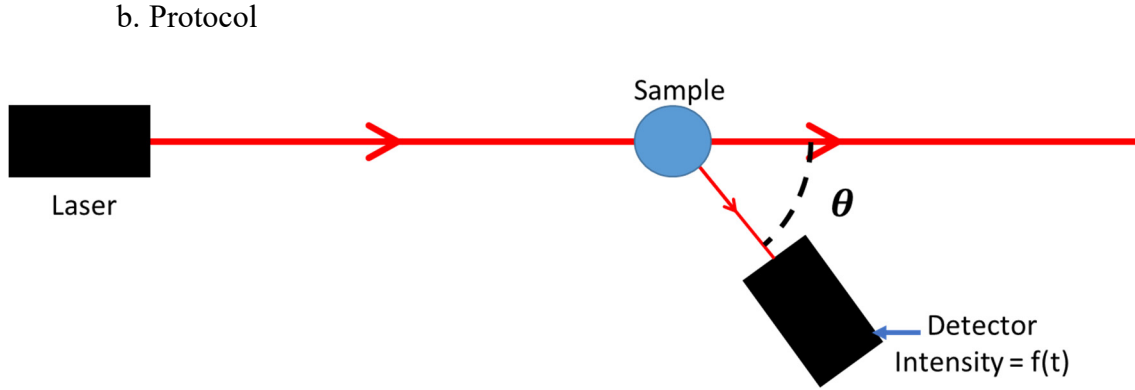
This experiment will allow us to study the relaxation time of the polymer chains in a stress-free configuration, the idea being to link these times to the dynamic of the transient physical bond we have introduced in the network.

2.3.1. Dynamic Light Scattering – Principles and protocol

a. Principle of the method

Dynamic light scattering consists in analyzing the temporal fluctuations inside a solution or, here, a chemically crosslinked gel. More specifically, a monochromatic laser light is sent into a 10 mm-diameter test tube, containing the hydrogel to analyze. Inside any hydrogel, there are gradients of concentration of polymer chains. Those differences in concentration will scatter the incident light. These gradients of concentrations evolve with time, at a time length that depends on the length of the polymer chains, their interactions... The scattered light intensity will then vary with time, at the same characteristic time lengths. By studying this scattered light intensity, and how it evolves with time, it is possible to go back to the movements of the polymer chains inside the hydrogel.

2. Preparation and microstructure of a dual-crosslink hydrogel



Scheme 2.3: Dynamic light scattering experiment.

Dynamic light scattering measurements were performed with an ALV CGS-3 goniometer system (ALV, Langen, Germany), equipped with a cuvette rotation/translation unit (CRTU) and a He-Ne laser (22 mW at $\lambda = 632.8$ nm). The system measures the time-averaged autocorrelation function of the scattered light intensity $I(t)$ at a scattering vector q defined as

$$q = \frac{4\pi n}{\lambda} \sin\left(\frac{\theta}{2}\right) \quad \text{Eq. 2.6}$$

Where n is the refractive index and θ the scattering angle (see Scheme 2.3).

Once $I(t)$ is known, the second-order intensity auto-correlation function $g^{(2)}(t)$ is generated, with t the decay time, with Eq. 2.7.

$$g^{(2)}(t) = \frac{\langle I(\tau)I(t + \tau) \rangle}{\langle I(\tau) \rangle^2} \quad \text{Eq. 2.7}$$

This intensity auto-correlation function is then converted into the field auto-correlation function $g^{(1)}(t)$ with the Siegert relation, given by Eq. 2.8.

$$g^{(2)}(t) = \beta(1 + g^{(1)}(t))^2 \quad \text{Eq. 2.8}$$

For ergodic samples, it is possible to explore the whole phase space in the course of the experimental time at a fixed sampling position when the duration of acquisition is sufficiently long compared to the slowest characteristic time of the system. Thus, the time averaged autocorrelation function is equivalent to the ensemble averaged one: experimentally, we obtain a constant value of the amplitude of the autocorrelation function at $t = 0$ s and it goes to zero at long times.

In the case of non-ergodic samples, such as here with a chemically crosslinked gel, due to the static concentration gradient associated to the presence of frozen disorder in the system, the time averaged autocorrelation function does not probe all the configuration of the system. The time-averaged autocorrelation function is then different from the ensemble-averaged one. In order to circumvent this non-ergodicity, the sample cell was vertically translated steadily while time averaging. Thus $g^{(2)}$ coincides with the ensemble-averaged autocorrelation function, up to a cut-off decay time fixed by the sample translation speed (having here a characteristic time of around 10 s). The averaging duration was more than 3600 s. The obtained field correlation functions were fitted with stretched exponential functions having one, two or three relaxation modes. These functions fit well empirically the autocorrelation functions.

The gels studied were standard chemical gels and “one-pot” dual-crosslink hydrogels, with concentrations in Ni^{2+} ranging from 0 to 20 mmol/L. From what we computed previously, we know that almost all the ions are bound to the polymer chain in these cases. Studying higher concentrations of physical bonds is impossible with this technique. When increasing $[\text{Ni}^{2+}]$, the gels become more and more diffusing, and the scattered light intensity decreases drastically. It is then impossible to extract information from it.

2.3.2. Results for a bare chemical gel

A DLS measurement realized on a bare chemical gel, with no physical crosslinks, at a scattering angle of 90° , gives the results shown in Figure 2.7. In this figure, one can see the evolution of the normalized field auto-correlation function as a function of the time, in black circles. The line is a fitting result that we will detail later, only used as guide for the eye here. The autocorrelation function exhibits the follow characteristics:

- A decorrelation mode having a long characteristic time (a few seconds), which corresponds to the movement of the cuvette previously mentioned. It is not a dynamic mode of the hydrogel, and will be ignored in the rest of the experiments;
- A decorrelation mode with a characteristic time of about 10^{-4}s ;
- A plateau with an amplitude of 0.4.

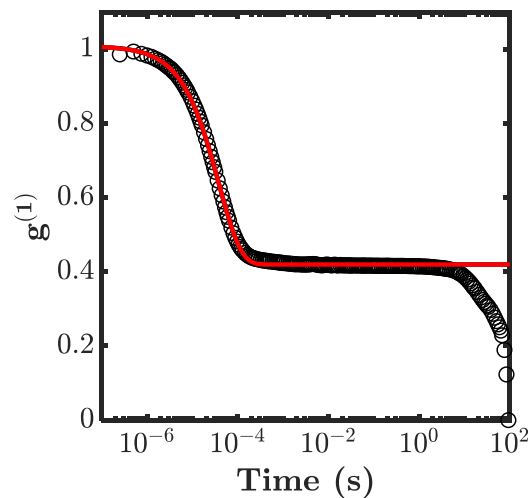


Figure 2.7: Normalized field autocorrelation function of the scattered light intensity measured at an angle of 90° , for the bare chemical gel. The black circles are the experimental data points, the lines are the fits, used as guides for the eye here..

The fast decorrelation is the so-called gel mode, linked to the collective motion of polymer chains in the network. The fact that the auto-correlation function does not fully decorrelate and shows a plateau indicates that a part of the scattered light intensity does not fluctuate with time as it comes from the spatially frozen concentration gradient in the polymer network³⁵.

In order to better characterize the nature of this mode, the autocorrelation function $g^{(1)}$ can be fitted by a stretched exponential decay, such as:

2. Preparation and microstructure of a dual-crosslink hydrogel

$$g^{(1)}(t) = A \exp \left[- \left(\frac{t}{\tau} \right)^\alpha \right] + d \quad \text{Eq. 2.9}$$

where A is the amplitude of the decorrelation mode, d is the value of the plateau, τ is the characteristic time of the decorrelation and α is the stretch factor of the exponential decay and represents the distribution of characteristic times around the mean value τ .

For the chemical gel, the only fit parameters are τ and α , since d is measured on the graph and we have the relationship $A = 1 - d$. The result of this fit is also plotted in Figure 2.7.

To determine the exact nature of this mode, we studied the scattering vector dependence of the characteristic times: the experiment was carried out at different scattering angles θ , thus varying the scattering vector q (see Eq. 2.6). The obtained values for τ are then plotted as a function of the scattering vector, in Figure 2.8.

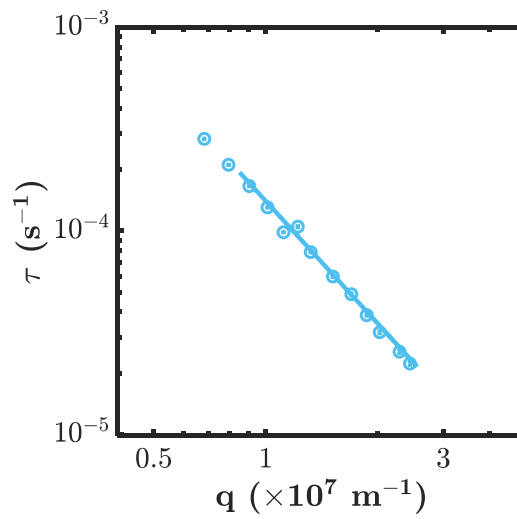


Figure 2.8: Characteristic decorrelation time observed in the bare chemical gel (light blue circles), as a function of the scattering vector q .

The characteristic time of this fast decorrelation scales as $\tau \sim q^{-2}$, which is representative of a diffusive gel mode. In such a mode, the characteristic time increases with the observation length scale $1/q$ following $\tau = 1/Dq^2$, where D is the collective diffusion coefficient. From this collective diffusion coefficient, we can compute a correlation length ξ thanks to Stokes-Einstein equation:

$$\xi = \frac{k_b T}{6\pi\eta D} \quad \text{Eq. 2.10}$$

With η the dynamic viscosity of water, $0.89e^{-3} Pa.s$ at $T = 298 K$. The values obtained are summarized in Table 2.5.

Table 2.5: Results of the linear fit $\ln(\tau) = a \ln(q) - \ln(D)$ and value of the correlation length ξ obtained from Eq. 2.10

a	D ($10^{-11} m^2/s$)	ξ (nm)
-1.98	6.2	4.0

These values will be used as reference later, when studying the dual-crosslink hydrogels.

2.3.3. Results for a “One-pot” dual-crosslink gel

a. $[\text{Ni}^{2+}] = 20 \text{ mmol/L}$ – Influence of the scattering vector q

We performed the same measurement on a dual-crosslink hydrogel with Ni^{2+} , synthesized by the “One-pot” method and directly prepared it in the measurement cell (glass test tube). The normalized field autocorrelation function of the dual crosslink gel is shown in Figure 2.9, with that for the bare chemical gel (previously shown in Figure 2.7) as references. Here, we observed three decorrelation modes (movement of the test tube at 10 s excluded), labeled as “fast”, “intermediate” and “slow”. The fast decorrelation mode, with a characteristic time of about 10^{-4} s, possessed a similar characteristic time as the diffusive decorrelation mode of the chemical gel. The intermediate and slow modes were not observed on the chemical gel. They are thus attributed to the dynamics related to the transient physical bonds.

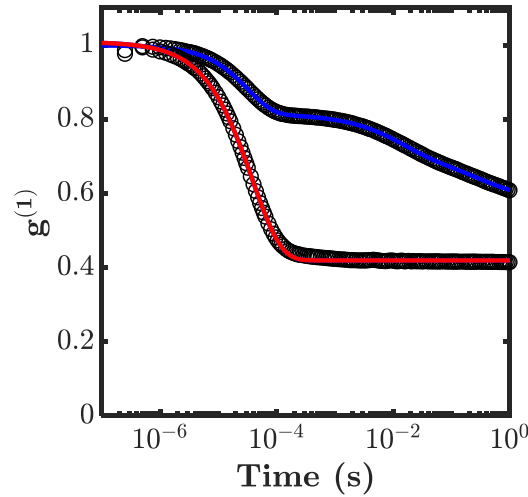


Figure 2.9: Normalized field autocorrelation functions of the scattered light intensity measured at an angle of 90° , for the bare chemical gel (red) and the dual-crosslinked gel with Ni^{2+} ions (blue). The black circles are the experimental data points, the lines are the fits.

In order to better characterize the nature of these different modes, the autocorrelation function $g^{(1)}$ were fitted by the following equation having three stretched exponential decay functions, which empirically well fit autocorrelation functions:

$$g^{(1)}(t) = \sum_{k=s,i,f} A_k \exp \left[- \left(\frac{t}{\tau_k} \right)^{\alpha_k} \right] + d \quad \text{Eq. 2.11}$$

For this dual-crosslink gel, three decorrelations are necessary. Here, there will be 9 fitting parameters: the amplitude, characteristic time and stretch exponent of each exponential decay (‘s’ for slow, ‘i’ for intermediate and ‘f’ for fast). Figure 2.10 shows the result of the fit: the fitting curve in red correspond well to the experimental value of $g^{(1)}$ for the whole time scale. The three decorrelation modes are also separately shown in the figure (the amplitude of the plateau $d = 0.6$, was added to the first decorrelation). The three characteristic times have at least one decade of difference from each other, and the amplitudes are about 0.1 or more, thus we can identify and distinguish them from each other.

2. Preparation and microstructure of a dual-crosslink hydrogel

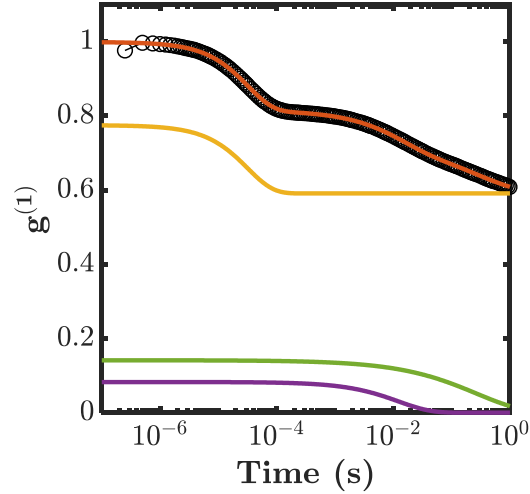


Figure 2.10: Autocorrelation function obtained from a dual-crosslink hydrogel with $[Ni^{2+}] = 20$ mmol/L (black circles), fitted (in red) by a sum of three exponential decays (plotted here in yellow, green and purple).

We studied the scattering vector dependence of the characteristic times: the experiment was carried out at different scattering angles θ , thus varying the scattering vector q (see Eq. 2.6). The obtained values for τ_f , τ_i and τ_s of the dual-crosslink gel are then plotted as a function of the scattering vector, in Figure 2.11.

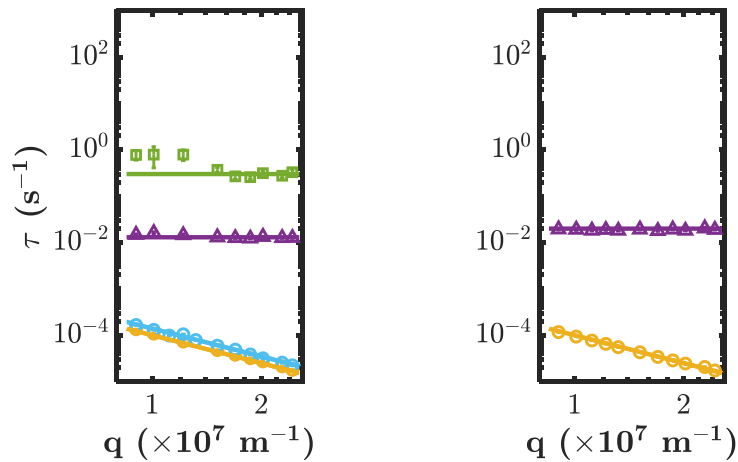


Figure 2.11: Left: Characteristic decorrelation times for the three decorrelations observed in the dual crosslink gel (circles, triangles and squares for the fast, intermediate and slow modes respectively), along with the unique decorrelation time observed in the bare chemical gel (light blue circles), as a function of the scattering vector q . Right: Same results, for a solution of physically crosslinked $P(AAm-co-VIm)-Ni^{2+}$

The characteristic time of the chemical gel is also plotted as a reference. The fast mode of the dual-crosslink hydrogel (blue symbols), whose characteristic time has practically the same values as that of the chemical gel, showed q^{-2} dependence. Thus, we attribute this fast mode to the gel mode, the collective diffusive movement of polymer chains in the gel.

The characteristic time of the intermediate and slow modes, did not evolve with the scattering vector q . This indicates that the corresponding dynamics do not depend on the length scale of observation, thus corresponding to a macroscopic relaxation [4,5]. As mentioned before, these two modes are related to the transient physical bonds in the hydrogel. Their average values here are 10^{-2} s and 3×10^{-1} s respectively. It should be noted that the slow decorrelation mode, being so close in time to the decorrelation linked to the movement of the sample, had larger errors than those for the fast and intermediate decorrelation modes.

The same experiment has been realized on a solution of P(AAm-co-VIm), crosslinked only with Ni^{2+} ions (no chemical bonds). The results are also shown on Figure 2.11 (right). The two modes observed in this solution are identical to the fast and intermediate modes previously observed in the dual-crosslinked hydrogel. A slow mode was not observed here: at the long times involved in the slow mode, we start to measure the characteristic time of terminal flow of the polymer solution. It is then impossible to differentiate the decorrelation linked to the flow of the polymer chains, and the decorrelation linked to a possible slow mode. It is however interesting to note that the presence of chemical bonds has no influence on the characteristic time of the intermediate mode.

b. $[\text{Ni}^{2+}] = 20$ mmol/L – Influence of temperature & Activation energy

In order to better understand the nature of these dynamic modes in the dual-crosslink hydrogel, their activation energy was further studied. The autocorrelation function of the scattered light of a dual-crosslink hydrogel, with $[\text{Ni}^{2+}] = 20$ mmol/L, was obtained at different temperatures (ranging from 5 to 45 °C) and the characteristic decorrelation times were determined by the fitting. The Arrhenius plot of the values of them at 90° are shown in Figure 2.12.

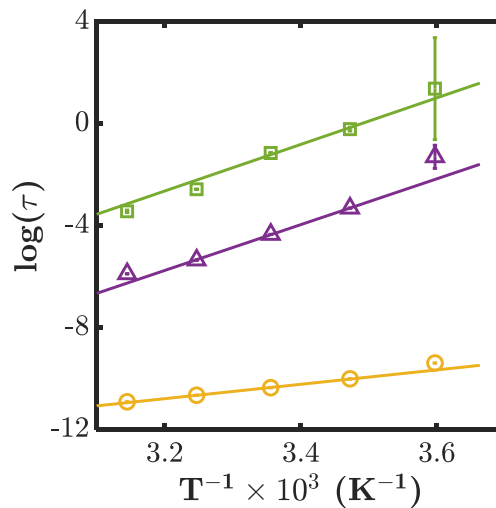


Figure 2.12: Arrhenius plot of the three decorrelation times, observed at 90° , of the dual-crosslink hydrogel with $[\text{Ni}^{2+}] = 20$ mmol/L.

An activation energy for each of these modes was calculated from the slope, we found around 20 kJ/mol for the fast mode and around 70 kJ/mol for the intermediate and slow modes. This result indicates that the intermediate and slow modes have the same energy barrier to overcome in order for the polymer chain to relax, presumably corresponding to the dissociation of the coordination bond with a ligand on a polymer chain.

2. Preparation and microstructure of a dual-crosslink hydrogel

c. Influence of $[\text{Ni}^{2+}]$

i. Auto-correlation functions

In order to understand the influence of the amount of physical bonds on the macroscopic modes of decorrelation we observed in the previous part (2.3.3.a), we studied the transient physical crosslinker concentration (or Ni^{2+} concentration) dependences of these three modes. Figure 2.13 shows the evolution of the auto-correlation function for dual-crosslink gels with varying concentrations in Ni^{2+} . It is confirmed that the same three modes were observed for all the dual crosslink gels at different Ni^{2+} concentrations, and that the normalized field autocorrelation functions $g^{(1)}(t)$ could be fitted with Eq. 2.11.

Let us first comment on the amplitude of the modes. We see here that the amplitude of the fast mode, A_f , as well as the amplitude of the plateau, d , showed complex Ni^{2+} concentration dependences. The value of A_f decreased with increase in Ni^{2+} concentration from 0 (chemical gel) to 5 mM, then it increased when Ni^{2+} concentration goes from 5 to 10 mM, above which the concentration dependence became less significant. The amplitude of the intermediate and slow modes showed less pronounced crosslinker concentration dependence. Thus, the amplitude of the plateau d decreased then increased. It is noteworthy that the plateau value for the bare chemical gel was higher than the plateau value of the gels with low Ni^{2+} concentration (2 and 5 mmol/L). Since this set of gels is made with the “one-pot” method, this decrease of the plateau value at lower concentrations might be linked to a change in the nature of the chemical network.

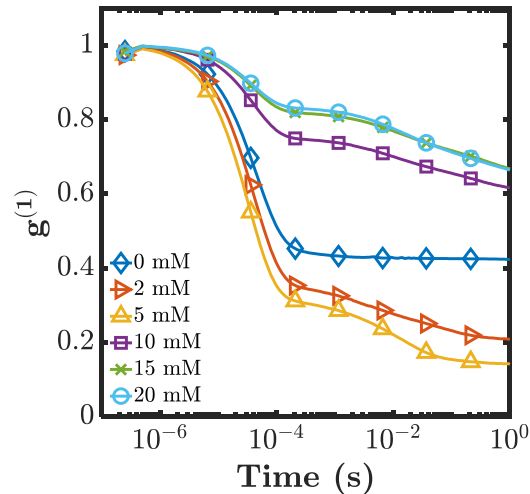


Figure 2.13: Evolution of the field auto-correlation function $g^{(1)}$ as a function of $[\text{Ni}^{2+}]$.

ii. Evolution of heterogeneity in the chemical network?

In order to understand this evolution of the plateau at low concentrations, we studied more closely the dependence of the amplitudes of decorrelations to the physical crosslinker concentration, as shown in Figure 2.14.

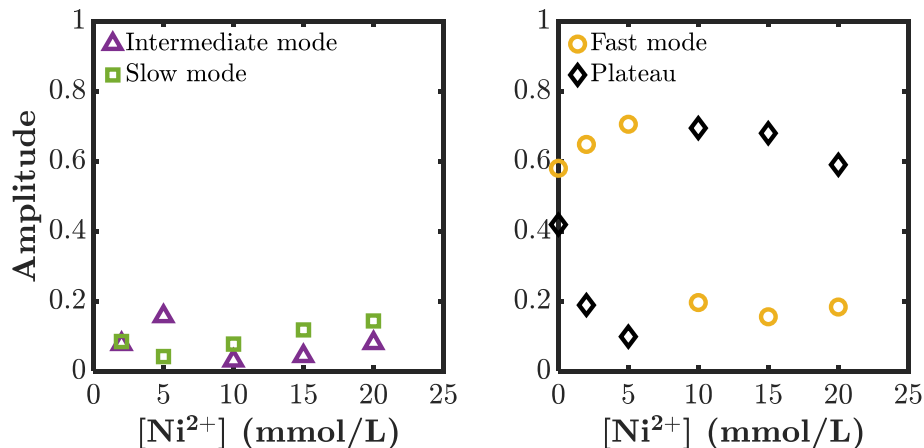


Figure 2.14: a) Amplitudes of the intermediate and slow decorrelation modes, as a function of Ni^{2+} ion concentration; b) Amplitude of the fast decorrelation mode and of the final plateau as a function of Ni^{2+} concentration.

At low Ni^{2+} concentrations, the amplitude of the fast mode was the largest. It dropped from about 0.7 to 0.2 when Ni^{2+} concentration increased from 5 to 10 mmol/L. At the same time, the amplitude of the plateau at long time d increased from 0.2 to 0.7. The amplitude of this plateau was related to the intensity of the scattered light from the static heterogeneity of the network: the chemical crosslinking induces the frozen-in concentration gradient of the polymer network and the scattered light intensity from the corresponding structure does not fluctuate with time. This result suggests that the static heterogeneity of the chemically crosslinked network increases with the transient physical crosslinker concentration. The amplitudes of the intermediate and slow modes did not have a clear dependence on the physical crosslinker concentration. Except for 5 mmol/L at which the structural change started to occur, the values of the amplitudes A_i and A_s were almost constant over the concentration range studied here.

The structural change between 5 and 10 mmol/L was also demonstrated by the scattered light intensity, shown in Figure 2.15 as a function of the scattering vector q . The scattered light intensity increased sharply with increase in Ni^{2+} concentration from 5 to 10 mmol/L. We do not have a clear explanation for this increase in the heterogeneity of the system. Presumably, the initiation of the radicals by the potassium persulfate initiator might be influenced by the presence of Ni^{2+} ions, thus modifying the polymerization and the obtained chemical network.

2. Preparation and microstructure of a dual-crosslink hydrogel

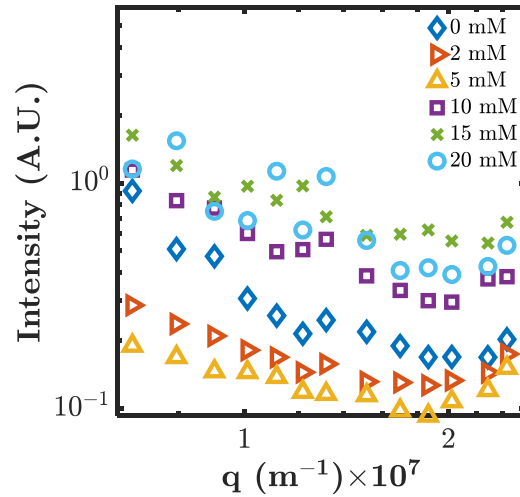


Figure 2.15: Scattered light intensity as a function of the scattering vector and Ni²⁺ ion concentration.

iii. Study of the decorrelation times

Here we characterized the characteristic time of the three modes of the dual-crosslink hydrogels with varying Ni²⁺ concentrations, by fitting the data from Figure 2.13 with Eq. 2.11. The fast mode, observed in the bare chemical gel and in the dual-crosslink hydrogel, is diffusive. As we have done in the previous paragraph, we estimated the diffusion coefficient and correlation length of the dual crosslink hydrogels by using Eq. 2.10. The results are plotted in Figure 2.16, as a function of [Ni²⁺].

The correlation length exhibited a very weak Ni²⁺ concentration dependence. We observed a decrease in it from 0 to 5 mmol/L of Ni²⁺, and this decrease however stopped at 10 mmol/L, where the correlation length reached an equilibrium value around 3 nm. This change might be partly explained by the polyelectrolyte effect: the physical crosslinking points are charged and due to the increasing amount of fast-moving counterions around the polymer chains, the diffusive movement of the chains can be accelerated (a small decrease in the fast decorrelation mode, which can also be seen in Figure 2.13). Thus, the correlation length decreases. This change in behavior of the correlation length can also be explained by the structural change in the chemical network we have observed between 5 and 10 mmol/L. For a more accurate evaluation, the heterodyne method is necessary to take into account of the static component of the scattered light. In this work we did not apply it to the system with the macroscopic relaxation mode. A detailed theoretical development of the heterodyne method in the presence of macroscopic modes is beyond the scope of this work.

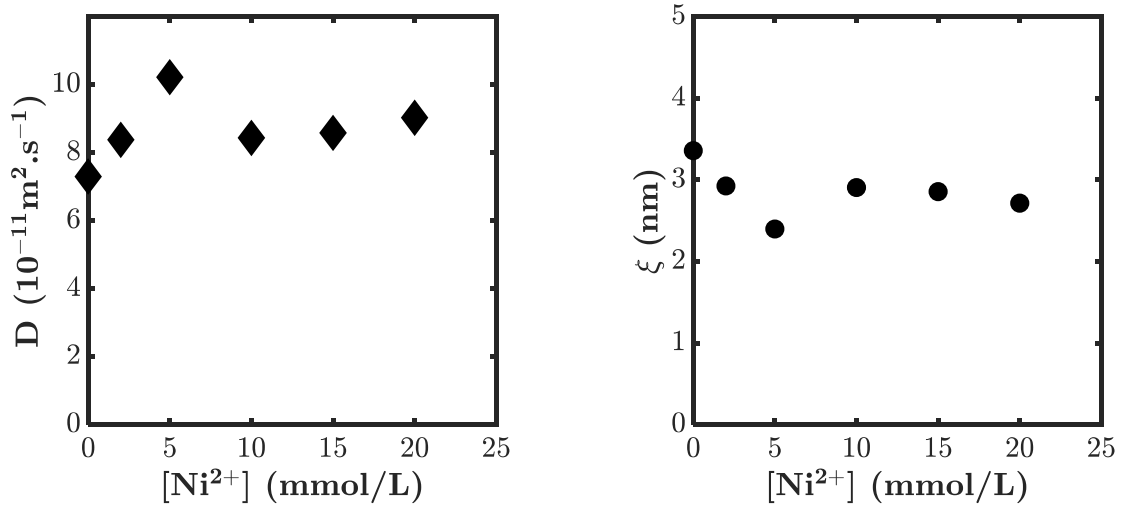


Figure 2.16: Left: Diffusion coefficient related to the fast decorrelation mode, as a function of Ni^{2+} ion concentration. Right: ξ , the correlation length obtained from Stokes-Einstein equation, as a function of Ni^{2+} ion concentration.

In Figure 2.17, we have plotted the decorrelation times of each mode, as a function of the concentration in Ni^{2+} ions. For the characteristic time of the intermediate and slow modes, we found a slight deceleration between 2 and 5 mmol/L, then at the higher concentrations both modes showed a constant characteristic time, around 10^{-2} s and 0.3 s, respectively.

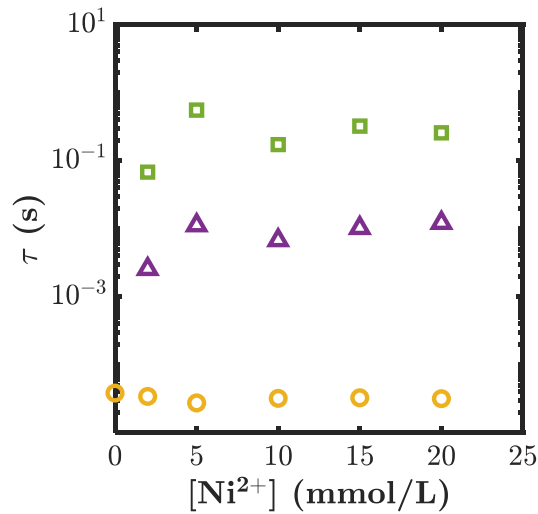


Figure 2.17: Decorrelation times of the fast (orange circles), intermediate (purple triangles) and slow (green squares) modes observed in a DLS measurement of a “One-pot” dual-crosslink hydrogel, as a function of Ni^{2+} ion concentration.

iv. Influence of temperature – Activation energy

The concentration dependence of the activation energy was examined for the three modes. The values of them were plotted Figure 2.18 as a function of the concentration in Ni^{2+} ions.

2. Preparation and microstructure of a dual-crosslink hydrogel

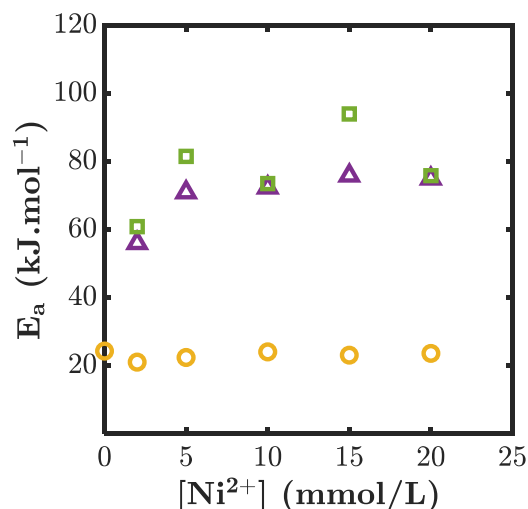


Figure 2.18: Activation energies of the fast (orange circles), intermediate (purple triangles) and slow (green squares) modes observed in a DLS measurement of a “One-pot” dual-crosslink hydrogel, as a function of Ni^{2+} ion concentration.

We see on this figure that the activation energy of the fast mode did not evolve with Ni^{2+} concentration, staying around 20 kJ/mol. The activation energies of the intermediate and slow mode however, slightly increased from 2 to 5 mmol/L, and then stay constant at a value of around 80 kJ/mol. We confirmed that both intermediate and slow modes showed a similar value of activation energy (the dispersion of data for the slow mode was larger). The evolution between 2 and 5 mmol/L does not seem to be correlated to the change in the heterogeneity of the chemical network structure we have demonstrated beforehand, since this change was happening between 5 and 10 mmol/L. A possible explanation of the increase in lifetime and activation energy between 2 and 5 mmol/L might be that the complexation state of the Ni^{2+} ions change between those two concentrations.

2.3.4. Conclusions

The only decorrelation mode observed in the bare chemical gel was also found in the dual-crosslink hydrogels. Its amplitude decreased with an increasing amount of physical bonds, while its characteristic decorrelation time was constant. This mode was attributed to the collective diffusive movement of the polymer chains inside the gel. The characteristic time of this dynamic mode was not affected by the presence of physical bonds.

We demonstrated the presence of two decorrelation modes in our dual-crosslink hydrogel, inexistent in the bare chemical gel thus linked to the physical crosslinks. These two modes did not evolve with the scattering vector q , meaning that they are macroscopic properties of the hydrogels. Their characteristic times and amplitudes did not evolve much with the concentration of physical crosslinks. More importantly, each mode possessed the same activation energy, meaning that they have the same energy barrier to overcome in order for the polymer chain to relax.

What is the origin of the two macroscopic modes? We introduced in our dual-crosslink gel one characteristic lifetime, breaking time of the transient physical crosslink. We attribute the intermediate mode, the faster of the two, to the chain relaxation due to the physical bond breaking. As we showed

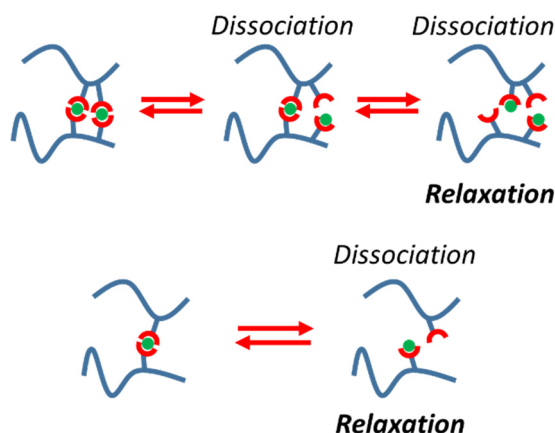
from the absorption isotherm, that $[\text{NiIm}_2]^{2+}$ complexes represent the majoritarian family of complexes, and these complexes can serve as physical crosslinks. It is very interesting to note that the intermediate mode, attributed to the dissociation of one physical bond, is identical in the dual-crosslink hydrogel and in the solution of physically crosslinked polymer. This implies that the presence of chemical bonds does not affect the lifetime of the physical bond – which will be very important in the last part of this manuscript.

For the slow mode, several interpretations are possible. It would be possible that complexes having higher coordination numbers result in the slow mode. However, such high coordination number complexes should be found at lower Ni^{2+} concentrations and less abundant than $[\text{NiIm}_2]^{2+}$ complexes. Note that at 2 mmol/L, the amplitude of the slow mode was not particularly higher than that of the intermediate mode, suggesting that the presence of high coordination complexes is improbable.

We believe that the slow mode is due to the presence of “clusters” of physical bonds on the polymer chains. When two (or more) $[\text{NiIm}_2]^{2+}$ complexes are present close to each other, they are expected to behave as a single crosslinking point, called here “cluster”. In order to completely relax the chain by breaking a cluster, the chain must wait for all the physical crosslinks from the clusters to be open at the same time (see Scheme 2.4). This relaxation time is then by definition, much longer than that linked to the opening of one physical bond (intermediate mode). The distribution of the lifetimes of clusters is supposed to be wider than the that of the single bond lifetime, which can explain the very low α parameter we observe for this relaxation.

Tito et al. [6] recently proposed a thermodynamic model to explain why those clusters should exist. It is entropically more interesting to create clusters of physical bonds in a polymeric material, instead of randomly spreading those bonds along the polymer chains. Moreover, in polyelectrolytes such as ours, the positive ion linked to the chain will gather anions around it (here, Cl^- anions). Those anions will in turn gather other cations, facilitating again the formation of clusters of cations (and physical crosslinks).

This hypothesis is coherent with what we observed in Figure 2.18: the full dissociation of the cluster being controlled by the dissociation of the last coordination bond composing the cluster, the energy needed to dissociate the cluster of bonds is the energy needed to dissociate the last bond composing the cluster. This explains why we found the same activation energy for both relaxation modes.



Scheme 2.4: Schematic explanation of the existence of two different lifetimes for the physical crosslinks

2.4. Linear mechanical behavior at small deformations

We have demonstrated by DLS the presence of the two macroscopic relaxation modes attributed to the physical bond breaking dynamics (or clusters of them). Since they should be macroscopic (q independent), it should be possible to detect them in rheological measurements. We thus performed linear rheology experiments. We will start from a brief study of the bare chemical gel. This will be followed by a systematic study of the dual crosslink gels. We will first compare the “Diffusion” and “One-pot” dual crosslink hydrogels. Complex rheological responses of the dual crosslink gels will be characterized with a fractional derivative method. We will be able to fit adequately the hydrogel storage and loss moduli, and determine those two different characteristic times and their evolution with Ni^{2+} concentration, which we will be compared with the DLS results.

2.4.1. Rheology of a chemical gel

Rheological experiments were conducted on a bare chemical hydrogel, with no physical bonds. First, we verified the range of the linear domain. A strain sweep test at an angular frequency of 1 Hz was performed with a parallel plate geometry and the results are presented in Figure 2.19.

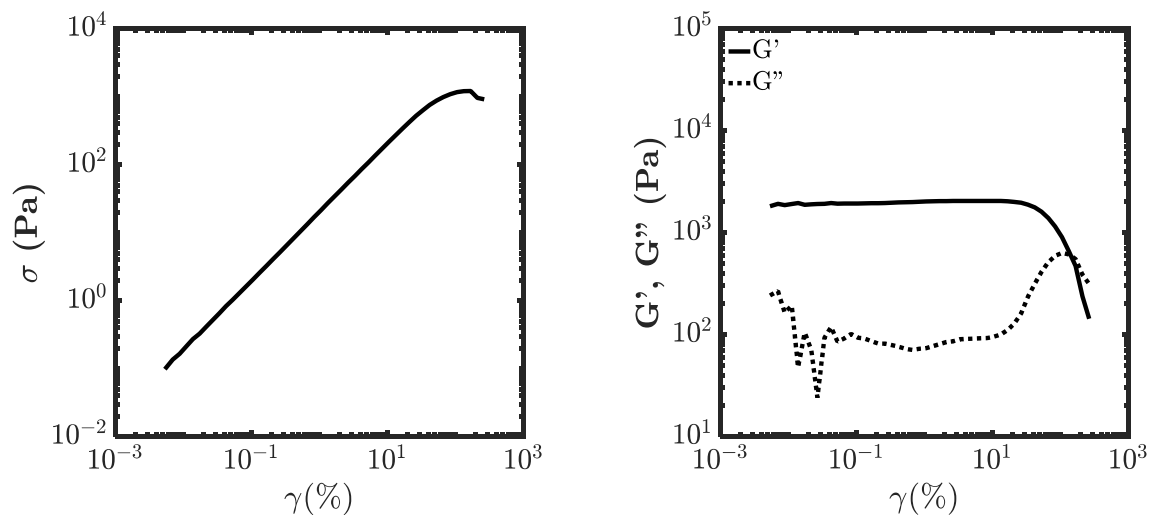


Figure 2.19: Shear stress-strain curve for a chemical gel (left), and corresponding storage and loss moduli (right).

The chemical gel exhibited a linear behavior until $\gamma = 10\%$ more or less. At large deformations, a strain softening behavior was observed: the elastic modulus started decreasing and the loss modulus increased. This behavior can be linked to a damaging of the material, or to the material slipping between the parallel plates at high shear. Since the sample exhibits the exact same behavior when we do once again the same experiment, we can imagine that it suffered no damage and simply slipped between the plates.

A frequency sweep test was performed, with a deformation rate set at 0.8% to ensure the gel stayed within its linear domain. The results shown in Figure 2.20 exhibited a typical rheological response of a chemical gel. We found an elastic plateau: the elastic modulus G' was almost constant with a weak frequency dependence, presumably due to the low chemical crosslinking ratio. The values of the loss modulus G'' were lower than those of G' for the whole frequency range. From the value of the plateau modulus, we can estimate a mesh size Ξ , with Eq. 2.12:

$$G' = \frac{kT}{\Xi^3} \quad \text{Eq. 2.12}$$

Using $G' \approx 1100$ Pa, we obtained $\Xi \approx 16$ nm.

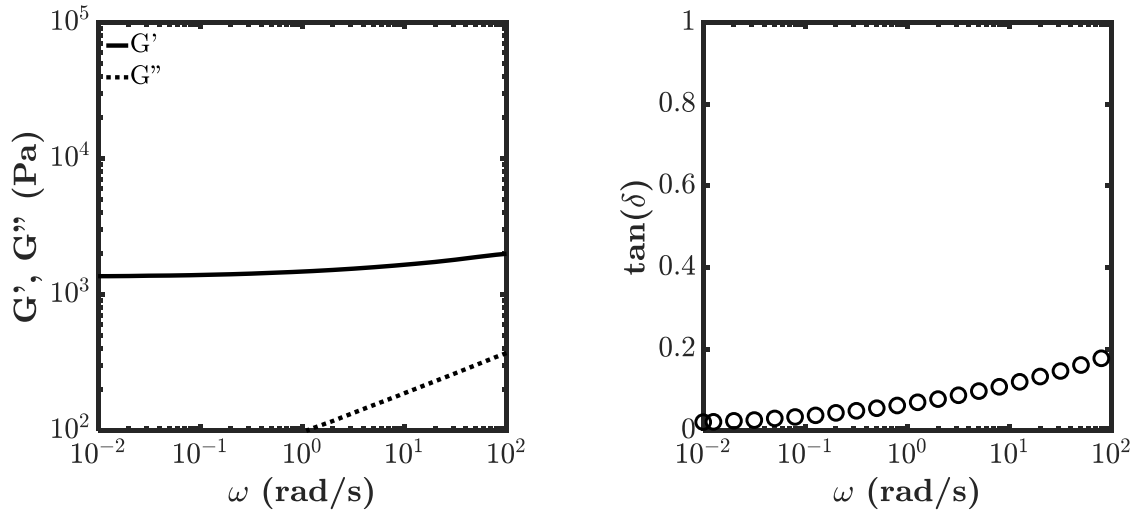


Figure 2.20: Storage and loss modulus (left) and corresponding $\tan(\delta)$ (right) for a chemical gel, at a deformation rate of 0.8%.

A stress relaxation test was also performed, in order to probe the dynamic behavior especially at long time scales. The values of the relaxation modulus were plotted as a function time in Figure 2.21.

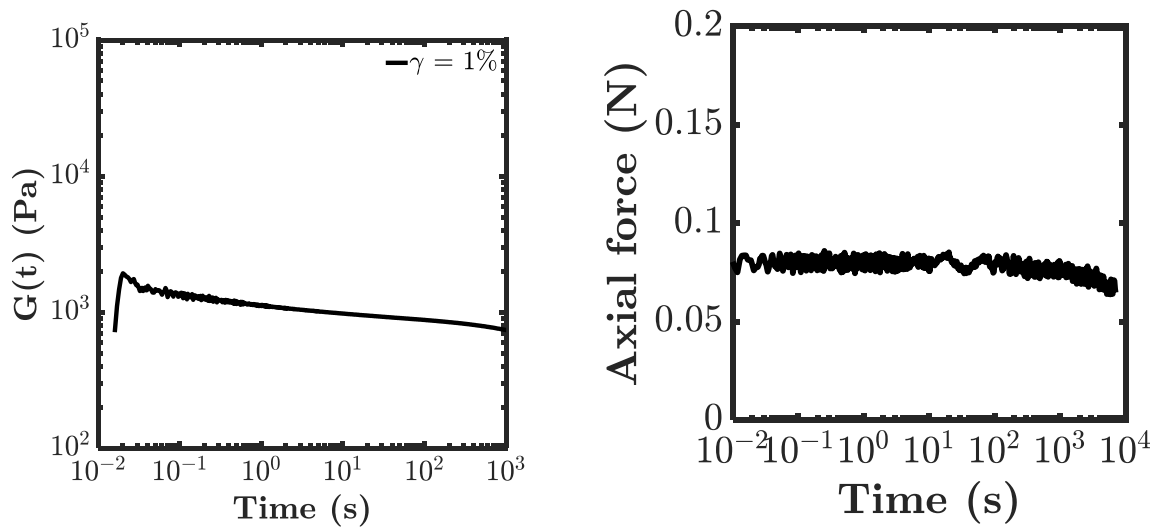


Figure 2.21: Shear modulus (left) and axial force applied by the rheometer (right) evolution over time under a constant shear strain of 1%, for three chemical gels with increasing crosslinker concentration.

Before the beginning of the experiment, we set the gap between the top and bottom plates of the rheometer so that the force applied to the sample was around 0.1 ± 0.03 N. The gap is usually around 1.2mm. The decrease in modulus we observe at longer times (around 10^3 seconds) is then linked to the material. We attributed this phenomenon to a poro-elastic behavior, the time scales being quite close to

2. Preparation and microstructure of a dual-crosslink hydrogel

what one can find when indenting a hydrogel with a sphere [7,8]. We will most certainly observe this behavior on the dual-crosslinked hydrogels.

2.4.2. Rheology of a “One-Pot” dual-crosslink hydrogel

a. General results

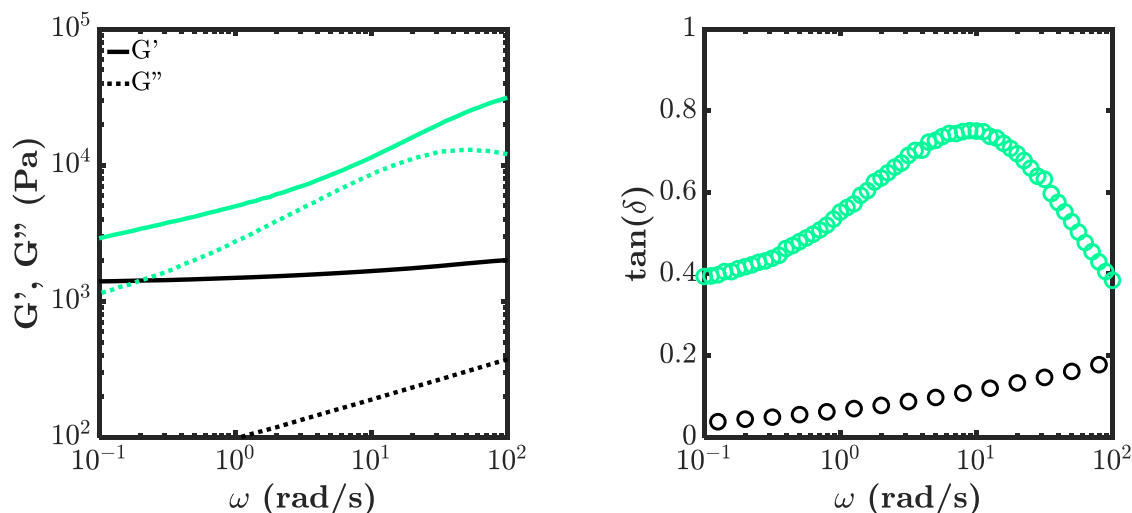


Figure 2.22: Storage and loss modulus (left) and corresponding $\tan(\delta)$ (right) of a “One-pot” dual-crosslinked hydrogel (light green) and the chemical gel (black), versus the frequency of the shear strain applied., with $[Ni^{2+}] = 100 \text{ mmol/L}$

During her PhD, Jingwen Zhao performed the same series of rheological measurements on the dual crosslink hydrogel prepared by the “one-pot” method [9]. In the following parts, we will try to extract characteristic times for these “one-pot” dual-crosslink hydrogels with varying Ni^{2+} concentration, and compare those times with the ones we found in DLS (Figure 2.17). Figure 2.22 shows the result of a frequency sweep test. The result of the chemical gel is also shown for comparison. First, we can see that the storage modulus increased after the incorporation of physical crosslinks, for the whole range of frequencies. The loss modulus also largely increased, which again is in agreement with the fact that our physical bonds should be dissipative. We noticed the following evolution in the moduli:

- At high frequencies, the storage modulus increased towards a plateau, and the loss modulus starts to decrease, giving a peak. This result suggests that the behavior of the dual crosslink gels moves toward that of a highly crosslinked chemical gel, where the physical bonds act as permanent bonds;
- At low frequencies, the storage modulus decreased towards that of the bare chemical gel. The dissipation modulus also decreases. This result suggests that the physically crosslinked chains will fully relax at lower frequency and will have no influence on the moduli of the network.

There is however one unexpected phenomenon: with decreasing frequency, the decrease in moduli seems to be slowed down, or the power-law behavior between 10^{-1} and about 2 rad/s was weaker than that in the higher frequency. This suggests the presence of a slower dissipation mechanism. This observation may be more visible in the evolution of $\tan(\delta)$ shown in Figure 2.22 (right), which seems to tend towards a plateau at lower moduli.

b. Influence of the temperature

In order to expand the accessible frequency range, a time-temperature superposition was performed. First the same frequency sweep test was done on this “One-pot” dual-crosslink gel at different temperatures (5 – 25 °C), as shown in Figure 2.23. We obtained the same rheological responses for all the temperature tested, while the curves were horizontally shifted to lower frequency with increase in the temperature. Practically no vertical shift was observed. A time-temperature superposition was performed with $T = 25\text{ °C}$ as reference temperature. The resulting mastercurves are plotted in Figure 2.24. Both moduli in the whole frequency range were well superposed on the mastercurves. These curves allow us to complete the observations that we did for a single temperature: the data at higher shifted frequency were added to evidence clearly the dissipation peak as well as the elastic plateau at high frequencies. It is also important to note that, from the Arrhenius plot of the horizontal shift factors shown in Figure 2.24, we can estimate an activation energy of around 70 kJ/mol, which is very close to the value determined by the DLS measurement in 2.3.3. The vertical shift-factors showed no significant evolution with temperature, or the change in the enthalpy of crosslinking was small at this condition. Note that the chemical gel did not show particular temperature dependence (data not shown).

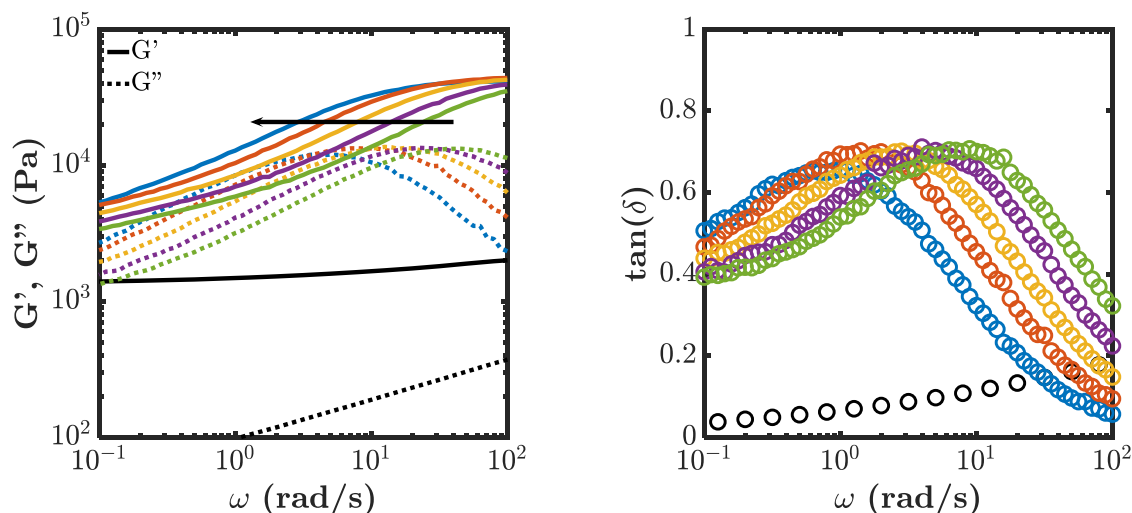


Figure 2.23: Storage and loss modulus (left) and corresponding $\tan(\delta)$ (right) of a “One-pot” dual-crosslinked hydrogel with $[Ni^{2+}] = 100\text{ mmol/L}$ versus shear frequency, at decreasing temperatures (arrow).

To summarize, we observed two relaxation modes due to the transient physical crosslinks and a low-frequency elastic plateau due to the permanent chemical crosslinks. Those three evolutions additively contribute to the the dynamic moduli of the dual crosslink gel. The fact that the whole curves can be shifted and well superposed indicates that the dynamics in this frequency range are governed by the same process, which is the dissociation of the transient crosslinks followed by the chain relaxations. Both dynamic relaxations have then, as shown with DLS experiments, the same activation energy and are linked to the same phenomenon.

2. Preparation and microstructure of a dual-crosslink hydrogel

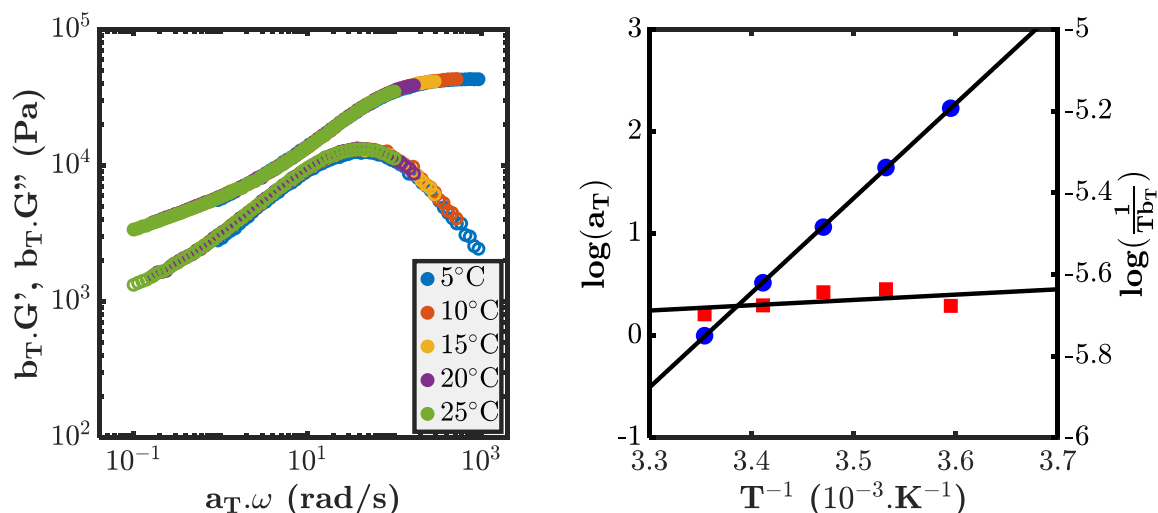


Figure 2.24: Mastercurves of G' and G'' (left) for a “One-pot” dual-crosslink hydrogel with $[Ni^{2+}] = 100$ mmol/L, and corresponding horizontal (a_T , blue) and vertical (b_T , red) shift-factors. $T_{ref} = 25^\circ C$, from the data in Figure 2.23.

2.4.3. Comparing “One-pot” and “Diffusion” dual-crosslink hydrogels.

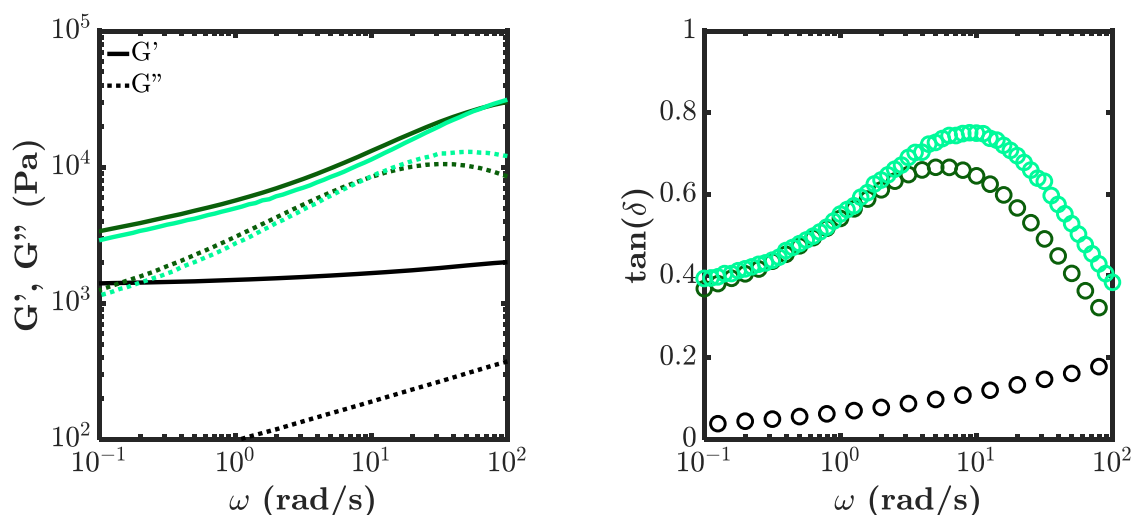


Figure 2.25: Storage and loss moduli (left) and corresponding $\tan(\delta)$ (right) as a function of the shear frequency, for a chemical gel (black), a “One-pot” dual-crosslink gel (light green) and a “Diffusion” dual-crosslink gel (dark green), both with $[Ni^{2+}] = 100$ mmol/L.

Let us briefly comment on the comparison between the “one-pot” and “diffusion” dual crosslink hydrogels. Figure 2.25 shows the results of a small amplitude oscillatory shear experiment for both types of dual-crosslink gels. Their rheological responses were found practically the same. The “One-pot” hydrogel exhibited slightly higher values of G'' and frequency at the peak, while the differences in G' are little. At the low frequency range, no difference was observed.

2.4.4. Fitting with fractional model

a. Fractional model

Since the frequency sweep suggested the presence of two relaxation modes, it is necessary to compare them with those found by DLS measurements (Part 2.3). Though quantitative characterizations are required, a simple Maxwell model did not fit this data. Thus, we used a fractional derivative model [10-12], with two fractional elements (one for the fast relaxation time, one for the slower) and a purely elastic element (representing the chemical network), additively contributing to the shear modulus as shown in Eq. 2.13:

$$G^* = G_0 + \frac{G_1(j\omega\tau_1)^{\alpha_1}}{1 + (j\omega\tau_1)^{\alpha_1}} + \frac{G_2(j\omega\tau_2)^{\alpha_2}}{1 + (j\omega\tau_2)^{\alpha_2}} \quad \text{Eq. 2.13}$$

where G_0 is the modulus at the low frequency range, supposed to be equivalent to the modulus of the chemical gel (around 1100 Pa here), G_1 and G_2 the moduli of the fractional derivative elements, τ_1 and τ_2 their characteristic times. The parameters α_1 and α_2 represent the fact that the dynamic of each fractional element is not defined by one characteristic time, but by a distribution of characteristic times around a mean value (here τ_i), just as the same parameters α_i were used in DLS.

The result of the fit for the “One-pot” dual-crosslink hydrogel is shown, for the storage modulus, in Figure 2.26. In this figure, we can see clearly the contribution of each of the three elements of the model. Both dynamic fractional elements show very distinct characteristic times.

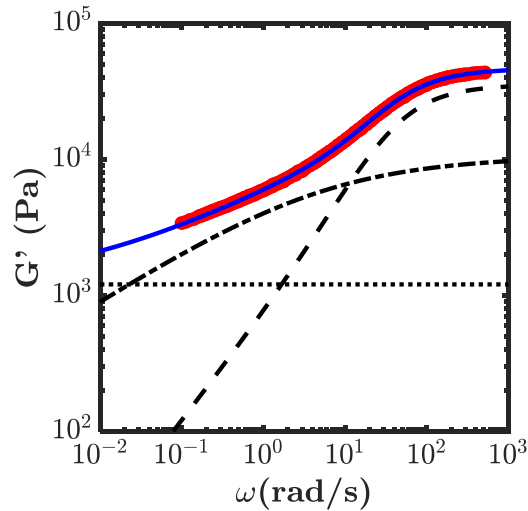


Figure 2.26: Fitting of the storage modulus G' of a dual-crosslinked gel with $[Ni^{2+}] = 100 \text{ mmol/L}$, by the model given in Eq. 2.13.. Red circles: experimental data – Blue line: Complete fit – Dotted black lines: contributions of each of the elements in the model.

b. Moduli evolution

Thanks to this fitting, we obtained a value for the plateau of the storage modulus at high angular frequencies, for each mode. The obtained values of the elastic moduli are shown in Table 2.6. Both G'_1 (for high frequency mode) and G'_2 (for low frequency mode) increased with the Ni^{2+} concentration, and for all the concentrations tested here we found $G'_1 > G'_2$.

2. Preparation and microstructure of a dual-crosslink hydrogel

In order to further study the efficiency of the transient crosslinks in this dual crosslink hydrogel, from the value of the moduli G_1' and G_2' , we calculated the concentration of the effective physical crosslinks per volume, corresponding to the two elastic modes, by using a formula given by the affine network theory:

$$G' = \frac{f}{2} \nu RT \quad \text{Eq. 2.14}$$

where ν is the density of crosslinks in the gel (in mol/L) and f is the functionality of the crosslinks. From the results shown in part 2.2, we supposed that the valence of the metal-ligand coordination bond is two (one Ni^{2+} ion with two imidazole ligands) for the majority of the transient crosslinks, thus it results in a functionality $f = 4$.

In Table 2.6 the concentrations of the elastically active transient crosslinker concentrations, which are equivalent to Ni^{2+} concentrations in the crosslinks are plotted as a function of the Ni^{2+} concentration in the feed. From the binding isotherm, we estimated the concentration of Ni^{2+} forming complexes in the hydrogel (Table 2.4). We thus calculated the efficiency of the crosslinks, $(\nu_1 + \nu_2) / [\text{Ni}^{2+}]_{\text{crosslinking}} = \nu_{\text{total}} / [\text{Ni}^{2+}]_{\text{crosslinking}}$.

Table 2.6: Storage moduli of both fractional elements G_i' and corresponding crosslinking density ν_i for “One-pot” dual-crosslink hydrogels with varying Ni^{2+} concentration.

$[\text{Ni}^{2+}]$ (mmol/L)	G_1' (kPa)	G_2' (kPa)	G_{total}' (kPa)	ν_1 (mM)	ν_2 (mM)	ν_{total} (mM)	efficient crosslinks
5	4.66	1.62	6.28	0.94	0.33	1.27	25.4%
20	24	5.38	29.38	4.85	1.09	5.94	36.4%
100	35.5	10.6	46.1	7.16	2.13	9.29	23.5%

We found relatively low crosslinking efficiencies, about 25 – 35%. However, it should be noted that the experiments realized in a rheometer with a plate-plate geometry underestimate the values of modulus, compared to that measured with a cone-plate geometry, or that measured by tensile biaxial stretch tests. Comparison with the tensile tests suggests that a factor of 2 will be systematically found. Taking this into account, we reach cross-linking efficiencies of about 50 to 70%. These values are reasonable, as the absorption isotherm cannot distinguish the bis-complexes forming elastically active crosslinks from those forming elastically inactive crosslinks, and the true concentration of the elastically active crosslinks should be lower than $[\text{Ni}^{2+}]_{\text{crosslinking}}$.

For comparison purposes, the efficiency for the chemical crosslinks was calculated. From the plateau modulus of the chemical gel, $G_0' = 1100$ Pa, corresponding to the effective crosslinker concentration of 0.22 mmol/L, the crosslinking efficiency was estimated to be $0.22/3 * 100 = 7.4\%$, which is low but not unexpected for a chemical gel with a low crosslinking degree from what has already been shown in the literature.

c. Characteristic times and comparison to DLS measurements

As shown above, we found two dynamic modes corresponding to the macroscopic relaxation of the dual crosslink gel by the two different techniques, dynamic light scattering and rheology. We compared the results of the two methods. We investigated the physical crosslinker concentration dependences.

First we compared the characteristic times. Figure 2.27 shows the evolution of the characteristic times measured by DLS (intermediate and slow modes) and by rheology, as a function of Ni^{2+} concentration. For both modes, the results from the two experiments are in good agreement, indicating that by two independent techniques one can measure the macroscopic chain relaxation modes. The values of the faster characteristic time (for the DLS ‘intermediate mode’, and ‘high frequency mode’ in rheology) were found around 0.01 s, slightly increasing with crosslinker concentration. The same trend was observed for the slow mode, whose characteristic time was found between 0.1 and 1 s. This increase can be explained by the probability of the bond reassociating with the same ligand. At low Ni^{2+} concentrations, there are more imidazole ligands available, thus, when a Ni^{2+} - Imidazole complex dissociates, it is easy for the Ni^{2+} to complex with another Imidazole to change a pair, allowing chain relaxation. When Ni^{2+} concentration increases, there are less imidazole ligands available in the vicinity of the dissociated bond. Thus the probability for the Ni^{2+} to reform a complex with the same imidazole ligand that it has just dissociated with increases, preventing the chain relaxation to occur.

The parameter α in equations Eq. 2.11 and Eq. 2.13 describes the dispersity of the characteristic times of the dynamic modes. The values of α determined by the two techniques were plotted in Figure 2.27 as a function of $[\text{Ni}^{2+}]$ for comparison. The dispersion of the data from DLS was rather large, and we do not discuss the Ni^{2+} concentration dependence. Still, we can conclude that the values we obtained from both experiments are close. The values of α for the slow mode were reasonably smaller than those of the intermediate mode, suggesting that the slow mode shows a larger dispersion of characteristic times.

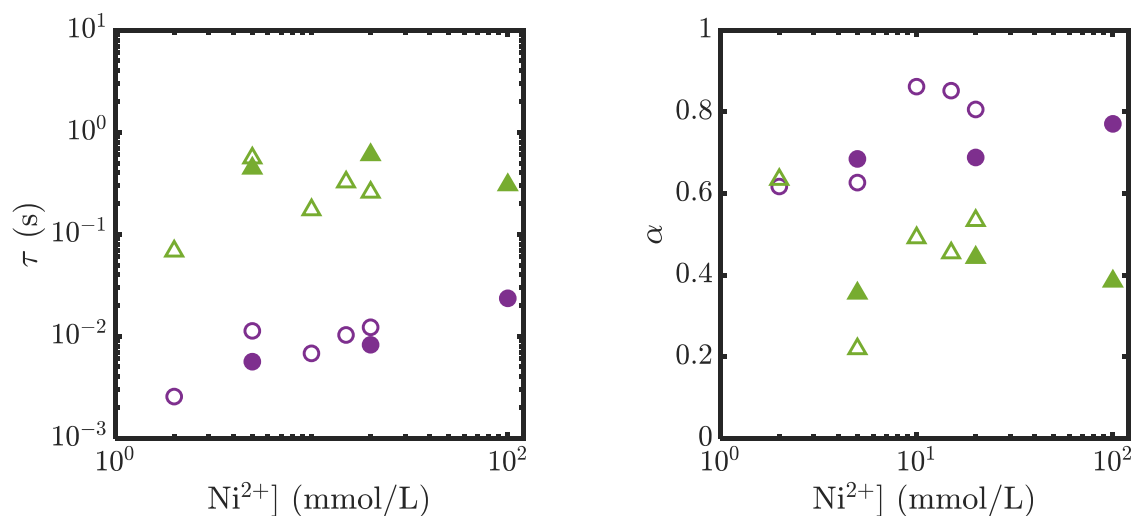


Figure 2.27: Left - Characteristic times measured in DLS (empty points) and rheology (filled points), for both intermediate (circles) and slow (triangles) modes, as a function of $[\text{Ni}^{2+}]$; Right - parameter α measured in DLS (empty points) and rheology (filled points), for both intermediate (circles) and slow (triangles) modes, as a function of $[\text{Ni}^{2+}]$.

From both experiments, we have determined the values of the activation energy, which we can now compare on Figure 2.28, as a function of Ni^{2+} ion concentration. By rheology we found only one horizontal shift factor to superpose both dynamics, thus the two modes have the same activation energy. And we found that the activation energies measured in rheology agreed well with those of the intermediate and slow modes observed in DLS. The activation energy of those two modes, linked to the

2. Preparation and microstructure of a dual-crosslink hydrogel

physical crosslinks, slightly increased at low Ni^{2+} concentrations, and saturated around a value of 80 kJ/mol.

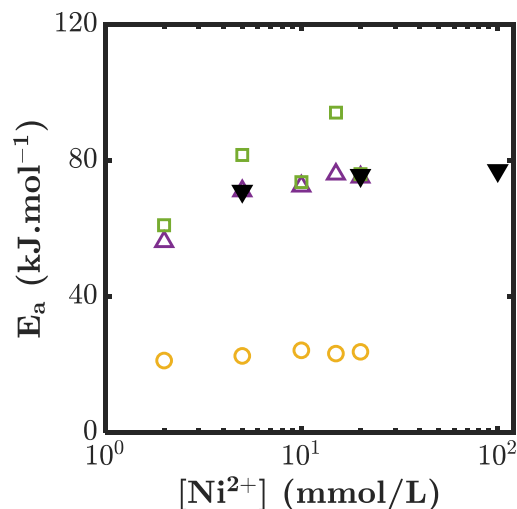


Figure 2.28: Activation energy measured in each experiment. Full triangles: rheology results – Empty shapes: DLS results for the three different modes (circles: fast mode; triangles: intermediate mode; squares: slow mode).

2.4.5. Relaxation experiments

While oscillatory shear is perfectly adapted to investigate fast relaxation modes, it becomes inconvenient to go above 10-30 seconds and relaxation experiments as a function of time become more convenient. Figure 2.29 shows the relaxation modulus measured at different strains for a “Diffusion” dual-crosslink gel. We observed a fast decrease at short times (< 1 s), followed by a second moderate decrease which continued until around 100 s. At a time of the order of several hundreds of seconds, the poro-elastic behavior started to appear. This behavior should be equivalent to that observed by a frequency sweep: the two relaxation modes are exhibited.

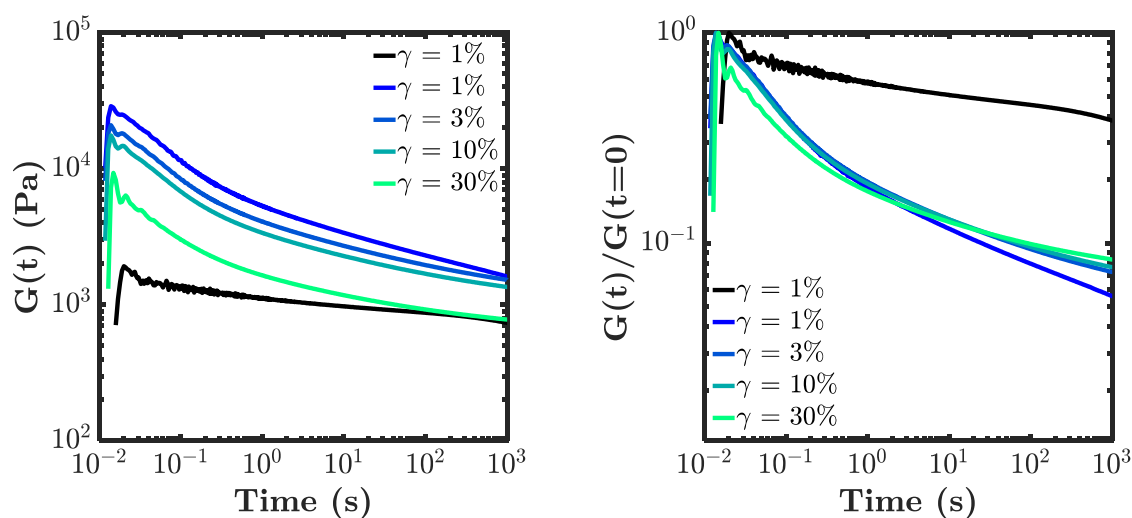


Figure 2.29: Shear modulus $G(t)$ versus time in a relaxation experiment for a chemical gel (black) and a “Diffusion” dual-crosslink hydrogel at different shear strains (from blue (lower strain) to green (higher strain)).

Importantly we found a strain dependence of the relaxation modulus: the relaxation modulus decreased with increasing strain. In the linear domain ($\gamma < 10\%$), the effect was weak, while for $\gamma = 30\%$ in the nonlinear domain, the slower mode seems to disappear, and/or the relaxation became faster (as seen in Figure 2.29 right). This result implies that the physical bonds are sensitive to the force applied on them. The higher the force, the lower the lifetime of the physical bond. This is to be expected for any transient physical system: the energy barrier to overcome in order for the physical bond to open is decreased by applying a tension on the physical bond. It is different, however, from what has been previously demonstrated in PVA-Borax gels.

2.4.6. Conclusions

We have seen that the difference of behavior, in linear rheology, between “One-pot” and “Diffusion” hydrogels is minor, justifying the DLS study of the “one-pot” hydrogel.

The close study of the results obtained from rheology, fitted with a fractional derivative model, show that two relaxation modes exist. All the results we find point to the fact that those two modes can be related to the ‘intermediate’ and ‘slow’ mode we have demonstrated with DLS measurements. They possess the same activation energy, the same characteristic times and very close stretching parameters α . The high frequency mode we see in rheology should then be the relaxation of polymer chains linked to the breaking of physical bonds. The mode at low frequencies is explained by the relaxation of the clusters of physical bonds, which we suspect exist in our dual-crosslinked hydrogel.

Finally, the characteristic relaxation time observed at high frequencies or short times, and related to the opening of a physical bond, is visibly dependent on the force applied on the hydrogel. Which in turn implies that, in large deformations where the loads applied on the crosslinks are much higher, the behavior of the gel might diverge from what we expected. A systematic study on the nonlinear mechanics of the dual crosslink gels will be shown in the next chapters.

2.5. Small-Angle X-Ray scattering experiments

In 2.3.4, we have attributed the slow dynamic of our dual-crosslink hydrogel to the presence of clusters of physical bonds. This slow dynamic could have some important influence on the mechanical properties of the dual-crosslink hydrogels. To try to prove the existence of clusters of physical crosslinks in our hydrogels, we will now see some Small-Angle X-ray Scattering (SAXS) experiments. These experiments were conducted at the Laboratoire Léon Brillouin, at CEA Saclay, with Dr. Annie Brûlet. This technique uses X-ray beams to quantify sizes and distances at the nanoscale. Those lengths may in turn be related to two characteristic lengths we have already found previously, in DLS and rheology measurements.

2.5.1. SAXS – Principle and protocol

a. Principle of the method

Small Angle X-Ray Scattering is a tool to analyze the spatial organization inside a material. This technique can identify spatial correlations present in the structure of the material. These correlations can for example be related to the size of or distance between the particles in a filled polymeric material. These elements will elastically scatter X-Rays, and the scattered light will create a pattern in reciprocal

2. Preparation and microstructure of a dual-crosslink hydrogel

space. This pattern is then studied, and structural information is gathered from it. In general, the diffraction pattern consists of peaks of intensity, and the angle at which is situated the peak can be related to a characteristic distance in the material.

The detector is a 2-D detector. The diffraction pattern measured is hence an image, with at the center the incident beam of unscattered X-rays. Each characteristic distance in the material will scatter X-rays at a certain distance on the image from the incident beam. In an isotropic material, the diffraction pattern will depend only on the distance from the incident beam. One characteristic length will give a ring centered on the incident beam. The distance between the incident beam and the position of the ring will give an angle θ (Figure 2.30).

The sample being isotropic, the image can be integrated along the azimuth (see Figure 2.30), giving a 1-D signal that can be plotted versus the scattering vector q :

$$I(q) = \int I(q, \psi) d\psi \quad \text{Eq. 2.15}$$

$$q = \frac{4\pi}{\lambda} \sin\left(\frac{\theta}{2}\right) \quad \text{Eq. 2.16}$$

The incident beam is of high intensity and can damage the detector. To avoid this, it is then hidden by a “beam stop” placed on the detector, which absorbs the X-Rays. Depending on the distance between the sample and the detector, not all θ angles are accessible: if the detector is too close, the smaller angles will be hidden by the beam stop. As we will see, we have used two configurations of the experimental set-up to collect data over a wider range of scattering vectors.

In our case, we hope to find a distance that we could relate to a distance between clusters of Ni^{2+} ions (i.e. physical bonds) in our dual-crosslink hydrogel.

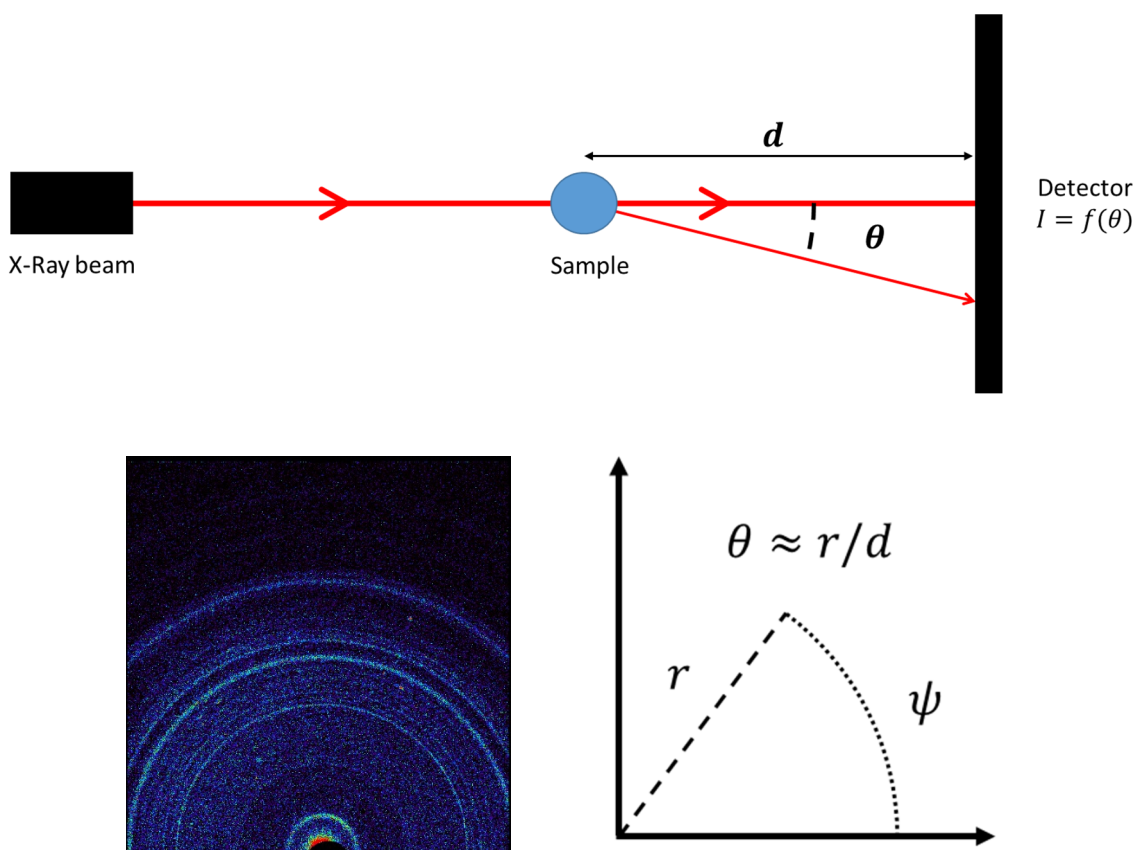


Figure 2.30: *Top:* Schematic representation of the X-Ray diffraction set-up and the angle θ . *Bottom:* 2-D acquisition of X-Ray scattering. Blue is low X-Ray intensity, red is high X-Ray intensity. Red point in the bottom is the incident beam, only half-hidden by the beam stop (black). Each ring is representative of one characteristic length that can be found in the sample. Image is the first X-ray view of Martian soil, 2012, from: https://www.nasa.gov/mission_pages/msl/multimedia/pia16217.html

b. Protocol

SAXS experiments were carried out on the Xeuss 2.0 apparatus of LLB installed in the SWAXS Lab (Saclay, France). The instrument uses a micro-focused Cu K_{α} source (wavelength of 1.54 Å, 8 keV). Mirrors placed just at the exit of the generator focus the X-rays. Two slits systems of variable aperture are placed at a fixed collimation distance of about 1.2 m from the mirrors. They define the width of the incident beam. Those slits are made of single crystals: they do not scatter the X-rays at low scattering vectors (so-called ‘scatterless slits’).

The beam passes through the sample, where it is scattered. The scattered X-rays are collected on a CCD screen sensitive to X-Rays (a Pilatus3 1M detector from Dectris, Switzerland), at a distance d from the sample, with an integration time t . The incident light ($\theta = 0^{\circ}$) is cut off by an X-Ray absorbing material called the beam stop. This creates a loss of data at the smaller angles, but protects the detector from high intensities.

Two configurations allow to cover a broad q range: first a sample to detector distance set to 2.494 m with a collimated beam size of $0.3 \times 0.3 \text{ mm}^2$ to achieve a q range from 0.003 to 0.035 \AA^{-1} ; second, a sample to detector distance set to 0.539 m with a collimated beam size of $0.8 \times 0.8 \text{ mm}^2$ to achieve a

2. Preparation and microstructure of a dual-crosslink hydrogel

q range from 0.02 to about 1 \AA^{-1} . For the “medium-angle” set-up, the scattered light was collected during an integration time $t = 15 \text{ min}$. For the “small-angle” set-up, $t = 120 \text{ min}$.

The sample of hydrogels were placed between two thin sheets of Nalophan (PET), tightly sealed with tape in order to avoid the drying of the hydrogel during the experiment. This “container” slightly scatters X-rays. This scattering was measured and subtracted from the experimental data (following protocol from [13] and [14]). The scattering of the beam itself, with no sample, was measured and subtracted in the same way. Finally, the electronic noise of the experiment was measured (with no incident beam) and also subtracted from the data. Data were normalized to absolute units using the calibration of the direct beam flux determination, and the thickness of the sample considered. All of these corrections were done for both set-ups. The data from both set-up were then simply concatenated, and superposed well. Lastly, a constant background, the value of the minimum scattering signal obtained at large scattering vector, has been subtracted to the scattering intensity.

The long exposure times mean that we need to make sure the hydrogel does not dry. To do so, we decomposed the two hours of acquisition in two acquisitions of 1h, the second acquisition done 5h after the first. The two experiments superposed well, proving that the state of the gel did not change.

Absorption of X-Rays by air can be very problematic, especially at long distances. Thus, the scattered X-Ray beam travels through a tube placed under vacuum.

2.5.2. Qualitative analysis

a. Results for a “One-pot” dual-crosslink hydrogel

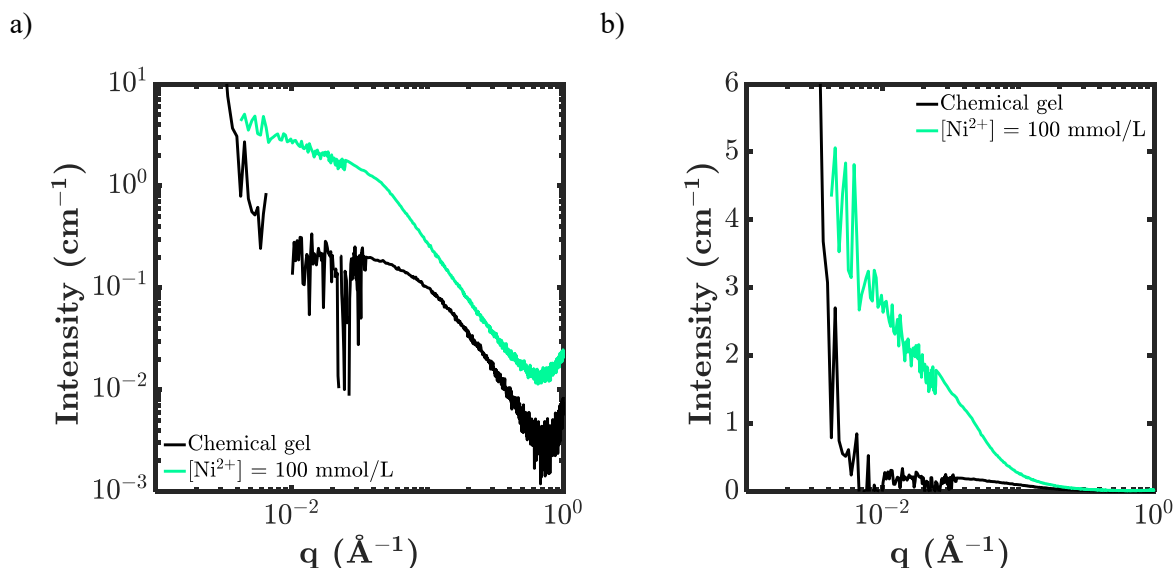


Figure 2.31: X-Ray intensity, normalized by the thickness of the sample, as a function of the scattering vector, for a Chemical gel (black) and a “One-pot” dual-crosslink hydrogel with $[\text{Ni}^{2+}] = 100 \text{ mmol/L}$ (green); a) log-log plot; b) linear-log plot

A SAXS measurement realized on a “One-pot” dual-crosslink hydrogel with $[\text{Ni}^{2+}] = 100 \text{ mmol/L}$ gives the scattered intensity curve shown in Figure 2.31 (in log-log plot in figure a, and in semi-log plot in figure b). The chemical gel did not show any clear peak of scattered intensity. The dual-crosslink gel however showed a shoulder of a peak at lower q -values. The dual-crosslink gel also shows an increase

in the scattered intensity at $q > 0.8 \text{ \AA}^{-1}$, but this increase is very low (not visible on the linear plot for example) and corresponds to distances or sizes that are largely inferior to what we expected to find in our hydrogel ($d \sim 2\pi/q < 7.8 \text{ \AA}$), certainly linked to monomer-monomer interactions [14].

It is also possible to study the same data in a so-called ‘‘Kratky’’ plot, as shown in Figure 2.32. A polymer in solution, whose orientation follows a random walk, would have a scattered X-Ray intensity decreasing in q^{-2} . Hence, plotting $I(q) \times q^2$ (as done in the Kratky plot) on that polymer should give a plateau at intermediary values of q (typically below 0.3). This graph allows one to see how the organization of the studied polymer deviates from the ideal situation. We see here in Figure 2.32 a shoulder appearing at $q \approx 0.05 \text{ \AA}^{-1}$, showing again the existence of an organization of the Ni^{2+} ions inside the gel.

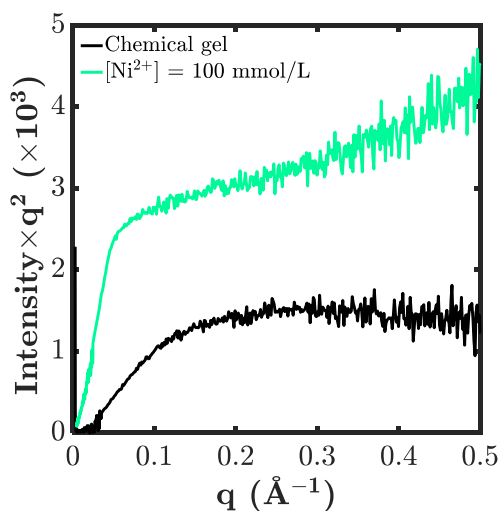


Figure 2.32: Kratky plots showing $I(q) \times q^2$ as a function of the scattering vector, for a Chemical gel (black) and a ‘‘One-pot’’ dual-crosslink hydrogel with $[\text{Ni}^{2+}] = 100 \text{ mmol/L}$ (green).

b. Influence of the preparation method

With this technique, it is possible to compare the structure of a ‘‘One-pot’’ and a ‘‘Diffusion’’ dual-crosslink gel. This is what Figure 2.33 shows. In this figure, we can see that the 1-D scattering is different between the two gels: there seems to be a structural difference at the small q range. The shoulder we observed for the ‘‘One-pot’’ hydrogel seems to have been shifted to lower q values, and is partially hidden by the increase in intensity linked to incident beam. This shift implies that the characteristic distance between the clusters of bonds increases if the dual-crosslink gel is prepared by diffusion. At the intermediate q range around 0.1 \AA^{-1} , the values of the intensity for the two gels were identical. On the Kratky plot, we also see a change in the scattering at higher q -values between 0.1 and 0.4: where the ‘‘Diffusion’’ gel shows a slightly decreasing plateau, the ‘‘One-pot’’ gel shows a steady increase. However, the values at low intensity could be influenced by the precision and repeatability of the baseline measurements, it is difficult to conclude that this difference is related to change in the microstructures.

It is reasonable to think that the existence of the ion complexes before the initiation of the polymerization might influence the creation of clusters, either by electrostatic interaction or by changing the reactivity of the vinyl-imidazole. In this second scenario, the vinylimidazole would then react more slowly than the acrylamide and be integrated in the network in clusters, after all the acrylamide monomers.

2. Preparation and microstructure of a dual-crosslink hydrogel

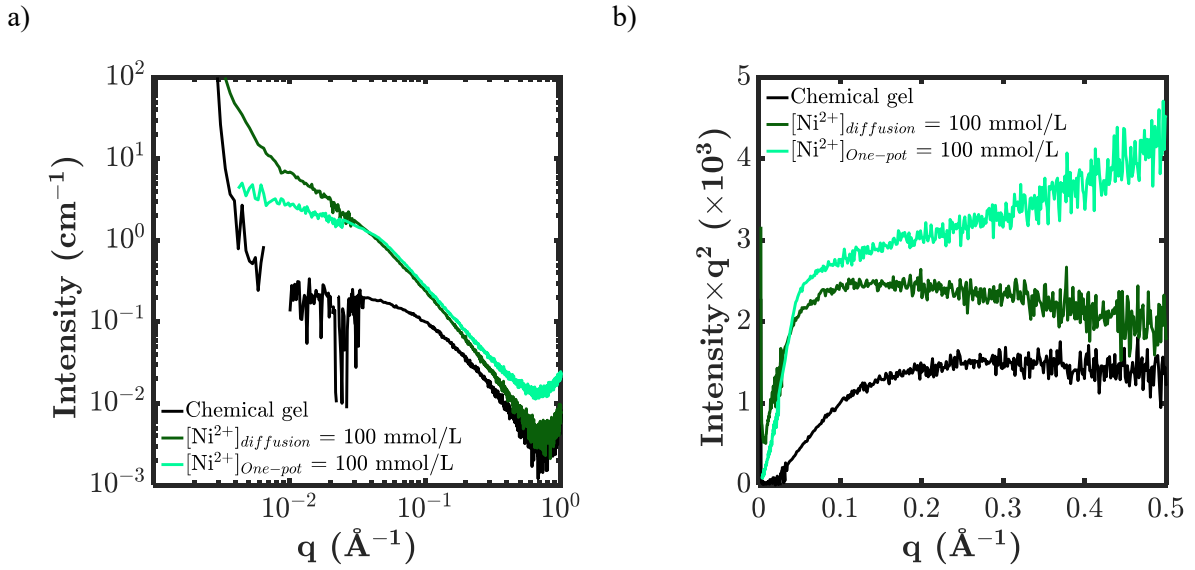


Figure 2.33: a) log-log plot of X-Ray intensity, normalized by the thickness of the sample, as a function of the scattering vector and b) Kratky plots for a chemical gel (black), a “One-pot” dual-crosslink hydrogel (aquamarine) and a “Diffusion” dual-crosslink hydrogel (dark green).

c. Influence of Ni²⁺ concentration

It is also interesting to study the influence of the concentration in Ni²⁺ ions on the structure of the gel. In Figure 2.34, we can see 1D SAXS scattering patterns for “Diffusion” dual-crosslink hydrogels with an increasing concentration in Ni²⁺ ions. We can see, especially on the Kratky plots, a clear change of behavior in those dual-crosslink gels. There is still a peak at $q \approx 0.05 \text{ \AA}^{-1}$ for each of them, but the gel with the lower ionic concentration shows a different behavior at larger q -values, with a clear plateau implying a dependence in q such as $I(q) \sim q^{-2}$, while the gels at $[\text{Ni}^{2+}] = 40$ and 100 mmol/L show a decrease, with this time $I(q) \sim q^{-m}$ with $m > 2$.

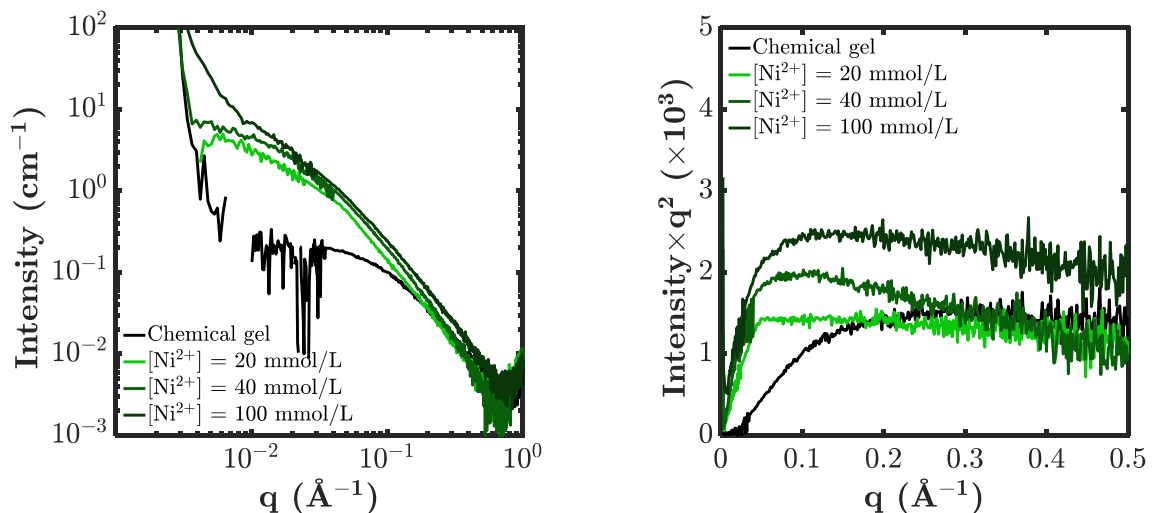


Figure 2.34: a) log-log plot of X-Ray intensity, normalized by the thickness of the sample, as a function of the scattering vector and b) Kratky plots for a chemical gel (black) and “Diffusion” dual-crosslink hydrogels with increasing concentration in physical crosslinks (light green to dark green).

2.5.3. Attempt at quantitative analysis

With these SAXS measurements, we could obtain an idea of the size of the clusters in the hydrogel. However, in order to do that, we need to select the right model to fit the data among the many possibilities existing in the literature. Let us first study the case of a “Diffusion” dual-crosslink hydrogel with $[Ni^{2+}] = 100 \text{ mmol/L}$.

a. Choice of a fitting model

In neutron-scattering experiments, in the case of polymer solutions, in a semi-dilute regime and for $q\xi \gg 1$, the scattered intensity is well described by a Lorentzian equation:

$$I(q) \sim \frac{I_L}{1 + q^2\xi^2} \quad \text{Eq. 2.17}$$

Where ξ represents the polymer-polymer correlation length in the solution, or the size of a “blob” composing the polymer chain. In order to take into account the crosslinking of the polymers, some modifications of this equation can be made. For now, we can try fitting equation Eq. 2.17 to our SAXS results. With $\xi = 30 \text{ \AA}$ and $I_L = 2.5$, it gives the result in Figure 2.35.

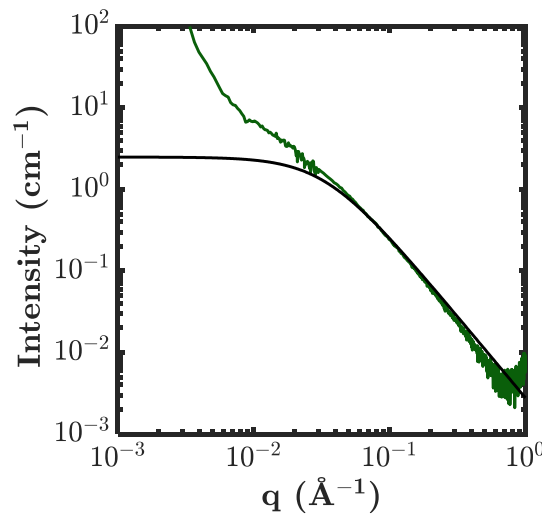


Figure 2.35: SAXS measurement of a “Diffusion” dual-crosslink gel with $[Ni^{2+}] = 100 \text{ mmol/L}$ (green) and corresponding Lorentzian equation (black).

The fitting is not perfect, especially at low values of the scattering vector since this equation is thought for the case where $q\xi \gg 1$. However, we still can see in our scattering data a trend that almost corresponds to the scattering of neutrons made by blobs of polymers in solution, when in our gels the scattering objects are the Ni^{2+} ions. This observation leads us to believe that the Ni^{2+} are split into two families: one, shown in 2.3, where the physical bonds (hence the ions) are grouped in clusters of bonds, and the other where the physical bonds are randomly distributed along the polymer network. This second family will then give a map of the polymer chains when analyzed by SAXS, which is why the scattered intensity shows a profile corresponding to an organization of polymers.

This hypothesis is further confirmed by the value of ξ we have used in Figure 2.35: $\xi = 3 \text{ nm}$ corresponds to the mean value of the correlation length of the polymer chains we have observed in DLS experiments (see Figure 2.16 right).

2. Preparation and microstructure of a dual-crosslink hydrogel

This means that we can try using the models commonly used in neutron scattering experiments to represent gels.

From Figure 2.35, we can extract two other useful information:

- There is a supplementary structural organization at lower values of q , implying the presence of a larger characteristic distance in the material;
- The slope of the logarithmic data curve, at higher values of the scattering vector, is a little bit lower than the slope of the Lorentzian (-2), which is what we observed on the Kratky plots.

The Lorentzian equation given in Eq. 2.17 represents well a polymer solution at equilibrium, but in a chemically crosslinked gel the polymer concentration fluctuations are perturbed. Certain arrangements of polymer chains are excluded because of the crosslinks and as a result, Eq. 2.17 no longer describes the scattering intensity. A supplementary contribution from those regions of the sample where movement is restricted must also be included in the equation. Mallam et al. have assumed a Gaussian spatial distribution for these regions, giving:

$$I(q) \sim I_G * \exp(-q^2 \Xi^2) \quad \text{Eq. 2.18}$$

This Gaussian spatial distribution of polymers can also be read here as a so-called ‘‘Guinier’’ function $I(q) = I_G \exp(-R_g^2 q^2/3)$, where $R_g = \sqrt{3}\Xi$ is the radius of gyration of the polymer rich (or poor) domains. This Gaussian contribution is therefore the same as the Guinier function. In addition to those long distance fluctuations in the local concentration, short-range solution-like fluctuations still need to be taken into account. These two contributions are assumed to be decoupled, which leads to:

$$I(q) = \frac{I_{L0}}{1 + q^2 \xi^2} + I_{G0} * \exp\left(-\frac{\Xi^2 q^2}{3}\right) \quad \text{Eq. 2.19}$$

This solution should take into account the structural organization at lower values of the scattering vector that we observe on our data, and the Guinier-part of this equation might give us an insight on the clustering of physical bonds in the gel.

However, it still assumes a decay in q^{-2} at larger values of q , which is not exactly the case for our dual-crosslink gels.

In order to represent properly the data we have from our SAXS experiments, we can try using this model developed by Mallam et al. and Shibayama et al. [16,17], and successfully applied to PVA-borate gels:

$$I(q) = \frac{I_{L0}}{\left(1 + \frac{m+1}{3} * q^2 \xi^2\right)^{m/2}} + I_{G0} * \exp\left(-\frac{\Xi^2 q^2}{3}\right) \quad \text{Eq. 2.20}$$

where they assumed that gels were composed of closely packed and uncorrelated domains of size ξ , in which the polymer chains were correlated to each other with the fractal dimension m . In their PVA gel in water, the reported value of m was ~ 2.6 to 2.8 . This exponent $m > 2$ was attributed to the presence of hydrogen bonding in the system. Since we also have here physical bonding between the polymer chains, this equation seems well adapted.

Considering the situation were $q \gg \xi^{-1}$, we could assume that the Guinier-part of Eq. 2.20 is negligible. Hence,

$$I(q) \sim \frac{I_{L0}}{\left(1 + \frac{m+1}{3} q^2 \xi^2\right)^{m/2}} \quad \text{Eq. 2.21}$$

Which in turn leads to

$$\ln\left(\frac{I_{L0}}{I(q)}\right) = \ln\left[\left(\frac{m+1}{3}\right)^{\frac{m}{2}} \xi^m q^m \left(1 + \frac{3}{(m+1)\xi^2 q^2}\right)^m\right] \quad \text{Eq. 2.22}$$

And if we consider $q \gg \xi^{-1}$,

$$\ln\left(\frac{I_{L0}}{I(q)}\right) = \ln\left[\left(\frac{m+1}{3}\right)^{\frac{m}{2}} \xi^m q^m\right] = m \cdot \ln(q) + m \cdot \ln\left[\xi \left(\frac{m+1}{3}\right)^{1/2}\right] \quad \text{Eq. 2.23}$$

Thus, by plotting $\ln(I(q)^{-1})$ versus $\ln(q)$, we should obtain (at high enough q values) a line which slope will be m as shown on Figure 2.36

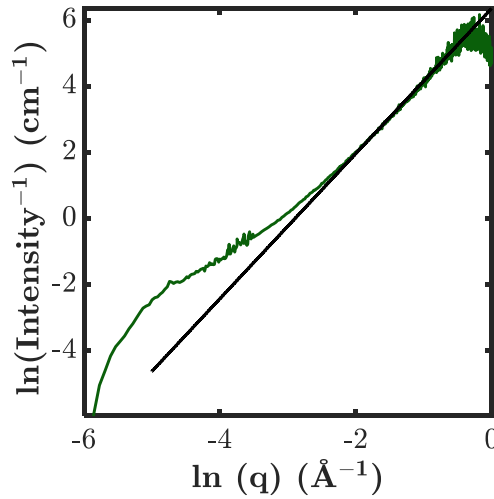


Figure 2.36: Natural logarithm of the inverse of the scattered intensity, as a function of the natural logarithm of the scattered vector.

The linear fitting made with $q > 10^{-1} \text{ \AA}^{-1}$ gives a slope $m = 2.19$. With this value, we can fit Eq. 2.20 to our data with $\xi = 3 \text{ nm}$, and I_{L0} , I_{G0} and R_g as fitting parameters. The result is shown on Figure 2.37.

2. Preparation and microstructure of a dual-crosslink hydrogel

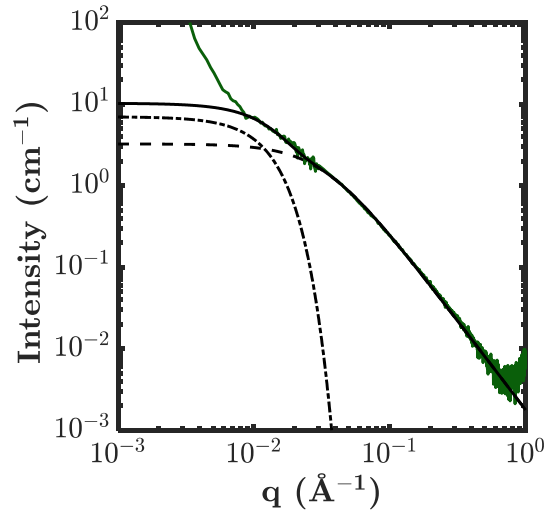


Figure 2.37: Scattered intensity versus the scattering vector for a “Diffusion” dual-crosslink gel with $[Ni^{2+}] = 100 \text{ mmol/L}$, fitting obtained with Eq. 2.20 (solid black line), and Guinier and stretched-Lorentzian components of Eq. 2.20 (dashed black lines).

The fit seems to be quite good. The strong increase in intensity at low q -values is related to the incident beam (according to Annie Brûlet). The values used and obtained from this fit are summarized in Table 2.7. Again, m and ξ are not fitting parameters but measured values. The value obtained for R_g is very interesting, since we actually find something of the same order of magnitude as the mesh size we obtained for the chemical gel in linear rheology (see 2.4.1).

Table 2.7: Parameters of Eq. 2.20 for “Diffusion” dual-crosslink gel with $[Ni^{2+}] = 100 \text{ mmol/L}$

Coefficient (units)	Value
I_{L0}	3.25
ξ (Å)	30
m	2.19
I_{G0}	7
Ξ (Å)	138

These results suggest that we have two scales of concentration fluctuations:

- At 3 nm, a concentration fluctuation of physical bonds associated to the free arrangement of polymer chains in the solution;
- At 14 nm, a fluctuation of concentration of the physical bonds associated to a clustering of those bonds. This length scale being very similar to the mesh size of the chemical network we could extract from rheology data (in 2.4.1), we can suppose that the physical bonds are clustering around the chemical crosslinks.

b. Fit results for other Ni^{2+} gels

We can now apply this model to the data obtained for the “Diffusion” dual-crosslink hydrogels with different $[Ni^{2+}]$ concentrations. Again, m was measured thanks to Eq. 2.23 as shown on Figure 2.36.

However, to ensure a good fitting of the model to our data ξ was set as a fitting parameter, with a starting value at 30 nm and free to move between reasonable bounds.

The fitted curves for the gels with $[\text{Ni}^{2+}] = 20$ and 40 mmol/L are shown on Figure 2.38.

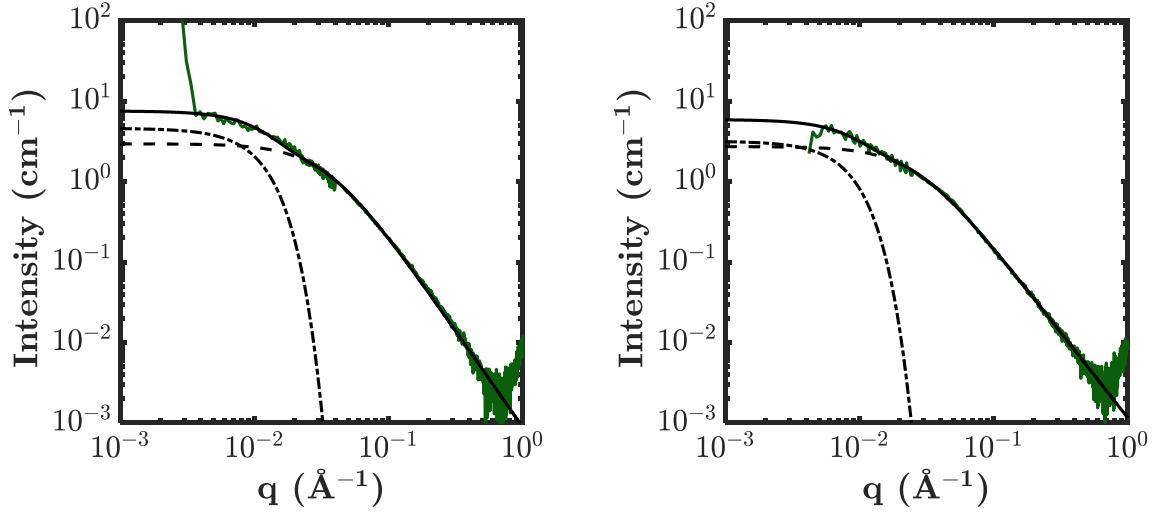


Figure 2.38: Scattered X-Ray intensity versus the scattering vector for a “Diffusion” dual-crosslink gel with $[\text{Ni}^{2+}] = 40$ mmol/L (left) and $[\text{Ni}^{2+}] = 20$ mmol/L (right); fitting obtained with Eq. 2.20 (solid black line), and Guinier and stretched-Lorentzian components of Eq. 2.20 (dashed black lines).

Both sets of data seem to be represented quite well by Eq. 2.20. The obtained parameters are summed up in Table 2.8. In this table, we can see that the intensity of the “stretched-Lorentzian” function decreases with $[\text{Ni}^{2+}]$, as does the intensity of the Guinier function. This seems quite natural, since we are decreasing the amount of scattering objects. However, I_{G0} decreases significantly more than I_{L0} , suggesting that the clustering of physical bonds is favored by a higher $[\text{Ni}^{2+}]$ concentration.

Both correlation lengths do not evolve much between 100 and 40 mmol/L. In the case of $[\text{Ni}^{2+}] = 20$ mmol/L, R_g increases to 20 nm and ξ to 3.74 nm. To explain this change in organization, we can try looking at the Kratky plot of this particular gel. It is presented in Figure 2.39.

Table 2.8: Parameters of Eq. 2.20 for “Diffusion” dual-crosslinked gels with $[\text{Ni}^{2+}] = 100, 40$ and 20 mmol/L, and for the “One-pot” dual-crosslinked hydrogel.

Coefficient (units)	$[\text{Ni}^{2+}] = 100$ mmol/L	$[\text{Ni}^{2+}] = 40$ mmol/L	$[\text{Ni}^{2+}] = 20$ mmol/L	$[\text{Ni}^{2+}] = 100$ mmol/L “One Pot”	Error
I_{L0}	3.25	2.94	2.72	1.99	± 0.01
ξ (Å)	30	27.5	37.4	29.6	± 0.15
m	2.19	2.4	2.13	1.84	± 0.05
I_{G0}	7	4.58	3.17	0.53	± 0.3
Ξ (Å)	138	155	201	33.1	± 20

In this figure, we can see that the model from Eq. 2.20 does not quite catch the form of the data obtained. The data shows a sharp transition from a linear behavior at low values of q to a plateau at higher values, which the model fails to represent. Since we are observing two linear evolutions, a closer model would be:

2. Preparation and microstructure of a dual-crosslink hydrogel

$$I(q) = \begin{cases} Aq^{-1} & \text{if } q \leq q_c \\ Cq^{-2} & \text{if } q > q_c \end{cases} \quad \text{Eq. 2.24}$$

This equation is completely empirical and has no real physical meaning. However, this might imply that Eq. 2.20 is not giving the exact picture of the structural organization in our gels, and that this picture might need to be refined to improve the model.

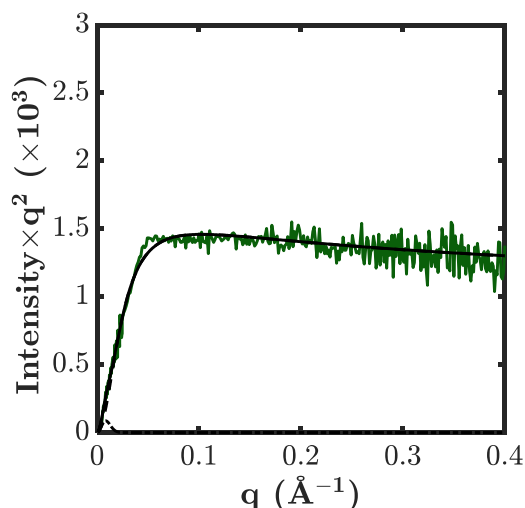


Figure 2.39: Kratky plot for a “Diffusion” dual-crosslink hydrogel with $[Ni^{2+}] = 20 \text{ mmol/L}$ (green) and corresponding fit by Eq. 2.20

This observation is also valid for the “One-pot” dual-crosslink hydrogel, shown in Figure 2.40 and in Table 2.8.

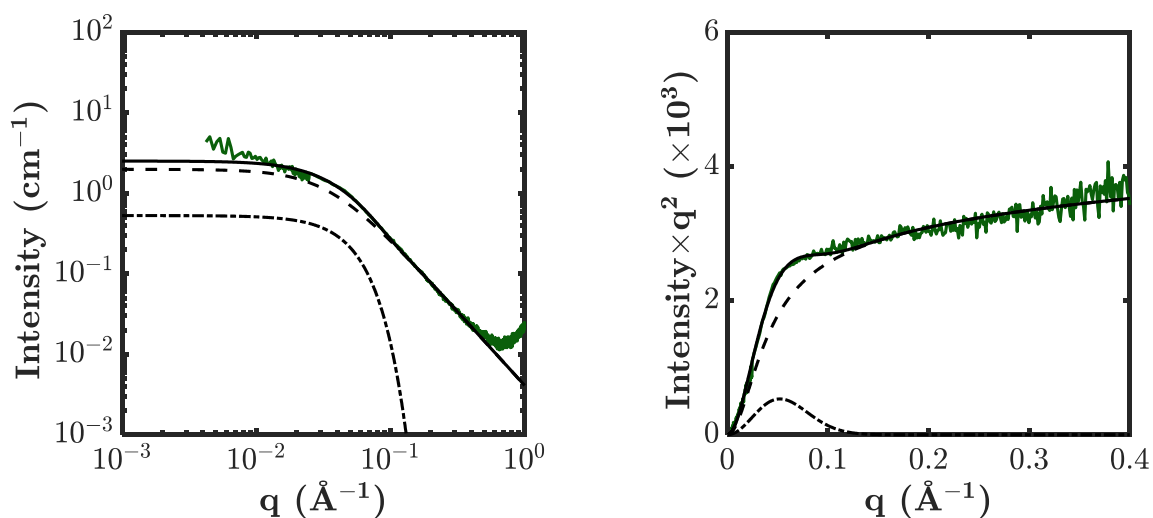


Figure 2.40: Scattered X-Ray intensity versus the scattering vector for a “One-Pot” dual-crosslink gel with $[Ni^{2+}] = 100 \text{ mmol/L}$, corresponding fit obtained with Eq. 2.20 (solid black line), and Guinier and stretched-Lorentzian components of Eq. 2.20 (dashed black lines). Left: log-log representation; Right: Kratky representation

The fits seem to be quite good on the graphs, but some problems arise with the computed parameters. First, Ξ is of the same order of magnitude as ξ . The fractal parameter m is slightly low compared to what

we have observed previously on the diffusion gels. The intensity of the Guinier scattering is also very low compared to the stretched-Lorentzian scattering.

The polymerization in the presence of the Ni^{2+} ions seems to change the structure of the clusters of physical bonds: we see at low q that the Gaussian we have used does not work, the length scale of the clusters might be larger than what we can see with the scattering set-up that we used.

2.5.4. Conclusions from X-ray scattering

Dual-crosslink hydrogels presented here clearly show a structural organization of the Ni^{2+} ions at length scales much larger than the length of a physical bond. Looking more closely into those results, we found that the X-Ray is scattered by the Ni^{2+} ions just as neutrons would be scattered by polymer chains when going through a chemically crosslinked gel of PVA-borate or PDMS.

It seems that the model given by Shibayama et al. that we used here does not work perfectly when the gel is synthesized following the “One-Pot” method. However, it gives realistic insights on the length scales in “Diffusion” gels, with length scales that correspond to what we can find in other experiments.

The results imply that the physical bonds are organized in two families. The first one randomly distributed along the polymer chains, with a correlation length of around 3 nm that corresponds to the correlation length between polymer chains we have measured in DLS. The other representing the clusters of physical bonds, which correlation length of around 15 nm is very close to the mesh size of the chemical network (16 nm) we have measured in rheology, implying that the clusters might actually be organized around chemical crosslinking points.

With these observations, and their coherence with what we have found before, we are now quite convinced of the existence of clusters of physical crosslinks around chemical crosslinking points.

2.6. Conclusion on microstructure and dynamics

We have successfully prepared chemically crosslinked P(AAm-co-VIm) hydrogels and incorporated into that network dynamic physical crosslinks based on metal-ligand coordination bond with a controlled lifetime. We developed two methods to incorporate the physical bonds, one more simple experimentally (“One-pot”), and the other giving us the ability to use a larger range of metallic ions as crosslinkers (“Diffusion”). The “Diffusion” method allowed us to characterize the complexation state of the Ni^{2+} ions in the network. We have shown that a large proportion of ions create crosslinks between polymer chains.

By light scattering experiments, we have demonstrated the existence of two dynamics in a hydrogel crosslinked by Ni^{2+} ions. One is related to the lifetime of the physical bond, with a characteristic time of about 10^{-2} s evolving with the concentration in Ni^{2+} ions; the other, with a characteristic time of about a second, we assumed to be linked to the existence of clusters of physical bonds.

Rheological experiments allowed us to prove that the preparation method (“One-pot” or “Diffusion”) has very little influence on the dynamic of the dual-crosslink hydrogel. It also demonstrated again the existence of two dynamics. Using a fractional derivative model, we managed to extract two characteristic times from these rheology results, which were quite similar to the ones we had found in DLS experiments. These rheology results, combined with our previous results on the complexation state

2. Preparation and microstructure of a dual-crosslink hydrogel

of the Ni^{2+} in the network, suggested a good cross-linking efficiency of about 60% for the physical crosslinks.

The characterization of the dynamics in both DLS and rheology experiments can be related to two length scales in our material: the mesh size of the chemical network, around 16 nm, and the correlation length of the polymer chains, around 3 nm.

We have proven the existence of aggregates of physical crosslinks with X-Ray scattering experiments. Using a model from neutron scattering by polymer gels, we could extract two length scales from the SAXS experiments. Those length scales were quite close to the ones we previously measured in our dynamic experiments. This similarity might imply that the physical bonds are randomly distributed along the polymer chains, but that those chains are more closely packed in some places (maybe around the chemical crosslinks). This creates aggregates of physical bonds that have a lifetime much longer than that of the simple physical crosslink.

We can now focus on the main objective of this PhD: the behavior of these hydrogels in large deformations. We will try to correlate the toughness of the material with its capacity to dissipate energy.

References

1. Sjöberg, S. Critical evaluation of stability constants of metal-imidazole and metal-histamine systems. *Pure & Appl. Chem.* **69**, 1549–1570 (1997).
2. Hammes, G. G. & Steinfeld, J. I. Relaxation Spectra of Some Nickel(II) and Cobalt(II) Complexes. *Journal of the American Chemical Society* **84**, 4639–4643 (1962).
3. Sato, H., Yui, M. & Yoshikawa, H. Ionic Diffusion Coefficients of Cs⁺, Pb²⁺, Sm³⁺, Ni²⁺, SeO₂⁻⁴ and TcO₄⁻ in Free Water Determined from Conductivity Measurements. *Journal of Nuclear Science and Technology* **33**, 950–955 (1996).
4. Rose, S., Marcellan, A., Hourdet, D., Creton, C. & Narita, T. Dynamics of Hybrid Polyacrylamide Hydrogels Containing Silica Nanoparticles Studied by Dynamic Light Scattering. *Macromolecules* **46**, 4567–4574 (2013).
5. Rossow, T., Habicht, A. & Seiffert, S. Relaxation and Dynamics in Transient Polymer Model Networks. *Macromolecules* **47**, 6473–6482 (2014).
6. B. Tito, N., Creton, C., Storm, C. & G. Ellenbroek, W. Harnessing entropy to enhance toughness in reversibly crosslinked polymer networks. *Soft Matter* **15**, 2190–2203 (2019)
7. Hui, C.-Y., Lin, Y. Y., Chuang, F.-C., Shull, K. R. & Lin, W.-C. A contact mechanics method for characterizing the elastic properties and permeability of gels. *Journal of Polymer Science Part B: Polymer Physics* **44**, 359–370 (2006).
8. Chan, E. P., Hu, Y., Johnson, P. M., Suo, Z. & Stafford, C. M. Spherical indentation testing of poroelastic relaxations in thin hydrogel layers. *Soft Matter* **8**, 1492–1498 (2012).
9. Zhao, J. Structure et propriétés des hydrogels à réticulation chimique et physique. (PSL Research University, 2018).
10. Schiessel, H., Metzler, R., Blumen, A. & Nonnenmacher, T. F. Generalized viscoelastic models: their fractional equations with solutions. *J. Phys. A: Math. Gen.* **28**, 6567 (1995).
11. Jaishankar, A. & McKinley, G. H. A fractional K-BKZ constitutive formulation for describing the nonlinear rheology of multiscale complex fluids. *Journal of Rheology* **58**, 1751–1788 (2014).
12. Aime, S., Cipelletti, L. & Ramos, L. Power law viscoelasticity of a fractal colloidal gel. *Journal of Rheology* **62**, 1429–1441 (2018).
13. Brûlet, A., Lairez, D., Lapp, A. & Cotton, J.-P. Improvement of data treatment in small-angle neutron scattering. *J Appl Cryst* **40**, 165–177 (2007).
14. Cotton, J.P. (1991). In: *Neutron, X-Ray and Light Scattering*, Eds. P. Lindner, Th. Zemb, p.19, Elsevier, North-Holland, Delta series.
15. Filippidi, E. et al. Toughening elastomers using mussel-inspired iron-catechol complexes. *Science* **358**, 502–505 (2017).
16. Mallam, S., Horkay, F., Hecht, A. M., Rennie, A. R. & Geissler, E. Microscopic and macroscopic thermodynamic observations in swollen poly(dimethylsiloxane) networks. *Macromolecules* **24**, 543–548 (1991).
17. Shibayama, M. et al. Small-angle neutron scattering from poly(vinyl alcohol)-borate gels. *Polymer* **33**, 2883–2890 (1992).
18. Shibayama, M., Tanaka, T. & Han, C. C. Small angle neutron scattering study on poly(N-isopropyl acrylamide) gels near their volume-phase transition temperature. *Polymer* **97**, 14 (1992).

Chapter 3

Large deformations of dual-crosslink hydrogels with Ni²⁺ ions

3. Large deformations of dual-crosslink hydrogels with Ni²⁺ ions

3. Large deformations of dual-crosslink hydrogels with Ni²⁺ ions

Table of contents

3.1. Standard uniaxial tensile tests: continuous loading	92
3.1.1. Comparison of “One-pot” and “Diffusion” gels with [Ni ²⁺] = 100 mmol/L	92
3.1.2. Continuous loading.....	93
3.1.3. Discussion	99
3.2. Cyclic testing	101
3.2.1. Influence of stretch and stretch-rate	101
3.2.2. Damage during cycles?	105
3.3. Relaxation.....	109
3.4. Fracture of Ni²⁺ dual-crosslink hydrogels	113
3.4.1. Single-notch fracture under continuous stretching.....	113
3.4.2. Delayed fracture of “pure-shear” samples.....	115
3.5. Conclusions and discussions	120
References	123

3. Large deformations of dual-crosslink hydrogels with Ni²⁺ ions

Now that we have addressed the microstructure of the Ni²⁺ dual-crosslinked hydrogel, in this chapter we will focus on the main part of this PhD project: the mechanical properties of the dual-crosslink hydrogels at large deformations, and their resistance to fracture. In this chapter, we will only consider the P(AAm-co-VIm)-Ni²⁺ dual crosslink gel with $[Ni^{2+}] = 100 \text{ mmol/L}$, in comparison with the corresponding chemical gel. This dual crosslink gel, prepared in optimized conditions in terms of toughness and detectable dynamics, will be a good reference for comparisons with other dual crosslink gels that will be studied in the subsequent chapters.

Many experiments have already been carried out by J. Zhao during her PhD on “One-pot” P(AAm-co-VIm)-Ni²⁺ dual-crosslink hydrogels [1-3]. However, she also showed that this “One-pot” method does not allow a large variety of metallic ions to be used, since only hydrogels with Ni²⁺ ions can be obtained with no visible problems. In this PhD, as mentioned before, the focus is on “Diffusion” dual-crosslink hydrogels because of the versatility of this preparation method, presented in the previous chapter. We will start by exposing the differences in mechanical properties under uniaxial tensile tests between those gels made with the two different preparation methods (which are quite small in the case of Ni²⁺ ions). We will then focus on the “Diffusion” dual crosslink hydrogels for the rest of this study.

Next, we will show how the dual-crosslink gels behave under cyclic loading and briefly characterize their remarkable recovery after such cycles. We will use these cycles at high strains and some relaxation experiments to demonstrate the existence of damage inside the polymer network at large deformations before the failure of the hydrogel, and the existence of a mechanism of inhibition of crack nucleation inside the dual-crosslink hydrogel. Finally, some systematic fracture experiments will show the resistance of the material to the propagation of a crack in different geometries.

3.1. Standard uniaxial tensile tests: continuous loading

In this part, the behavior of a pristine sample of the dual crosslink hydrogel in large deformations will be studied. We will first observe the difference between the two synthesis methods presented in the previous chapter. Then, we will make some observations on the large deformations of the “Diffusion” dual-crosslink hydrogel, especially its pronounced stretch-rate dependence. We will then focus on the mechanical properties of the dual crosslink hydrogel under cyclic tests, to better characterize its energy dissipation during stretching. In addition, we will demonstrate the existence of some damage to the polymer structure at very large deformations. We will also look into the relaxation process of this material and how it evolves with stretch.

Finally, the fracture properties of the material will be studied, in single-notch fracture and delayed fracture experiments. We will show some unexpected behaviors, especially at higher stretch-rates.

3.1.1. Comparison of “One-pot” and “Diffusion” gels with $[Ni^{2+}] = 100 \text{ mmol/L}$

We performed uniaxial tensile tests on strips of dual-crosslink hydrogels prepared by the “one-pot” and by the “diffusion” methods. The results are shown in Figure 3.1 as stress-strain curves. We can see in this figure that the behaviors of the hydrogels prepared by both methods are similar, with a strain softening at low deformations, followed by a strain hardening at high deformations. The “One-pot” hydrogel showed slightly higher values of stress than the “Diffusion” hydrogel, presumably due to the slight difference in the Ni²⁺ concentration in the gels. It should be noted that the dual crosslink hydrogel

made by ion diffusion contains NaCl (107 mmol/L) while the one-pot hydrogel has no added salt. The electrostatic interactions between the charged physical crosslinking points may play a role in the dynamics. Further systematic studies are necessary.

From now, all reported results were obtained with the “Diffusion” dual-crosslink hydrogel with $[\text{Ni}^{2+}] = 100 \text{ mmol/L}$. All mentions of ‘dual-crosslink hydrogels’ in this chapter will refer to the “Diffusion” dual-crosslink hydrogel with $[\text{Ni}^{2+}] = 100 \text{ mmol/L}$.

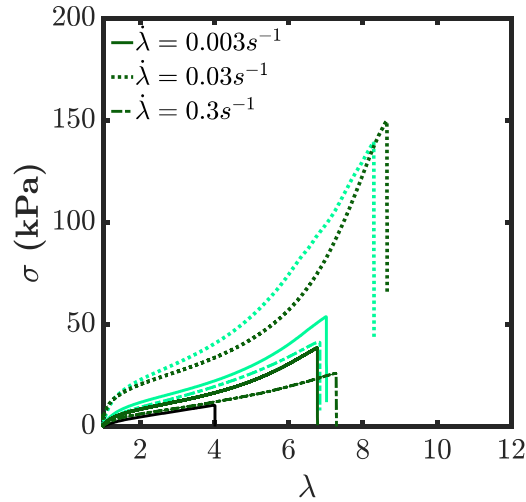


Figure 3.1: Stress versus strain for tensile tests of a chemical gel (black), a “One-pot” dual-crosslink hydrogel (light green) and a “Diffusion” dual-crosslink hydrogel (dark green) realized at different stretch-rates, both hydrogels with $[\text{Ni}^{2+}] = 100 \text{ mmol/L}$.

3.1.2. Continuous loading

In this section, in order to characterize the dynamics and the stretch rate dependence of the mechanical properties of the dual crosslink gel from small to large deformations, we realized uniaxial tensile tests at different stretch-rates on un-notched dogbone-shaped samples of Ni^{2+} dual-crosslink hydrogel by continuous loading to rupture. The stress stretch curves are shown in Figure 3.2. Compared to the corresponding chemical gel (black curve, $\dot{\lambda} = 0.03 \text{ s}^{-1}$), the dual crosslink gel showed much higher stress levels at high stretch rates that decreased with decreasing stretch rate and approached that of the chemical gel. The extensibility was largely improved by dual crosslinking: the stretch at break, λ_c , was above 9 for all the stretch rates while that for the chemical gel was only about 5.5.

3. Large deformations of dual-crosslink hydrogels with Ni²⁺ ions

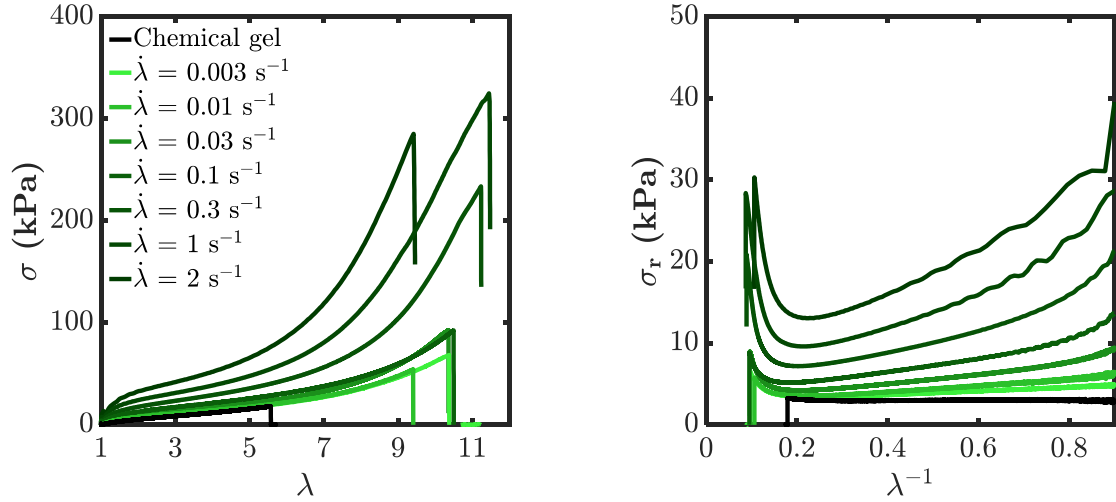


Figure 3.2: Stress versus strain (left) and reduced stress versus inverse of strain (right) for tensile tests of a chemical gel (black) and a Ni²⁺ dual-crosslink hydrogel, realized at different stretch-rates.

The initial modulus and stretch at break as a function of stretch rate are shown in Figure 3.3 (in green filled triangles). The value of the modulus increased with stretch-rate and reached a plateau (about 80 kPa) at high stretch-rates, showing the same behavior as G' obtained from rheological measurements (Figure 2.25). Interestingly, the strain at break λ_c increased dramatically between the chemical and the dual-crosslink hydrogel, and was then relatively independent of the strain-rate. It seems to decrease once reaching higher stretch-rates ($\dot{\lambda} = 2 \text{ s}^{-1}$), which is consistent with our theory: at higher stretch rates, the physical crosslinks start to behave more like permanent crosslinks, with low dissipation. Here it should be pointed out that at as very low stretch-rate as $\dot{\lambda} = 0.003 \text{ s}^{-1}$, the value of the modulus was close to that of the chemical gel thus the physical crosslinks did not contribute to the elasticity, while the stretch at break remained as high as $\lambda_c = 10$.

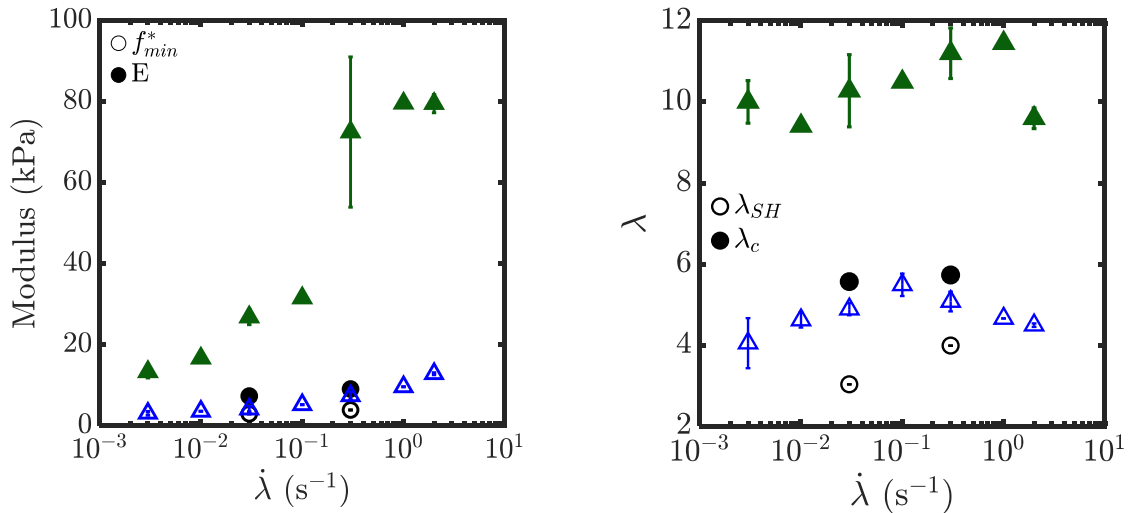


Figure 3.3: Left: Young's modulus (filled symbols) and reduced stress at the onset of strain-hardening (empty symbols) versus the stretch-rate, for the reference chemical gel (black) and the Ni²⁺ dual-crosslink hydrogel (Young's modulus in green, f_{min}^* in blue). Right: stretch at break (filled symbols) and stretch at the onset of strain-hardening (empty points) versus strain-rate for a chemical hydrogel (black) and a Ni²⁺ dual-crosslink hydrogel (λ_{max} in green, λ_{SH} in blue).

Because the stress-strain representation of the data is not the most convenient to separate effects of stretch and stretch rate [4], we also show the Mooney representation of the same data, with the reduced stress (defined in chapter 1) as a function of the inverse of the stretch. This representation is based on a Neo-Hookean model. In the original Mooney-Rivlin model [5,6], developed for elastic rubbers, the reduced stress σ_r can be decomposed into a stretch-independent term C_1 and a stretch-dependent term C_2 :

$$\sigma_{reduced} = \frac{\sigma_N}{\lambda - 1/\lambda^2} = C_1 + \frac{C_2}{\lambda} \quad \text{Eq. 3.1}$$

When $C_2 = 0$, the model corresponds to the classical Neo-Hookean theory; $C_2 > 0$ means that a softening occurs during the uniaxial tension; $C_2 < 0$ means that a strain hardening appears. These so-called Mooney plots for the dual crosslink gel and the chemical gel are shown in Figure 3.2 (right). We can see that in uniaxial tension, the chemical gel followed well the Neo-Hookean model, with $C_2 = 0$, up until $\lambda \approx 3$ where a slight hardening appears. There was no softening in this hydrogel. The value of σ_r before the slight strain hardening thus corresponded to the modulus of the chemical hydrogel $E/2(1 + \nu) \approx E/3$ (around 3 kPa here).

The Mooney-Rivlin model does not apply to our Ni^{2+} dual-crosslink hydrogel. In this model, C_2 is constant. Here, the value C_2 depends on the stretch λ . The reduced stress shows a clear non-linear softening ($C_2(\lambda) > 0$), until a certain λ_{SH} . It is followed by a hardening at large λ . The softening is presumably linked to the physical bond breaking, since the chemical network showed no softening. There is a decrease of the number of polymer chains in the network, which decreases the reduced stress.

After this λ_{SH} , the reduced stress increases, $C_2(\lambda)$ becomes negative. It is possible to determine the value of the stretch at which the hardening starts, thanks to the Mooney plot. We define it as the point of minimal value of $\sigma_{reduced}$, which gives the stretch of onset of strain-hardening λ_{SH} and the minimal reduced stress f_{min}^* .

The values of the minimum reduced stress f_{min}^* and the corresponding stretch λ_{SH} are plotted in Figure 3.3 (in blue empty triangles). One can see that the minimal reduced stress increases with stretch-rate. This increase is less pronounced than that of the elastic modulus and does not show a plateau value at high stretch rates. At low stretch-rates, the value of the minimal stress reaches that of the chemical hydrogel (black empty circles). The increasing minimal stress suggests that the lifetime of the physical bonds is of the order of magnitude of the inverse of the stretch-rate and hence the number of physical crosslinks contributing to strain-hardening increases as the strain-rate increases.

The onset of the strain hardening, λ_{SH} , however, occurs at a larger strain than that for the chemical gel at all the stretch rates studied. λ_{SH} is observed to increase and decrease slightly with stretch rate, with a peak at $\dot{\lambda} = 0.1 \text{ s}^{-1}$. It is noteworthy that at low stretch-rates, the reduced stress only varies little with stretch and that in those conditions the measurement of λ_{SH} involves a large measurement error.

The values observed at $\dot{\lambda} > 0.1 \text{ s}^{-1}$ follow a law in $(f_{min}^*)^{-1/2}$ (shown in Figure 3.4), as expected in this kind of situation [7,8].

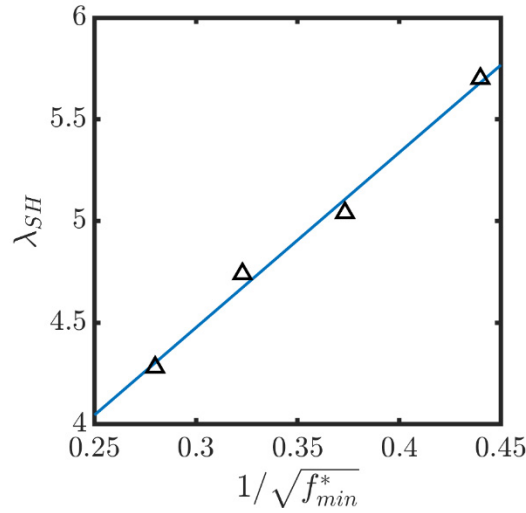


Figure 3.4: Onset stretch of strain hardening λ_{SH} versus $1/\sqrt{f_{min}^*}$, for a Ni²⁺ dual-crosslink hydrogel at $\dot{\lambda} \geq 0.1 \text{ s}^{-1}$

The reduced stress values of Figure 3.2 clearly exhibited a stretch-rate dependence, implying an increasing influence of the physical crosslinks with stretch-rate. The characteristic values of stretch (the stretch at break or the onset of strain hardening), however, did not evolve much with the stretch-rate. This observation leads us to apply a time-strain separability to the stress of these dual-crosslink hydrogels, as has been previously done on the PVA-borax dual-crosslink hydrogel [4]:

$$\sigma(\lambda, t) = G(t) \cdot \left(\lambda - \frac{1}{\lambda} \right) \quad \text{Eq. 3.2}$$

We plotted the reduced stress $\sigma_{reduced}(t)$ as a function of time in Figure 3.5 for different stretch-rates. The curves superposed reasonably well on a master curve, indicating that the time-strain separability worked for this system. At short times (between 10⁻¹ and 10¹ s) the superposition was less clear with the lower stretch-rates (0.01 and 0.003 s⁻¹), due to low value of the stress. The steep increase of reduced stress at the end of each experiment corresponds to a strain stiffening effect, where this separability does not work. This separation allows us to define a linear relaxation mode $G(t)$, independent on the stretch or the stretch-rate. In this mode, the stress decreases during stretching because of the breaking of active physical bonds. The number of polymer chains in the network decreases hence the stress relaxes.

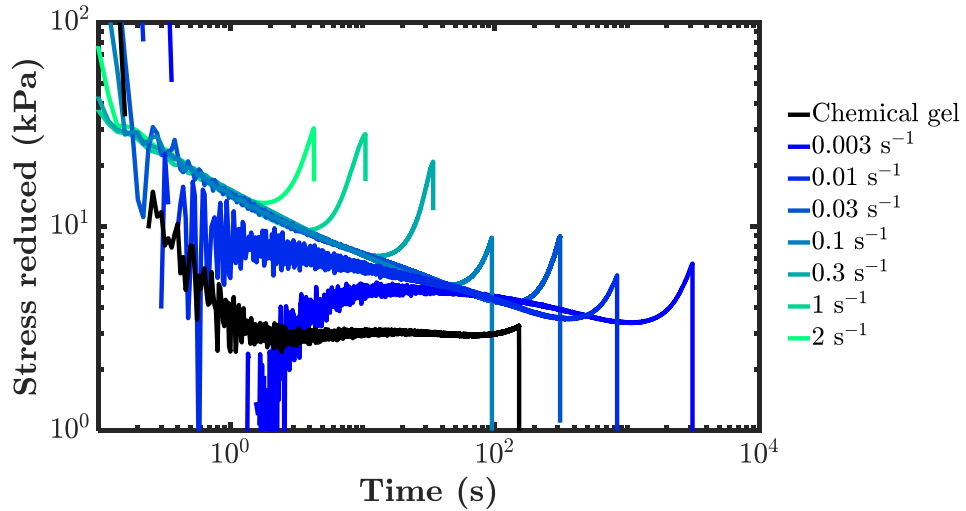


Figure 3.5 Time dependence of the reduced stress f^* under uniaxial continuous loading for the Ni^{2+} dual cross-link hydrogel at various initial stretch rates.

This representation also highlights the strain hardening, happening at the higher strains for each hydrogel. To characterize it further by separating the time effect, the reduced stress was normalized by the linear behavior. More precisely, the values of the reduced stress for the stretch rates from $\dot{\lambda} = 2 \text{ s}^{-1}$ to $\dot{\lambda} = 0.1 \text{ s}^{-1}$ were normalized by the stress from $\dot{\lambda} = 0.03 \text{ s}^{-1}$ (the superposition was less clear for lower stretch-rates). This should give a normalized stress always equal to 1, except when the behavior deviates because of strain hardening. The results are presented in Figure 3.6 (left). The samples reach different levels of relative stress, increasing with the stretch-rate and then slightly decreasing at $\dot{\lambda} = 2 \text{ s}^{-1}$.

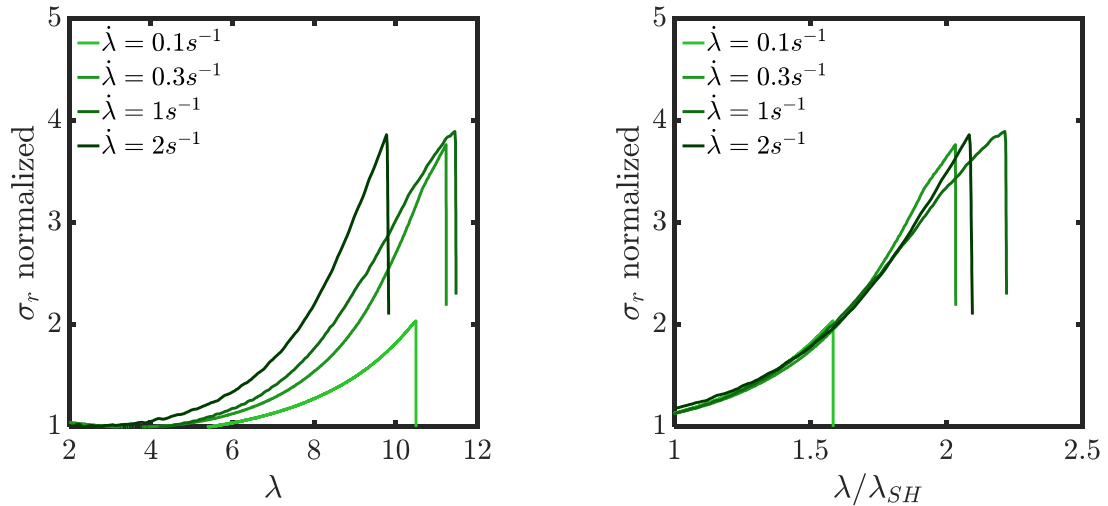


Figure 3.6: Reduced stresses from $\dot{\lambda} = 2 \text{ s}^{-1}$ (dark green) to $\dot{\lambda} = 0.1 \text{ s}^{-1}$ (light green), normalized by the reduced stress from $\dot{\lambda} = 0.03 \text{ s}^{-1}$, as a function of the stretch λ (left) and time shifted by the onset of strain hardening (right).

It is also possible to shift these curves, by normalizing the x axis by the onset stretch of strain hardening λ_{SH} , as done also in Figure 3.6 (right). Interestingly this normalized strain hardening follows exactly the same increase rate, for each stretch rate.

3. Large deformations of dual-crosslink hydrogels with Ni²⁺ ions

When increasing the stretch-rate, one increases the number of active physical bonds, thus the number of polymer chains between two physical crosslinks. This in turn decreases the mean length of a polymer chain. This explains why λ_{SH} decreases at higher stretch-rates: the strain-hardening begins sooner because chains are shorter.

The results of Figure 3.6 imply that the strain hardening itself is not dependent on the strain rate (in that range of strain rates) but only on the ratio λ/λ_{SH} . There is a critical deformation λ_{SH} above which the strain-hardening becomes a dominant phenomenon, and the stress increases in the material, following a function f independent on the stretch-rate such as:

$$\sigma_{r,normalized}(\lambda, t) = 1 + f\left(\frac{\lambda}{\lambda_{SH}}\right) \quad \text{Eq. 3.3}$$

Seeing how we normalized the reduced stress by a linear relaxation function, we can try to implement a phenomenological model defining the stress as:

$$\sigma_N(\lambda, t) = G(t) \times \left(\lambda - \frac{1}{\lambda^2}\right) \times \left(1 + f\left(\frac{\lambda}{\lambda_{SH}}\right)\right) \quad \text{Eq. 3.4}$$

Where $G(t)$ is defined as the linear relaxation function (in our case, we took it as the curve from the experiment realized at $\dot{\lambda} = 0.03 \text{ s}^{-1}$, before the onset of strain-hardening) and $f(\lambda/\lambda_{SH})$ is the function defining the increase in stress linked to the strain-hardening. Long et al. proposed an exponential function to model the strain-hardening in a PVA-borax dual-crosslink hydrogel [9].

In order to obtain more information on this function f , we plotted it against λ/λ_{SH} on a log-log plot in Figure 3.7 (left). The result gives a linear curve after the onset of strain-hardening (which is here at $\log(\lambda/\lambda_{SH}) = 0$), which suggests that f is a power law.

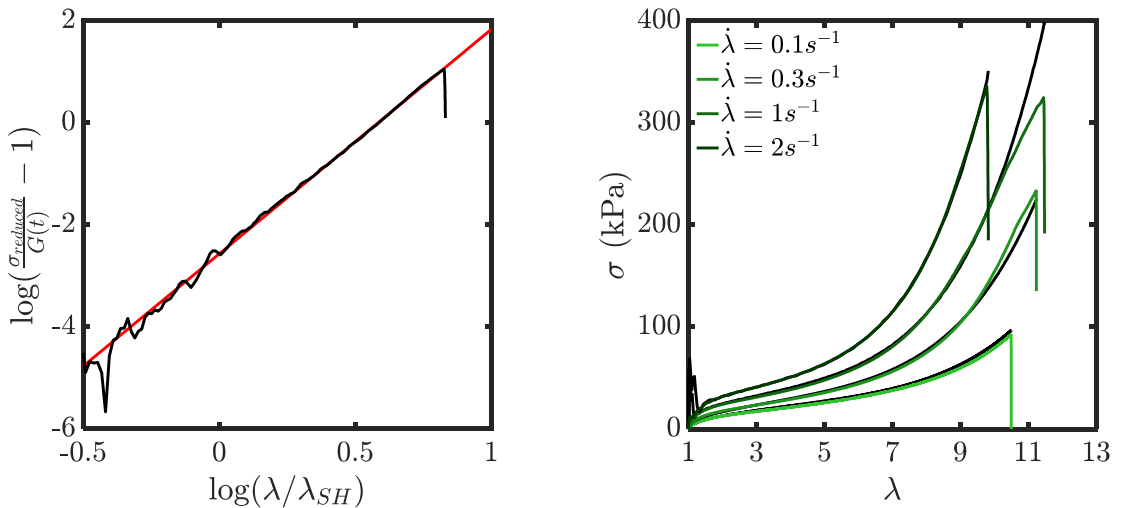


Figure 3.7 Left: log-log plot of the strain-hardening function $f(\lambda/\lambda_{SH})$ versus the normalized stretch λ/λ_{SH} , along with its fitted curve, for $\dot{\lambda} = 2 \text{ s}^{-1}$. Right: stress-stretch curves for the stretch-rates studied in strain-hardening, along with their respective fits from Eq. 3.4.

Fitting this linear plot, we obtained the formula given in Eq. 3.7:

$$f\left(\frac{\lambda}{\lambda_{SH}}\right) = 0.077 \times \left(\frac{\lambda}{\lambda_{SH}}\right)^{4.4} \quad \text{Eq. 3.5}$$

This result is completely independent on the stretch-rate, as mentioned before and as Figure 3.7 (right) further demonstrates. The curves from this phenomenological model follow quite well the experimental data.

However, this description of the strain-hardening does not work at lower stretch-rates, where f_{min}^* and λ_{SH} are relatively constant. The strain-hardening seems to follow two different behaviors: at $\dot{\lambda} \geq 0.1 \text{ s}^{-1}$, it is defined by the presence of the physical bonds, which number will set its intensity and its onset; at $\dot{\lambda} < 0.1 \text{ s}^{-1}$, the physical bonds are not mechanically active since the observation time is much longer than their characteristic time, which makes the strain-hardening insensitive to the stretch-rate.

A last interesting parameter, the stress at break σ_{max} , was also plotted as a function of the stretch rate in Figure 3.8. Contrary to the stretch at break, and similarly to the initial modulus, the stress at break increased markedly with the stretch-rate. This result confirms that the dual-crosslink hydrogel breaks when reaching a critical stretch, and not a critical stress.

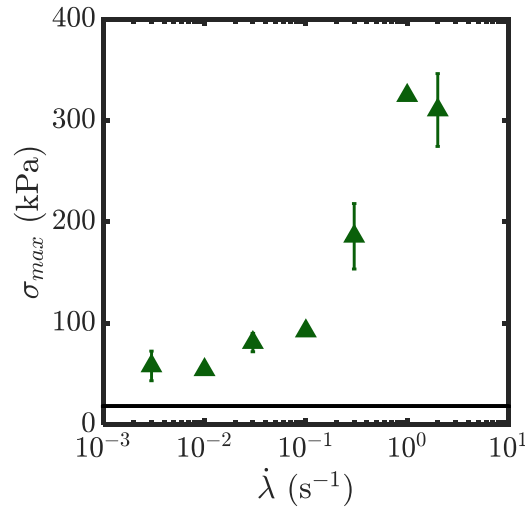


Figure 3.8: Stress at break as a function of the stretch-rate, for the Ni^{2+} dual-crosslinked hydrogel. The black line represents the value obtained for the corresponding bare chemical gel.

3.1.3. Discussion

The number of active physical crosslinks at the beginning of the stretching is dependent on the stretch-rate: the higher the stretch-rate, the more physical bond active at the beginning of the experiment. The Young's modulus of the hydrogel will then increase with the number of polymer chains in the network. While stretching, the number of active physical crosslinks (and hence the number of polymer chains) decreases, leading to a softening of the material. This stress relaxation can be decomposed into two factors, one strain-dependent and one time-dependent. The strain-dependent factor was taken from the Mooney-Rivlin model, and the time-dependent relaxation is completely independent on the stretch-rate.

When increasing the stretch, a strain-hardening behavior appears. The intensity of this behavior is directly related to the number of polymer chains that have reached their strain-hardening regime. The

3. Large deformations of dual-crosslink hydrogels with Ni²⁺ ions

strain-hardening regime begins at a stretch λ_{SH} dependent on the modulus of onset of the strain-hardening, following a classical law. This macroscopic strain-hardening is caused by the existence of a percolating network of polymer chains in their strain-hardening regime. The number of these polymer chains modifies the intensity of the strain-hardening, which is the case here: with increasing stretch-rate, the number of active physical bonds (and hence the number of polymer chains) increases, which in turn increases the number of chains in their strain-hardening regime. However, the stretch of onset of strain-hardening depends on the size of the polymer chains: the more active physical bonds in the network there are, the lower λ_{SH} is. The evolution of this strain-hardening, at high stretch-rates, is independent on the stretch-rate itself and can be described by a phenomenological power law. At lower stretch-rates, where the observation time is much longer than the characteristic lifetime of the physical bond and the number of active physical bonds is consequently low, this strain-hardening behavior seems to be independent on the stretch-rate.

The evolution of the stress in the tensile experiment is then simply a competition between the linear relaxation linked to the decrease of the number of polymer chains with time, and the stress increase linked to the increased influence on the stress of the polymer chains in their strain-hardening regime.

The stretch at break of the bare chemical network was found $\lambda_c \approx 5 \pm 0.5$ (fracture of un-notched samples of the brittle network results in relatively large errors). Since the dual crosslink network was prepared by adding transient dynamic crosslinks to the permanent chemical network, it is reasonable to suppose that the ultimate chain extensibility (with all physical crosslink dynamics) would be the same in the chemical gel and in the dual-crosslink gel (as it has been found in elastomers for example [10]). As demonstrated above, the experimental results showed an opposite case: although the dual crosslinked gel has a higher modulus and hence more active elastic chains, the extensibility of the dual crosslink gel was much higher than that of the chemical gel.

To understand this phenomenon, we can decompose the fracture process into two different steps: the nucleation of a fracture and its propagation. In a perfectly elastic network in tension, the polymer chains are unfolded and stretched in the traction direction; the more they are stretched, the more stress or energy is stored in those polymer chains. At a certain stretch, the shortest of these polymer chains will reach their maximal extensibility (or the maximal amount of energy it can store) and break. All the energy carried by the broken chain will be transferred to its neighbors in the plane orthogonal to the traction direction. Those chains will in turn exceed their critical energy level, break, and transfer their energy to their neighbors (Figure 3.9). From one chain to another, a crack will nucleate and propagate. This successive breaking of polymer chains is what happens in a bare chemical gel, for example.

One plausible explanation for the toughening we observe on a dual-crosslink hydrogel is then that the chemical chains indeed break during loading, but no fracture is nucleated from this breaking. The energy released by a broken chain is not transferred to its neighboring chains, but dissipated by the physical bonds in-between those chains (Figure 3.9). The successive breaking of polymer chains is inhibited, until a critical point.

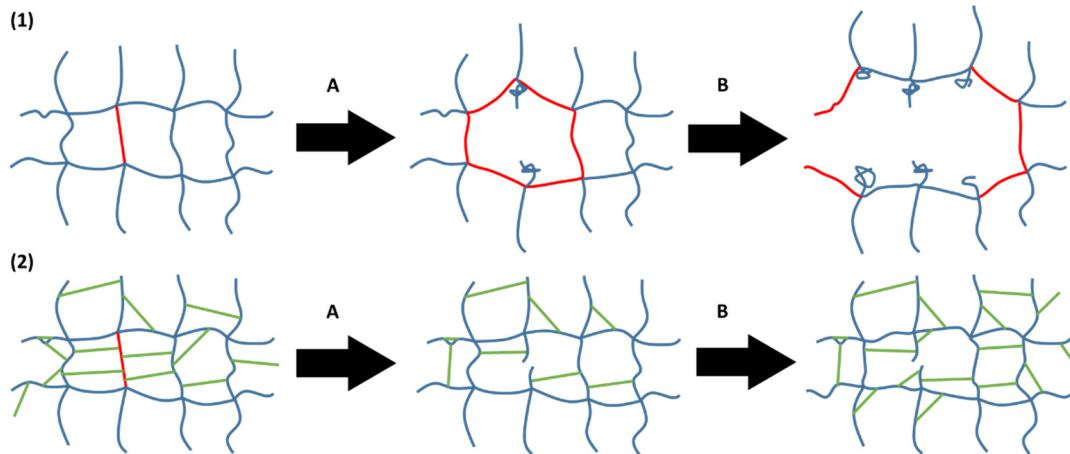


Figure 3.9: *Top:* Correlated breaking of polymer chains in a perfectly elastic network. *Bottom:* Prevention of correlated breaking by physical bonds in a dual-crosslink hydrogel. The physical bonds will break and allow a rearrangement of the polymer chains that will prevent the correlated breaking.

Thus, the physical bonds act on not only the force (or energy) needed to propagate a crack, but also on the nucleation of this crack. This explanation implies that during loading, at stretches above the critical stretch of the chemical gel, there should be diffuse damage of the chemical network inside the dual-crosslink hydrogel before a crack appears and propagate.

3.2. Cyclic testing

The results presented in the previous part imply the possibility of dissipation of energy and permanent damage in the material at deformations between the maximal stretch of the chemical gel (≈ 5) and the maximal stretch of the dual-crosslink hydrogel. In order to evaluate the dissipation and damage, cyclic experiments were conducted at different stretches and different stretch-rates. The objective of these experiments was to demonstrate damage inside the material, by a change in the mechanical properties (lower modulus, higher strain at break) of a dual-crosslink hydrogel previously stretched at $\lambda > \lambda_{c,chemical\ gel}$

3.2.1. Influence of stretch and stretch-rate

First, we confirmed that the bare chemical gel did not have any energy dissipation when stretched, as shown in Figure 3.10. We observed that the unloading curve perfectly superposed on the loading curve when the bare chemical gel was stretched up to $\lambda = 3$. There was no dissipation during this cycle. The artifact observed at $\lambda = 3$ is related to the inertia of the load cell used for this experiment. This cycle was repeated 50 times with no waiting time between each cycle, giving always the same result (data not shown). The bare chemical gel thus was perfectly elastic and showed no change of behavior with cycles (no damage) in this range of stretches.

3. Large deformations of dual-crosslink hydrogels with Ni²⁺ ions

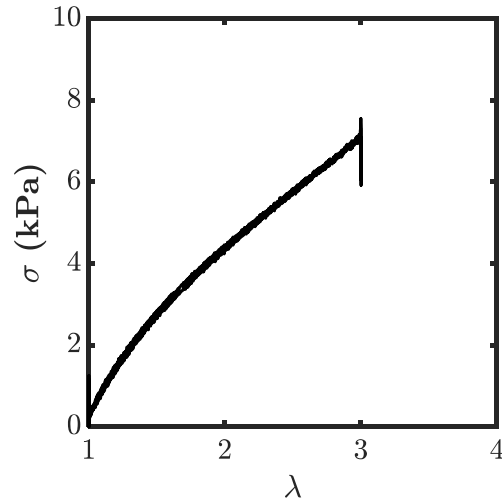


Figure 3.10: Stress versus stretch obtained from a loading-unloading uniaxial tensile test of the bare chemical gel, realized at a stretch-rate $\dot{\lambda} = 0.03 \text{ s}^{-1}$.

Then we studied the dissipation of the dual-crosslink hydrogel. We performed a series of cyclic loading-unloading tests of a dual-crosslink hydrogel, at different stretch rates and at different maximal stretches. In Figure 3.11 we show the results for two maximal stretches at different stretch rates as example. We observed a hysteresis for all the condition tested and the dissipated energy increased with increasing stretch-rate. We also noticed the appearance of a residual stretch: the value of the stretch did not come back to zero when the stress came back to zero. We will discuss this residual stretch later in this section.

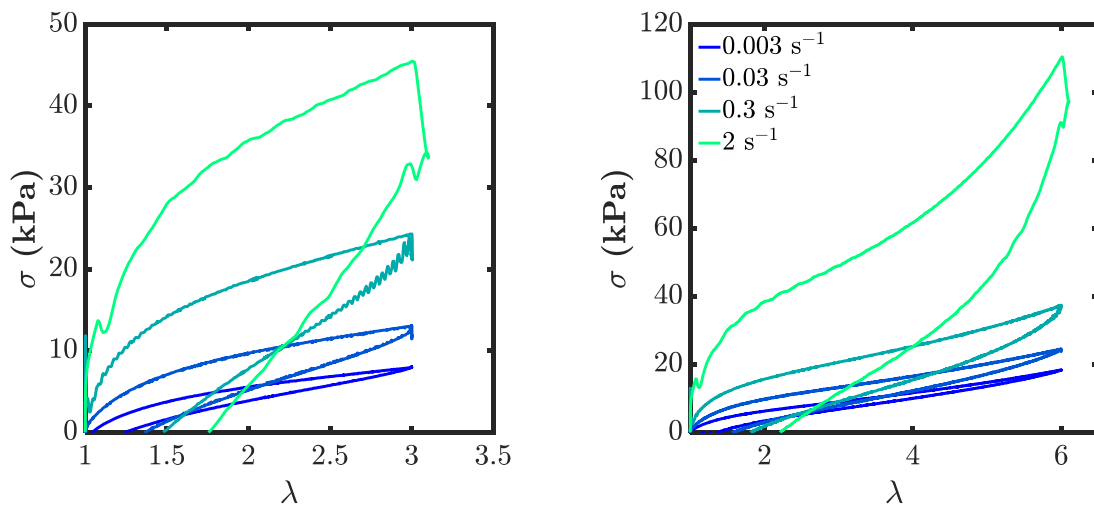


Figure 3.11: Stress vs. Stretch for cyclic loading/unloading of the dual-crosslinked hydrogel with $[\text{Ni}^{2+}] = 100 \text{ mmol/L}$, at different stretch rates. Left: $\lambda_{\text{max}} = 3$. Right: $\lambda_{\text{max}} = 6$.

Figure 3.11 shows a clear visco-elastic behavior of the material, with a characteristic hysteresis between the loading and unloading curves. This hysteresis can be further quantified, by computing the stored and dissipated energies. The stored energy is the integral of the unloading curve (see Figure 3.12), and represents the energy that was stored in the material as elastic energy and that can be recovered. This energy is different from the total mechanical energy brought to the system, which is the integral of the

loading curve. The difference between these two energies is the energy that was dissipated during the loading, the hysteresis.

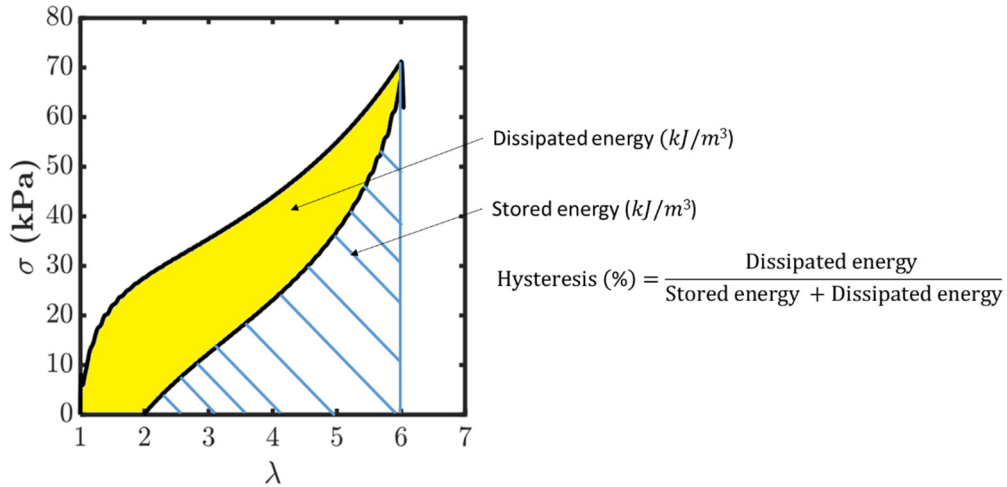


Figure 3.12: calculation of the stored and dissipated energies.

As shown in Figure 3.13, the stored energy shows a sharp increase with applied maximal stretch. It is noteworthy that the stored energy should represent the elastic part of a material, and should therefore follow an evolution in λ^2 . Indeed, since $Energy \sim \sigma \lambda$ and, in an elastic network, $\sigma \sim \lambda - 1/\lambda^2$, we can conclude that $Energy \sim \lambda^2$ for an elastic network. Here, this energy depends on the stretch-rate. The energy recovered during the unloading of the sample was stored not only in the chemical network, but also in the physical network. With increasing stretch-rate, the number of active physical bonds increases. The energy stored in the network, which depends on the number of polymer chains, will then increase.

The increase in dissipated energy with stretch follows what seems to be a linear relationship with λ . It is very sensitive to the stretch-rate. We can also observe a sharp increase of this dissipated energy at $\lambda = 10$ for the stretch-rate of 0.3 s^{-1} , which might indicate some breaking of the chemical bonds at those high deformations.

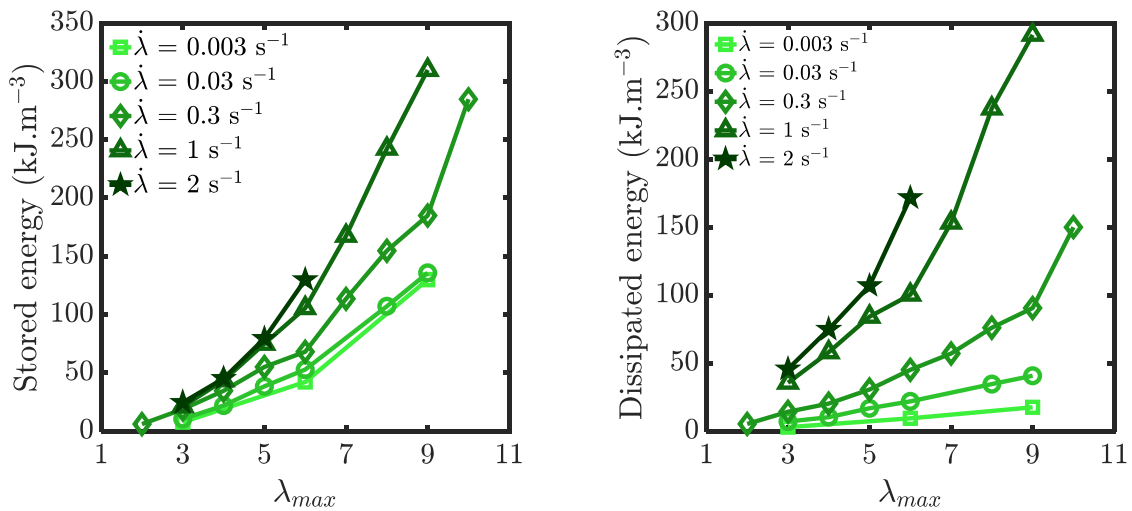


Figure 3.13: Stored (left) and dissipated (right) energies during a cyclic loading/unloading of the dual-crosslink hydrogel with $[Ni^{2+}] = 100 \text{ mmol/L}$, as a function of the maximal stretch of the cycle, realized for different stretch-rates.

3. Large deformations of dual-crosslink hydrogels with Ni²⁺ ions

The ratio of the dissipated energy to the total energy is shown in Figure 3.14, as a function of maximal stretch for different stretch rates. The value of hysteresis in percentage decreased with stretch, as well as stretch rate. This indicates that the material becomes more elastic with stretch, a classical feature of dissipative crosslinked networks that do not break, precisely because the elastic energy increases with λ^2 while the dissipated energy is linear with λ .

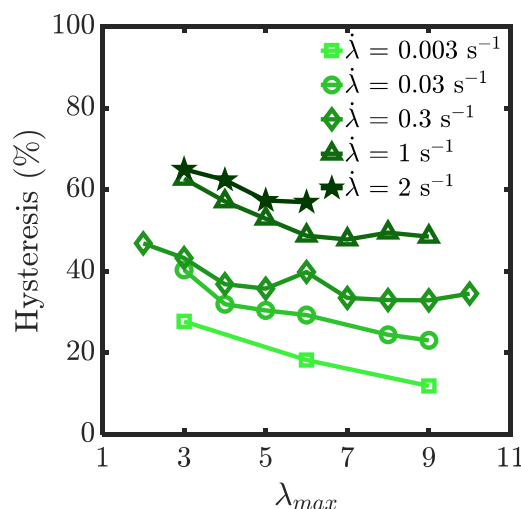


Figure 3.14: Proportion of dissipated energy to the total energy (in percentage) for the dual-crosslink hydrogel under cyclic deformation, as a function of the maximal stretch at different stretch-rates.

In an effort to renormalize the data and separate time dependent effects from strain dependent ones, these previous points can be plotted as a function of the time needed to reach the maximal stretch, as was done in Figure 3.15. The points superpose well for the higher stretch-rates. The points at low stretch-rates and low stretch ($\dot{\lambda} = 0.03 \text{ s}^{-1}$ and $\lambda = 3$ for example) seem a bit higher in hysteresis than the general trend, which might imply a higher dissipation at low stretches – and therefore an influence of the stretch on the energy dissipation. It is also interesting to note on this graph that we never reach a perfectly elastic network with 0% of dissipated energies even at times 10^3 higher than the main relaxation time of the hydrogel observed in rheology (0.16 s) that we attributed to the opening of a physical bond.

As previously mentioned, we also observed a residual stretch on the material after unloading. We found that the sample length did not follow the imposed stretch change and the sample exhibited buckling as shown in Figure 3.16. When the stretch was kept to 1 after unloading, the residual stretch disappeared with time, as shown by the pictures in Figure 3.16. It took about 1 h of waiting time for the buckling to disappear, in the case of a stretch at $\lambda = 3$.

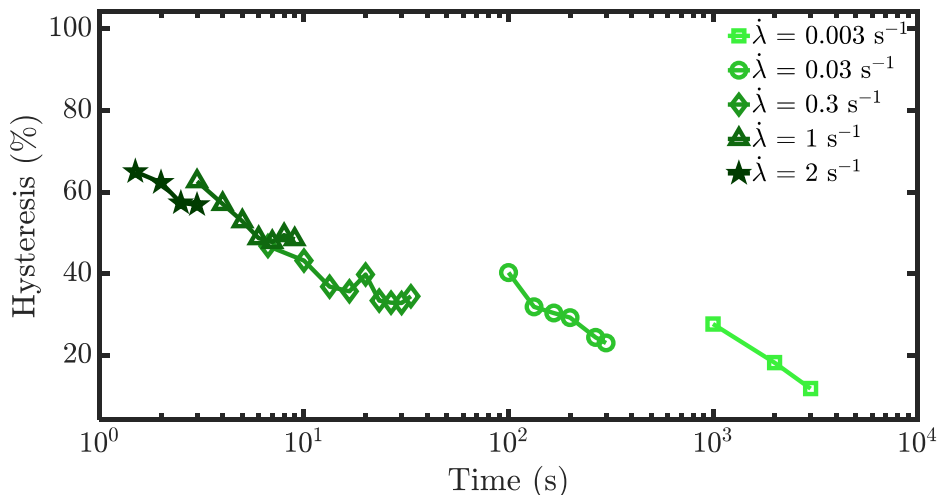


Figure 3.15: Hysteresis = Dissipated energy/Total energy (in percentage) in a dual-crosslink hydrogel under cyclic deformation, versus the time to reach maximal stretch

To understand whether this residual stretch is linked to the visco-elasticity of the sample or to a damage of the network, we realized cyclic experiments at low and high deformations, and studied the recovery of the hydrogel.

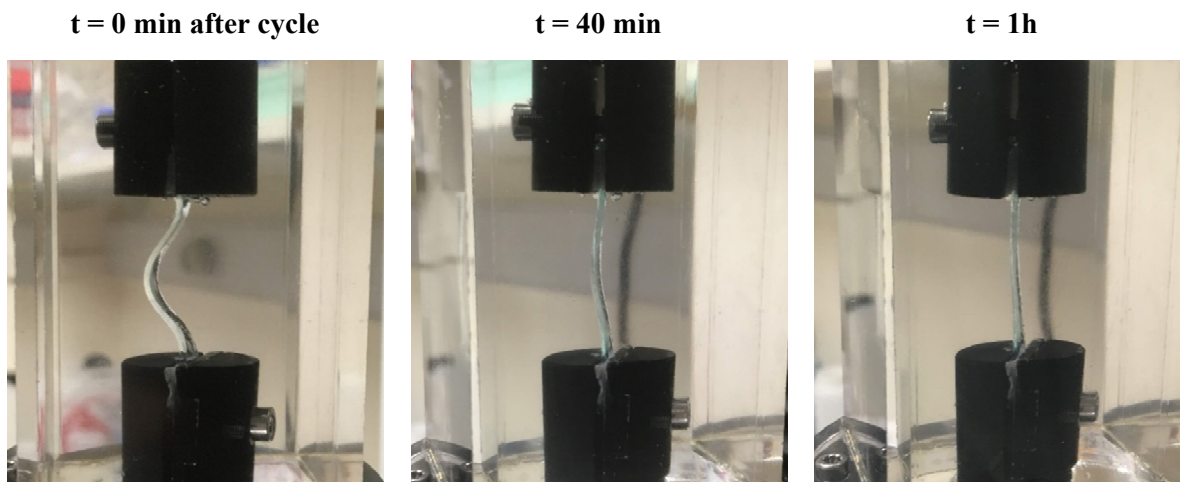


Figure 3.16: Pictures of a sample of the dual-crosslink hydrogel with $[\text{Ni}^{2+}] = 100 \text{ mmol/L}$, taken at different times after the end of the cycle ($\lambda = 1$ on the pictures).

3.2.2. Damage during cycles?

From the results shown in the previous sections, we have hypothesized that the physical bonds inhibit the nucleation of a crack in the dual-crosslink hydrogel. To prove this hypothesis, we attempted to detect the existence of broken polymer chains in the network before the complete rupture of the hydrogel. By applying cyclic deformations to a hydrogel at $\lambda > \lambda_{c,0}$ with $\lambda_{c,0}$ the stretch at break of the bare chemical gel, we should start breaking the chemical network. This damage might appear in the form of a change of mechanical properties (permanent residual strain, decrease in the elastic modulus,...).

First, we studied the behavior of the dual-crosslink hydrogel under cycles at $\lambda < \lambda_{c,0}$. This will give us a baseline of the viscous, non-permanent deformations occurring in the hydrogel when stretched. 50 cycles were applied to a sample of the dual-crosslink hydrogel, at $\lambda = 0.03 \text{ s}^{-1}$ and up to $\lambda = 3$. Figure

3. Large deformations of dual-crosslink hydrogels with Ni^{2+} ions

3.17 shows the stress measured during such a test, as a function of time. We observed a decrease of the maximal stress of each cycle, from 16 kPa for the first cycle until reaching a plateau at around 10 kPa.

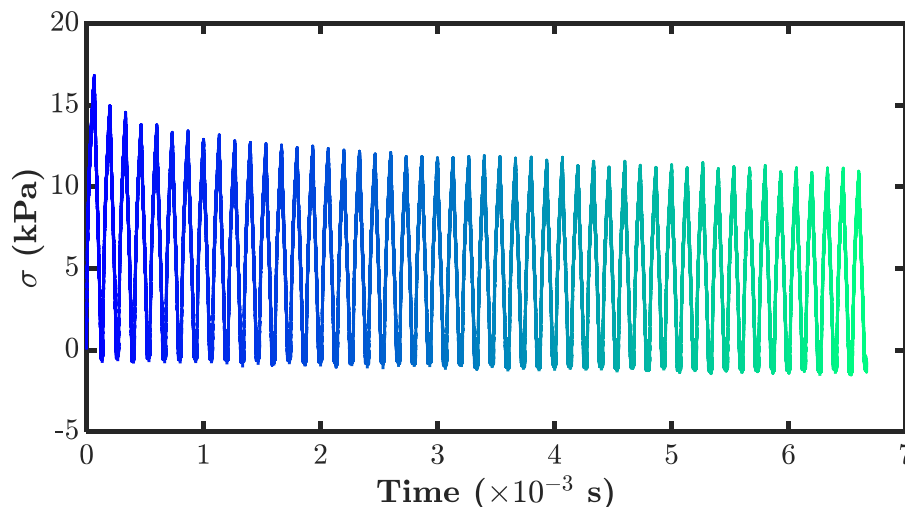


Figure 3.17: Time profile of the stress during the repeated cyclic deformations at $\lambda = 3$ and $\dot{\lambda} = 0.03 \text{ s}^{-1}$ for the dual-crosslink hydrogel.

Figure 3.18 shows the stress vs. strain curves of four of those 50 cycles (1st, 16th, 32th and 50th). We observed a very clear decrease of the hysteresis loop, along with this residual stretch we observed in Figure 3.16. We also found a decrease of the elastic modulus with the cycles.

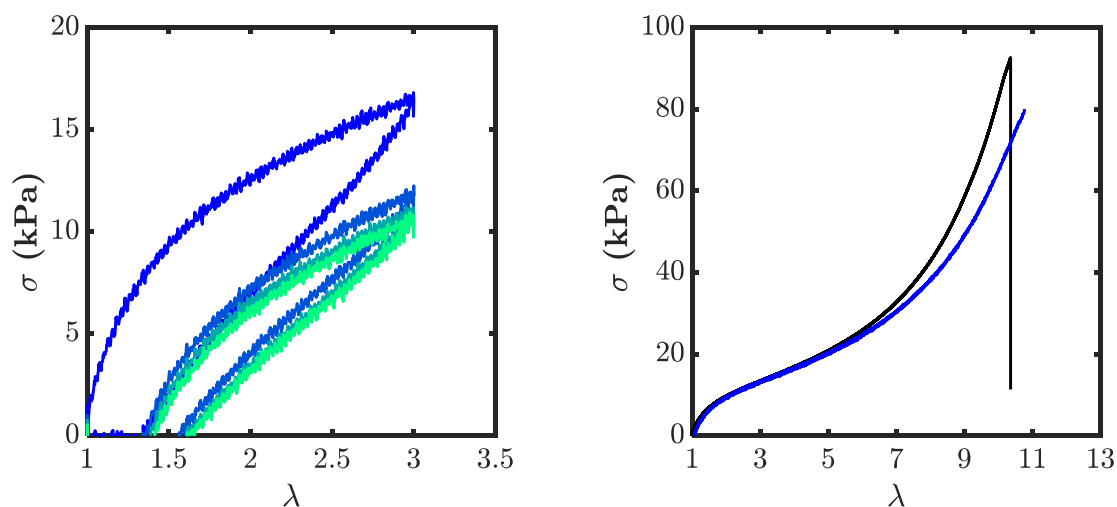


Figure 3.18: Left: Stress versus stretch for a cyclic loading/unloading test, realized on the dual-crosslink hydrogel with $[\text{Ni}^{2+}] = 100 \text{ mmol/L}$, at $\lambda = 3$ and $\dot{\lambda} = 0.03 \text{ s}^{-1}$. Are represented only the cycles $n^{\circ}1, 16, 32$ and 50 . Right: stress versus stretch of a continuous loading test realized on the dual-crosslink hydrogel before (black) and after (blue) the cycle test, with a waiting time of 60 min.

In order to check the recovery of the properties, after the 50 cycle tests with a waiting time of 60 min, we performed a continuous loading test to rupture. The stress stretch curve is shown in Figure 3.18 (right) with the curve for an intact sample (without cycle tests). The two curves superposed, thus the mechanical properties in tension of the dual-crosslink hydrogel were completely recovered after waiting

for around an hour. The only difference we can observe is in a lower level of strain-hardening, but this difference is within the repeatability of the experiment.

The same experiments were then realized at the same stretch-rate, but up to a maximal stretch $\lambda = 6 > \lambda_{c,0}$. The results are shown in Figure 3.19.

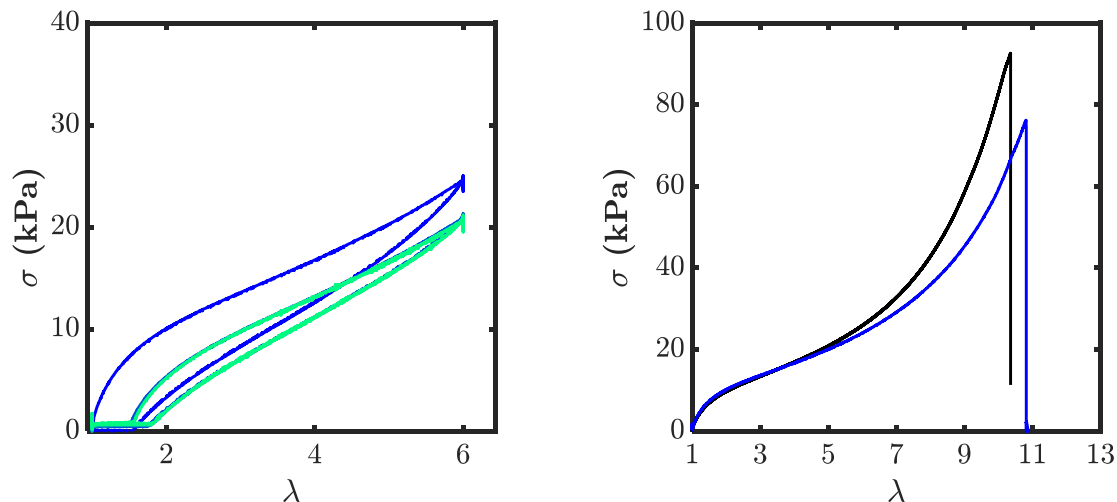


Figure 3.19: Left: Stress versus stretch for a cyclic loading/unloading test, realized on the dual-crosslink hydrogel with $[Ni^{2+}] = 100 \text{ mmol/L}$, at $\lambda = 6$ and $\dot{\lambda} = 0.03 \text{ s}^{-1}$. Are represented only the cycles $n^{\circ}1, 16, 32$ and 50. Right: stress versus stretch of a continuous loading test realized on the dual-crosslink hydrogel before (black) and after (blue) the cycle test, with a waiting time of 60 min.

The same observations as Figure 3.18 can be made here: we see the appearance of a clear residual strain after the first cycle, the modulus decreases with the cycles and the hysteresis loop between the loading and unloading curve seems to decrease. After a certain resting time, here between 1 and 2 hours, the material recovers its initial properties (as shown on the right graph of Figure 3.19). Again, there is a decrease of the intensity of strain-hardening, again within the repeatability margin of the experiment. However, since this observation can be made on both experiments (cycles at $\lambda = 3$ and $\lambda = 6$), it might be a real phenomenon. In this case, we could argue that the cycles provoke the breaking of the smallest polymer chains, which have the more influence on the strain-hardening. Breaking those chains can then in turn provoke a decrease of the level of strain-hardening reached by the material at high stretches.

The results of the cyclic tests were further analyzed with the values of the elastic modulus, the residual stretch and the different energies mentioned previously, plotted as a function of the cycle number in Figure 3.20 and Figure 3.21.

3. Large deformations of dual-crosslink hydrogels with Ni²⁺ ions

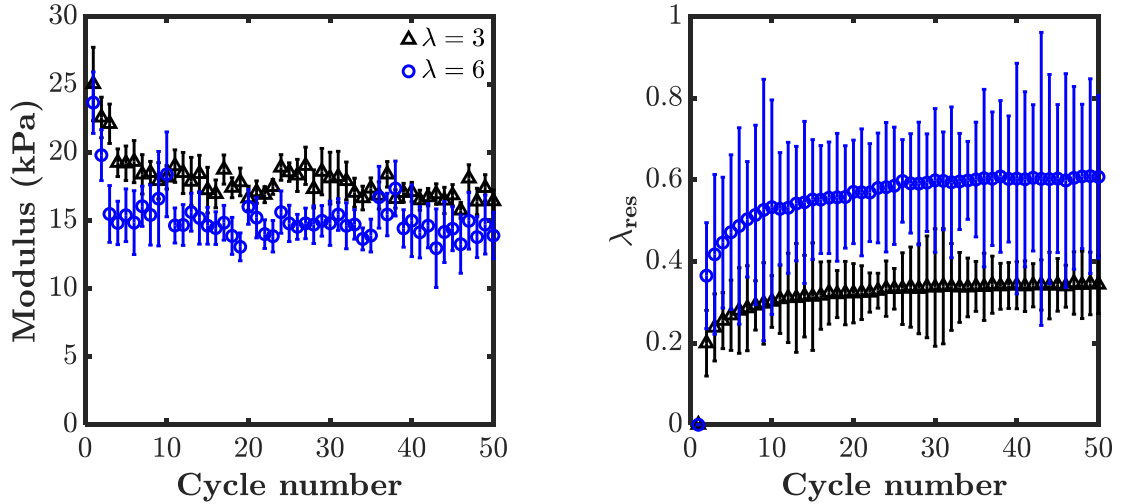


Figure 3.20: Modulus (left) and residual stretch after each cycle (right), versus the number of the cycle, for $\lambda_{stretch} = 3$ (black) and $\lambda_{stretch} = 6$ (blue).

The elastic modulus and the residual stretch reached a steady state after around 20 cycles for $\lambda_{stretch} = 3$, with a residual stretch of around 0.35 and a modulus decreased from 30 to 20 kPa. For the cycles at $\lambda_{stretch} = 6$, equilibrium is reached after around 30 cycles for the residual stretch, which reaches a plateau around 0.6. The Young's modulus drops this time to 15 kPa, which is slightly lower than for $\lambda_{stretch} = 3$.

The dissipated and stored energies also decreased with the cycle number for both maximal stretches (Figure 3.21). The decrease of the stored energy could be linked to a decrease in the number of chains of the elastic network if we were sure this energy was purely elastic. We showed in Figure 3.13 that we still have some visco-elastic phenomena during unloading, so the decrease might simply be a decrease of the visco-elastic properties of the material. Which can be confirmed by the clear decrease of the dissipated energy. Both decreases are much more important for $\lambda_{stretch} = 6$. The hysteresis decreases slightly with the cycles, but remains constant after the first 2 or 3 cycles.

In summary, we observed no clear evidence of damage of the material when stretching it multiple times above the critical stretch of the chemical network. However, the time needed for the hydrogel to relax to its initial length is much longer than what was found in linear rheology (one hour, compared to 0.1 second). This behavior, quite classic in dynamic materials with no chemical crosslinks [11,12] is certainly linked to the high levels of deformation imposed here.

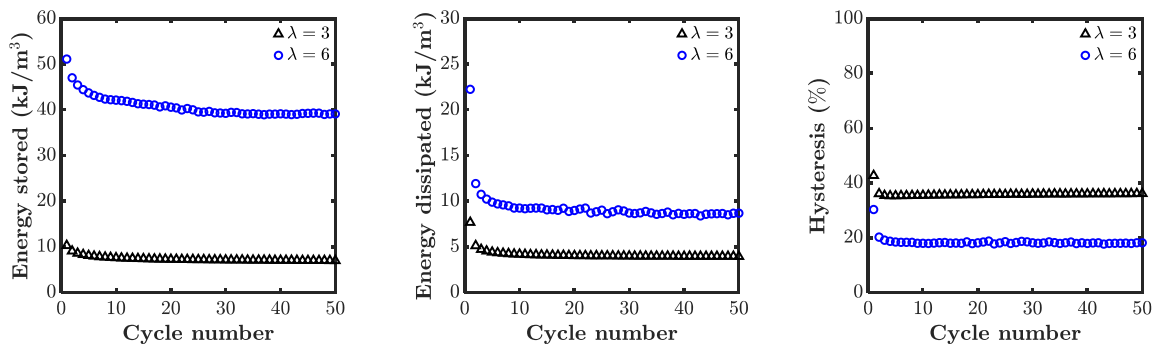


Figure 3.21: Stored energy (left), dissipated energy (center) and the ratio of dissipated energy over the total mechanical energy (right) for the dual-crosslink hydrogel during the cyclic test, as a function of the cycle number, for $\lambda_{stretch} = 3$ (black) and $\lambda_{stretch} = 6$ (blue).

The same experiments have been realized on the Ni^{2+} dual-crosslink hydrogel at $\dot{\lambda} = 0.3 \text{ s}^{-1}$ (ten times faster). The results (presented in the annexes) show the exact same behavior as what we just presented: decrease of the elastic modulus (from around 50 kPa to around 30 kPa), apparition of a residual stretch (0.5 at $\lambda = 3$, 0.9 at $\lambda = 6$), decrease in the energy dissipated with the number of cycles and slight decrease in hysteresis in the first few cycles. All these changes in properties are erased after a sufficiently long resting time, equivalent to the one observed at $\dot{\lambda} = 0.03 \text{ s}^{-1}$. The graphs are not presented here, in an attempt at clarity in this already long chapter.

When stretching the dual-crosslink hydrogel, the physical bonds break and reform themselves on another place on the polymer chain. The configuration of the “physical network” changes. When unloading the sample, in a perfectly elastic network, the chains would immediately go back to their initial, entropically stable state. Here, in the dual-crosslink network, this recovery is slowed down by the presence of physical bonds, which act as “sticky points” along the chains. Hence the longer relaxation time observed in large deformations than in rheology.

By applying multiple cycles to those gels, we ensure that we reach a steady state, where the behavior of the gel becomes always the same: during stretching, the network organization oscillates around an equilibrium state that is deformed, presenting an anisotropy. It then takes for the gel a long time (one hour for $\lambda = 3$, two hours for $\lambda > 6$, independent on the stretch-rate) to go back to its initial state: the physical bonds might break quite fast (dissociation kinetics measured at around 0.1 seconds in rheology), but they reform even faster (10^5 faster according to the kinetics of association and dissociation of complexes). We can imagine that they tend to reform in the place they just left, except from time to time when the chain has had the time to move between the dissociation and re-association. This would explain why it takes a long time for the gel to go back to its initial state.

3.3. Relaxation

One important question is the evolution of the dynamic of the network when a force is applied on the transient bond. In theory, the lifetime of the physical bond should decrease (or increase in the case of so-called ‘catch-bonds’) exponentially with the force applied [13,14], although the physical bond in the PVA-borax has been shown to be independent on the force [15]. In order to characterize the evolution of the bond lifetime with stretch or stress, relaxation tests were carried out on samples of the dual-crosslink hydrogel, at varied stretch values. The stretching was carried out at a constant stretch-rate

3. Large deformations of dual-crosslink hydrogels with Ni²⁺ ions

of $\dot{\lambda} = 0.3 \text{ s}^{-1}$. The results are shown in Figure 3.22. We observe an increase in the tensile stress after relaxation with the stretch, which was to be expected. We also observe that, at $\lambda \geq 5$ (which is the critical stretch of the chemical gel), the sample breaks while relaxing (the breaking of the samples at $\lambda = 5, 6$ happened after 1h of relaxation). We will first focus on the samples that did not break.

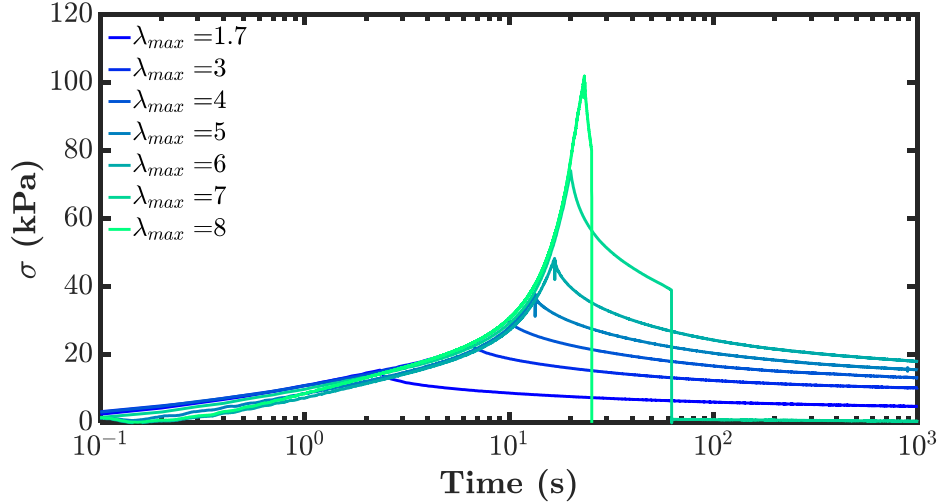


Figure 3.22: Stress relaxation tests for the dual-crosslink hydrogel at different stretches. Stretch-rate: $\dot{\lambda} = 0.3 \text{ s}^{-1}$

The reduced stress can also be represented in a way designed to minimize the effect of the initial stretch, as shown in Figure 3.23. In this figure, the time origin has been shifted so that the stress relaxation begins at 0.1 s. After an hour of relaxation, the reduced stress reaches a value around 3 kPa, which corresponds exactly to the value of the reduced stress of the bare chemical gel found in Figure 3.2. The ‘physical network’ has entirely relaxed and all the stress is now stored in the chemical network.

To compare the evolution of the relaxation time, we can normalize the stress by its initial value when the stress relaxation starts, which is represented on the right graph in Figure 3.23. The proportion of stress relaxed decreases slightly with applied stretch.

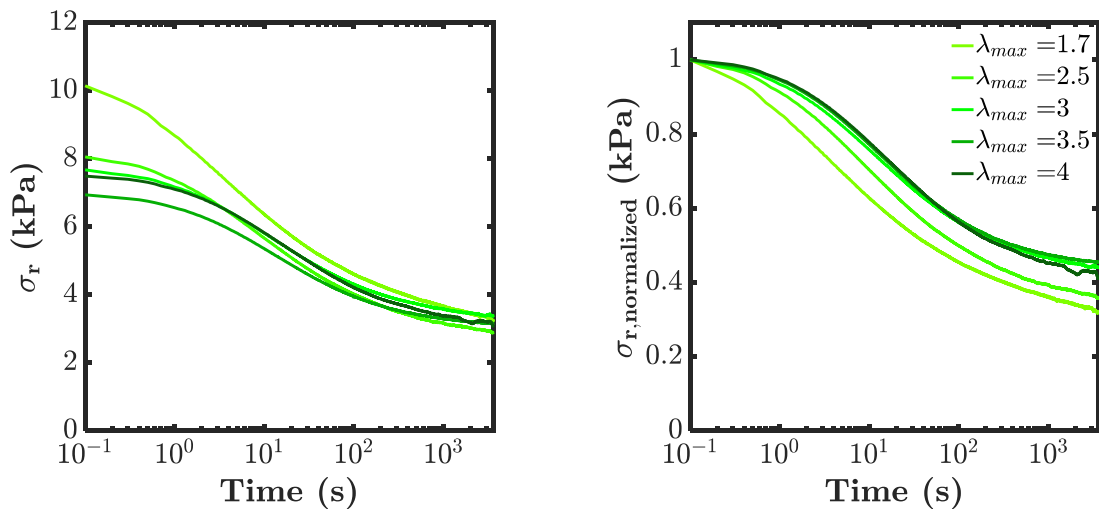


Figure 3.23: Reduced stress (left) and normalized reduced stress (right) vs. time for relaxation tests on dual-crosslink hydrogels at different levels of stretch. Time is shifted so that $t = 0.1 \text{ s}$ corresponds to the beginning of the relaxation.

This effect can be related to what we have shown in Figure 3.14: dissipation decreases as the stretch level increases. More precisely the relaxation time seems to increase with the level of stretch, until $\lambda = 3$ where it reaches a constant value. This is contrary to what we had shown in linear rheology. However, in linear rheology, the time needed to reach the applied strain is independent of deformation. In large strain, a finite time is needed to reach the desired stretch where the relaxation experiment starts and the material has already relaxed. It is thus difficult to compare the different relaxation times with this graph

However, we can look at the reduced stress σ_r versus the ‘real’ unshifted time, as done in Figure 3.24. In this figure, we can see that the stress relaxation at $\lambda = 4$ occurs faster than the relaxation at lower stretches. The reduced stress reaches the plateau of $\sigma_r = 3 \text{ kPa}$ before the others, ‘crossing’ the curves at $\lambda = 1.7$ and 3 for example. The curve obtained for $\lambda = 1.7$ seems to relax significantly more slowly than the others do. This would imply a decrease in the relaxation time with increasing stretch, which is more coherent with what we have seen in rheology.

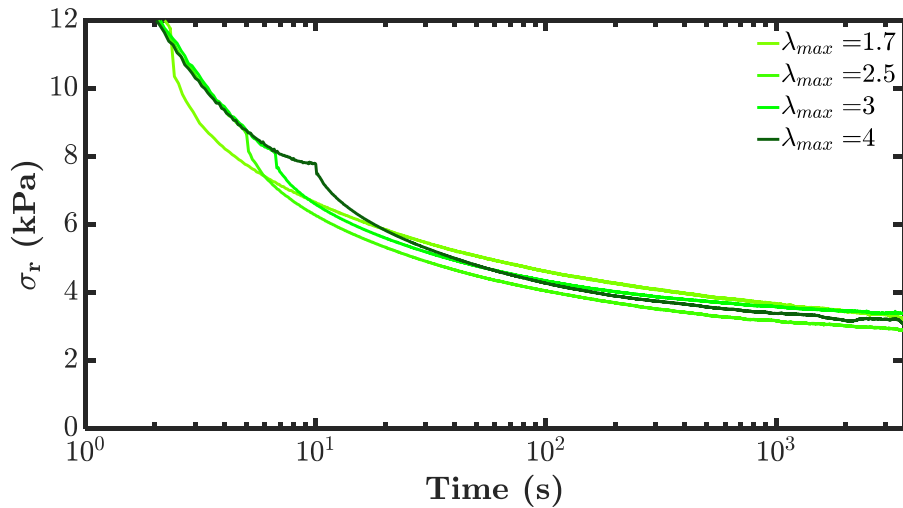


Figure 3.24: Reduced stress versus time for relaxation tests on Ni^{2+} dual-crosslink hydrogels up to different stretches, at $\dot{\lambda} = 0.3 \text{ s}^{-1}$.

The difference is however quite small. We can try to improve this experiment, by realizing relaxations at different stretches and ensuring that the desired stretch is always reached in 1 s. This was done in Figure 3.25. The differences between both relaxations are rather small. One might see faster relaxation dynamics in the higher stretched experiment, especially when looking at the normalized reduced stress.

3. Large deformations of dual-crosslink hydrogels with Ni²⁺ ions

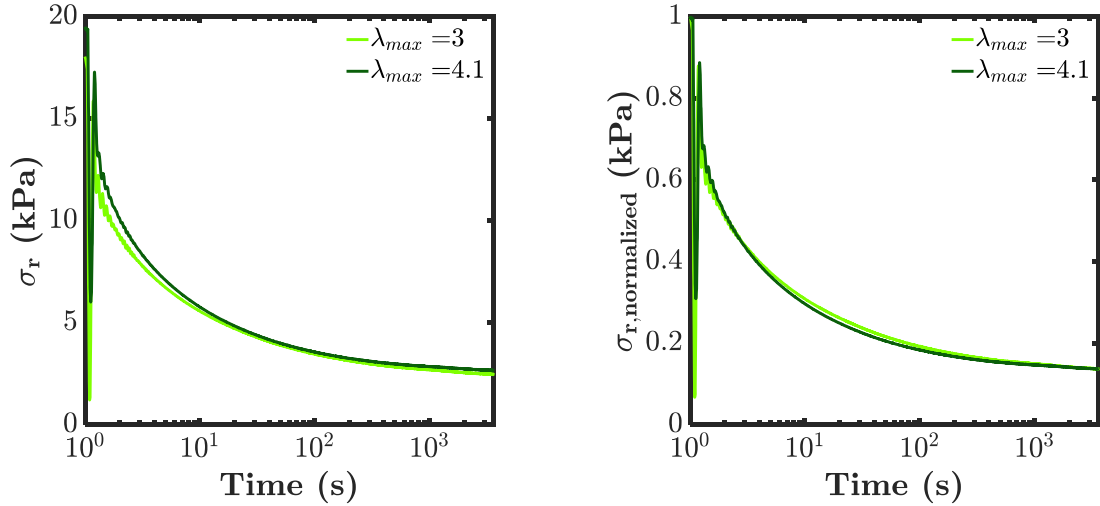


Figure 3.25: Reduced stress (left) and normalized reduced stress (right) vs. time for relaxation tests of the dual-crosslink hydrogels at different stretches. Maximal stretched was reached in 1 second.

As mentioned before, at higher stretches ($\lambda \geq 5$ with a fixed stretch-rate of $\dot{\lambda} = 0.3 \text{ s}^{-1}$), the sample breaks during the relaxation. This is obviously expected: since the material relaxes, the stress is being transferred from the physical network to the chemical network. The chemical bonds are subject to increasing stresses (and stretches), and start to break. The mechanism of prevention of crack nucleation we mentioned before (3.1.3) might delay the fracture of the sample, but at some point too many bonds are broken and a fracture nucleates and propagates.

This time to reach complete failure (for $\lambda \geq 5$) is shown in Figure 3.26, as a function of the imposed stretch or the reduced stress at break. The time to break follows exponentially the imposed stretch. The fact that the reduced stress at break, for lower stretches, is equal to σ_r for the chemical gel implies that, even after full relaxation of the physical network, bonds keep breaking in the material.

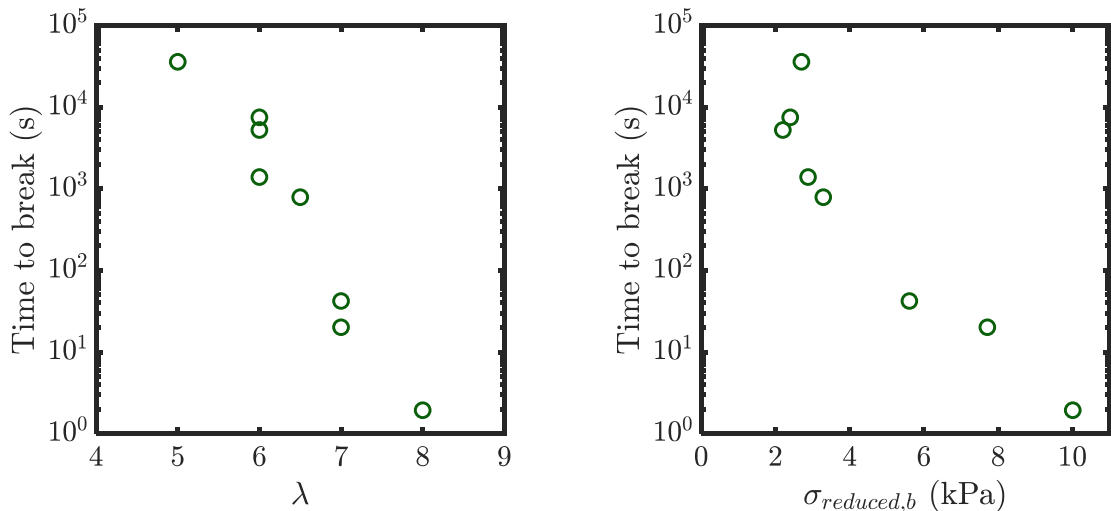


Figure 3.26: Time to break during relaxation, versus the imposed stretch (left) and the reduced stress at break (right)

This result further proves that the physical bonds delay the nucleation of a fracture, by preventing the correlated breaking of chemical bonds.

3.4. Fracture of Ni²⁺ dual-crosslink hydrogels

We have seen that the Ni²⁺ dual-crosslinked hydrogel is much tougher than the chemical gel, with higher stress and stretch at break. In this section, we will characterize more accurately this toughening of the material. Our hypothesis is that the fracture properties of our dual-crosslink hydrogel will directly evolve with its dynamics [16,17,18], being the toughest at a stretch-rate corresponding to the characteristic frequency of the physical bond.

3.4.1. Single-notch fracture under continuous stretching

We first realized tensile tests on single edge notch samples. The samples were 10 mm wide and the notch was around 1 mm long, measured accurately. This single edge notch geometry is the simplest geometry to study fracture, and Greensmith proposed a simple expression to quantify the energy release rate \mathcal{G} of single-edge notch samples for neo-Hookean elastomers:

$$\mathcal{G} = \frac{6}{\sqrt{\lambda}} c W(\lambda) \quad \text{Eq. 3.6}$$

With c the length of the notch and $W(\lambda)$ the stored energy density calculated from the uniaxial stress-strain curve of the un-notched sample. When $\lambda = \lambda_c$, the crack starts to propagate and $W(\lambda_c)$ can be estimated from the area under the stress-strain curve of the un-notched sample:

$$W(\lambda_c) = \int_1^{\lambda_c} \sigma d\lambda \quad \text{Eq. 3.7}$$

The energy release rate is then equal to the fracture energy Γ :

$$\Gamma = \frac{6 c W(\lambda_c)}{\sqrt{\lambda_c}} \quad \text{Eq. 3.8}$$

It should be noted that this formula has been established for non-linear elastic materials, where all the energy given to the material is available for the propagation of a crack. It has been used for some visco-elastic materials although in those materials, part of the energy has been dissipated and the energy available for the crack propagation is then less than what is given by the area under the loading curve. The true fracture energy is then lower than what is calculated by Eq. 3.8.

The computed values of Γ for a Ni²⁺ dual-crosslink hydrogel are presented in Figure 3.27, as a function of the stretch-rate employed in the test, along with the values of λ_c .

For the elastic chemical gel, there was no influence of the stretch-rate on its fracture properties. The critical stretch λ_c and the corresponding fracture energy Γ were constant, respectively around 1.8 and 10 J·m⁻².

The stretch at break of the notched dual-crosslink samples increases with the stretch-rate (from 3 to 6), which was not the case for the un-notched samples (constant around 10). This is followed by an increase in fracture energy Γ , from 80 to 800 J·m⁻². It is interesting to note that, even at low stretch-rates, the fracture energy of the dual-crosslink hydrogel was found much higher than that of the chemical gel. The fracture energy kept increasing at higher strain-rates, with no sign of a plateau. On the contrary, the critical stretch λ_c increased from 3.5 to 6 and then slightly decreased.

3. Large deformations of dual-crosslink hydrogels with Ni^{2+} ions

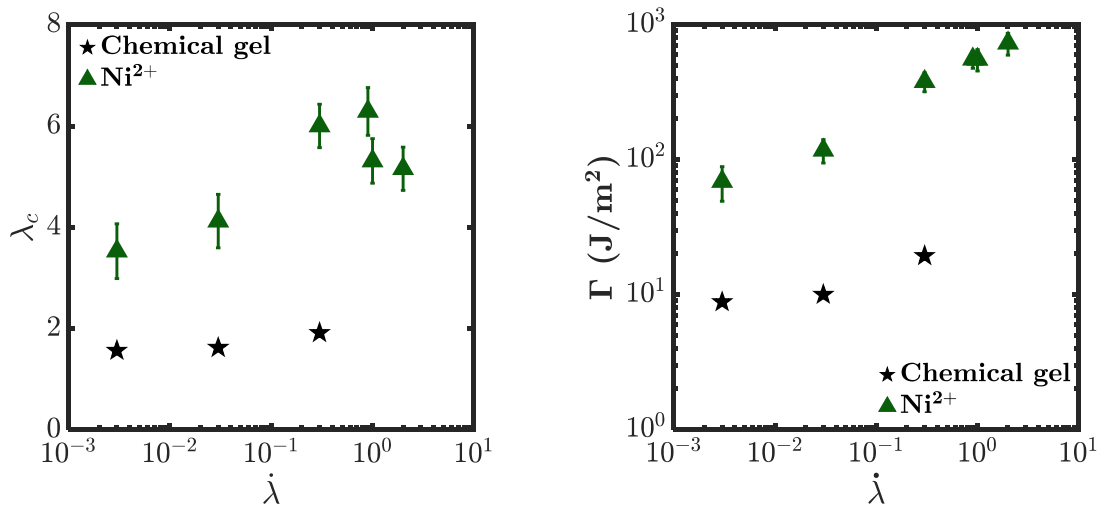


Figure 3.27: Critical stretch λ_c at which the crack starts to propagate (left) and corresponding fracture energy Γ (right) as a function of the stretch-rate, for a Ni^{2+} dual-crosslink hydrogel (green) and the corresponding chemical gel (black).

The crack speed increased slightly with stretch rate for the chemical gel (Figure 3.28). Since increasing the stretch rate does not really increase the fracture energy it is interesting to note that the average crack speed actually increases more significantly with strain-rate suggesting less dissipative conditions of propagation. For the visco-elastic dual-crosslinked hydrogel, the increase in crack speed with stretch-rate was much steeper: the crack propagation rate was one decade lower than that of the elastic chemical gel at low stretch-rates, and one decade higher at high stretch-rates.

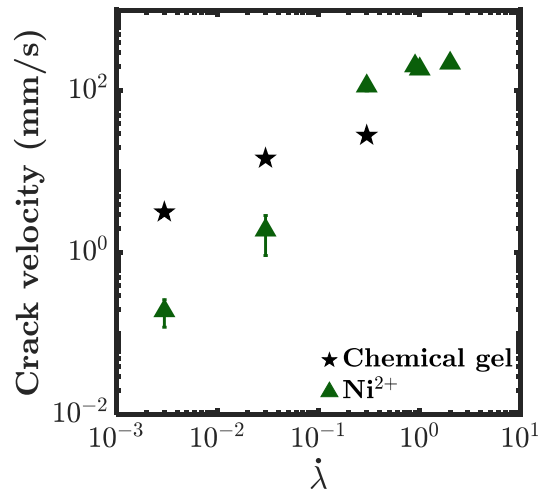


Figure 3.28: Propagation speed of the crack versus the stretch-rate, for the Ni^{2+} dual-crosslink hydrogel with $[\text{Ni}^{2+}] = 100 \text{ mmol/L}$ (green) and the corresponding chemical gel (black).

However, the value of Γ calculated in these results includes the energy dissipated during the loading stage. The real energy Γ_{local} available for fracture is lower than the energy Γ previously computed with a conventional method [16]. It is possible to estimate this energy available when the fracture propagates for each stretch-rate, using the data obtained in the cyclic experiments shown in Section 3.2. The results

are shown in Figure 3.29 (for the elastic chemical gel, $\Gamma_{local} = \Gamma$, as there is no hysteresis). The values of Γ_{local} evolved similarly to Γ at low stretch-rates, while at high stretch-rates they started to level off, showing the beginning of a plateau.

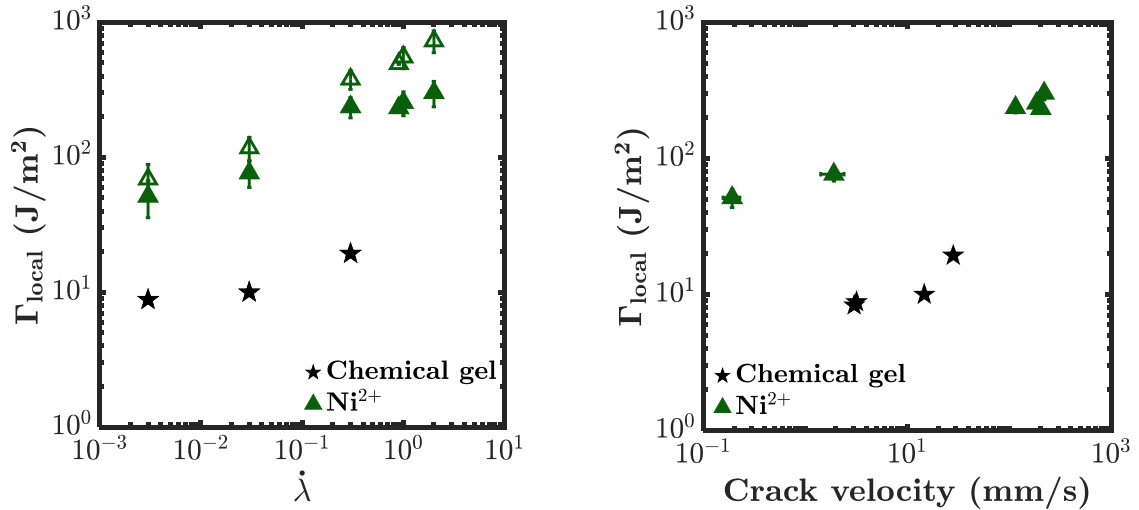


Figure 3.29: Left: Γ (empty symbols) and Γ_{local} (filled symbols) versus stretch-rate. Right: Γ_{local} versus the crack velocity.

Even taking into account the energy dissipated during the loading stage, the fracture energy at low stretch-rates was higher than that of the elastic chemical gel. It seems that the physical bonds enhance the fracture resistance of the dual-crosslinked hydrogel (λ_c and fracture energy) at stretch-rates where their input on the stress-strain curve of the hydrogel is minimal. It is also interesting to note that the critical stretch reaches a peak at $\dot{\lambda} = 0.1$ s⁻¹, a stretch-rate where, in the tensile tests, the elastic modulus just begins to show an influence of the physical bonds. This could imply that the imposed stretch-rate is not the effective stretch-rate at the crack tip, which is an expected behavior [8].

The speed at which the crack propagates could be a more relevant parameter, since it gives an idea of how fast the energy is transferred from one broken bond to its unbroken neighbor in the chemical network. This is shown on Figure 3.29 (right). Γ_{local} seems to follow a power law with the crack speed, increasing as $v^{0.25}$ (with v the crack speed).

3.4.2. Delayed fracture of “pure-shear” samples

In order to obtain a velocity of crack propagation independent from the stretch-rate, we realized experiments of delayed fracture: a pure-shear sample (with a height of around 20 mm, lower than its width around 60 mm) was notched, and stretched up to a certain deformation λ_{max} , at a stretch-rate $\dot{\lambda} = 0.3$ s⁻¹. Once the desired λ_{max} was reached, we maintained the stretch to follow the crack propagation. This experiment will allow us to reach much slower crack velocities.

3. Large deformations of dual-crosslink hydrogels with Ni²⁺ ions

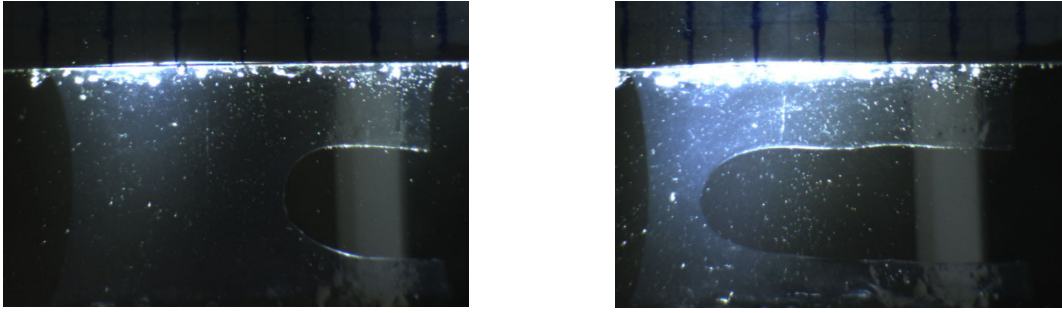


Figure 3.30: Propagation of a crack in a pure-shear sample.

For the elastic chemical gel, two cases appeared – either the fracture propagated (when $\lambda_{max} \geq 1.5$ in this geometry) or it did not propagate ($\lambda_{max} < 1.5$)

For the dissipative dual-crosslink hydrogel, at $\lambda_{max} \geq 1.5$, the crack should propagate at a velocity dependent on the applied stress, with a certain delay time dependent on the visco-elasticity of the material.

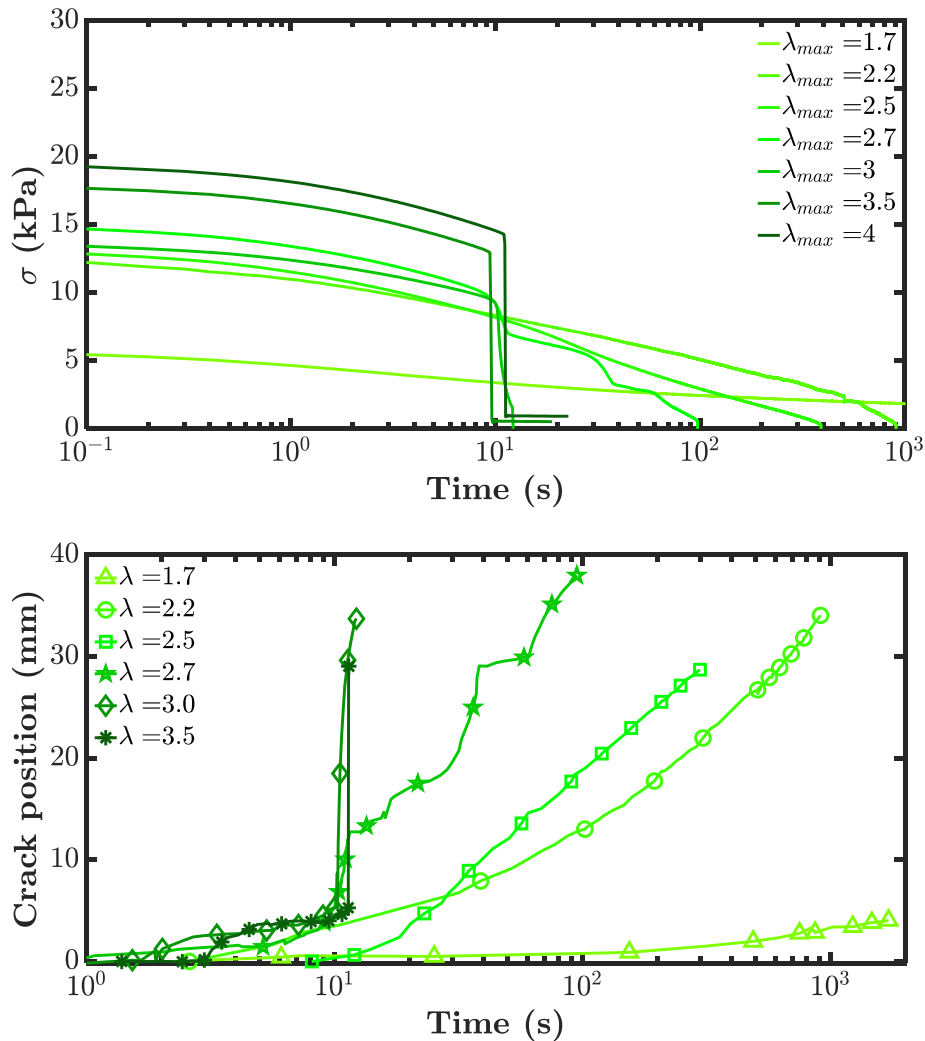


Figure 3.31: Stress vs. time (top) and Crack position vs. time (bottom) for relaxation tests on notched “pure shear” samples. The time $t = 0$ s corresponds to the beginning of the relaxation.

The fracture propagation in this experiment, shown in Figure 3.31, exhibited a peculiar profile:

- At $\lambda_{max} \leq 1.5$, the crack did not propagate. This was expected, since the chemical gel did not break at these small deformations either;
- At $1.5 < \lambda_{max} < 2.5$, the fracture propagated slowly, accelerating with time until complete fracture of the hydrogel. This propagation was particularly slow at $\lambda = 1.7$, close to the critical stretch value of the chemical gel in this geometry;
- At $\lambda_{max} \geq 2.5$, an unexpected behavior appears. Upon reaching $\lambda = 2.5$ during stretching, the crack propagated a little and immediately deviated vertically, i.e. along the loading direction, towards the top or the bottom of the sample (see Figure 3.32). Once the desired λ_{max} was reached, the crack continued to propagate slowly vertically. At a time $t \approx 10$ s, the crack propagated then fast and horizontally, i.e. normal to the propagation direction.



Figure 3.32: Propagation and deviation of a fracture at $\lambda \approx 2.5$ in a pure-shear sample of Ni^{2+} dual-crosslink hydrogel.

This behavior implies the appearance of an anisotropy in the material. This is certainly unexpected, and quite hard to explain. We have seen in the previous chapter the presence of clusters in the network. These clusters might have an influence on this anisotropy. To characterize it better, we plot the stretch and the fracture energy of the sample at the point of the crack deviation in Figure 3.33. The deviation always appears at a stretch around 2.4, and more precisely with a fracture energy of around $300 \text{ J} \cdot \text{m}^{-2}$.

This anisotropy at the crack tip that causes a deviation might be related to the anisotropy we have evidenced in Section 3.2. The orientation of the polymer chains in the tensile direction might change the organization of the physical bonds. This, along with the fact that our stretch-rate is of the order of magnitude of the opening frequency of the physical bond, might explain the difficulty for the crack to propagate horizontally.

The onset of crack propagation, for these samples where the crack deviates, will be taken as the beginning of the horizontal propagation (at around 10 seconds for those samples, in Figure 3.31).

3. Large deformations of dual-crosslink hydrogels with Ni²⁺ ions

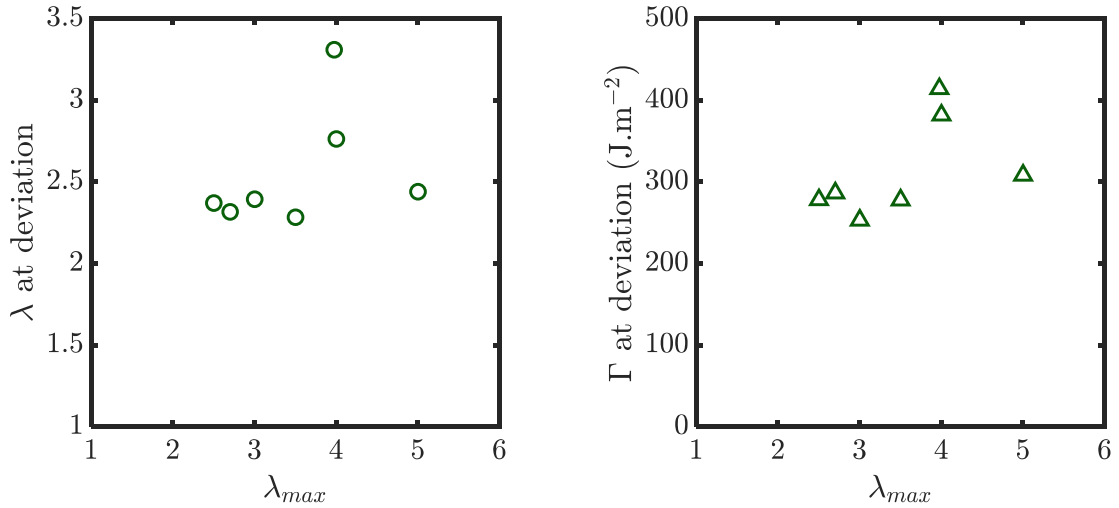


Figure 3.33: Stretch (left) and fracture energy (right) measured when the crack deviates in the pure shear sample of Ni²⁺ dual-crosslink hydrogel.

It is interesting to examine the time at which the propagation begins for all those samples, as done in Figure 3.34. We can see three different groups of samples:

- A sample at low λ_{max} (close to λ_{break} of the chemical gel) with an onset time (around 100 s here);
- Samples with no onset time at $\lambda_{max} \approx 2.2$;
- Samples with an onset time of around 10 s, at $\lambda_{max} \geq 2.5$.

The mean fracture velocity, also shown in Figure 3.34, increased with maximal stretch until reaching a plateau at around 2×10^4 s. It must be noted that, for these last three samples ($\lambda_{max} > 3.5$), the fracture was particularly fast and happens between two or three images of the video. The measure of time (resp. speed) of fracture might be overestimated (resp. underestimated).

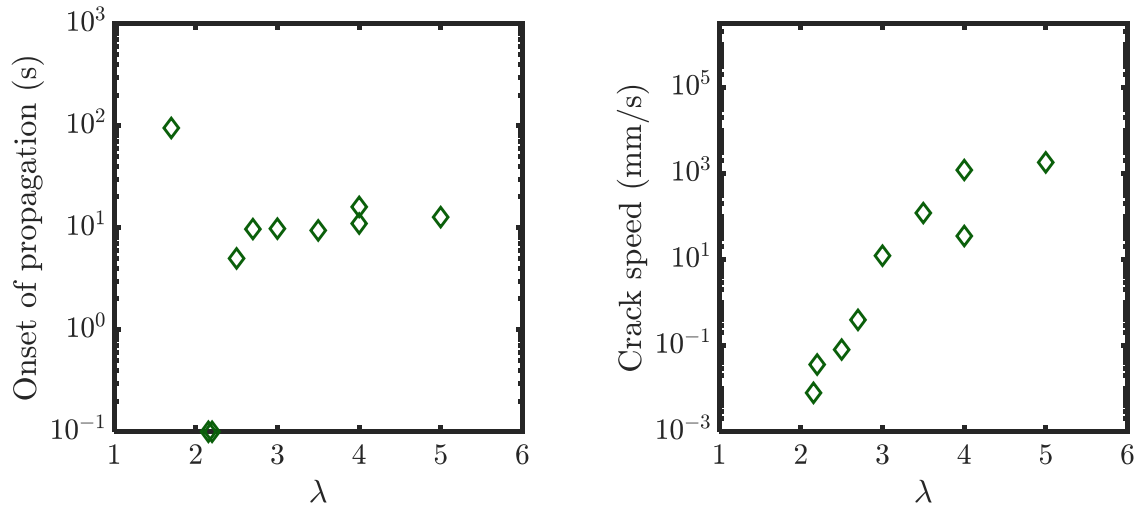


Figure 3.34 Onset time of propagation (left) and mean crack velocity (right) as a function of the maximal stretch, for pure-shear samples of Ni²⁺ dual-crosslinked hydrogels.

Some of the samples (at $\lambda = 2.2$ and $\lambda = 4$) have been repeated with different heights (around 14 mm) and width (40 mm), explaining the differences in crack velocity. It is then interesting to look at the

fracture energy of those samples, to understand how this crack velocity distributes with the fracture energy. To obtain this fracture energy, we must first compute the energy \mathcal{G} brought to the system:

$$\mathcal{G} = \int_1^\lambda \sigma d\lambda \quad \text{Eq. 3.9}$$

And the fracture energy Γ is simply:

$$\Gamma = \mathcal{G}(\lambda_{break}) * H * \text{Energy dissipated} \quad \text{Eq. 3.10}$$

with H the height of the sample. The “energy dissipated” factor is here to take into account the bulk relaxation of the material while the fracture does not propagate. This way, Γ represents the energy in the material when the crack starts propagating. This factor is taken from the relaxation curves on pristine samples shown in Figure 3.23.

The results are plotted in Figure 3.35 (left). As expected, the fracture energy for the two samples with different geometry is different. Finally, when looking at the energy release rate \mathcal{G} versus the crack velocity (Figure 3.35 right), all these points fall nicely into a single curve. Here, it seems that the fracture energy controls the velocity of the crack propagation.

The points obtained for the reference chemical gel have been added on the graphs. They show a clear toughening of the material thanks to the physical bonds. A crack in this chemical hydrogel propagates immediately once reaching $\lambda \approx 1.8$.

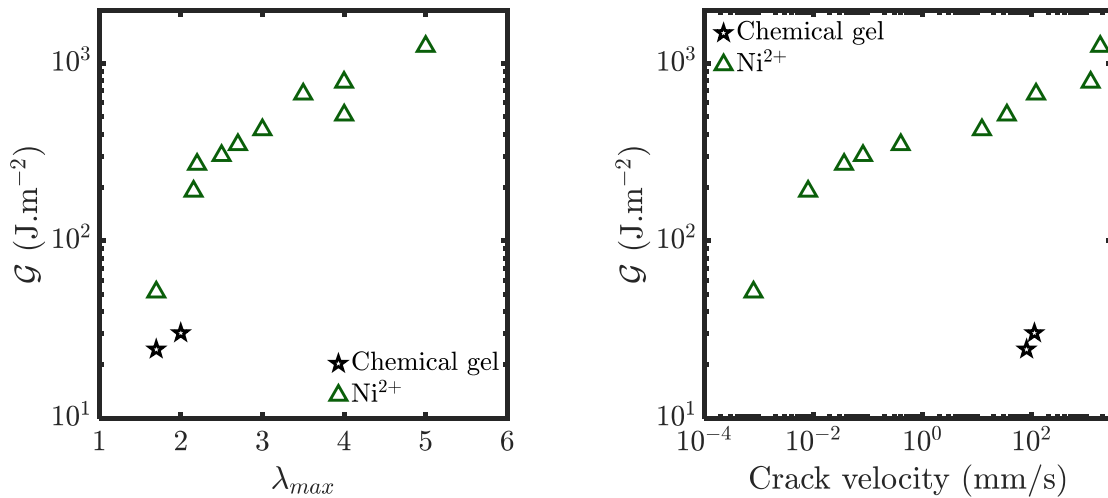


Figure 3.35: Left: Fracture energy versus the applied stretch. Right: Energy release rate versus mean crack velocity.

Plotting the onset of crack propagation versus the energy or the crack velocity (Figure 3.36) reveals again the three groups of samples we previously mentioned: one with a slow propagation and a large time of onset; one with immediate and moderately fast propagation; and a last one showing this crack deviation, with an onset time of 10 s and a fast propagation.

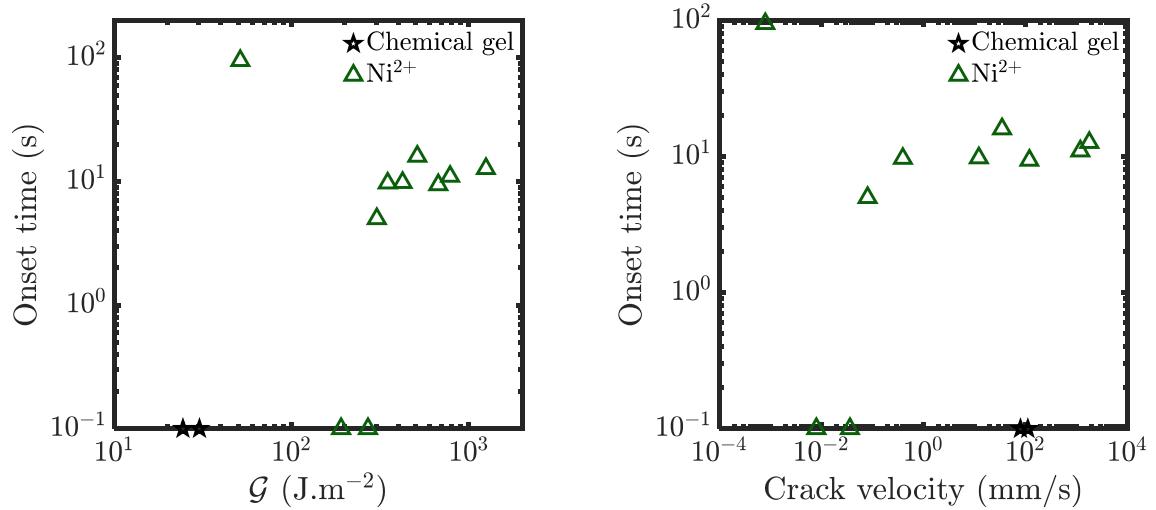


Figure 3.36: Time of onset of crack propagation, versus the energy release rate imposed (left) or the mean crack velocity (right).

3.5. Conclusions and discussions

In this chapter, we have studied the mechanical properties in large deformations of the P(AAm-co-VIm)-Ni²⁺ dual-crosslink hydrogel we had prepared in the last chapter. The rheology shown a behavior extremely dependent on the frequency at which the material was deformed, a result we clearly confirm in this chapter.

The properties in large deformations of this hydrogel are quite interesting. Its Young's modulus increases with the stretch-rate. This suggests that the lifetime of the physical bonds is of the order of magnitude of the inverse of the stretch-rate and hence the number of physical crosslinks increases with the stretch-rate, leading to an increase in Young's modulus. This first steep increase in stress is followed by a softening of the material, which we have shown to be independent on the stretch. This softening is indeed a stress relaxation linked to the breaking of the physical bonds, and the subsequent decrease in the number of physical bonds in the network.

Upon reaching a certain stretch, the material starts showing a strain-hardening behavior. At low stretch-rates, where the physical bonds have a low influence on the mechanical properties, this onset was quite independent on the stretch-rate. At higher stretch-rates however, the intensity of this strain-hardening starts to increase and its onset to decrease, following a well-known law. We have shown that this strain-hardening (at high stretch-rates) depends only on the stretch and can be normalized. In competition with the linear relaxation we have seen when stretching the material, there is an increase in the stress the network bears because of the increasing number of polymer chains in their strain-hardening regime. When increasing the stretch-rate, one increases the number of active physical bonds and hence, increases the number of polymer chains. This in turn increases the level of strain-hardening observed. The onset and the intensity of this strain-hardening behavior are dependent on the stretch-rate, but the strain-hardening itself follows a law independent on the stretch-rate.

Interestingly, the stretch at break of the dual-crosslink hydrogel was found to be independent on the stretch-rate, apart from the highest stretch-rate where it decreases slightly. Our hypothesis was that the fracture properties of this material would be greatly increased at stretch-rates around the characteristic

frequency of the physical bond. Here however, at stretch-rates much lower than the characteristic frequency of the bond (marked by a steep increase of the Young's modulus), the material is much more stretchable than its elastic counterpart. This behavior was explained by the fact that the nucleation of a crack happens at a characteristic speed relatively independent on the stretch-rate. The physical bonds will then be active at this speed, delaying the nucleation of a crack inside the network by preventing the correlated breaking of polymer chains. The slight decrease we observe at higher stretch-rates might be linked to our initial hypothesis: when reaching observation times (or stretch-rates) much shorter than the characteristic lifetime (or higher than the characteristic frequency) of the physical bond, those bonds begin to act as permanent bonds. They do not break, do not dissipate energy, and cannot toughen the network.

To better characterize the energy dissipation inside such a hydrogel at large deformations, we have realized cyclic experiments at certain levels of stretch and stretch-rates. These experiments evidenced the high stretch-rate dependence of the energy dissipation inside the material. This dissipated energy also follows linearly the imposed stretch. These experiments also highlighted the time-dependence of the percentage of energy dissipated during a loading experiment. This percentage decreases with the time to stretch the sample, which corresponds to our conclusions: the shorter the observation time, the more physical bonds are active, and the more physical bonds can break and dissipate energy.

To prove our hypothesis that the physical bonds delay the nucleation of a crack by preventing the correlated breaking of polymer chains, we realized some cyclic experiments at high deformation. They showed no sign of molecular damage inside the hydrogel. All the changes observed were of visco-elastic nature, and disappeared after a certain resting time. These experiments allowed us however to evidence the apparition in the network, at high deformations, of an anisotropic organization dependent on the stretch and stretch-rate. Upon stretching the network, the polymer chains align in the tensile direction. When unloading, because of the physical bonds, the polymer chains do not relax immediately to their original position. This anisotropy takes quite a long time to disappear.

The relaxation experiments we realized to try to evidence an influence of the stretch on the relaxation time were not very conclusive, which tends to confirm our argument of a separation between time and stretch.

Finally, we focused on the fracture properties of the Ni²⁺ dual-crosslink hydrogel. This material shows a particularly clear toughening compared to the reference chemical gel. We observed a significant increase of the fracture energy with the stretch-rate, along with an increase in the crack velocity. Contrary to those two values, the critical stretch at which the crack propagates showed a peak at intermediary stretch-rates. This could imply the beginning of the fragilization of the material, but the fracture energy does not decrease accordingly. The fracture energy increases quite closely with the crack velocity. We tried to confirm this result by realizing some delayed fracture experiments, where we impose a certain energy release rate to the material, and measure the resulting crack velocity. These experiments showed that the energy controls the velocity of the crack. They also showed a particularly interesting behavior: upon reaching a certain stretch or fracture energy, at the stretch-rates we used, the crack starts propagating and immediately deviates at an angle of 90°. This deviation could be related to an anisotropy in the network, happening at large deformations, induced by the orientation of the polymer

3. Large deformations of dual-crosslink hydrogels with Ni²⁺ ions

chains along the tensile direction and the long lifetime (at the observation times considered here) of the physical bonds, which tends to ‘freeze’ this anisotropy.

We have shown that this dual-crosslink hydrogel does not follow exactly the behavior we expected: it seems to behave as we expected at higher stretch-rates, with a decrease in extensibility and a beginning of a plateau in the fracture energy; however, it is still quite stretchable and tough at low stretch-rates. We cannot explore these low- and high-stretch-rate domains in our laboratory: the experiments would be too long in the first case, and our machines do not allow us to reach higher stretch-rates than what we have done here. In the next chapters, we will see how we overcame these two issues.

References

1. Zhao, J. Structure et propriétés des hydrogels à réticulation chimique et physique. (PSL Research University, 2018).
2. Zhao, J., Mayumi, K., Creton, C. & Narita, T. Rheological properties of tough hydrogels based on an associating polymer with permanent and transient crosslinks: Effects of crosslinking density. *Journal of Rheology* 61, 1371–1383 (2017).
3. Zhao, J., Narita, T. & Creton, C. Dual Crosslink Hydrogels with Metal-Ligand Coordination Bonds: Tunable Dynamics and Mechanics Under Large Deformation. in *Self-Healing and Self-Recovering Hydrogels* vol. 285 1–20 (Springer International Publishing, 2020).
4. Mayumi, K., Marcellan, A., Ducouret, G., Creton, C. & Narita, T. Stress–Strain Relationship of Highly Stretchable Dual Cross-Link Gels: Separability of Strain and Time Effect. *ACS Macro Lett.* 2, 1065–1068 (2013).
5. Mooney, M. A Theory of Large Elastic Deformation. *Journal of Applied Physics* 11, 582–592 (1940).
6. Rivlin, R. S. Large elastic deformations of isotropic materials. I. Fundamental concepts. *Philosophical Transactions of the Royal Society of London. Series A, Mathematical and Physical Sciences* 240, 459–490 (1948).
7. Degrandi-Contraires, E., Lopez, A., Reyes, Y., Asua, J. M. & Creton, C. High-Shear-Strength Waterborne Polyurethane/Acrylic Soft Adhesives. *Macromolecular Materials and Engineering* 298, 612–623 (2013).
8. Creton, C. & Ciccotti, M. Fracture and adhesion of soft materials: a review. *Reports on Progress in Physics* 79, 046601 (2016).
9. Long, R., Mayumi, K., Creton, C., Narita, T. & Hui, C.-Y. Time Dependent Behavior of a Dual Cross-Link Self-Healing Gel: Theory and Experiments. *Macromolecules* 47, 7243–7250 (2014).
10. Filippidi, E. et al. Toughening elastomers using mussel-inspired iron-catechol complexes. *Science* 358, 502–505 (2017).
11. Zheng, S. Y. et al. Metal-Coordination Complexes Mediated Physical Hydrogels with High Toughness, Stick–Slip Tearing Behavior, and Good Processability. *Macromolecules* 49, 9637–9646 (2016).
12. Sun, J.-Y. et al. Highly stretchable and tough hydrogels. *Nature* 489, 133–136 (2012).
13. Pereverzev, Y. V. & Prezhdov, O. V. Force-induced deformations and stability of biological bonds. *Physical Review E* 73, (2006).
14. Sarangapani, K. K. et al. Low Force Decelerates L-selectin Dissociation from P-selectin Glycoprotein Ligand-1 and Endoglycan. 9.
15. Guo, J., Long, R., Mayumi, K. & Hui, C.-Y. Mechanics of a Dual Cross-Link Gel with Dynamic Bonds: Steady State Kinetics and Large Deformation Effects. *Macromolecules* 49, 3497–3507 (2016).
16. Mayumi, K., Guo, J., Narita, T., Hui, C. Y. & Creton, C. Fracture of dual crosslink gels with permanent and transient crosslinks. *Extreme Mechanics Letters* 6, 52–59 (2016).
17. Arora, S., Shabbir, A., Hassager, O., Ligoure, C. & Ramos, L. Brittle fracture of polymer transient networks. *Journal of Rheology* 61, 1267–1275 (2017).

3. Large deformations of dual-crosslink hydrogels with Ni²⁺ ions

18. Zheng, S. Y. et al. Fracture of tough and stiff metallosupramolecular hydrogels. *Materials Today Physics* 13, 100202 (2020).

Chapter 4

Dual-crosslink hydrogels with faster dynamics

4. Dual-crosslink hydrogels with faster dynamics

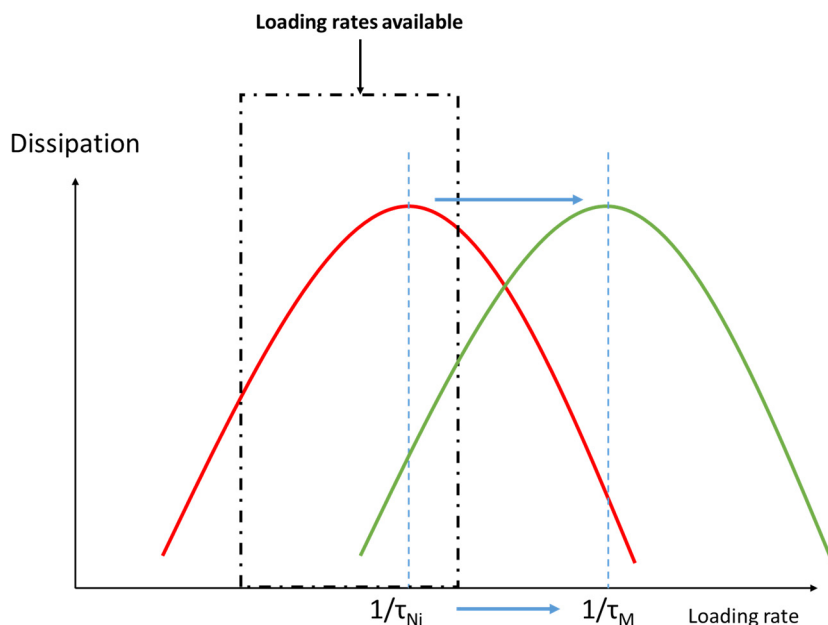
Table of contents

4.1. Preparation	129
4.1.1. Cu ²⁺ dual-crosslink hydrogel.....	129
4.1.2. Zn ²⁺ dual-crosslink hydrogels	130
4.1.3. Absorption isotherms	130
4.2. Rheology	131
4.2.1. Cu ²⁺ and Zn ²⁺ dual-crosslink hydrogels	131
4.2.2. Zn ²⁺ dual-crosslink hydrogel – “One-pot” vs. “Diffusion”	132
4.3. Small-angle X-Ray scattering.....	132
4.3.1. General observations	133
4.3.2. Fitting	134
4.3.3. Scattered intensity normalization method	135
4.3.4. Normalized results – comparison between Ni ²⁺ and Zn ²⁺ dual-crosslink hydrogels	137
4.3.5. Conclusions	139
4.4. Large deformations	139
4.4.1. “One-Pot” vs “Diffusion” Zn ²⁺ hydrogels.....	140
4.4.2. Tensile tests on Zn ²⁺ and Cu ²⁺ dual-crosslink hydrogels.....	140
4.5. Cyclic tests.....	145
4.5.1. Influence of stretch-rate and stretch	145
4.5.2. Damage during cycles?	147
4.6. Fracture of a fast dual-crosslink hydrogel.....	150
4.6.1. Single-notch fracture under continuous stretching.....	150
4.6.2. Delayed fracture of “pure-shear” samples of Zn ²⁺ dual-crosslinked hydrogel.....	152
4.7. Conclusions	154
References	157

4. Dual-crosslink hydrogels with faster dynamics

As shown in the previous chapters, we have intensively studied the properties of the dual-crosslink hydrogel with Imidazole- Ni^{2+} coordination bonds. Since its main characteristic time (related to the transient physical bonds breaking) was experimentally easily accessible, the frequency- and stretch rate-dependences of the mechanical properties were successfully characterized. At the characterization time scales close to the dissipation peak, stiffening (increase in the modulus) and toughening having stretch-rate dependences were evidenced.

Now a next question arises: what are the mechanical properties and their stretch rate dependences when the dissipation by the dynamic bonds does not occur? The dissipation decreases at two extremities: (1) at slow experimental time scales or with short-lived dynamic bonds, and (2) at fast experimental time scales or equivalently with long-lived dynamic bonds. In this chapter, we will investigate the former case, slow experiments or fast dynamics, as one might expect recovery of the properties of the corresponding chemical gel without the dissipation. It is rather difficult to expand the experimental time scales to the slower range: the experiments are time consuming, and drying and poroelasticity of hydrogels could limit the accuracy of measurements. Alternatively, we will now try to change the dynamics of the hydrogel, by using different metal ions than Ni^{2+} . In this chapter, we will prepare hydrogels whose dynamics are faster than that of the Ni^{2+} dual-crosslink hydrogel. The stretch-rates and frequencies available on our experiments would then be slow compared to the dynamics of the hydrogel, which should not dissipate much energy (see Scheme 4.1). We will then be able to study the toughness of a low-dissipation dual-crosslink hydrogel. Ideally, this will allow us to create a mastercurve of the dissipation as a function of the relative stretch-rate (see Scheme 4.2), and we would be able to compare this evolution of dissipation with an evolution of the fracture properties.



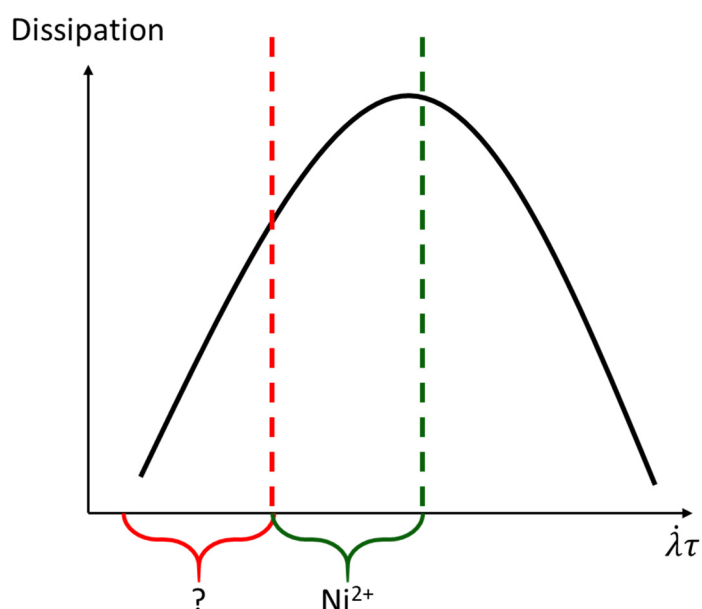
Scheme 4.1: By changing the metal ion used in the physical bonds, it is possible to change the dynamics of the hydrogel and thus, its behavior

The study of the Ni^{2+} dual-crosslink hydrogels has also raised many questions on the organization of the physical bonds inside the gel and the influence of this organization on the material properties. Thus, we will evaluate the influence of the lifetime of the physical bond on the microstructure.

In this chapter, we will characterize two dual crosslink gels: with Cu^{2+} ions and with Zn^{2+} ions, the latter being the most extensively studied. Those ions are expected to give hydrogels with faster dynamics than the Ni^{2+} dual-crosslink hydrogel, as shown on Table 4.1.

*Table 4.1: Stability constant of Imidazole-metal complexes, and corresponding association and dissociation kinetic constants for the dissociation of one imidazole from a $[\text{MIm}_2]$ complex. *computed from value at $T=0^\circ\text{C}$. Data from [1,2,3,4]*

Metal ion	$\log(K_1)$	$\log(K_2)$	$\log(K_3)$	$\log(K_4)$	k_{ass} ($\text{M}^{-1}\cdot\text{s}^{-1}$)	k_{diss} (s^{-1})
Ni^{2+}	3.03	2.51	2.01	1.47	4.3×10^3	8.9
Zn^{2+}	2.56	2.37	2.23	2.03	4×10^9 *	2×10^7 *
Cu^{2+}	4.2	3.51	2.95	2.25	-	-



Scheme 4.2: (By shifting the stretch-rates with the lifetime of the physical bond, we could reconstruct the behavior of a dual-crosslink hydrogel over a wide range of Weissenberg numbers.

4.1. Preparation

The same P(AAm-co-VIm) chemical gel was used. The synthesis was described in Chapter 2.

4.1.1. Cu^{2+} dual-crosslink hydrogel

The synthesis of “One-pot” P(AAm-co-VIm) dual-crosslink hydrogels with Cu^{2+} ions is not possible, as Jingwen Zhao previously showed during her PhD. The only hydrogels studied with Cu^{2+} ions will therefore be “Diffusion” hydrogels. P(AAm-co-VIm)- Cu^{2+} dual crosslink gels were prepared with the same method described in Chapter 2.

Cu^{2+} ions were found however less stable in the preparation solution than Zn^{2+} or Ni^{2+} ions: after a few days in solution, we observed some precipitations of those ions, which decreased the accuracy of the ion concentration measurements and obviously changed the behavior of the hydrogel. A control of the pH

4. Dual-crosslink hydrogels with faster dynamics

was needed to conserve them for longer times. Unless otherwise stated, the Cu^{2+} dual-crosslink hydrogels used in this chapter were tested during the week after their preparation.

4.1.2. Zn^{2+} dual-crosslink hydrogels

“Diffusion” dual-crosslink hydrogels with Zn^{2+} ions were prepared in the same manner as the other “Diffusion” dual-crosslink hydrogels.

Jingwen Zhao has previously synthesized during her PhD a “One-pot” dual-crosslink hydrogels with Zn^{2+} ions, with the same method as the dual-crosslink hydrogels with Ni^{2+} ions shown in the previous chapter. Though their mechanical properties corresponded well to those of the dual crosslink gel systems, her hydrogels exhibited opacity, presumably due to precipitation of small amounts of zinc oxide particles. We will briefly compare the “one-pot” hydrogel properties to the properties of the “Diffusion” hydrogel, to highlight the interest of using the “Diffusion” method.

4.1.3. Absorption isotherms

The absorption isotherms of Zn^{2+} and Cu^{2+} are presented in Figure 4.1. We see, for Cu^{2+} , that we reach a plateau at around 0.5, just as for Ni^{2+} , which suggests a majority of $[\text{CuIm}_2]^{2+}$ coordination complexes in the hydrogel and thus, physical crosslinks with a functionality $f = 4$. This result is different from what was observed in the literature for the absorption of Cu^{2+} by a poly(vinyl-imidazole), where the main complexes are formed with 4 ligands [6]. However, this result is not overly surprising: a complex with 4 ligands is sterically much more complicated to realize in a network with only 10% of ligand, than in a network where all the monomers are ligands.

The trend is less clear for Zn^{2+} , but it would seem that we have a plateau at 0.25, followed by another increase in bound ions. This suggests that at concentrations in ions in the feed similar to what we have imposed in the Ni^{2+} gels (around 10 mmol/L), there is a majority of $[\text{ZnIm}_4]^{2+}$ complexes and thus, physical crosslinks with a functionality $f = 8$. In order to reach the same functionality as the Ni^{2+} hydrogels, we need to increase the Zn^{2+} in the feed to higher concentrations (around 25 mmol/L here).

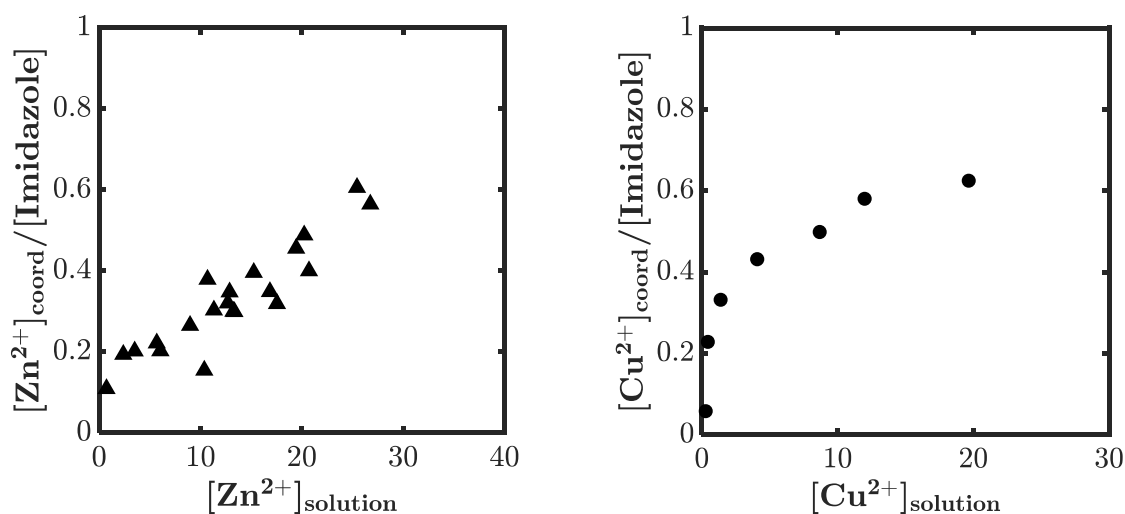


Figure 4.1 Concentration of complexed metal ions, normalized by the concentration of Imidazole moieties, as a function of the concentration of metal ions in the diffusing solution. All concentrations are at equilibrium.

In Figure 4.2 the same data are shown compared with the results from Ni^{2+} presented in the last paragraph. We see that Cu^{2+} and Ni^{2+} have very close diffusion behaviors. This can be explained by looking at the stability constants of each Ni^{2+} or Cu^{2+} complex with imidazoles (Table 4.1): their values of K_1 and K_2 are equivalent, suggesting the same thermodynamic behavior and hence the same absorption behavior. Those values are also much higher than their values of K_3 and K_4 , justifying the majority of $[\text{MIm}_2]^{2+}$ complexes. Zn^{2+} has instead similar values for all its K_i constants with imidazole, justifying a more significant presence of $[\text{ZnIm}_4]^{2+}$ complexes.

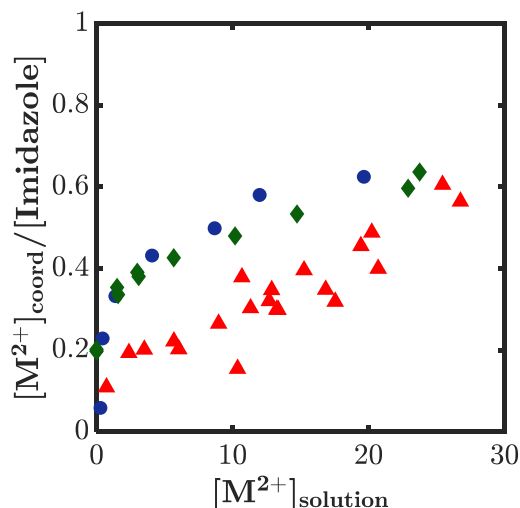


Figure 4.2: Absorption isotherms from Figure 4.1 and previous chapter, for Cu^{2+} (circles), Zn^{2+} (triangles) and Ni^{2+} (diamonds).

4.2. Rheology

4.2.1. Cu^{2+} and Zn^{2+} dual-crosslink hydrogels

In Figure 4.3 are presented the results of small amplitude oscillatory shear measurements for both Cu^{2+} and Zn^{2+} “Diffusion” dual-crosslink hydrogels, compared with the corresponding chemical gel. Both gels exhibited the same behaviors. The elastic modulus was higher than that of the chemical gel for the whole frequency range studied and increased with increasing test frequency. The loss modulus followed a similar frequency dependence. However, contrary to the Ni^{2+} gels, we did not observe a peak in the loss modulus or $\tan(\delta)$, which we could have associated to a lifetime of the physical bonds. This result suggests that the physical bond breaking happens at much higher frequencies [1,2,5], indicating a much shorter lifetime for those two physical bonds than for the Imidazole- Ni^{2+} bond. At low frequencies, the linear behavior of the dual-crosslink hydrogel was almost the same as that the chemical gel, just as if the physical bonds were invisible. The elastic modulus drops to around 2 kPa and the loss modulus decreases to 400 Pa. This result indicates that the Cu^{2+} and Zn^{2+} hydrogels with faster dynamics than the Ni^{2+} hydrogel are good candidates to characterize the regime with less dissipation.

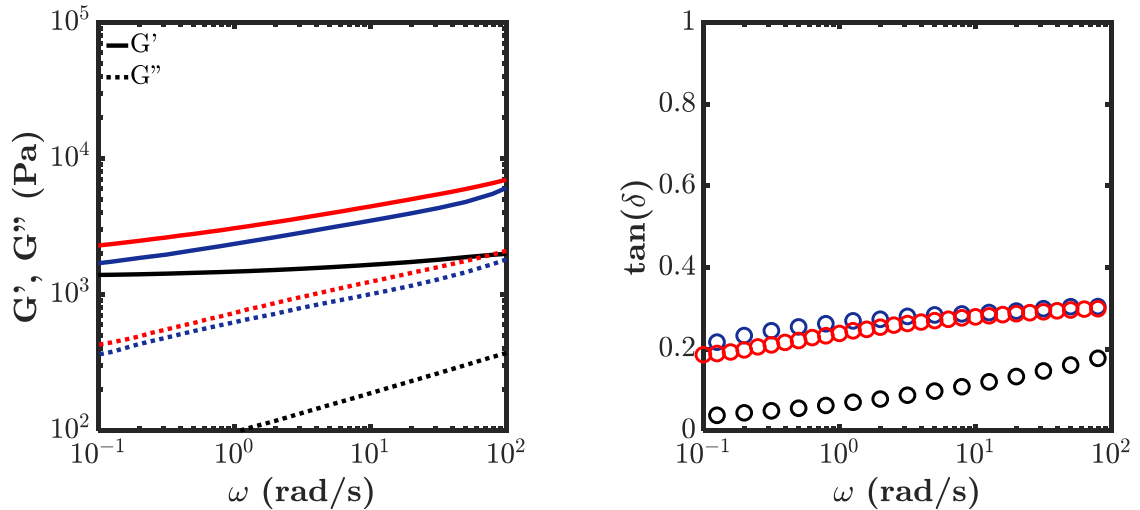


Figure 4.3: Storage and loss modulus (left) and corresponding $\tan(\delta)$ (right) of a Cu^{2+} dual-crosslink hydrogel (blue) and a Zn^{2+} dual-crosslink hydrogel (red), versus the frequency of the shear strain applied.

4.2.2. Zn^{2+} dual-crosslink hydrogel – “One-pot” vs. “Diffusion”

As previously mentioned, we briefly compared the properties of the “One-pot” and “Diffusion” dual-crosslink hydrogels with Zn^{2+} ions. In Figure 4.4 are plotted the storage and loss moduli of each hydrogel, along with the corresponding values of $\tan(\delta)$. The rheological response of the two gels was nearly identical, exhibiting a power-law behavior. The slight difference can be interpreted as the difference in the absolute values of moduli, or as that in the relaxation time. The “One-pot” gel showed slightly higher moduli or slower dynamics than the “Diffusion” gel with a factor of less than 1.5.

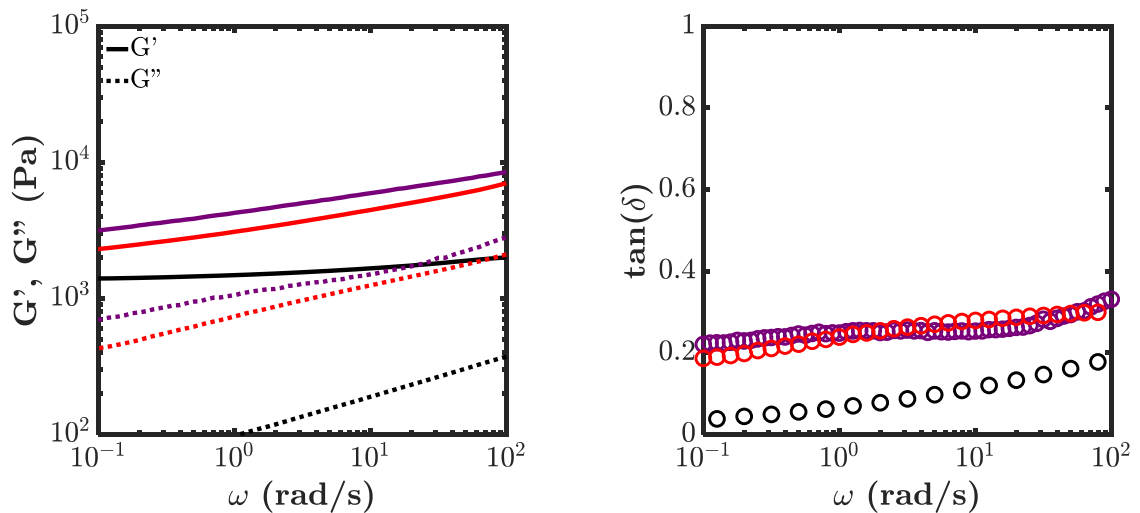


Figure 4.4: Storage and loss moduli (left) and corresponding $\tan(\delta)$ (right) as a function of the shear frequency, for a chemical gel (black), a Zn^{2+} “One-pot” dual-crosslink gel (purple) and a Zn^{2+} “Diffusion” dual-crosslink gel (red).

4.3. Small-angle X-Ray scattering

Knowing the differences in bond lifetime between Ni^{2+} and Zn^{2+} dual-crosslink hydrogels, we wanted to compare the organization of those physical bonds along the polymer network. In this part, we will

start by studying small-angle X-Ray scattering of Zn^{2+} dual-crosslink hydrogel, with different concentrations in Zn^{2+} . We will then try to normalize the scattering data by the scattering capacity of the metal ions considered, in order to compare the data from Ni^{2+} and Zn^{2+} dual-crosslink hydrogels.

4.3.1. General observations

For these SAXS experiments on dual-crosslink hydrogels with Zn^{2+} ions, the same protocol as before (Chapter 2, part 5) was applied. Figure 4.5 shows the results for 4 different Zn^{2+} ion concentrations. We see an increase in the X-ray scattering with concentration up to 60 mmol/L, after which the maximal intensity decreases. On the Kratky plot, we see the appearance of a clear peak at small scattering angles, which is better defined relatively to the rest of the scattering at high Zn^{2+} concentration.

The minimal value of scattering (at $q \approx 0.7 \text{ \AA}^{-1}$) seems also higher for the gel with $[\text{Zn}^{2+}] = 20 \text{ mmol/L}$, but the difference remains very small. The acquisition for this particular dual-crosslink hydrogel was realized during a different set of experiments than the acquisitions of the other $[\text{Zn}^{2+}]$ concentrations, and the difference in this “background level” can be attributed to the small variations in the set-up between two different series of experiments.

At first glance, it would seem that increasing the concentration in Zn^{2+} ions increases the clustering in the hydrogel and that a characteristic distance emerges from the scattering experiment.

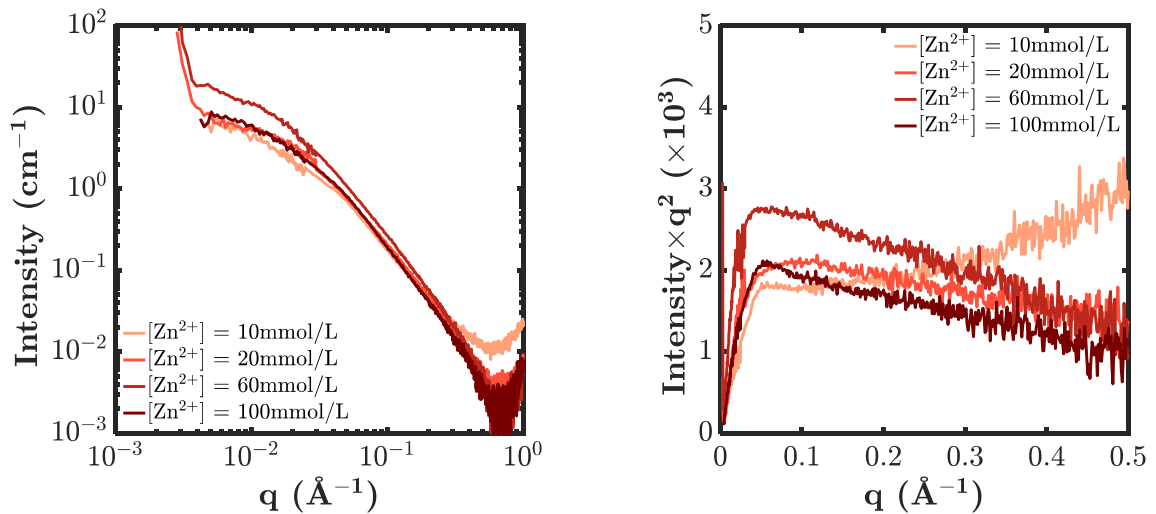


Figure 4.5: Log-log plot of X-Ray intensity, normalized by the thickness of the sample, as a function of the scattering vector (left) and Kratky plots (right) for dual-crosslink hydrogels with Zn^{2+} ions at different concentrations in ions.

4.3.2. Fitting

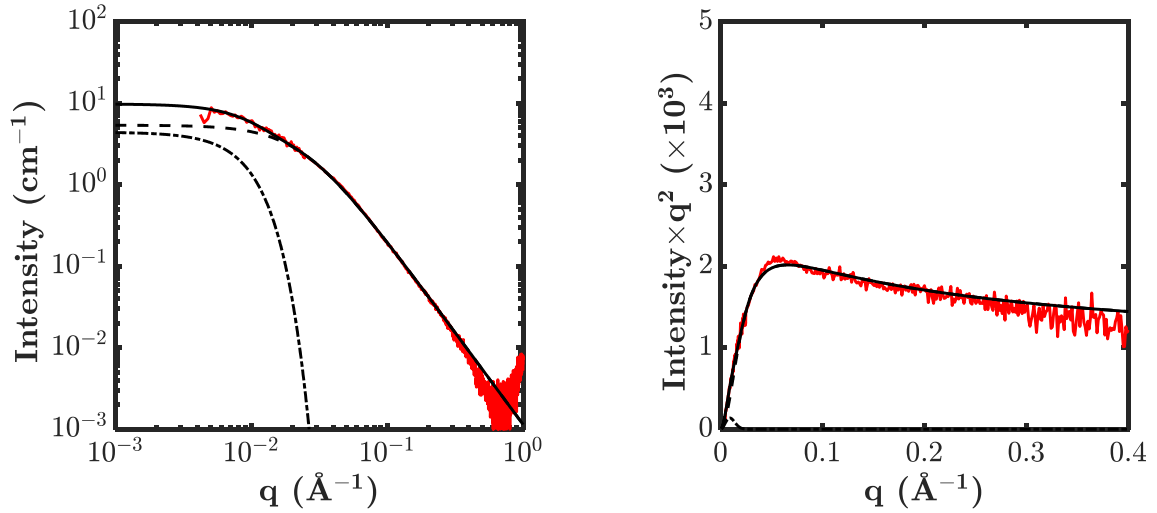


Figure 4.6: Log-log plot of X-Ray intensity, normalized by the thickness of the sample, as a function of the scattering vector (left) and Kratky plots (right) for dual-crosslink hydrogels with $[Zn^{2+}] = 100$ mmol/L along with the corresponding fit.

The model from Shibayama et al. [7] was again applied here to the dual-crosslink hydrogels with Zn^{2+} ions and correctly fits the results (Figure 4.6), giving interesting insights on the length scales inside the material (listed in Table 4.2).

As for the Ni^{2+} hydrogels, we see two length scales: one at 4 nm and the other around 18 nm. It is impossible to do DLS experiments on these hydrogels, since they are opaque when synthesized by the “One-pot” process and DLS requires a one-pot synthesis. We have thus no reference for this 4 nm characteristic length, still it is comparable to that for the Ni^{2+} hydrogels, a length corresponding to the organization of the chains between clusters. The intensities of each component of the model are also changed, with the intensity of the stretched-Lorentzian now being higher than the intensity of the Gaussian – contrary to what we have seen in the Ni^{2+} hydrogels.

Table 4.2: Parameters of Shibayama et al. model for “Diffusion” dual-crosslinked gels with $[Zn^{2+}] = 100, 60, 20$ and 10 mmol/L

Coefficient (units)	$[Zn^{2+}] = 10$ mmol/L	$[Zn^{2+}] = 20$ mmol/L	$[Zn^{2+}] = 60$ mmol/L	$[Zn^{2+}] = 100$ mmol/L	Error
I_{L0}	4.82	4.7	10.3	5.37	± 0.01
ξ (Å)	50	40	48.8	40.5	± 0.15
m	1.956	2.179	2.235	2.259	± 0.05
I_{G0}	3.43	3.8	6.18	4.41	± 0.3
Ξ (Å)	230	127	133	188	± 10

We also observe a great discrepancy between the intensities of diffraction at 60 mmol/L and the others. It is possible that this difference in intensity is linked to a change in the contrast of scattering between the bound ions and the free ions in the solvent: at $[Zn^{2+}]_{\text{bound}} = 60$ mmol/L, the ratio of bound ions to free ions is at its maximum, thus implying a better contrast and a higher intensity.

4.3.3. Scattered intensity normalization method

a. How to normalize the scattered intensity

Comparing intensity levels directly between Zn^{2+} and Ni^{2+} hydrogels is impossible, since both ions do not scatter X-rays in the same way. The scattered X-ray intensity follows

$$I(q) = \phi \cdot v \cdot (\Delta\rho)^2 \cdot P(q) \cdot S(q) \quad \text{Eq. 4.1}$$

Where ϕ is the volume fraction of ions, v is the volume of one scattering object and $(\Delta\rho)^2$ is the contrast factor between the scattering objects and the solvent. $P(q)$ and $S(q)$ are the form and structure factor of the ensemble. They account for the form of the objects and their organization.

In the case of our dual-crosslink hydrogels, the “scattering objects” should be the bound Ni^{2+} or Zn^{2+} ions. In order to be able to compare the results in intensity for gels with both ions, we need to normalize our $I(q)$ data by $\phi \cdot v \cdot (\Delta\rho)^2$. This will give us $I_{norm}(q) = P(q) \cdot S(q)$, where the intensity will not depend on the nature of the ions but on their organization.

The volume fraction ϕ is easily known, since we know accurately the concentration in ions inside the hydrogel:

$$\phi = [ions] \cdot N_A \cdot v \quad \text{Eq. 4.2}$$

The contrast factor is defined by:

$$\Delta\rho^2 = (\rho - \rho_{solvent})^2 \quad \text{Eq. 4.3}$$

Where ρ represents the electronic density of the scattering object, the number of electrons close to a certain point at a certain time. A good estimation of this value can be obtained by:

$$\rho = r_e Z / v \quad \text{Eq. 4.4}$$

Where Z is the number of electrons of the typical scattering object (or solvent molecule when considering $\rho_{solvent}$, in which case v is the molecular volume of the solvent). The value $r_e \equiv e^2 / (4\pi\epsilon_0 mc^2)$ is a characteristic length, equal to 2.82×10^{-13} cm, usually considered as the radius of the electron.

All these equations depend then on the value of the ion volume inside our hydrogel v , which we need to measure.

Knowing the radius of an ion, we can compute an approximation of the theoretical volume of a free ion in solution assuming the ion is a sphere (Table 4.3).

Table 4.3: Theoretical radii and volumes of free metal ions in solution

Ion	Radius (pm)	v (cm ³)
Ni^{2+}	69	1.38e-24
Zn^{2+}	74	1.70e-24

4. Dual-crosslink hydrogels with faster dynamics

However, there is no reason for these values to correspond to the volume of the scattering objects we have in our dual-crosslink hydrogel. In order to compute the normalized intensity values, we need to find a better approximation of this value.

We will do so thanks to Small-Angle Neutron Scattering experiments.

b. Molecular volumes

In neutron scattering, a beam of neutrons is sent on a sample, and scattered by the nuclei of the sample atoms. The process is very similar to the scattering of X-rays, except that we will be mapping the nuclei of the atoms instead of the electrons. We will apply this technique to our dual-crosslink hydrogels.

The contrast between the atoms of the polymer chains (C, H, N, O) and the solvent (H and O) will be very small, so the scattered neutron intensity linked to the polymer chains will be negligible. The scattering we will measure will be caused only by the metal ions, whose contrast with the solvent will be the greatest.

The same formula as in Eq. 4.1 applies for the scattered intensity. The form and structure factors $P(q)$ and $S(q)$ should not change, since we will be studying the same hydrogels with the same scattering objects. The volume v and the volume fraction ϕ will also remain constant between the two experiments. Only the contrast factor $(\Delta\rho)^2$ is dependent on the radiation used (X-rays or neutrons). In neutrons scattering, ρ the scattering length density is computed by

$$\rho = \frac{\sum_{i=1}^n b_i}{v_m} \quad \text{Eq. 4.5}$$

Where b_i is the bound coherent scattering length of i-th of n atoms in the scattering molecule with molecular volume v_m . In our case, considering that the scattering objects are the ions we have $\rho = b_{ion}/v_{ion}$ and $\rho_{solvent} = 2 * b_H + b_O$.

Knowing the scattered intensity in X-rays and neutrons scattering, we can then compute their ratio:

$$\frac{I_{SAXS}(q)}{I_{SANS}(q)} = \frac{(\Delta\rho_{SAXS})^2}{(\Delta\rho_{SANS})^2} = \frac{\left(\frac{r_e Z_{ion}}{v} - \rho_{X,solvent}\right)^2}{\left(\frac{b_{ion}}{v} - \rho_{N,solvent}\right)^2} \quad \text{Eq. 4.6}$$

Which in turn leads to

$$\left(\frac{b_{ion}}{v} - \rho_{N,solvent}\right) \cdot \sqrt{\frac{I_{SAXS}}{I_{SANS}}} = \frac{r_e Z_{ion}}{v} - \rho_{X,solvent}$$

Giving

$$v = \frac{b_n \sqrt{\frac{I_{SAXS}}{I_{SANS}}} - r_e Z_{ion}}{\rho_{N,solvent} \sqrt{\frac{I_{SAXS}}{I_{SANS}}} - \rho_{X,solvent}} \quad \text{Eq. 4.7}$$

With Eq. 4.7, knowing the scattered intensities in X-rays and neutrons, we can compute the molecular volume of an ion and normalize the scattered intensity data. The computed volumes are listed in Table 4.4.

Table 4.4: Molecular volumes of the free ion (based on Table 4.3) and the scattering object (computed from Eq. 4.7), along with the ratio between both volumes.

Ion concentration (mmol/L)	$v_{free\ ion}$ (cm^3)	v (cm^3)	Ratio -
$[Ni^{2+}] = 40$	1.38e-24	6.46e-23	47
$[Ni^{2+}] = 100$	1.38e-24	6.37e-23	46
$[Zn^{2+}] = 10$	1.70e-24	7.64e-23	45
$[Zn^{2+}] = 60$	1.70e-24	7.61e-23	45

We find a volume for the scattering object 45 times larger than the volume of a free ion in solution (corresponding to a radius 3.56 times greater). The ratio between both volumes is stable and does not depend on the metal ion.

4.3.4. Normalized results – comparison between Ni^{2+} and Zn^{2+} dual-crosslink hydrogels

The normalized scattered intensities in SAXS and SANS are plotted in Figure 4.7. They well superposed on each other. The difference at low scattering vector should be due to the influence of the incident beam in the X-ray scattering data; and that at high scattering vector is due to the high background value of neutron scattering.

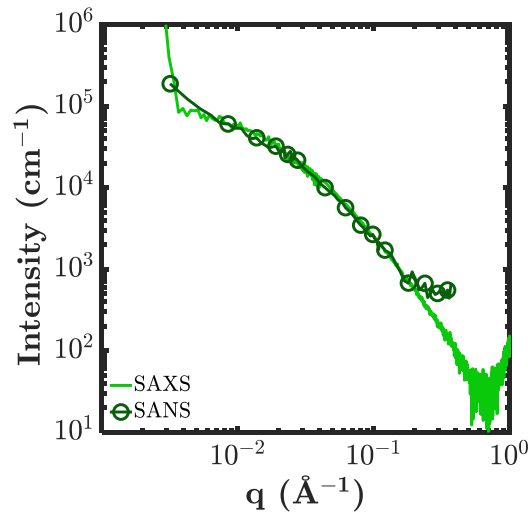


Figure 4.7: X-Ray and Neutron scattered intensities, normalized with Eq. 4.1, for the dual-crosslink hydrogel with $[Ni^{2+}] = 40\text{ mmol/L}$.

We can now plot the normalized scattered intensities as a function of the scattering vector for different ions and concentrations in Figure 4.8. We see a decrease of the scattered intensity with increasing ion concentration, at all scattering vectors.

4. Dual-crosslink hydrogels with faster dynamics

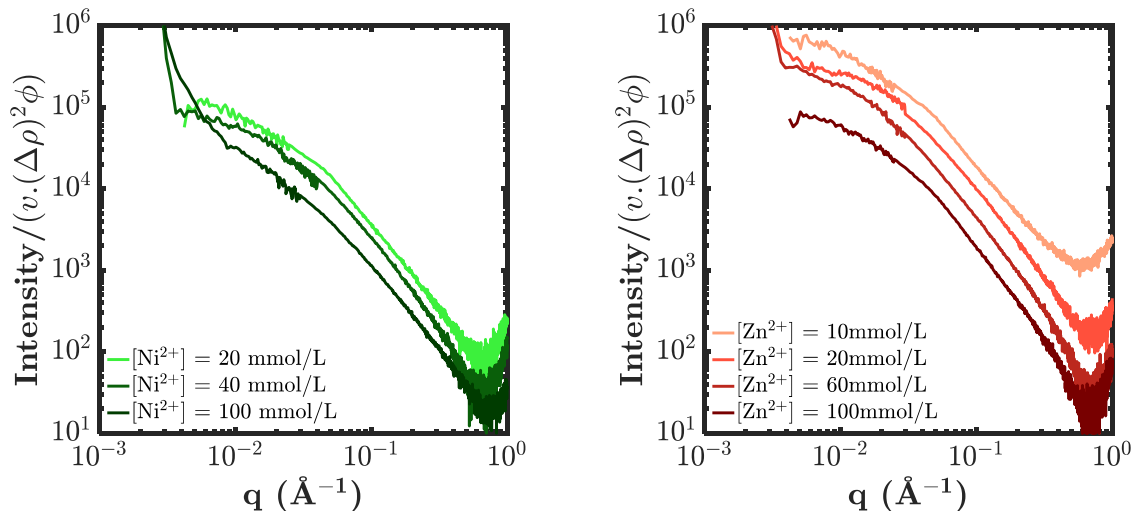


Figure 4.8: Normalized scattered X-Ray intensities for Ni^{2+} (left) and Zn^{2+} (right) dual-crosslink hydrogels.

There are two clear and distinct effects we can comment on these results. First, the normalized intensities we measure decrease with the concentration in metal ions. Our explanation is that, at low concentration in ions, the physical bonds organize in clusters. When increasing the ion concentration, an increasing amount of physical bonds forms randomly along the polymer chains, hence decreasing the heterogeneities in the network.

Second, the intensities of diffraction are higher for the dual-crosslink hydrogels with Zn^{2+} ions than for those with Ni^{2+} ions, implying that the former create more clusters of physical bonds than the latter. This particular result can be rationalized by considering the same energy balance as was done in part 2.5 of this manuscript: Imidazole – Zn^{2+} complexes have a lower thermodynamic binding constant than Imidazole – Ni^{2+} complexes. Thus, the relative entropic benefit of creating clusters of physical bond is increased in Zn^{2+} hydrogels, compared to Ni^{2+} hydrogels [8], which explains the difference in normalized scattered intensities between both dual-crosslink hydrogels.

Finally, Figure 4.9 shows the evolution of the length scales found in each dual-crosslink hydrogel, versus the concentration in metal ion. Overall, the two lengths we measure do not change much with the concentration, apart from a decrease of the longer length Ξ with increasing concentration in ions at low concentrations. The structure of the clusters does not really evolve with ion concentration or by changing the ion.

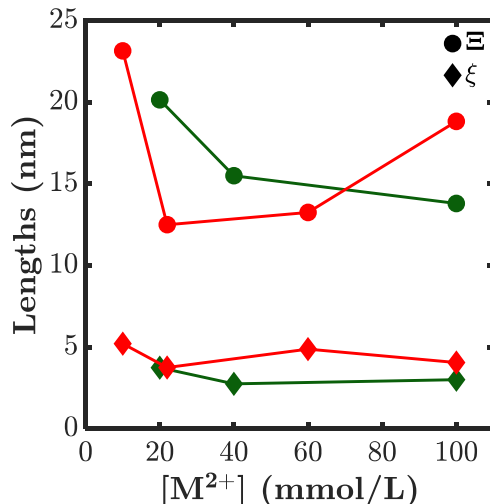


Figure 4.9: Length-scales Ξ (circles, relative to the Gaussian scattering) and ξ (diamonds, relative to the Lorentzian scattering) versus the metal ion concentration, for the Ni^{2+} (green) and Zn^{2+} (red) dual-crosslink hydrogels. Data from Table 4.2 and Part 2.5.3.

4.3.5. Conclusions

Using Small-Angle X-Ray scattering experiments, we have demonstrated here the presence of clusters of physical bonds in the Zn^{2+} dual-crosslink hydrogel. Using the same model than the one we used in Part 2.5.3, we could extract two length scales from the SAXS data of the Zn^{2+} hydrogel. Those two length scales were found to be similar in the Zn^{2+} dual-crosslink hydrogel than in the Ni^{2+} dual-crosslink hydrogel.

In order to compare the scattering intensities of both Ni^{2+} and Zn^{2+} dual-crosslink hydrogels, we have normalized the raw scattering data by parameters linked to the nature of the ion (concentration, volume and contrast with the media). The normalized data showed us a decrease in scattered intensity between the Zn^{2+} and the Ni^{2+} hydrogel, suggesting that the latter possesses less clusters of physical bonds than the former. This result is coherent with the theoretical background developed by Tito et al. [8]

4.4. Large deformations

The large deformation properties of the fast dual-crosslink hydrogels will now be studied. The ion concentration will be fixed at 100 mmol/L, just as the study in large deformations realized on the Ni^{2+} dual-crosslink hydrogel. To obtain the same concentration in polymer as the chemical gel and the Ni^{2+} dual-crosslink hydrogel, we introduce NaCl ions in the solution (see Chapter 2). In the Zn^{2+} dual-crosslink hydrogel, only 3 mmol/L of NaCl were necessary. In the Cu^{2+} dual-crosslink hydrogel, 90 mmol/L of NaCl had to be introduced.

The rheological results showed that the physical bonds we introduced in the network are very short-lived, we consequently expect them to have very little influence on the mechanical behavior of our dual-crosslink hydrogel. However, it has been previously shown that some fast-exchange bonds can still make a material more stretchable [9].

4.4.1. “One-Pot” vs “Diffusion” Zn²⁺ hydrogels

Uniaxial tensile tests for the “One-Pot” and “Diffusion” Zn²⁺ hydrogels were performed and the stress stretch curves at different stretch rates are shown in Figure 4.10. Although the global behaviors were found similar, we noticed slight differences between the two gels. The “One-Pot” hydrogel showed higher stress at all studied stretch-rates. Particularly, the “Diffusion” dual-crosslink hydrogel did not show an evolution in the stress at the stretch rates $\dot{\lambda}$ between 0.003 and 0.03 s⁻¹, and the values of the stress were the same as that for the chemical gel, as if the physical crosslinks had no effect on the properties of the gel at these strain-rates. This is coherent with what we have observed in rheology: the dynamics of the “One-pot” seemed slower than those of the “Diffusion” hydrogel. The difference in stretch at break between the two hydrogels was likely within the error of the experiment.

For the rest of the chapter, we only investigate The “Diffusion” hydrogels for the following reasons. The “Diffusion” method allows a more controlled preparation of the hydrogel. As mentioned before, this method ensures that every hydrogel studied possesses the same chemical network thus we can discuss differences in the properties between different ions having different relaxation times.

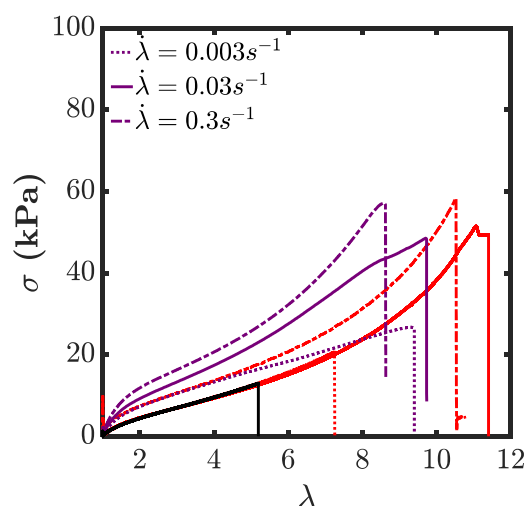


Figure 4.10: Stress-strain curves for a “One-pot” (purple) and a “Diffusion” (red) dual-crosslink hydrogels at different stretch rates. Data from Chemical gel (black) is also shown for comparison purposes. Both dual-crosslink hydrogels have an ion concentration [Zn²⁺] = 100 mmol/L

4.4.2. Tensile tests on Zn²⁺ and Cu²⁺ dual-crosslink hydrogels

Uniaxial tensile tests at different stretch-rates were performed on ‘dogbone’ shaped samples of the Cu²⁺ and Zn²⁺ dual-crosslink hydrogels. The results are shown in Figure 4.11.

a. Results

Both gels showed very weak stretch rate dependences, the values of the stress were very close to each other and to that of the chemical gel. Interestingly, the extensibility of these dual crosslink gels was found larger than that of the chemical gel. The physical bonds were mechanically invisible at these stretch-rates since we saw no change in the elastic modulus – as seen in rheology at low frequencies – but they still protect in some way the chemical network and prevent its breaking.

The Cu^{2+} dual-crosslink gel has a behavior very close to the one of the Zn^{2+} dual-crosslink hydrogel. This was expected, since their rheological behaviors and dynamics were found almost identical.

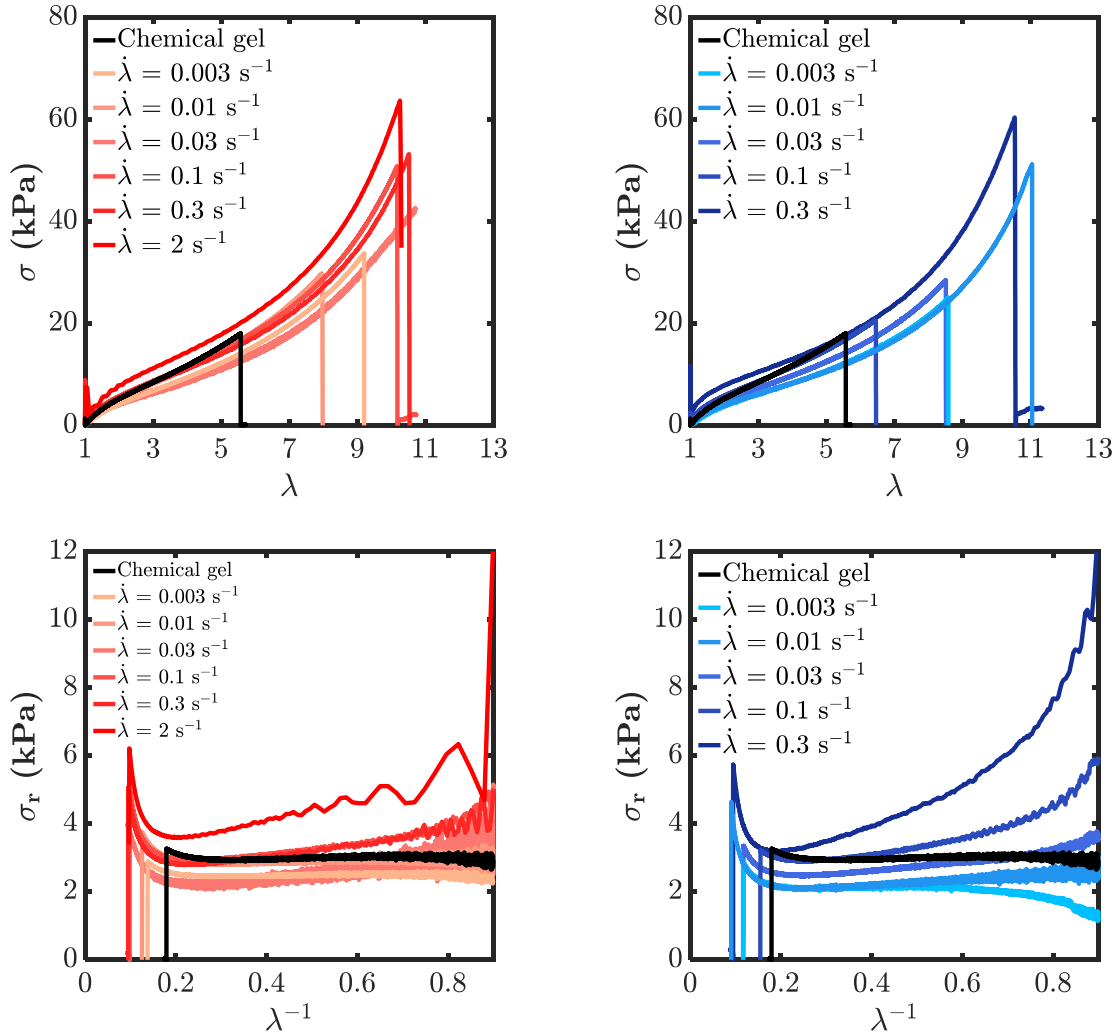


Figure 4.11: Stress vs. strain (top) curves and corresponding Mooney-stress vs. λ^{-1} (bottom) for Zn^{2+} (red) and Cu^{2+} (blue) dual-crosslink hydrogels.

From these curves, we can extract the same parameters as we did in the previous chapter (part 3.1.2), the initial modulus and the stretch at break. The value and the variation in Young's modulus with stretch-rate was very low compared to the increase we saw in the Ni^{2+} dual-crosslink hydrogel, and was found equal to that of the modulus of the bare chemical gel. The stretch at break increased slightly on the range of stretch-rates from 8 to 10, always significantly higher than the stretch at break of the chemical gel (about 5.5), while the physical bonds had absolutely no influence on the modulus. The Mooney plots in Figure 4.11 bottom indicate that the reduced stress did not strongly depend on the stretch, as the stretch rate dependence was found weak. Still some strain hardening was observed for all the conditions. Knowing that the accuracy was low, we estimated the onset of the strain hardening λ_{SH} and the corresponding stress f_{min}^* . The value of λ_{SH} slightly increased with stretch-rate, but this observation is not conclusive as the error of the measurements were large especially for the low stretch-rates. The value of f_{min}^* , however, did not evolve with stretch-rate. It remained close to that obtained for the bare

4. Dual-crosslink hydrogels with faster dynamics

chemical gel (around 3 kPa). This shows the low impact of the physical bonds on the stiffness of the gel at these strain-rates.

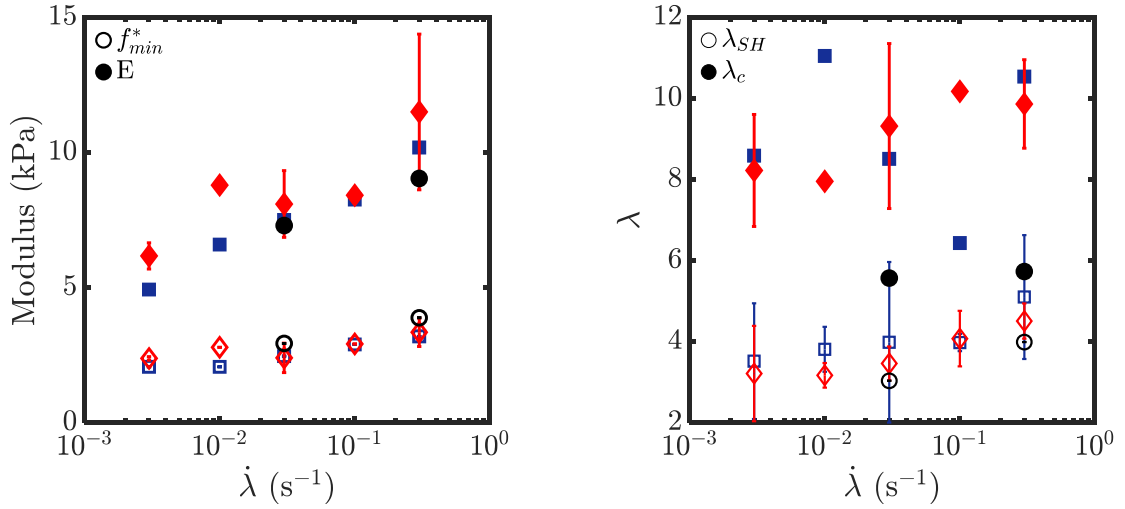


Figure 4.12: *Left:* Young's modulus (filled symbols) and reduced stress at the onset of strain-hardening (empty symbols) versus the stretch-rate. *Right:* stretch at break (filled symbols) and stretch at the onset of strain-hardening (empty symbols) versus stretch-rate. In both graphs, results for a chemical hydrogel (black), a Cu^{2+} (blue) and a Zn^{2+} dual-crosslink hydrogel (red).

This low impact of the physical bonds on the hydrogel mechanical properties is further confirmed by looking at the reduced stress versus time on Figure 4.13. The idea of this figure was to examine the separability of the time and strain effects on this dual-crosslink hydrogel, as done in Chapter 3 [10].

$$\sigma(\lambda, t) = G(t) \cdot \left(\lambda - \frac{1}{\lambda} \right) \quad \text{Eq. 4.8}$$

However here, the superposition is much less clear. This is mainly due to the low forces that the dual-crosslink hydrogel undergoes. We are, especially at low stretches, close to the limits of detection of the load cell of our instrument.

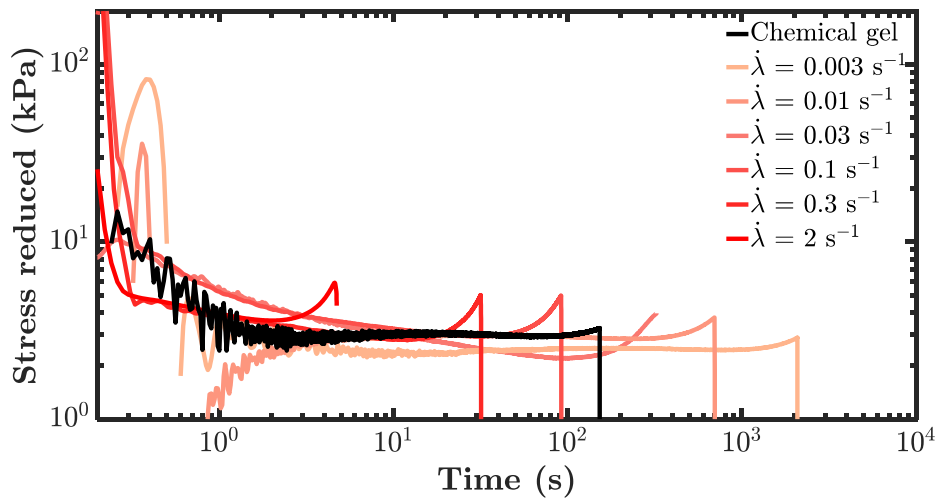


Figure 4.13: Time dependence of the reduced stress f^* under uniaxial deformation for the Zn^{2+} dual cross-link hydrogel at various initial strain rates.

The superposition of strain-hardening we found for the previous dual-crosslink hydrogel (part 3.1.2) was also realized on the Zn^{2+} dual-crosslink hydrogel and is shown in Figure 4.14. In this kind of fast-dynamic hydrogel, the strain-hardening was much less pronounced. The shift by λ_{SH} we have previously done on the Ni^{2+} dual-crosslink hydrogel did not result in a master curve, as the strain-hardening follows a clear evolution with λ .

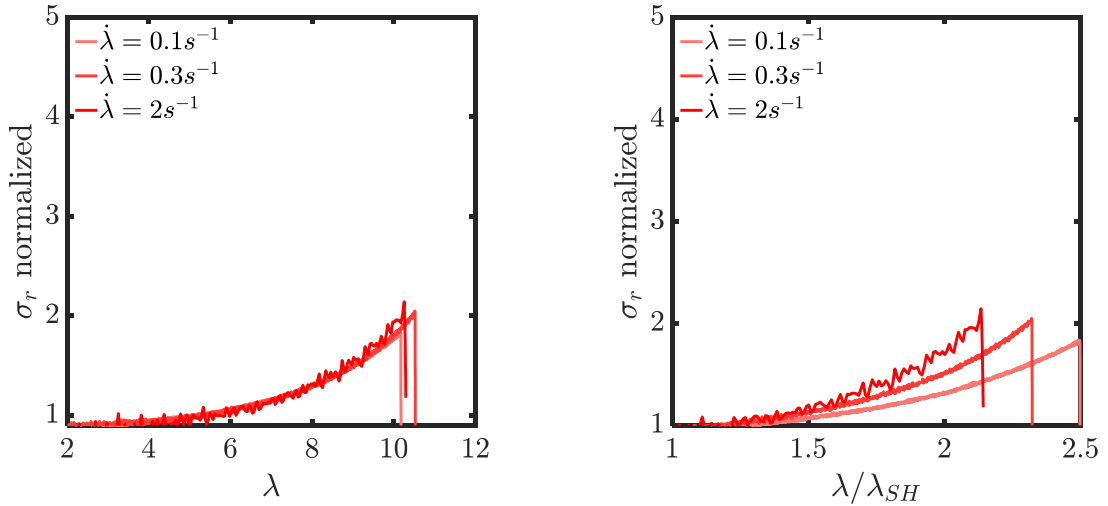


Figure 4.14: Reduced stresses from $\dot{\lambda} = 0.3 \text{ s}^{-1}$ (red) to $\dot{\lambda} = 0.03 \text{ s}^{-1}$ (light red), normalized by the reduced stress from $\dot{\lambda} = 0.01 \text{ s}^{-1}$, as a function of time shifted by the onset of strain hardening (left) and of λ (right), for a Zn^{2+} dual-crosslink hydrogel.

The strain-hardening is here close to the behavior at low stretch-rates we had tentatively observed on the Ni^{2+} dual-crosslink hydrogel. The observation time of the experiments we have done here is much longer than the lifetime of the physical bond. During stretching, not many physical bonds are active. Hence, the intensity of the strain-hardening does not increase with the stretch-rate and the stretch of onset of the strain-hardening remains constant. Both values are dependent only on the chemical network.

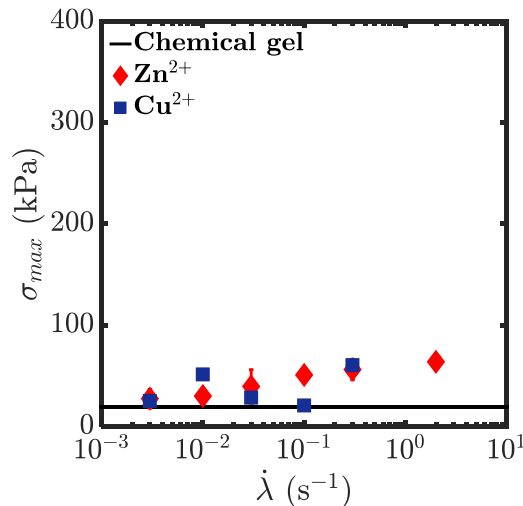


Figure 4.15: Stress at break (in kPa) as a function of the strain-rate, for a Ni^{2+} dual-crosslink hydrogel. The black line represents the value obtained for the associated bare chemical gel.

4. Dual-crosslink hydrogels with faster dynamics

The stress at break (Figure 4.15) increased with the stretch-rate, just as it did for the Ni^{2+} dual-crosslink hydrogel. The increase is however much less visible here, going from 20 to 80 kPa over 3 decades of stretch-rates.

b. Discussion

We characterized here two dual crosslink hydrogels with a fast characteristic dynamic, much faster than the Ni^{2+} dual-crosslink hydrogel we have previously studied. The physical bonds have little influence on the different moduli we can observe here, whether the elastic modulus or the onset of strain hardening. This is comparable to the results of the rheological tests, showing that the storage modulus was very close to that of the chemical gel. When increasing the stretch-rate applied to those materials, the number of active physical bonds does not increase much compared to what we observed in the Ni^{2+} hydrogel: the stretch-rates (or observation times) we can achieve in our lab are much lower than the characteristic frequency (resp. longer than the lifetime) of the physical bond. This low number of elastically active physical bonds does not change much the elastic modulus measured in rheology or large deformations. The strain-hardening, which as we have seen is also influenced by the physical bonds, is here quite close to a classical strain-hardening from an elastic network. It is indeed closely dependent on λ , which makes sense if we consider what we just stated. At the stretch-rates considered here, there are few elastically active physical bonds in the network, hence when the strain-hardening regime is reached, the increase in stress observed (linked to the number of bonds having reached this regime) does not change much with the stretch-rate. In this range of stretch-rates, the clusters of physical bonds we have observed will have a marked influence on the intensity of the strain-hardening regime. Acting as highly functional crosslinking points, with a relatively long lifetime, they will participate in the apparition of a percolating network of polymer chains in their Langevin entropic elasticity by increasing the number of polymer chains in that regime. Being long-lived, their influence is independent on the stretch-rate here.

The onset of strain-hardening λ_{SH} we observed is independent on the stretch rate. As stated in the previous chapter (section 3.1), the onset of strain-hardening is determined by a competition between the decrease of stress linked to the decrease in the number of polymer chains (or active physical bonds), and the number of polymer chains in their strain-hardening regime. Here, the linear relaxation is almost negligible. Hence, the strain-hardening behavior of the dual-crosslink hydrogel is the one of an elastic network. At the highest stretch-rate, the modulus of the dual-crosslink hydrogel increases slightly. The number of physical bonds increases accordingly, leading to a higher number of physical bonds able to break. This will delay the moment when the strain-hardening regime becomes dominant, but this effect is very small here.

However, even when they are mechanically invisible (with little to no influence on the elastic properties or the strain-hardening), the physical bonds have an influence on the deformation of the material. Whatever the characteristic dissipation frequency of such a dual-crosslinked hydrogel, its stretch at break is increased to a value of around 10 (with a slight decrease at lower stretch-rates).

This phenomenon has been observed in organogels [9]. We explain it by our hypothesis from the previous chapter: the physical bonds inhibit the correlated breaking of polymer chains, which happens at a velocity uncorrelated to the stretch-rate. When a polymer chain breaks, the energy transfer to its neighbors happens at a rate much higher than the strain-rate, which provokes an energy dissipation by

the physical bonds. The physical bonds prevent the nucleation of a crack, therefore delay the breaking of the sample.

4.5. Cyclic tests

4.5.1. Influence of stretch-rate and stretch

We show in Figure 4.16 the results of cyclic loading-unloading tests realized on the Zn^{2+} dual-crosslink hydrogel, at different stretch rates and different maximal stretches. We observed that the loading and unloading curves were close and the hysteresis was unremarkable, compared to that of the Ni^{2+} dual-crosslink hydrogel studied in the previous chapter. Still we noticed an increase of the hysteresis with stretch-rate as well as with maximal stretch. A small residual stretch of about 0.1 was observed when unloading the hydrogel.

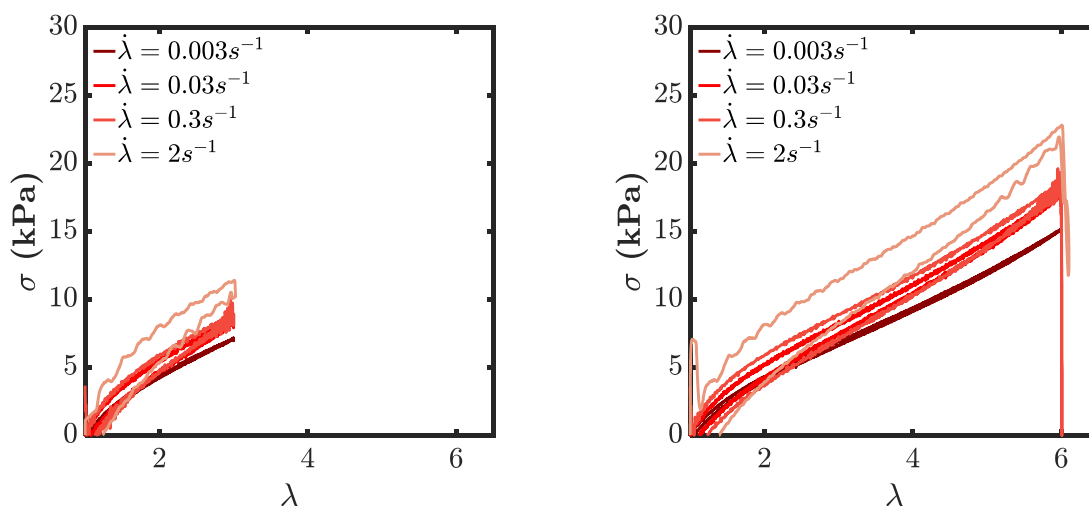


Figure 4.16: Stress vs. Stretch for cyclic loading/unloading of a dual-crosslinked hydrogel with $[Zn^{2+}] = 100\text{mmol/L}$, at different stretch rates. Left: $\lambda_{max} = 3$. Right: $\lambda_{max} = 6$.

We evaluated more closely the energies involved in these cyclic experiments. In Figure 4.17 are plotted the stored and dissipated energies, as a function of the maximal stretch, for different stretch-rates. The values of the dissipated energy corresponding to the hysteresis were less than 20 kJ/m^3 , which were much lower than those for the Ni^{2+} dual-crosslink hydrogel (up to 180 kJ/m^3). A weak stretch rate dependence was seen. The recovered energy increased with the maximal stretch and was found independent on the stretch-rate, implying that the short-lived physical crosslinks had little influence on the unloading of the material and that this energy was stored in the permanent chemical network.

4. Dual-crosslink hydrogels with faster dynamics

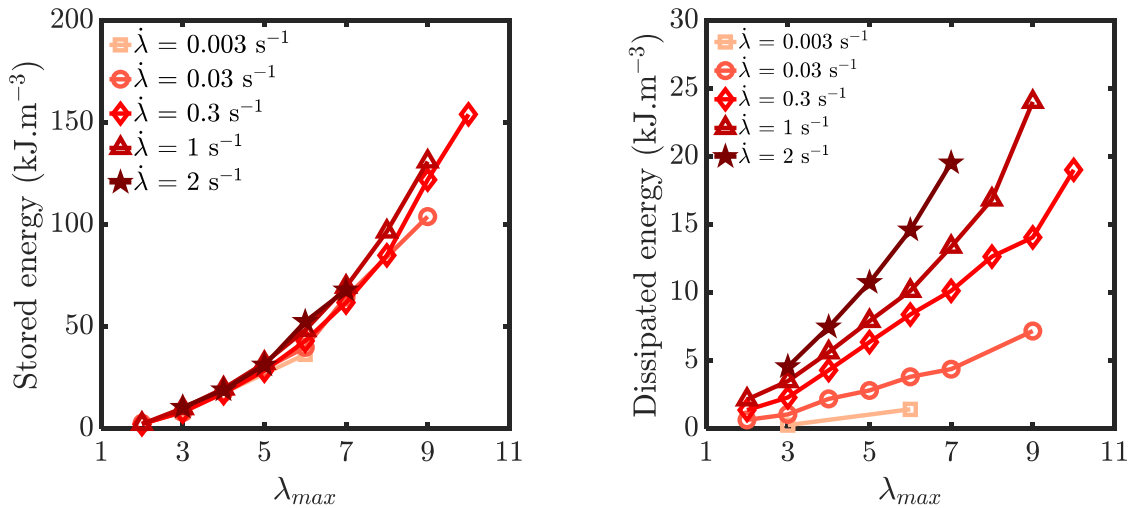


Figure 4.17: Stored (left) and dissipated (right) energies during a cyclic loading/unloading of a dual-crosslink hydrogel with $[\text{Zn}^{2+}] = 100 \text{ mmol/L}$, versus the maximal stretch of the cycle, realized at different stretch-rates.

The hysteresis (ratio of the dissipated energy over the total loading energy, shown on Figure 4.18) increased with the stretch-rate, and decreased slightly with increasing stretch – as a reminder, the Ni^{2+} hydrogels also showed a decrease of the hysteresis with increasing stretch.

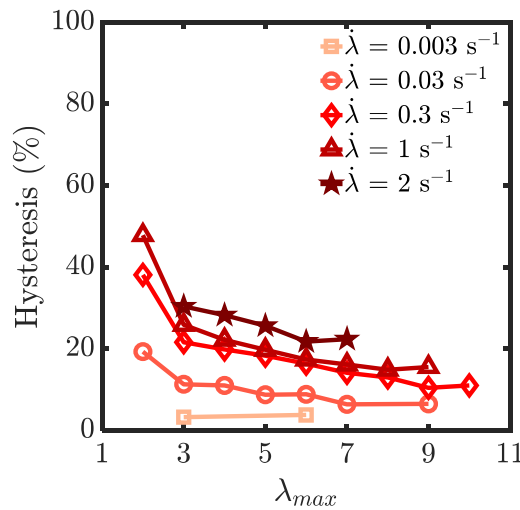


Figure 4.18: Proportion of dissipated energy to the total energy (in percentage) for the dual-crosslink hydrogel under cyclic deformation, as a function of the stretch-rate of the deformation.

Figure 4.19 shows the same data from Figure 4.18, plotted versus the time needed to reach the maximal deformation. The superposition is good at short times (just as for the Ni^{2+} dual-crosslink hydrogel), apart from the values obtained at low deformation. This might imply an influence of the stretch on the energy dissipation. The hysteresis clearly decreases with time, to reach a constant level close to 0% at long times. However, it is interesting to note that the hysteresis is non negligible even at observation times around 100 s, although the main relaxation time of the physical bonds, as estimated from the linear rheology, is lower than 0.01 s (the lower observation time reached during the rheology experiment). It is also clear from this data that the energy dissipation at low stretches does not follow the same behavior, being much higher than the rest. We can also remark, just as we did on the Ni^{2+} dual-crosslink hydrogel, that the superposition does not hold as well at longer times (or lower stretch-rates).

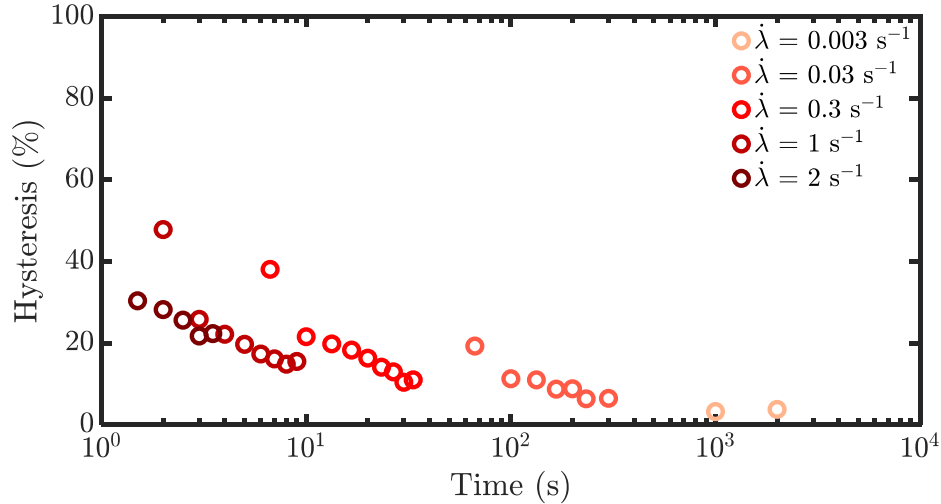


Figure 4.19: Hysteresis versus time to reach the maximal stretch.

These observations confirm what we have seen in linear rheology: the Zn^{2+} hydrogel has faster dynamics than the Ni^{2+} hydrogel, making it less dissipative at the same stretch-rates. When loading this dual-crosslink hydrogel with fast dynamics, since the observation times are much longer than the lifetime of the physical bond, a negligible number of those bonds are active. The energy they can dissipate becomes then negligible.

We however notice a significant hysteresis even at long times, which we associate to the existence of aggregates (or clusters) of physical crosslinks. The lifetime of such aggregates is much longer than that of the single physical crosslink, which explains their influence at long times or low stretch-rates.

Again, this shows a behavior quite unexpected: one would think that a low dissipation would be associated with an increased fragility of the material, yet the strain at break remains relatively unchanged compared to the Ni^{2+} hydrogel (which dissipates much more energy). This observation tends to confirm our hypothesis from the previous chapter, that the physical bonds also prevent the nucleation of a crack. This particular property seems to be independent of the stretch-rate and the lifetime of the physical bond, since the stretch at break of the Ni^{2+} and Zn^{2+} hydrogels are similar.

4.5.2. Damage during cycles?

Just as for the Ni^{2+} hydrogels, we figured out the possible damage of the chemical network at stretch-rates higher than the maximal stretch of the bare chemical gel $\lambda_{c,0} \approx 5$.

At stretches lower than the maximal stretch of the chemical network, one can expect no permanent change in the material properties. We applied 50 cycles up to $\lambda = 3$ to a sample of Zn^{2+} dual-crosslink hydrogel, let it rest for 100 seconds and loaded it up to fracture. Some of those cycles and the final tensile test are shown in Figure 4.20. It is clear from the graphs that there was almost no dissipation during the loading of the gel, the loading and unloading curves were very close. The tensile test realized after the cycles was identical to a tensile test realized on a pristine sample, implying that the material did not suffer any damage during these 50 cycles.

4. Dual-crosslink hydrogels with faster dynamics

As seen for the Ni^{2+} dual-crosslink hydrogel, we saw a residual stretch appear during the cycles, although it was as small as 0.1. The hysteresis between the loading and unloading curves seems to decrease after the first cycle.

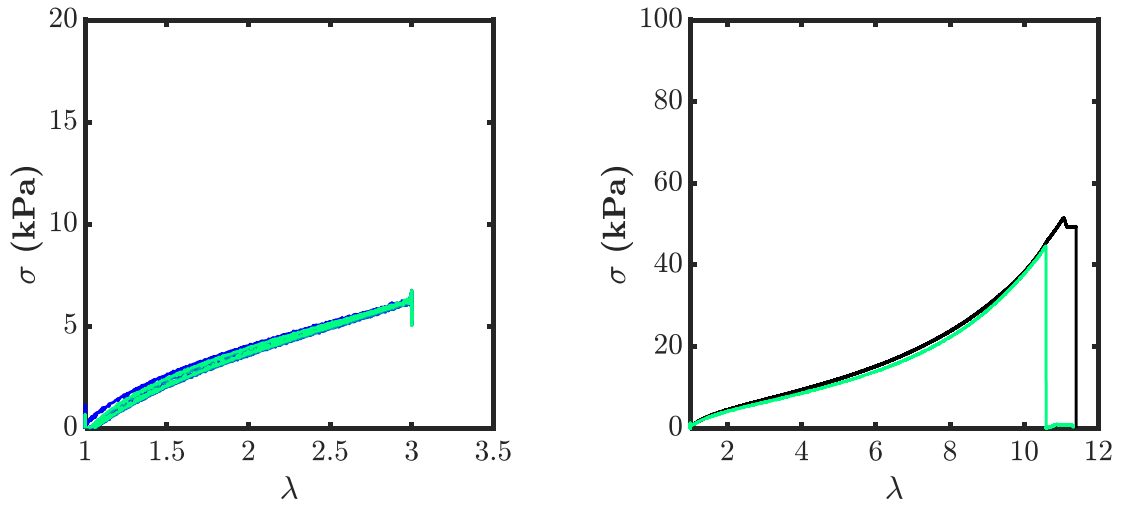


Figure 4.20: Left: Stress versus strain for a cyclic loading test, realized on a dual-crosslink hydrogel with $[\text{Zn}^{2+}] = 100 \text{ mmol/L}$. Are represented only the cycles n°1, 16, 32 and 50. Right: stress versus strain of a tensile test realized on a dual-crosslink hydrogel before (black) and after (green) applying to it 50 cycles of deformation at $\lambda = 3$ and $\dot{\lambda} = 0.03 \text{ s}^{-1}$ and waiting 100 seconds.

The same experiments were then realized at the same stretch-rate, but up to a maximal stretch $\lambda = 6 > \lambda_{c,0}$. The results are presented on Figure 4.21. The same observations as Figure 4.20 can be made here: we see very little hysteresis between the loading and unloading of the sample and the dual-crosslink hydrogel recovers completely its properties after a rest time of 100 seconds. The only difference with Figure 4.20 is the increase in residual stretch after a few cycles.

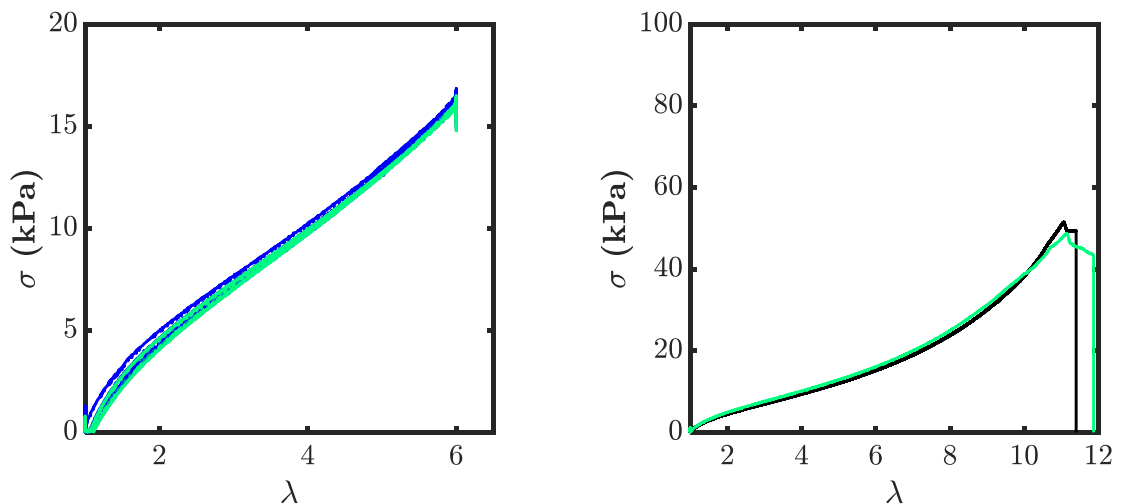


Figure 4.21: : Left: Stress versus strain for a cyclic loading test, realized on a dual-crosslink hydrogel with $[\text{Zn}^{2+}] = 100 \text{ mmol/L}$. Are represented only the cycles n°1, 16, 32 and 50. Right: stress versus strain of a tensile test realized on a dual-crosslink hydrogel before (black) and after (green) applying to it 50 cycles of deformation at $\lambda = 6$ and $\dot{\lambda} = 0.03 \text{ s}^{-1}$ and waiting 100 seconds

Figure 4.22 shows more closely the evolution of the modulus and the residual strain with the cycle number. We see that the modulus does not change (constant at 7 kPa), even if we see this small residual stretch (around 0.1 for $\lambda = 3$ and 0.2 for $\lambda = 6$) appearing.

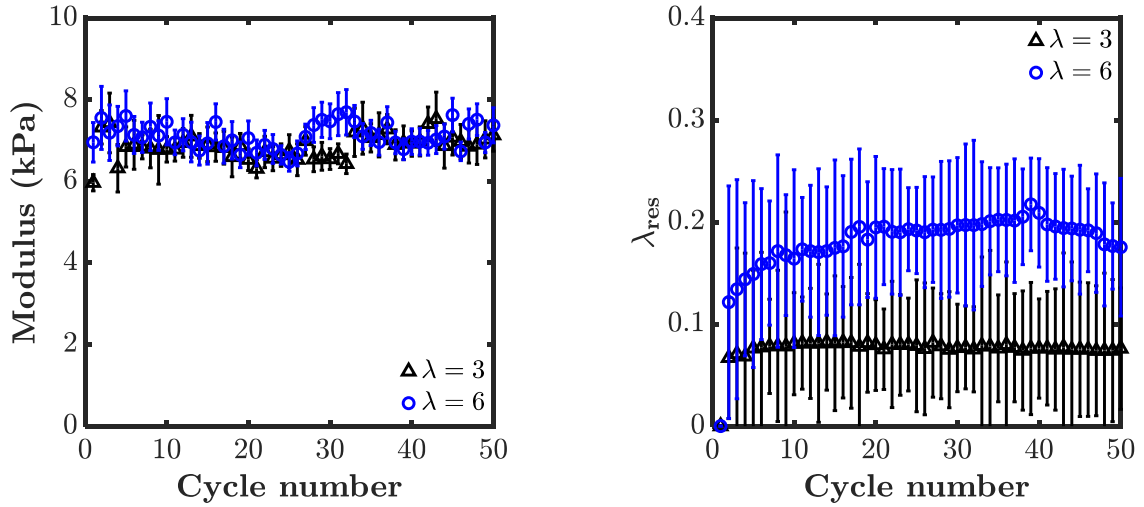


Figure 4.22: *Left:* Young’s modulus (kPa) versus the cycle number, for a Zn^{2+} dual-crosslink hydrogel at two different maximal stretches and $\dot{\lambda}\tau = 0.03 \text{ s}^{-1}$. *Right:* Residual stretch versus the cycle number, for a Zn^{2+} dual-crosslink hydrogel at two different maximal stretches and $\dot{\lambda}\tau = 0.03 \text{ s}^{-1}$.

This residual stretch disappeared completely after 100 seconds of recovery. In Figure 4.23 are plotted the stored and dissipated energy and the hysteresis measured in those experiments. There is no clear evolution of the stored energy over the cycles (constant at 7 J/m² for $\lambda = 3$ and 35 J/m² for $\lambda = 6$). The dissipated energy decrease slightly between the first and second cycle at $\lambda = 3$, following the appearance of the residual stretch (both remaining constant afterwards). The same can be said for the cycles at $\lambda = 6$, although the decrease of the hysteresis and increase of λ_{res} take place over the first 5 to 10 cycles.

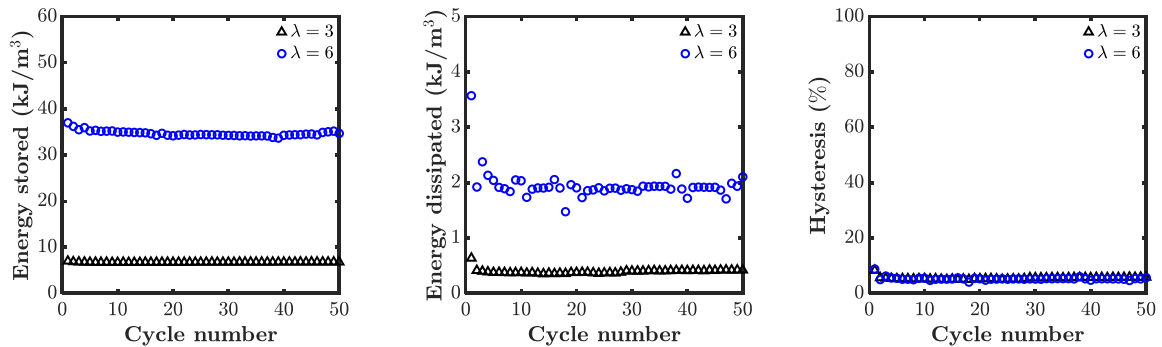


Figure 4.23: *Stored energy (left), dissipated energy (center) and the ratio of dissipated energy over the total mechanical energy (right) in a dual-crosslink hydrogel under cyclic deformation, as a function of the cycle number, for $\lambda_{stretch} = 3$ (black) and $\lambda_{stretch} = 6$ (blue).*

The Zn^{2+} hydrogel dissipates a very small amount of energy during stretching, yet does not show any sign of permanent damage at high deformations (up to $\lambda = 6$). All the changes in properties it goes through are non-permanent, linked to the physical network. The recovery time was much shorter than that for the Ni^{2+} hydrogel, which is coherent with the observations made in rheology. The Imidazole – Zn^{2+} complexes have faster dynamics than the Imidazole – Ni^{2+} complexes, which makes them less

“sticky” and allows the chains to go back to their initial conformation much faster. There was no sign of mechanical damage on the network, no permanent plasticity or decrease of the modulus that we could have attributed to molecular breaking inside the material.

4.6. Fracture of a fast dual-crosslink hydrogel

4.6.1. Single-notch fracture under continuous stretching

As we did for the Ni^{2+} dual-crosslink hydrogels, we now investigate the properties of fracture propagation of a dual-crosslink hydrogel with fast dynamics. We started doing so by studying the conditions of propagation of a notch in a sample under tensile loading. Using the same experimental conditions and formula as in the previous chapter (part 3.4, equation 3.8), we obtain the data presented in Figure 4.24. The critical stretch and the fracture energy both show an increase with the stretch-rate.

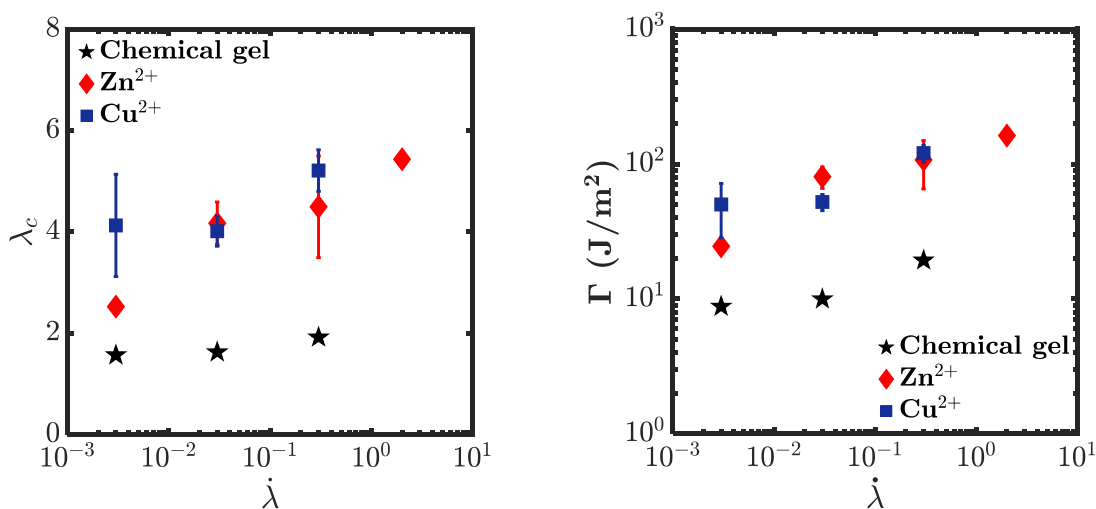


Figure 4.24: Critical stretch λ_c at which the crack starts to propagate (left) and corresponding fracture energy Γ (right) as a function of the stretch-rate, for the Zn^{2+} (red) and Cu^{2+} (blue) dual-crosslink hydrogels and the corresponding reference chemical gel (black).

The critical stretch and fracture propagation energy were higher for the Zn^{2+} and the Cu^{2+} dual-crosslink hydrogels than for the bare chemical gel, even at the lowest stretch-rates. This observation is inconsistent with our initial hypothesis on how energy dissipation would influence fracture properties, but tends to confirm what we have seen in Figure 4.11. Even when the physical bonds have no influence on the mechanical behavior of the gel (unchanged elastic modulus), they still toughen the material.

It is possible to use the results of cyclic experiments from Figure 4.17 to compute the local value of the fracture energy Γ_{local} , by removing the bulk dissipation from the computed Γ [11]. This gives the results shown in Figure 4.25 (data for the Cu^{2+} dual-crosslinked hydrogels were removed, since we did not realize cyclic experiments on those gels). The idea here is to subtract from Γ the energy that has been dissipated during loading in the bulk of the material, which is not available for crack propagation. The values obtained are still much higher than those of the bare chemical gel, implying the existence of a mechanism toughening the network even at low stretch-rates. This mechanism cannot be related to the clusters of physical crosslinks at $\dot{\lambda} = 0.003 \text{ s}^{-1}$: at this stretch-rate, the dual-crosslink hydrogel does not dissipate any significant energy.

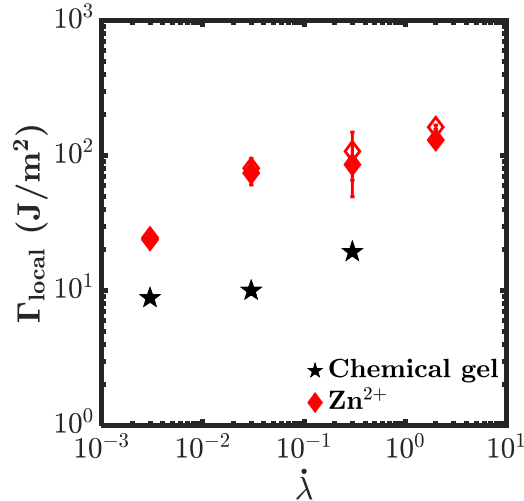


Figure 4.25: Local fracture energy Γ_{local} (filled symbols), along with the related fracture energy Γ (empty symbols), as a function of the stretch-rate, for a Zn^{2+} dual-crosslinked hydrogel (red) and the reference chemical gel (black).

We believe the propagation of a notch in such a sample to be prevented by the same mechanism mentioned in 4.4.2: the physical bonds prevent the correlated fracture of polymer chains, delaying it until higher stretches and fracture energies. Since this mechanism of protection is independent from the stretch-rate, it is still active at low stretch-rates when the physical bonds have no influence on the stiffness of the hydrogel.

The crack velocity is plotted in Figure 4.26. Just as for the Ni^{2+} dual-crosslinked hydrogel, the velocity is slower than the reference chemical hydrogel at low stretch-rates and increases faster with the stretch-rate, reaching 2 mm/s at $\dot{\lambda} = 2 \text{ s}^{-1}$. In the same figure, we plotted Γ_{local} versus crack velocity. We observe an increase of Γ_{local} with this velocity, although it is much less strong than in the Ni^{2+} dual-crosslink hydrogel.

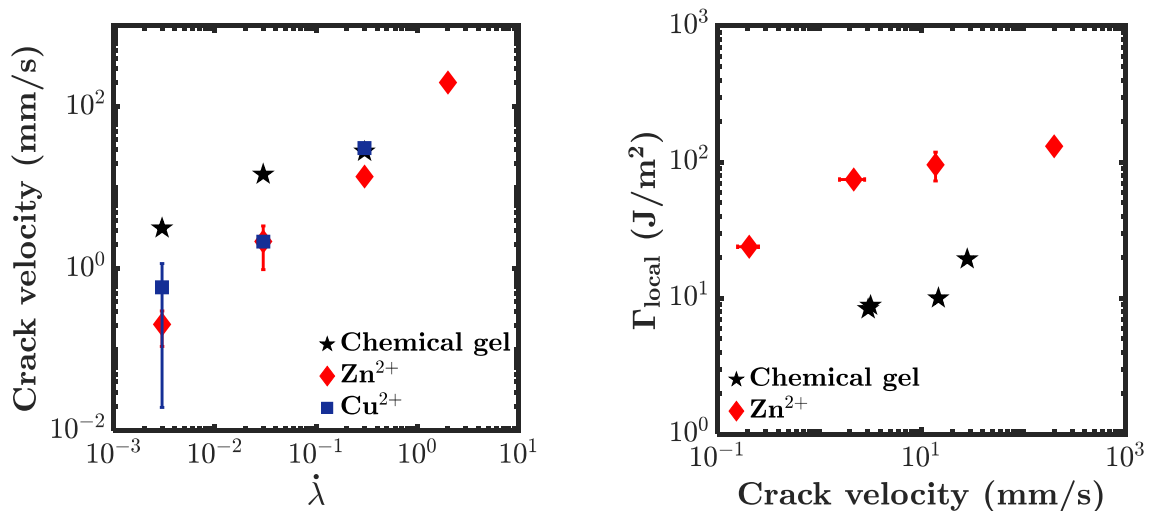


Figure 4.26: Left: Crack velocity as a function of the stretch-rate, for Zn^{2+} (red) and Cu^{2+} (blue) dual-crosslinked hydrogels, and the reference chemical gel (black). Right: Local fracture energy versus the crack velocity, for a Zn^{2+} dual-crosslink hydrogel (red) and the corresponding reference chemical gel (black).

4.6.2. Delayed fracture of “pure-shear” samples of Zn^{2+} dual-crosslinked hydrogel

Again, it might be interesting to look at how a crack propagates under constant stretch. We realized, on the Zn^{2+} dual-crosslink hydrogel, the same ‘delayed fracture’ experiments as in the previous part – applying a constant stretch to a notched sample in a “pure-shear” geometry. The stretching is realized at $\dot{\lambda} = 0.3 \text{ s}^{-1}$, just as for the Ni^{2+} hydrogel.

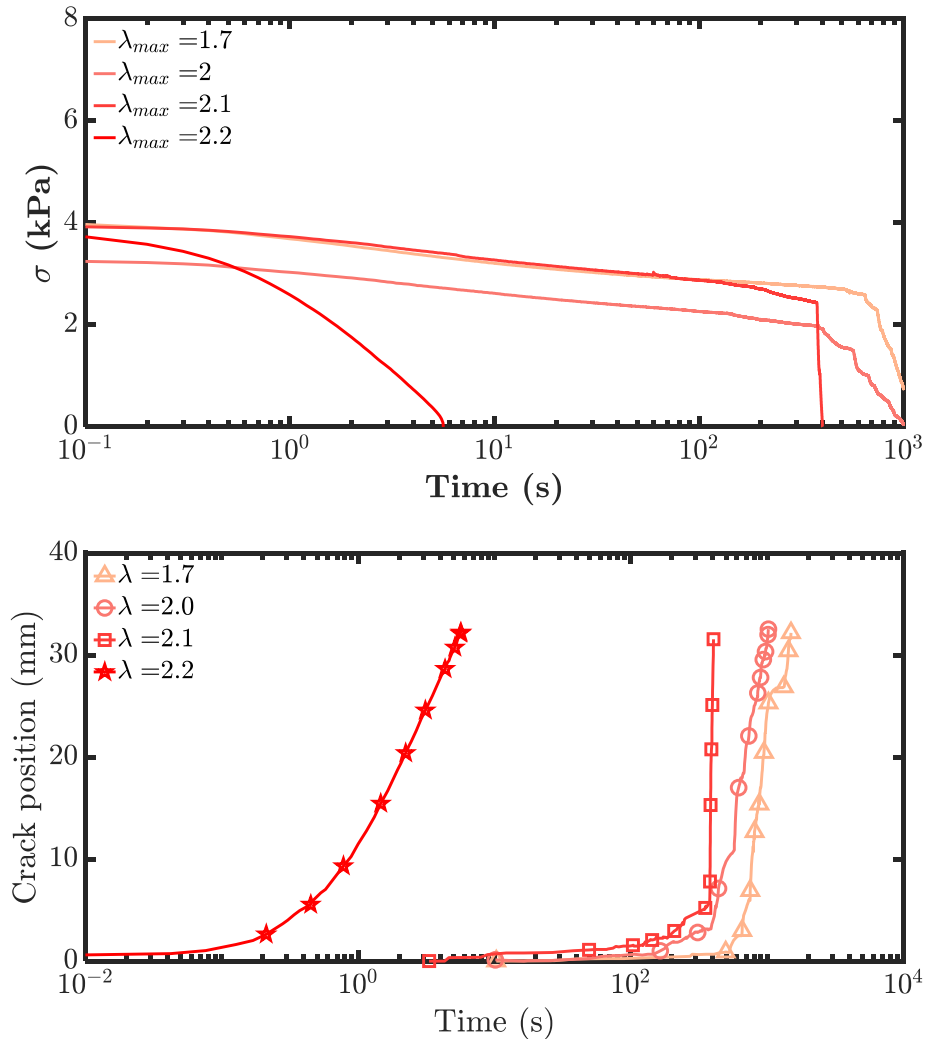


Figure 4.27: Stress vs. time (top) and Crack position vs. time (bottom) for relaxation tests on notched “pure shear” samples of a Zn^{2+} dual-crosslink hydrogel. The time $t = 0 \text{ s}$ corresponds to the beginning of the relaxation.

The fracture propagation in this experiment, shown in Figure 4.27, presents different profiles depending on the stretch:

- When $\lambda_{max} \leq 1.5$, the fracture does not propagate (which is expected since the chemical gel does not break at these small deformations either);
- When $\lambda_{max} = 1.7$ or 2 , the fracture propagates after a certain time (called delay time). This propagation is not steady-state, but shows a peculiar “stick-slip” behavior;
- When $\lambda_{max} = 2.1$, the fracture propagates with a stick-slip behavior after a certain delay time, followed by a fast propagation with no stick-slip behavior;

- When $\lambda_{max} \geq 2.2$, the fracture propagates immediately when the stretching stops. Furthermore, upon reaching $\lambda_{max} = 2.4$, the fracture propagates immediately during the stretching.

The stick-slip behavior is unexpected. When the energy is not high enough, the Zn^{2+} bond dissipates fast enough to stop the fracture. Once the fracture is stopped, the stresses relax at the tip of the fracture. At some point, the physical bonds cannot stop the correlated rupture of polymer chains, and the fracture propagates again. Figure 4.28 is a zoom on three experiments showing a delay before the beginning of the propagation (the stick-slip behavior of the sample stretched at $\lambda = 2.1$ happens before 390 s, where the crack propagates quickly).

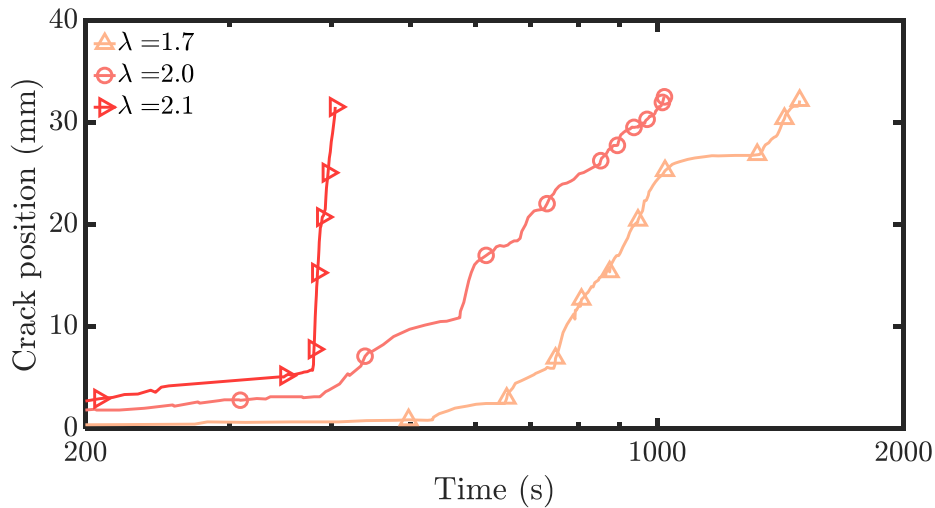


Figure 4.28: Crack position vs. time (zoom from Figure 4.27).

The onset of crack propagation (in seconds) and the crack speed (in mm/s) are shown in Figure 4.29. As mentioned earlier, the delay time decreases sharply with the stretch, until reaching a value of 0 (shown as 0.1s on the logarithmic graph). The mean crack velocity increases with the stretch.

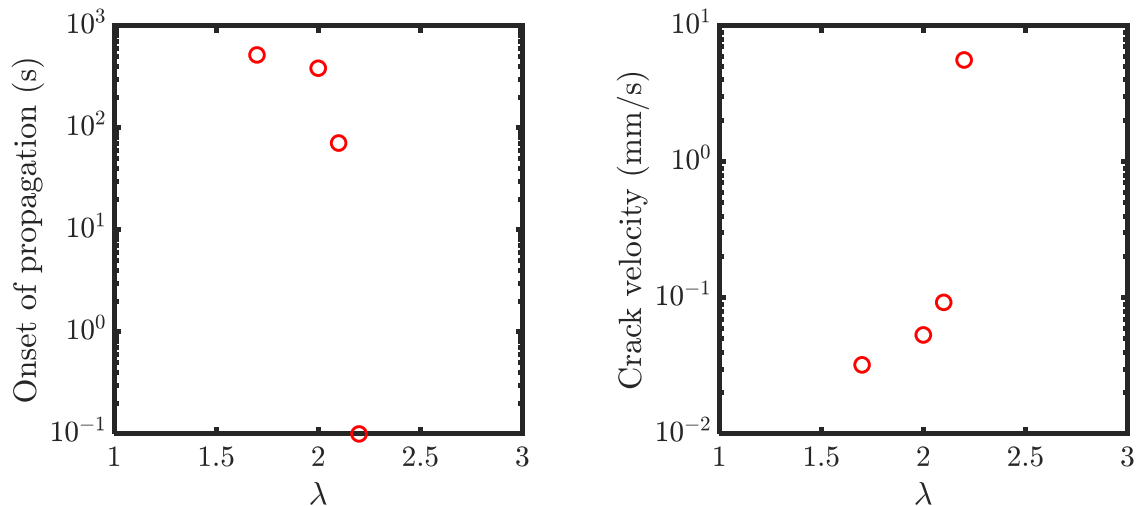


Figure 4.29: Onset of propagation (left) and mean crack velocity (right) versus the imposed stretch.

We noted in the previous chapter that, in this experiment, the main parameter controlling crack propagation was the strain energy imposed to the sample (and not the stretch). Figure 4.30 shows the

4. Dual-crosslink hydrogels with faster dynamics

computed strain energy release rate brought to the sample, and how it evolves with the crack velocity. The energy increases with the stretch, and provokes an increase in the velocity of the crack.

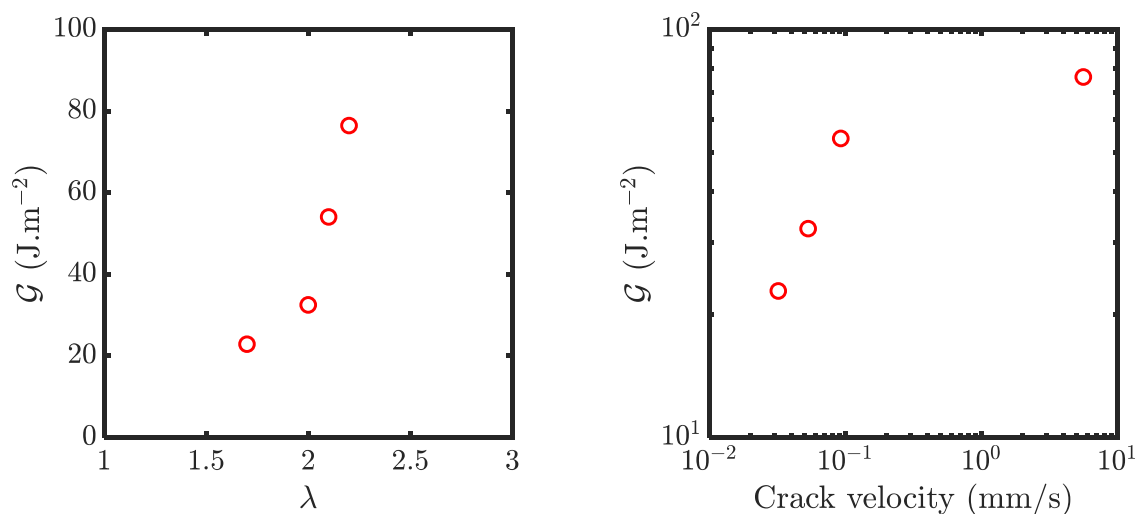


Figure 4.30: Left: Energy release rate versus the imposed stretch. Right: Mean crack velocity versus the energy release rate.

The materials studied here do not show the crack deviation we observed for the Ni^{2+} dual-crosslink hydrogel. At the stretch values where the crack deviates in the Ni^{2+} dual-crosslink hydrogel, the crack simply propagates here. The difference between those two hydrogels is simply their dynamic (fast here, slower in the previous one). At the same stretch-rate ($\dot{\lambda} = 0.3 \text{ s}^{-1}$), there are much more physical bonds active at the tip of the crack in the Ni^{2+} hydrogel than in the Zn^{2+} . At $\lambda \approx 2.4$, when the crack starts propagating in both hydrogels, a difference in anisotropy arises in both hydrogels: either the Zn^{2+} hydrogel has dynamics too fast to create an anisotropy that will force the crack to deviate, or this anisotropy exists and is linked to the existence of physical crosslinks and is here too short-lived to influence the crack. The crack propagates easily in this fast hydrogel.

4.7. Conclusions

We have prepared in this chapter two different dual-crosslink hydrogels with fast dynamics, simply by changing the metallic ion used as a physical crosslinker. Zn^{2+} and Cu^{2+} exhibit very similar behaviors, with Cu^{2+} maybe slightly slower in dynamics than Zn^{2+} . The rheology results show a low influence of the frequency on both storage and loss moduli. The peak in energy dissipation we observed in the Ni^{2+} dual-crosslink hydrogel is shifted to higher frequencies, suggesting that the Imidazole- Zn^{2+} (or Imidazole- Cu^{2+}) bond is much more short-lived than the Imidazole- Ni^{2+} bond. This was suggested by literature results on the dissociation kinetics of such complexes.

This result proves that the important factor in these dual-crosslink hydrogels is not the thermodynamic constant of association of the metal ion and the imidazole ligand, but its dissociation kinetic constant: while Cu^{2+} and Ni^{2+} possess very similar thermodynamic constants of complexation with imidazole, the lifetimes of such complexes is very different. The thermodynamic constant controls however the complexation state of such ions in the network. Cu^{2+} ions show an absorption isotherm very similar to the one of the Ni^{2+} ions, indicating a similar complexation state. Absorption is a thermodynamic-driven phenomenon, while the energy dissipation is a kinetic problem.

We have also shown that, just as in the Ni^{2+} dual-crosslink hydrogel, these fast-dynamic dual-crosslink hydrogels show evidence of aggregates of physical bonds. These aggregates, whether caused by the physical bonds or by the heterogeneities inherent to the chemical network, possess a characteristic lifetime that will influence the behavior of the dual-crosslink hydrogel. Their size was again related to the lengths we could measure in other experiments. More importantly, we evidenced a difference in the clustering between the Ni^{2+} and the Zn^{2+} dual-crosslink hydrogels, the latter showing higher clustering than the former. We were also able to identify a characteristic volume of the X-ray (or neutron) diffusing object, which was 45 times bigger than the volume of the free ion in solution.

The properties in large deformations of those fast dynamic dual-crosslink hydrogels are very interesting. Since the characteristic time of their physical bonds is much lower than the observation time of our experiments, the number of stretched elastic chains between physical bonds during the experiments we realized was negligible. We saw no increase in the elastic modulus that would indicate an increase in the number of active polymer chains. The strain-hardening behavior is here, contrary to the Ni^{2+} hydrogel, strain controlled. There was no increase of the number of polymer chains in their strain-hardening regime with the stretch-rate, which is what provokes the strain-hardening in the Ni^{2+} dual-crosslink hydrogel. However, the slight increase in the number of physical bonds is enough to provoke a delay of the onset of strain-hardening.

More interestingly, the stretch at break of such a fast dynamic dual-crosslink hydrogel was almost the same as that of the Ni^{2+} dual-crosslink hydrogel. Even at stretch-rates where the physical bonds were not active, and had no influence on the elastic modulus for example, the stretch at break was much higher than that of the bare chemical gel. We explained this behavior by the mechanism of prevention of crack nucleation we detailed in the previous chapter.

The energy dissipated by those materials during cyclic deformation is much lower than what the Ni^{2+} dual-crosslink hydrogel dissipates, because of the lower number of active physical bonds. However, energy dissipation is observed over a range of stretch-rates (or observation times) which is much longer than what could be expected from the rheology experiments. The lifetime of the Zn^{2+} -Imidazole bond is lower than 0.01 s, but the experiments we realized over 100 s still show a significant energy dissipation, which we attributed to the existence of aggregates of physical bonds.

We have seen no sign of molecular damage of the chemical network on the properties of the dual-crosslink hydrogels after cycles at high deformations. Just as for the Ni^{2+} dual-crosslink hydrogels, they recovered their properties after a time long enough to allow the polymer chains to go back to their initial state.

The materials studied in this chapter show no particularly significant increase of their deformation properties with increasing physical bonds (low dissipation until reaching high stretch-rates, slight increase in Young's modulus), but they are much tougher than the bare chemical gel. We observed a significant increase in the local fracture energy, even at very low stretch-rates, along with a significant increase of the stretch at break. We attributed this increase at low stretch-rates to the mechanism of nucleation prevention previously mentioned in Chapter 3. At the tip of the crack, the correlated molecular breaking is delayed by the presence of the physical bonds. This delays the onset of crack propagation, and hence increases the toughness of the material. At increasing stretch-rates, the number of active physical bonds in the network increases slightly. However, the stretch-rates at the crack tip are

4. Dual-crosslink hydrogels with faster dynamics

much higher than what we impose in the bulk. This implies a higher number of active physical bonds at the tip of the crack, which will average the stresses over a larger zone and help toughening the material.

These fast-dynamic materials allowed us to invalidate our initial hypothesis that, at low stretch-rates compared to the characteristic frequency of the physical bond, the low amount of energy dissipation would make the material as fragile as the elastic chemical network. Its mechanical properties (other than fracture) however follow our idea that the number of active physical bonds – which is a time-controlled parameter – controls the behavior of the dual-crosslink hydrogel.

References

1. Ahmadi, M. & Seiffert, S. Dynamic Model Metallo-Supramolecular Dual-Network Hydrogels with Independently Tunable Network Crosslinks. *Journal of Polymer Science* 58, 330–342 (2020).
2. Fullenkamp, D. E., He, L., Barrett, D. G., Burghardt, W. R. & Messersmith, P. B. Mussel-Inspired Histidine-Based Transient Network Metal Coordination Hydrogels. *Macromolecules* 46, 1167–1174 (2013).
3. Rorabacher, D. B. The Kinetics of Formation and Dissociation of the Monoammine Complexes of the Divalent, First-Row, Transition Metal Ions. *Inorganic Chemistry* 5, 1891–1899 (1966).
4. Sjöberg, S. Critical evaluation of stability constants of metal-imidazole and metal-histamine systems. *Pure & Appl. Chem.* 69, 1549–1570 (1997).
5. Yount, W. C., Loveless, D. M. & Craig, S. L. Strong Means Slow: Dynamic Contributions to the Bulk Mechanical Properties of Supramolecular Networks. *Angewandte Chemie International Edition* 44, 2746–2748 (2005).
6. Pekel, N. & Güven, O. Separation of heavy metal ions by complexation on poly (N-vinyl imidazole) hydrogels. *Polymer Bulletin* 51, 307–314 (2004).
7. Shibayama, M., Tanaka, T. & Han, C. C. Small angle neutron scattering study on poly(N-isopropyl acrylamide) gels near their volume-phase transition temperature. *97*, 14 (1992).
8. B. Tito, N., Creton, C., Storm, C. & G. Ellenbroek, W. Harnessing entropy to enhance toughness in reversibly crosslinked polymer networks. *Soft Matter* 15, 2190–2203 (2019).
9. Kean, Z. S. et al. Increasing the Maximum Achievable Strain of a Covalent Polymer Gel Through the Addition of Mechanically Invisible Cross-Links. *Advanced Materials* 26, 6013–6018 (2014).
10. Mayumi, K., Marcellan, A., Ducouret, G., Creton, C. & Narita, T. Stress–Strain Relationship of Highly Stretchable Dual Cross-Link Gels: Separability of Strain and Time Effect. *ACS Macro Lett.* 2, 1065–1068 (2013).
11. Mayumi, K., Guo, J., Narita, T., Hui, C. Y. & Creton, C. Fracture of dual crosslink gels with permanent and transient crosslinks. *Extreme Mechanics Letters* 6, 52–59 (2016).

Chapter 5

Slowing down the dynamics

5. Slowing down the dynamics

Table of contents

5.1. P(AAm-co-VIm) – Hg²⁺ hydrogels	162
5.1.1. Preparation and absorption isotherms	162
5.1.2. Linear rheology	163
5.1.3. Small angle X-Ray scattering	164
5.1.4. Tensile tests	165
5.1.5. Conclusions on P(AAm-co-VIm)-Hg ²⁺ dual-crosslink hydrogel	166
5.2. Synthesis of P(AAm-co-tPy) hydrogels.....	166
5.3. Rheology of the P(AAm-co-tPy) chemical hydrogel.....	167
5.4. Incorporation of physical bonds.....	168
5.5. Rheology of the slow Terpyridine-Zn²⁺ hydrogel	169
5.6. Behavior in large deformations	170
5.6.1. Tensile tests	170
5.6.2. Cycles	172
5.6.3. Fracture – Single notch test	174
5.7. Discussion and conclusions	177
References	179

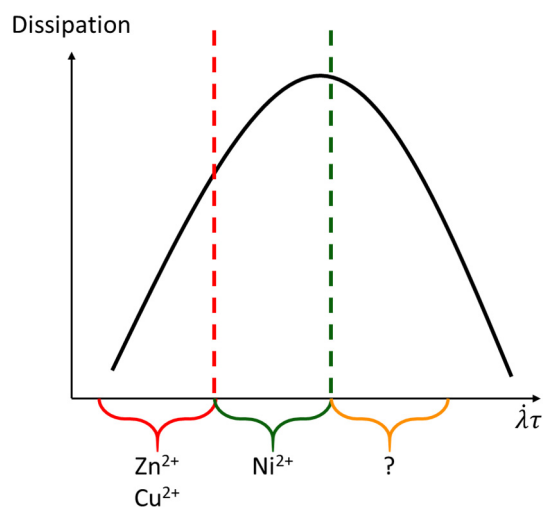


Figure 5.1: Dissipation of dual-crosslink hydrogels as a function of the stretch-rate, shifted by the lifetime of the physical bond.

In the previous chapters, we synthesized and characterized two types of dual-crosslink hydrogels based on the imidazole- M^{2+} chemistry : with fast dynamics (Zn^{2+}/Cu^{2+}) and with intermediate dynamics (Ni^{2+}). As shown in Figure 5.1, these two systems were suitable for the low Weissenberg number regions. Now the question is what is the dynamics of the dual-crosslink hydrogel system in the ‘high Weissenberg number’ domain of the dissipation curve. In order to answer this question, it is necessary to develop new dual crosslink gels based on coordination bonds with slower dynamics. Two options will be investigated. One is to keep the ligand (imidazole on the P(AAm-co-VIm) chains) and to change the metallic ions. We will study a dual crosslink gel physically crosslinked with mercury(II) ion Hg^{2+} , which thermodynamics complexation constants are $\beta_1 \approx 9$ and $\beta_2 \approx 18$. Another is to change the ligand with the same metallic ions; we will then study a dual crosslink gel based on a copolymer of acrylamide derivative with terpyridine.

In order to differentiate those two different hydrogels, we will name them P(AAm-co-VIm) for the one containing imidazole moieties and P(AAm-co-tPy) for the one containing terpyridine moieties.

5.1. P(AAm-co-VIm) – Hg^{2+} hydrogels

5.1.1. Preparation and absorption isotherms

This hydrogel was prepared by the “Diffusion” method, described in the previous chapters: first, the P(AAm-co-VIm) chemical gel was synthesized and then the physical bond was incorporated by diffusion.

Figure 5.2 shows the absorption isotherm obtained for Hg^{2+} , absorbed by the P(AAm-co-VIm) chemical hydrogel. The amount of the absorbed Hg^{2+} increased sharply in the low concentration range below 2 mmol/L, and the ratio $[Hg]/[Imidazole]$ exceeded 1 above $[Hg]_{solution} = 6$ mmol/L. This behavior can be explained either by an underestimation of $[Hg^{2+}]$ in solution by the titration method, or by a strong aggregation of metal ions in the hydrogel.

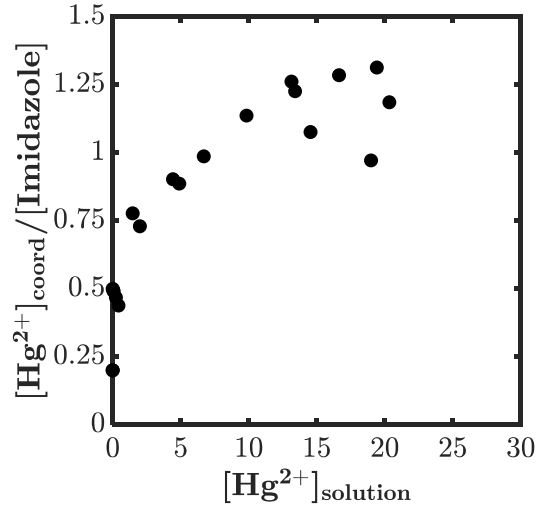


Figure 5.2: Absorption isotherm of Hg^{2+} ions in a P(AAm-co-VIm) hydrogel. The concentrations are in mmol/L.

In any case, it seems that the P(AAm-co-VIm) hydrogel absorbs much more Hg^{2+} ions than it absorbed Ni^{2+} or Zn^{2+} ions. This might lead to differences in the structure and in the properties of the dual-crosslink hydrogel. The equilibrium complexation of Hg^{2+} and Imidazole seems to be $[\text{HgIm}]^{2+}$, which should not create physical bonds between polymer chains.

5.1.2. Linear rheology

We selected the P(AAm-co-VIm) dual crosslink hydrogel with $[\text{Hg}^{2+}] = 100$ mmol/L, in order to compare it with P(AAm-co-VIm) dual crosslink hydrogel with Zn^{2+} and Ni^{2+} ions, the rheological properties of which have been demonstrated in the previous chapters. The results of rheological experiments carried out on the P(AAm-co-VIm)- Hg^{2+} dual crosslink hydrogels are shown in Figure 5.3. The results for the corresponding chemical gel are also shown.

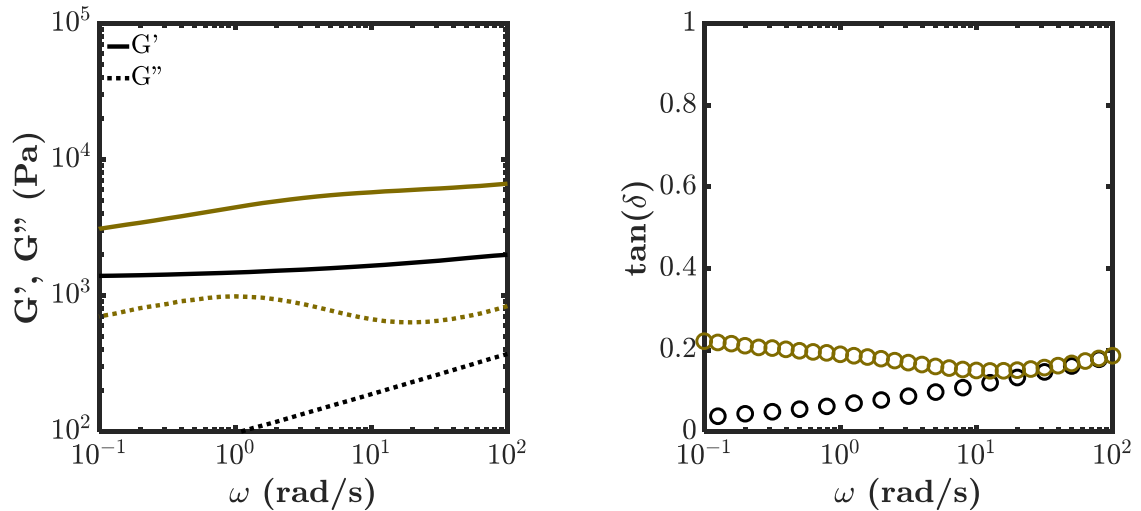


Figure 5.3: Storage and loss moduli (left) and corresponding $\tan(\delta)$ (right), as a function of the oscillation frequency for a dual-crosslink hydrogel with $[\text{Hg}^{2+}] = 100$ mmol/L (brown) and the corresponding bare chemical gel (black).

5. Slowing down the dynamics

The global rheological responses of the P(AAm-co-VIm)-Hg²⁺ dual-crosslink hydrogel showed the typical responses of the dual crosslink systems: by incorporating the transient crosslinks, the elastic modulus G' increases with increasing frequency. A peak in loss modulus is observed at low frequencies. For the P(AAm-co-VIm)-Hg²⁺ dual-crosslink hydrogels, we found the peak at 1 rad/s. However, it should be noted that the absolute values of the moduli were found to be much lower than those of the other P(AAm-co-VIm)-M²⁺ dual crosslink hydrogels. The storage modulus reached a much lower plateau at high frequencies (5.7 kPa at 100 rad/s) than what we observed in the Ni²⁺ dual-crosslink hydrogel (34 kPa). The loss factor $\tan(\delta)$ followed the same trend, with a maximal value around 0.25 when the Ni²⁺ dual-crosslink hydrogel reaches 0.67.

It seems that, in this Hg²⁺ dual-crosslink hydrogel, the physical bonds are much less effective than in the previous cases. We observe a slow dynamic, but the dissipation is very low. The low increase in elastic modulus relative to the chemical gel tends to confirm this observation. We have seen just before that the equilibrium complexation state seems to be with one Hg²⁺ ion for only one Imidazole moiety, which does not create physical crosslinks. These observations in rheology confirm this hypothesis: if we have in this Hg²⁺ dual-crosslink hydrogel very few [HgIm₂]²⁺ complexes, thus very few transient physical bonds, it would explain the low dissipation and elastic moduli observed.

5.1.3. Small angle X-Ray scattering

SAXS experiments were conducted on two P(AAm-co-VIm) hydrogels with [Hg²⁺] = 100 and 200 mmol/L. The results shown in Figure 5.4 reveal a very clear peak at low values of the scattering vector, corresponding to a distance of approximately 10 nm. There might be a shoulder at higher values of q , more clearly visible on the hydrogel with more Hg²⁺ ions, corresponding to a local organization of the ions at distances of the order of 1 nm.

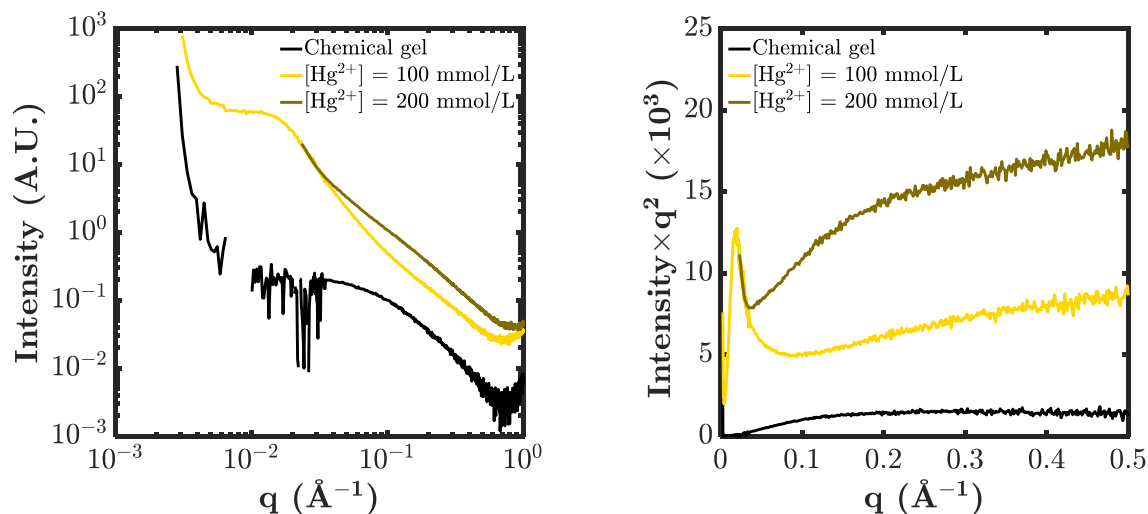


Figure 5.4: Log-log plot of X-Ray intensity, normalized by the thickness of the sample, as a function of the scattering vector (left) and Kratky plots (right) for dual-crosslink hydrogels with Hg²⁺ ions at different concentrations in ions. Results for the bare chemical gel are shown for comparison purposes

The organization of Hg²⁺ ions in the dual-crosslink hydrogel seems to be quite different from what we have seen before in the Ni²⁺ or Zn²⁺ dual-crosslink hydrogels, with a much clearer peak at low values of q , implying the existence of well-defined clusters of ions in this hydrogel.

5.1.4. Tensile tests

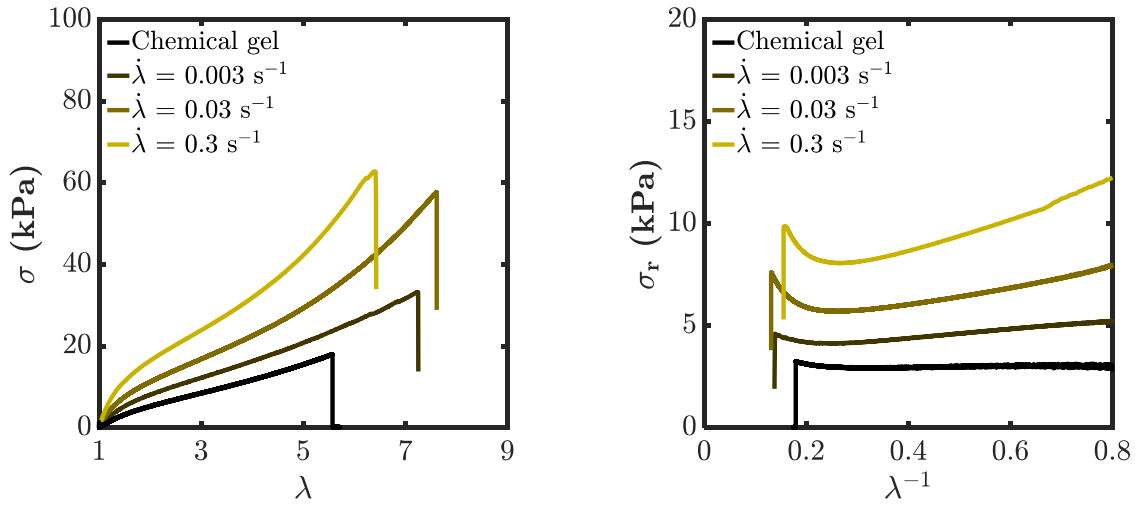


Figure 5.5: Stress vs. strain curves (left) and corresponding Mooney-stress vs. λ^{-1} (right) for an Hg^{2+} dual-crosslink hydrogel with $[\text{Hg}^{2+}] = 100 \text{ mmol/L}$ (brown) and a bare chemical gel (black).

Uniaxial tensile tests were realized on rectangular strips of $\text{P(AAm-co-VIm)-Hg}^{2+}$ dual-crosslink hydrogel with $[\text{Hg}^{2+}] = 100 \text{ mmol/L}$. The results are shown in Figure 5.5 and Figure 5.6. As for the previous hydrogels, the elastic modulus increased with strain-rate. The strain at break increased compared to the bare chemical gel, reaching values around $\lambda = 7$, while it evolved only a little with the stretch-rate. A slight decrease with increase in the stretch rate from 0.03 s^{-1} to 0.3 s^{-1} could be within the experimental error of the rupture of un-notched samples. Further experiments would be necessary for confirmation.

The data shown in Figure 5.5 were further analyzed as previously discussed. The onset of the strain hardening λ_{SH} occurred at more or less $\lambda = 4$, with a slight decrease with the stretch-rate. The reduced stress at which we see this strain hardening appears however, increases with the stretch-rate, and is multiplied by two between $\dot{\lambda} = 0.003 \text{ s}^{-1}$ and $\dot{\lambda} = 0.3 \text{ s}^{-1}$.

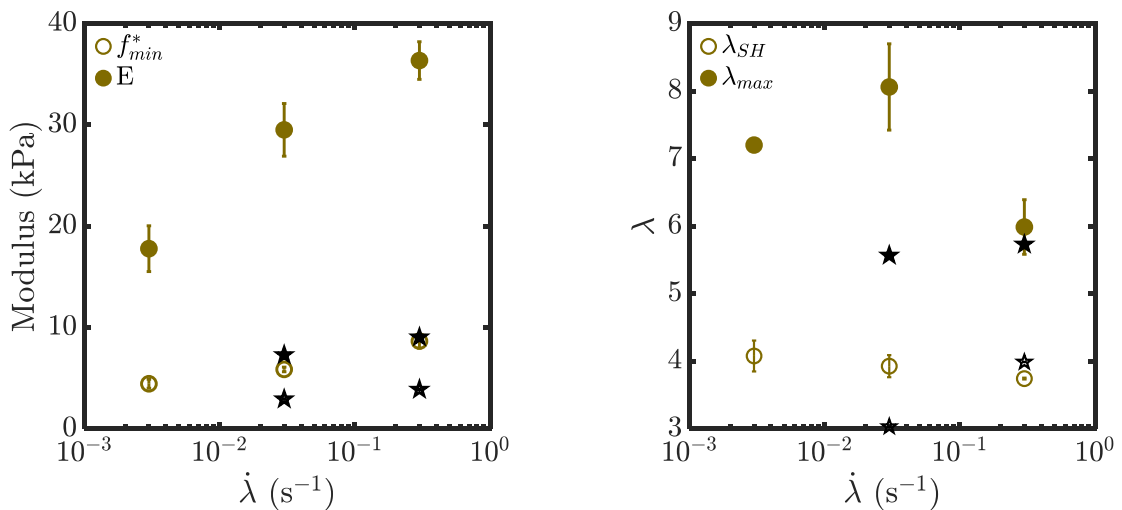


Figure 5.6: Elastic modulus and reduced stress at the onset of strain-hardening (left), stretch at break and stretch at the onset of strain-hardening (right) versus the stretch-rate, for a dual-crosslink hydrogel with Hg^{2+} ions (brown) and the corresponding chemical gel (black).

5.1.5. Conclusions on P(AAm-co-VIm)-Hg²⁺ dual-crosslink hydrogel

In this chapter, we aimed at preparing a dual-crosslink hydrogel with slow dynamics and characterizing their properties. The behavior in large deformations of this P(AAm-co-VIm)-Hg²⁺ dual-crosslink hydrogel was actually quite close to what we expected in a dual-crosslink hydrogel with slow dynamics: a continuous increase of the elastic modulus and a decrease of the stretch at break with increase in the stretch rate. Its long-lived physical bonds (relaxation time of 1 rad/s) allowed us to reach a rate of deformation at which they behave as permanent crosslinks. This should reduce the energy dissipation and make the material stiffer and more brittle, as we observed for this dual-crosslink hydrogel.

However, the study of the microstructure revealed many differences with the previously studied Zn²⁺ or Ni²⁺ dual-crosslink hydrogel. The absorption isotherm showed that the equilibrium complexation state was in majority one metal ion for one ligand, which implies the absence of physical crosslinks in the material. The rheological experiments confirmed that observation: with a storage and loss moduli much weaker than what was observed on the Ni²⁺ dual-crosslinked hydrogel. The slight increase in those moduli compared to the bare chemical gel could be explained by the presence of aggregates of mono-complexes. These aggregates will in turn act as physical crosslinkers, with a characteristic lifetime. Being much less numerous than the coordination crosslinks of the Ni²⁺ dual-crosslink hydrogel, the increase in storage modulus is much weaker than what was observed on the Ni²⁺ dual-crosslink hydrogel. The presence of those aggregates was confirmed by SAXS experiments.

All those observations, along with the safety issues that the use of HgCl₂ poses, are why we decided to abandon this hydrogel.

5.2. Synthesis of P(AAm-co-tPy) hydrogels

In order to obtain hydrogels with slower dynamics, another option was to change the ligand used in the complexes. In collaboration with Prof. Charles-André Fustin of Catholic University of Louvain, Belgium, we obtained a new monomer with a ligand, 2,6-bis(2-pyridyl), 4-N-ethoxy-propenamamide. This acrylamide-derivative has a terpyridine functionality that serves as ligand for coordination bond.

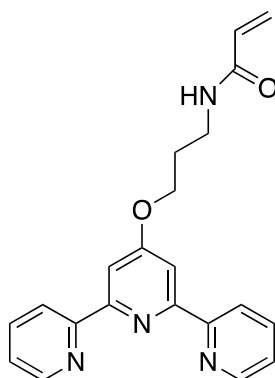


Figure 5.7: 2,6-bis(2-pyridyl), 4-N-ethoxy-propenamamide, pyridine monomer

The chemical structure of the monomer is shown on Figure 5.7. We integrated it in the chemical network of polyacrylamide using the formulation presented in Table 5.1.

*Table 5.1: Concentrations of each component in the chemical gel. *For the solvent, this is a weight percentage.*

	Molar mass (g/mol)	Specific gravity (g/mL)	Objective (mol %)	Concentration (mol/L)
AAm	71.1	-	90%	1.8
Terpyridine	94.1	1.039	10%	0.2
MBA	154.2	-	0.15%	0.003
VA-044	323.27	-	0.3%	0.006
Solvent	-	-	85.1%*	

We used a thermally activated azo initiator VA-044 (2,2'-Azobis[2-(2-imidazolin-2-yl)propane] dihydrochloride) obtained from Wako Pure Chemicals. It should be noted that with the KPS/TEMED polymerization, no gel was obtained. With VA-044, the polymerization was carried out at 30°C for 24 hours, in an inert N₂ atmosphere.

The synthesis was carried out in a slightly different mold than what was previously presented in Chapter II. Instead of using Teflon foils as interlayers between the hydrogel and the glass plate, we used PET foils. It was found that the Teflon inhibited the polymerization with the VA-044 initiator for unknown reasons.

It should be noted that the change in the ligand and the initiator could result in the difference in the structure of the chemical gel. We simply assessed possible difference by measuring the elastic modulus. We found that with this new synthesis, a P(AAm-co-tPy) chemical hydrogel synthesized with 0.15 mol% of chemical crosslinker (same as for the P(AAm-co-VIm) gel systems) had a higher elastic modulus than the reference P(AAm-co-VIm) chemical hydrogel studied before. In order to be able to compare both chemical hydrogels, the formulation needed to be modified. Formulations with a varied amount of MBA (ranging from 0.038 mol% to 0.15 mol%) were studied.

5.3. Rheology of the P(AAm-co-tPy) chemical hydrogel

We performed small amplitude oscillatory shear experiments on the P(AAm-co-VIm) and the P(AAm-co-tPy) chemical hydrogels, each with the same concentration in initiator, and varying the chemical crosslinker concentration in the P(AAm-co-tPy) hydrogels. The results are shown in Figure 5.8. The elastic modulus of the P(AAm-co-tPy), with 0.15 mol% of chemical crosslinker and initiated by VA-044, was 5 times higher than that of the P(AAm-co-VIm) hydrogel initiated by KPS. This forced us to change the formulation of the terpyridine hydrogel, as mentioned in the previous paragraph.

The formulation giving the gel closest to the reference chemical gel is that with a crosslinker concentration of 0.05 mol%. Lower concentrations gave a very soft hydrogel, approaching to the percolation point with a clearer visco-elastic behavior that should be avoided in the reference chemical network. This formulation was chosen as a reference in the following parts of this chapter.

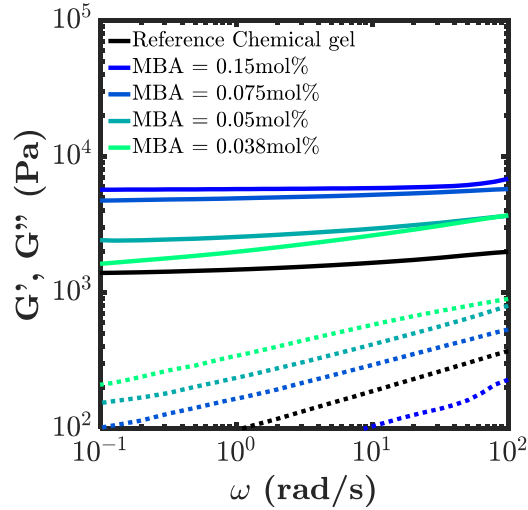


Figure 5.8: Storage and loss modulus of the reference P(AAm-co-VIm) chemical hydrogel synthesized with KPS/TEMED initiator (black) and of different P(AAm-co-tPy) hydrogel synthesized with VA-044 initiator and varying concentration of chemical crosslinker (blue to green).

5.4. Incorporation of physical bonds

P(AAm-co-tPy) dual crosslink hydrogels were prepared by the same diffusion method as the P(AAm-co-VIm) dual crosslink gels with NiCl₂ and ZnCl₂.

The absorption isotherm of Zn²⁺ ions by a P(AAm-co-tPy) hydrogel is shown in Figure 5.9. Error bars have been added, to take into account the possible experimental error on the measurement of the equivalent volume. The result suggested that the concentration of Zn²⁺ ions absorbed in the hydrogel saturated at [Zn²⁺]/[terpy] = 0.5 (thus [Zn²⁺] = 100 mmol/L) at a concentration in solution [Zn²⁺]_{solution} = 10 mmol/L. Thus the majoritarian component of the terpy-Zn²⁺ complex in this system is [Zn(terpy)₂]²⁺, one Zn²⁺ ion for two terpyridine moieties.

We have also tested the Ni²⁺ ions for the P(AAm-co-tPy) hydrogel system. They were also absorbed in a same manner by the P(AAm-co-tPy) chemical network. However, the obtained dual-crosslink hydrogels were very brittle at every Ni²⁺ concentration, thus it was difficult to handle. The lifetime of a [Ni(terpy)₂]²⁺ coordination complex is very long, around 6.10⁵ s [2] (to be compared with the 0.8 s of the [Zn(terpy)₂]²⁺ complex [2] or the 0.11 s of the [Ni(Im)₂]²⁺ complex [3], all listed in Table 5.2). This makes the physical bond introduced in the network very long-lived, almost permanent. This dramatic decrease in stretchability of the hydrogel with the long-lifetime physical bonds confirms our hypothesis: the longer the lifetime, the lesser the dissipation and the more fragile the material, behaving just like a highly crosslinked chemical gel.

Table 5.2: Stability constant of Ligand-M²⁺ complexes, and corresponding dissociation kinetic constants [1,2,3].

Metal-Ligand	K_1	K_2	k_{diss} (s ⁻¹)
Ni ²⁺ - Im	10 ^{3.03}	10 ^{2.51}	8.9
Ni ²⁺ - terpy	10 ^{10.7}	10 ^{11.1}	1.58 × 10 ⁻⁶
Zn ²⁺ - terpy	10 ⁶	> 10 ⁸	1.259

In the following, we characterize the hydrogel with $[Zn^{2+}]_{bound} = 100 \text{ mmol/L}$ and $[Zn^{2+}]_{free} = 10 \text{ mmol/L}$.

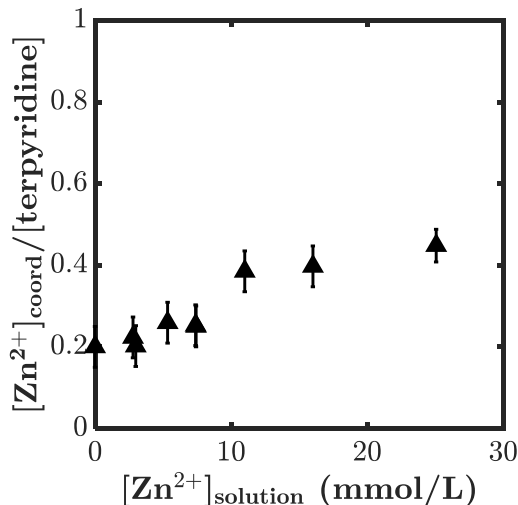


Figure 5.9: Concentration of complexed Zn^{2+} ions, divided by the concentration of Terpyridine moieties, as a function of the concentration of Zn^{2+} ions in the diffusing solution. All concentrations are at equilibrium.

5.5. Rheology of the slow Terpyridine- Zn^{2+} hydrogel

We performed small amplitude oscillatory shear experiments on the P(AAm-co-tPy)- Zn^{2+} hydrogel. The results are presented in Figure 5.10. At high frequencies, the elastic modulus G' reached a plateau around 90 kPa. At low frequencies, it decreased with decreasing frequency in a same manner as the other dual crosslink gels. The value of G' approached to but did not reach that of the chemical gel, suggesting the existence of a slower component. We see a clear peak in the loss modulus G'' around 3 rad/s, corresponding to the decrease of the elastic modulus. The loss factor $\tan(\delta)$ shows a peak around 0.6 rad/s.

The relaxation time of the P(AAm-co-tPy)- Zn^{2+} dual-crosslink hydrogel is around 10 times longer than the relaxation time of the P(AAm-co-VIm)- Ni^{2+} dual-crosslink hydrogel. The decrease in G'' at low frequencies is steeper for the P(AAm-co-tPy)- Zn^{2+} hydrogel than for the P(AAm-co-VIm)- Ni^{2+} dual-crosslink hydrogel. More importantly, the plateau reached at high frequencies is 2.5 times higher than what the P(AAm-co-VIm)- Ni^{2+} dual-crosslink hydrogel showed, implying that the P(AAm-co-tPy)- Zn^{2+} hydrogel possesses 2.5 times more elastically active physical crosslinks than the P(AAm-co-VIm)- Ni^{2+} hydrogel. We have computed in Chapter 2 the maximal amount of physical crosslinks in a P(AAm-co-VIm)- Ni^{2+} dual-crosslink hydrogel, estimated at around 40 mmol/L. This would imply that we have here a very high number of bis-complexes, with two ligands for one metal ion.

5. Slowing down the dynamics

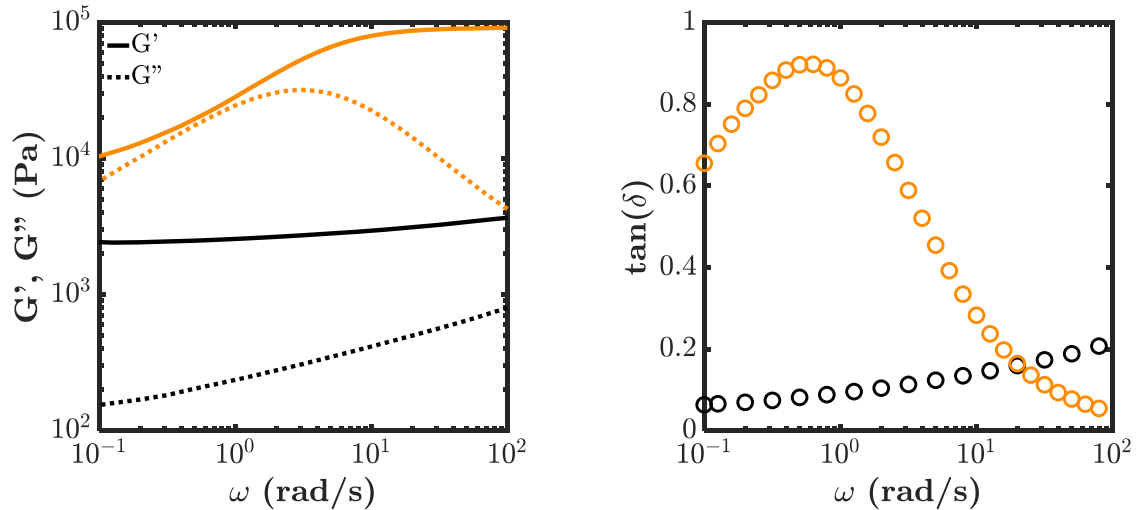


Figure 5.10: Storage and loss moduli (left) and corresponding $\tan(\delta)$ (right) as a function of the shear frequency, for a P(AAm-co-tPy)-Zn²⁺ “Diffusion” dual-crosslink gel (orange) and the corresponding chemical gel (black).

In order to explore longer relaxation times, we carried out relaxation experiments. Figure 5.11 shows the relaxation modulus of P(AAm-co-tPy)-Zn²⁺ dual-crosslink hydrogel and that of the corresponding chemical gel. We observed a relaxation of the modulus at a characteristic time around 0.6 s⁻¹, consistent with the relaxation time measured in the frequency sweep. Even at longer times up to 1000 s, the modulus of the chemical gel was not reached.

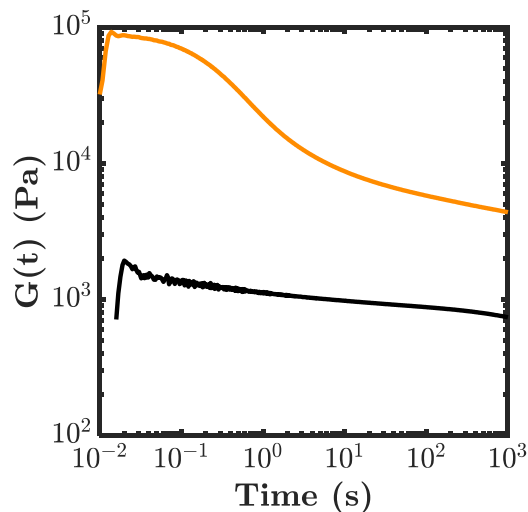


Figure 5.11: Shear modulus $G(t)$ versus time in a relaxation experiment, for a P(AAm-co-tPy)-Zn²⁺ “Diffusion” dual-crosslink gel (orange) and a chemical gel (black), at a strain of 1%.

5.6. Behavior in large deformations

5.6.1. Tensile tests

Figure 5.12 presents the results of uniaxial tensile tests realized on the P(AAm-co-tPy)-Zn²⁺ dual-crosslink hydrogels at different stretch rates. One can clearly see a decrease of the extensibility with increasing stretch rate, which was not observed with the P(AAm-co-VIm)-M²⁺ dual-crosslink hydrogels having faster dynamics. This can be explained by the long lifetime of the physical bond relative to the

stretch rate: at the fast stretch rate, the transient bond has no time to break and it behaves like a permanent crosslink, resulting in the increased brittleness. The Young's modulus of the hydrogel also increased drastically with stretch-rate (see also Figure 5.13), confirming the increase of the closed physical crosslinks at high stretch rates.

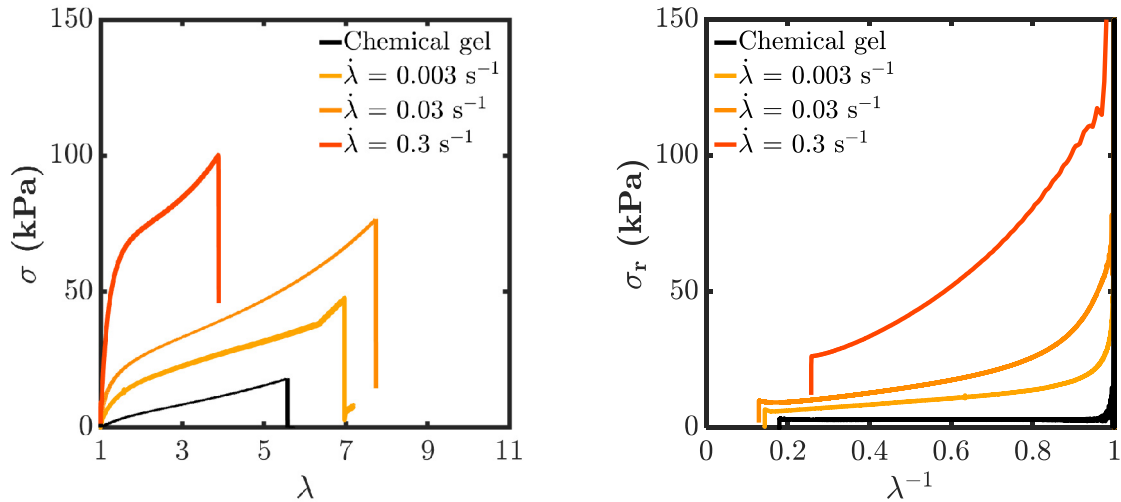


Figure 5.12: Stress-stretch curves (left) and Mooney plots (right) for a P(AAm-co-tPy) dual-crosslink gel with Zn^{2+} ions (orange) and the reference chemical gel (black).

The Mooney plots in Figure 5.12 (right) also show that the strain-hardening regime was not reached for this material at higher stretch-rates. The sample broke before. The unclear strain hardening can be seen by the values of f^*_{min} much lower than E as well as those of λ_{SH} close to λ_{max} (in Figure 5.13). It should be noted that, for $\dot{\lambda} = 0.3 \text{ s}^{-1}$, the material broke before showing a strain-hardening behavior. We see an increase in the minimal value of the reduced stress f^*_{min} , along with a decrease of the stretch of onset of strain-hardening λ_{SH} : just as was observed for the P(AAm-co-VIm)- Ni^{2+} hydrogel at higher stretch-rates.

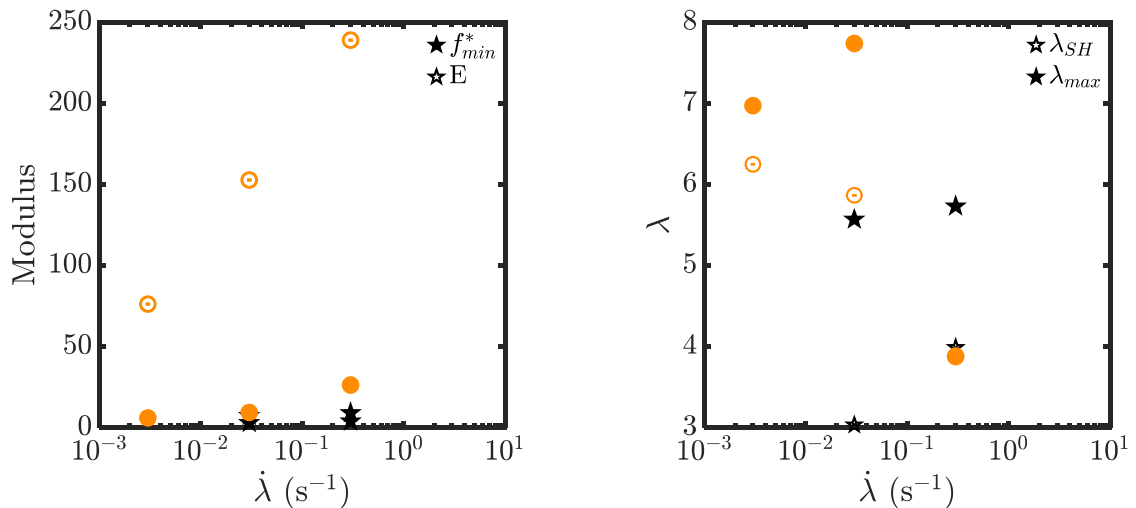


Figure 5.13: Young's modulus and reduced stress at the onset of strain-hardening (left), stretch at break and stretch at onset of strain-hardening (right) for a P(AAm-co-tPy) dual-crosslink gel with Zn^{2+} ions (orange) and the reference chemical gel (black).

5.6.2. Cycles

Figure 5.14 shows the results of a cyclic test up to $\lambda = 2$ at different stretch-rates. In this figure, we can see again the increase of modulus with the stretch-rate previously observed. The hysteresis between the loading and unloading curves also greatly increased. Just as for the other dynamic gels, the behavior of the P(AAm-co-tPy)-Zn²⁺ dual-crosslink hydrogel after those cycles remained unchanged: with a rest time of 30 min between each cycle, at a stretch-rate of $\dot{\lambda} = 0.3 \text{ s}^{-1}$, the material always recovers its initial behavior (Figure 5.14).

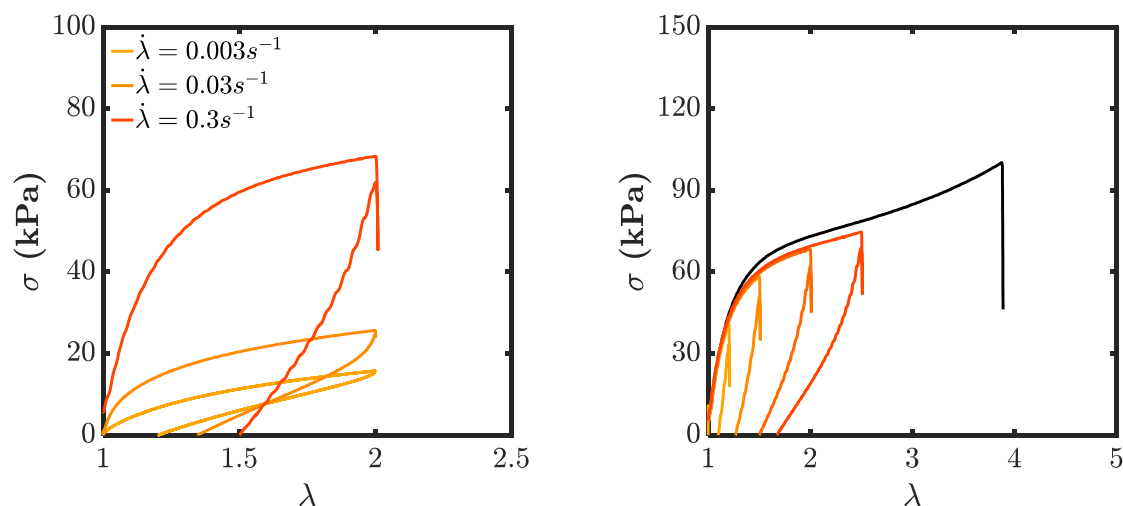


Figure 5.14: Stress-stretch curves of cyclic experiments in tension, realized on a tPy-Zn²⁺ hydrogel up to $\lambda = 2$ at varying stretch-rates (left) and at $\dot{\lambda} = 0.3 \text{ s}^{-1}$ and varying stretches (right). Data from a standard tensile test is added in black.

Realizing those cycles by varying stretch-rates and maximal stretches allowed us to estimate values of dissipated energy during traction, as a function of λ and $\dot{\lambda}$. These results are presented in Figure 5.15. The integral of the unloading curve, called here recovered or stored energy, showed a sharp increase with the maximal stretch, as expected. It was also slightly dependent on the stretch-rate, implying that a visco-elastic process also takes place during the unloading. Just as for the P(AAm-co-VIm)-Ni²⁺ hydrogel, there was a large increase of the dissipated energy (difference between the integral under the loading and unloading curves) with increasing stretch-rate. It is actually surprising to see this large increase in dissipation at $\dot{\lambda} = 0.3 \text{ s}^{-1}$: previous results on the PVA-Borax dual crosslink hydrogels having also slow dynamic bonds [4,5] showed reduced hysteresis as the materials became more brittle, thus explaining the decrease of the maximal extensibility of the material. This would follow our initial hypothesis that the energy dissipation inside the hydrogel controls its resistance to fracture. When the stretch-rate increases, the bonds act as permanent crosslinkers, energy dissipation decreases and the material becomes more fragile. It is not the case here, as the dissipation still increases when the stretch at break drops.

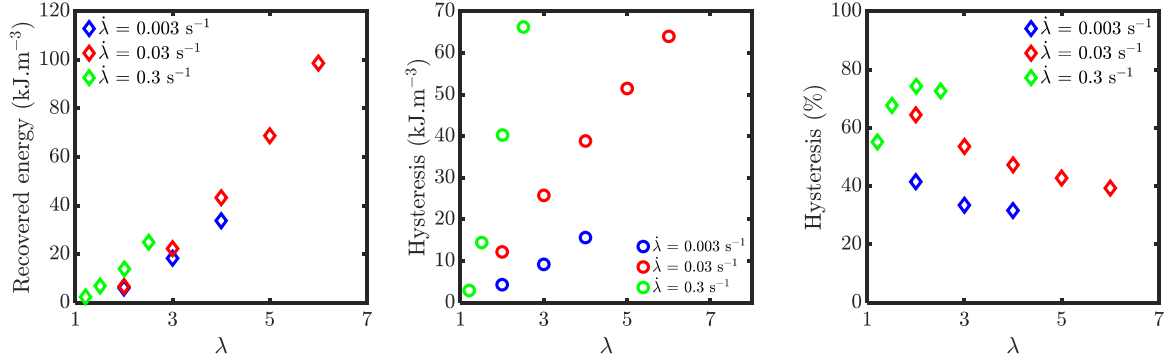


Figure 5.15: Recovered energy (left) dissipated energy (center) and percentage of energy dissipated (right) vs the stretch, for three different stretch-rates.

The hysteresis between the loading and unloading curves, shown in percentage of energy dissipated, has a different behavior from what we observed before:

- at lower stretch rates ($\dot{\lambda} = 0.003, 0.3 \text{ s}^{-1}$), it decreases with stretch just as we observed in the previous chapters;
- at $\dot{\lambda} = 0.3 \text{ s}^{-1}$, since the hydrogel breaks at lower values of λ , we realized cycles at lower maximal stretches. The hysteresis increases with the stretch up to $\lambda = 2$, then decreases.

This behavior might exist in the P(AAm-co-VIm)-Ni²⁺, Cu²⁺ or Zn²⁺ hydrogels previously studied, while we did not realize cycles at $\lambda < 2$ in those cases.

The decrease in hysteresis can be simply explained by the fact that the stored energy E_{rec} increases with λ^2 , whereas we observe that the dissipated energy E_{diss} follows λ linearly; thus,

$$Hysteresis = \frac{E_{diss}}{E_{diss} + E_{rec}} \sim \frac{\lambda}{\lambda^2} = \lambda^{-1}$$

The increase in hysteresis observed at lower stretches is a bit more challenging to explain. It implies that, when increasing the stretch up to $\lambda = 2$, the dissipation increases drastically, and by extension implies that the dissipation is very low at low stretches. This may be linked to an increase of the dynamics by increasing strain at these low stretches.

Figure 5.16 shows the hysteresis versus the time to reach the maximal stretch of the cycle (equal to $\lambda_{max}/\dot{\lambda}$). It shows a peak of hysteresis at a few tens of seconds, which was not visible for the previous hydrogels. The superposition is sketchy at longer times.

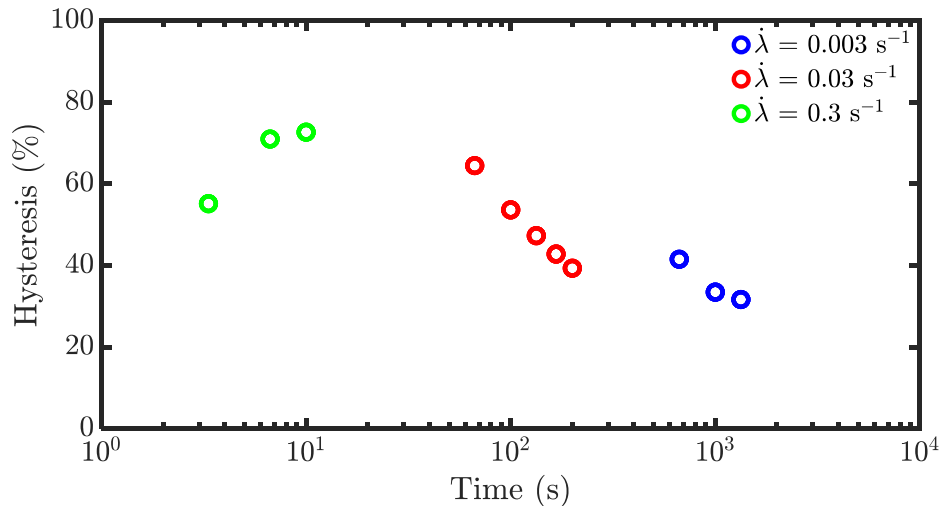


Figure 5.16: Percentage of energy dissipated versus time to reach the maximal stretch, for three different stretch-rates, for the tPy-Zn²⁺ dual-crosslink hydrogel.

5.6.3. Fracture – Single notch test

The same single-notch fracture tests shown in the previous chapters were carried out for this gel. The results are presented below, in Figure 5.17. We see a clear decrease of the stretch at which the fracture propagates with increasing stretch-rate. For certain samples we noticed some drops in the stress on the curve before the breaking, seen on the curve at $\dot{\lambda} = 0.03 \text{ s}^{-1}$ at $\lambda = 2.6$ for example. We will discuss this phenomenon later in this chapter.

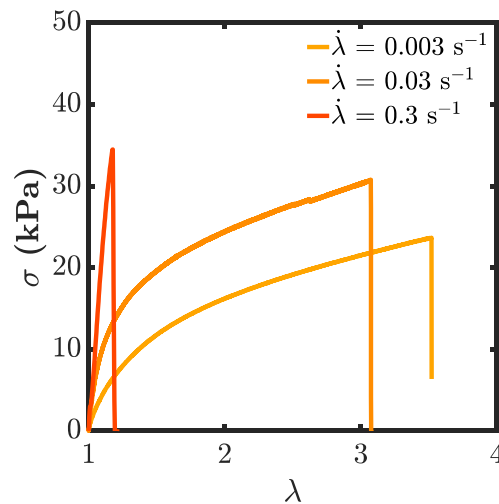


Figure 5.17: Stress vs. strain curves, for a notched P(AAm-co-tPy)-Zn²⁺ dual crosslink hydrogel at different stretch-rates

In Figure 5.18, we plotted the critical stretch λ_c at which the fracture propagates and the corresponding fracture energy. The values of λ_c were globally lower than those for the unnotched sample (Figure 5.13, left). The critical stretch decreased drastically with increasing stretch-rate, just as the fracture energy. The material becomes more brittle with the stretch-rate, which is what was expected from the previous results: the physical bonds being slow and long-lived, increasing the stretch-rate makes the material

more brittle. We are as expected on the “high Weissenberg number” part of the schematic curve presented in Figure 5.1.

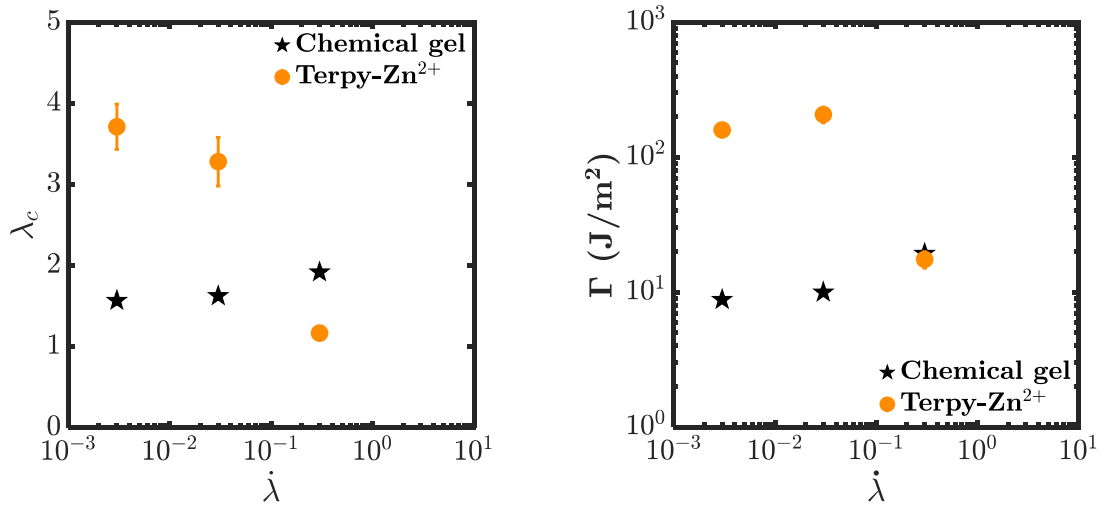


Figure 5.18: Critical stretch λ_c at which the crack starts to propagate (left) and corresponding fracture energy Γ (right) as a function of the stretch-rate, for a tPy- Zn^{2+} dual-crosslink hydrogel (orange) and the reference chemical gel (black).

The average crack velocity during propagation, measured from the time profile of the force, is shown in Figure 5.19. It increased sharply with stretch-rate, indicating the embrittlement of the material at higher stretch-rates.

It is interesting to note that, for those stretch rates, we never reach the same values as observed in Chapter 3 for the VIm- Ni^{2+} hydrogel (Γ up to $800 J.m^{-2}$, λ_c up to 6 and velocity up to $200 mm.s^{-1}$). This might be explained by the differences in the chemical network between those two hydrogels: to obtain the same G' (thus mesh size) measured in rheology, I had to divide by 3 the amount of chemical crosslinker in the terpyridine hydrogel. Which might imply a different distribution of chain size in each network, and thus different maximal fracture resistance values. This difference in fracture values might also be linked to the number of physical crosslinks present in the network: as seen in rheology, the present dual-crosslink hydrogel possesses much more elastically active physical crosslinks than the P(AAm-co-VIm)- Ni^{2+} dual crosslink hydrogel does.

Figure 5.20 shows the critical value of Γ_{local} , as defined in Chapter 3. On this graph, we see again a clear decrease of the fracture energy. However, this decrease is not linked to a decrease in the dissipated energy, on the contrary. The dissipated energy keeps increasing as the material becomes more brittle.

5. Slowing down the dynamics

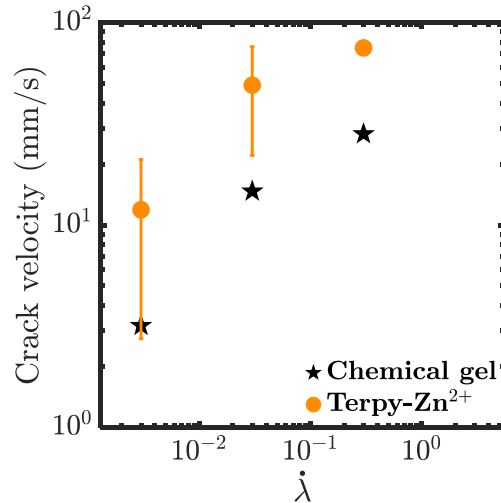


Figure 5.19: Propagation speed of the fracture versus the stretch-rate of the experiment, for a tPy-Zn²⁺ dual-crosslink hydrogel (orange) and the reference chemical gel (black).

Lastly, it is interesting to note that this dual-crosslink hydrogel shows a deviation of the crack at the two lowest stretch-rates, as shown in Figure 5.21. This implies an anisotropy of the material at the tip of the crack, just as the P(AAm-co-VIm)-Ni²⁺ hydrogel showed in the pure-shear geometry at high stretch-rates. This anisotropy seems to be dependent on the stretch-rate, hence dependent on the physical crosslinks only. It does not exist at low stretch-rates where the fracture energy and critical stretch are low (P(AAm-co-VIm)-Ni²⁺ hydrogel at $\dot{\lambda} = 0.03 \text{ s}^{-1}$ does not show this behavior), and disappears at higher stretch-rates (here, at $\dot{\lambda} = 0.3 \text{ s}^{-1}$) where the fracture energy and the critical stretch drop.

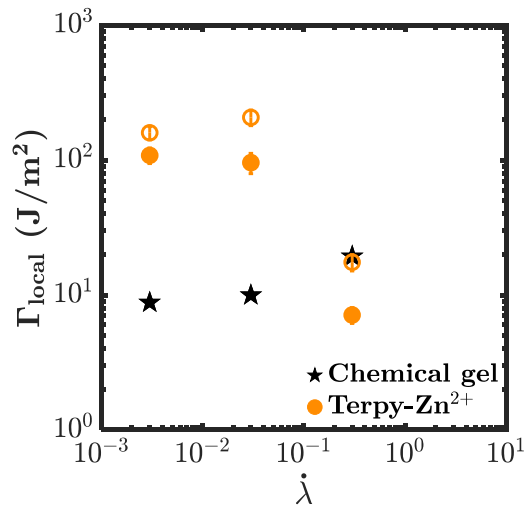


Figure 5.20: Γ (empty points) and Γ_{local} (filled points) versus stretch-rate.

This deviation can be seen on the stress-strain curves of Figure 5.17, as the drops in stress during loading.

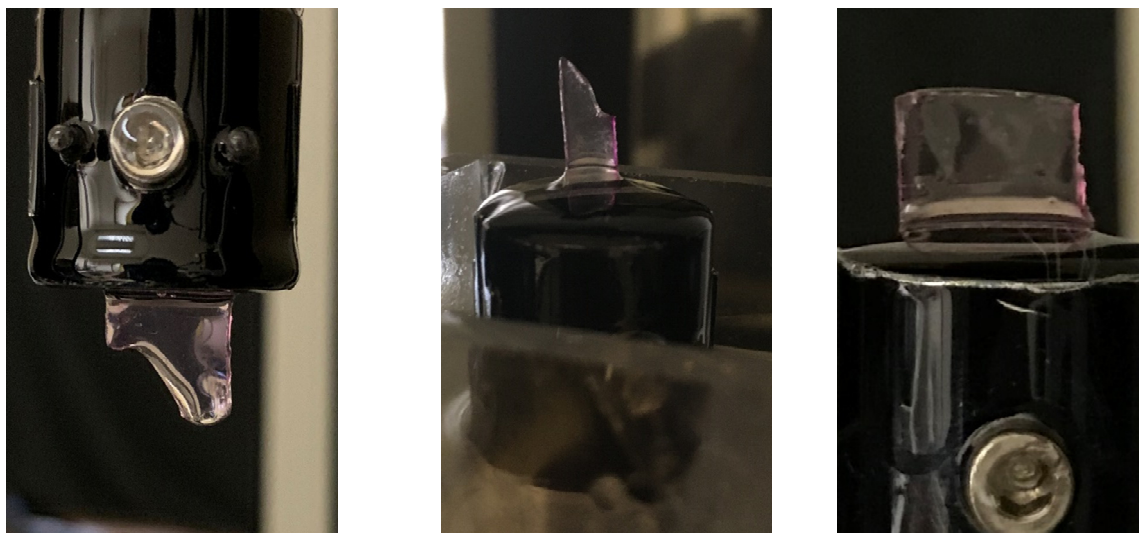


Figure 5.21: Sample of P(AAm-co-tPy)-Zn²⁺ hydrogel after a crack propagation, at $\dot{\lambda} = 0.003 \text{ s}^{-1}$ (left), $\dot{\lambda} = 0.03 \text{ s}^{-1}$ (center) and $\dot{\lambda} = 0.3 \text{ s}^{-1}$ (right).

This behavior might be directly linked to the evolution of energy dissipation inside the hydrogel, or to the evolution of the level of stretch reached when the fracture propagates – the anisotropy might be provoked by a high stretch.

5.7. Discussion and conclusions

The objective of this chapter was to prepare a dual-crosslink hydrogel on the same basis as the previous ones (P(AAm-co-VIm)-Ni²⁺, Zn²⁺ and Cu²⁺), with a much slower dynamic.

The imidazole-Hg²⁺ bond showed interesting promises, with high thermodynamic complexation constants. The experiments showed that, in such a network, the large majority of Hg²⁺ ions were bound with one imidazole only. The physical crosslinks were not made by coordination complexes, but by aggregates of mono-complexes. The behavior observed in rheology and the microstructure studied in SAXS were thus different from what we observed on the other dual-crosslink hydrogels, where the physical crosslinks were mainly made by single [M(Im)₂]²⁺ complexes with two ligands on different chains.

The hydrogels synthesized with terpyridine as a co-monomer, however, are very interesting. Their dynamics with Zn²⁺ ions were much slower than what we observed on the other gels, allowing us to study a dynamic dual-crosslink hydrogel at high Weissenberg numbers ($\dot{\lambda}\tau \sim 1$). The results in large deformations and fracture experiments followed our initial hypothesis, and what was observed on a PVA-Borax dual-crosslink hydrogel: when increasing the stretch-rate, the physical bonds start behaving as permanent bonds and energy dissipation decreases, the material becoming more brittle. Here, as the stretch-rate increases, we observe a decrease of the stretch at break of pristine samples and a decrease of the energy necessary to propagate a crack. The values reached by these measurements were a bit lower than expected, certainly due to differences in the microstructure network of the P(AAm-co-tPy) and P(AAm-co-VIm) hydrogels (different chemical network, and more importantly difference in number of physical crosslinks).

However, one result was surprising: according to our hypothesis, we expected the energy dissipation in cyclic loading-unloading tests to decrease at higher Weissenberg numbers (provoking the decrease of

5. Slowing down the dynamics

the fracture properties of the hydrogel). It is not what we observe here. On the contrary, the energy dissipation keeps increasing with the stretch-rate, even when the material becomes more brittle. This observation can be explained by the fact that the energy dissipation at the crack tip is not the same as in the rest of the network. When the bulk of the material is at a certain stretch and stretch-rate, the crack tip is much more stretched, with stretch-rates up to 100 times higher than the bulk [5]. This was observed on a PVA-borax dual-crosslink hydrogel. The crack tip then undergoes a much higher Weissenberg number, with much less dissipation, making the material more brittle there.

References

1. Sjöberg, S. Critical evaluation of stability constants of metal-imidazole and metal-histamine systems. *Pure & Appl. Chem.* 69, 1549–1570 (1997).
2. Holyer, R. H., Hubbard, C. D., Kettle, S. F. A. & Wilkins, R. G. The Kinetics of Replacement Reactions of Complexes of the Transition Metals with 2,2',2''-Terpyridine. *Inorg. Chem.* 5, 622–625 (1966).
3. Hammes, G. G. & Steinfeld, J. I. Relaxation Spectra of Some Nickel(II) and Cobalt(II) Complexes. *Journal of the American Chemical Society* 84, 4639–4643 (1962).
4. Long, R., Mayumi, K., Creton, C., Narita, T. & Hui, C.-Y. Time Dependent Behavior of a Dual Cross-Link Self-Healing Gel: Theory and Experiments. *Macromolecules* 47, 7243–7250 (2014).
5. Mayumi, K., Guo, J., Narita, T., Hui, C. Y. & Creton, C. Fracture of dual crosslink gels with permanent and transient crosslinks. *Extreme Mechanics Letters* 6, 52–59 (2016).

Chapter 6

One bond to rule them all

And in the network, bind them

(The Lord of the Bonds)

6. One bond to rule them all

6. One bond to rule them all

Table of contents

6.1. Linear rheology.....	184
6.2. Large deformations	186
6.2.1. Tensile tests	186
6.2.2. Cyclic	191
6.3. General remarks on the results in large deformations	194
6.4. Fracture.....	195
6.4.1. Single edge notch	195
6.4.2. Delayed fracture of pure shear samples.....	199
6.5. On the dynamic behavior of the dual-crosslink network.....	201
References.....	205

6. One bond to rule them all

We have successfully prepared three different types of dual-crosslink hydrogels, with very different dynamics and almost the same chemical network:

- two “fast” hydrogels, with physical bonds made of Imidazole-Zn²⁺ or Imidazole-Cu²⁺ coordination complexes;
- an “intermediate” hydrogel, with physical bonds made of Imidazole-Ni²⁺ complexes;
- a “slow” hydrogel, with a slightly different chemical network and physical bonds made of Terpyridine-Zn²⁺ coordination complexes.

The objective of this work was to investigate how energy dissipation due to dynamic bonds inside a hydrogel affects the toughness of the material. In this chapter, we will demonstrate that our dual-crosslink hydrogels allow us to reach a wide range of Deborah (in rheology) or Weissenberg (in large deformations) numbers, simply by shifting the results by the relaxation time introduced in the network with the physical bonds. By applying that method to the four different hydrogels we prepared, we will be able to understand the behavior of those dual-crosslink networks in a more general framework. We will evidence a difference in dynamics between rheology, large deformations properties such as energy dissipation or stretch at break, and fracture properties. We will also evidence a qualitative difference between two dual-crosslink hydrogels under slow crack propagation.

6.1. Linear rheology

Figure 6.1 shows the results of linear rheology experiments obtained for the different dual-crosslink hydrogels and the reference chemical gel. We can see a clear evolution of the frequency at which G'' or $\tan(\delta)$ reach a peak. The P(AAm-co-tPy)-Zn²⁺ dual-crosslink hydrogel exhibits the slowest dynamics, the P(AAm-co-VIm)-Ni²⁺ is 10 to 20 times faster, and the P(AAm-co-VIm)-Zn²⁺ or Cu²⁺ are the fastest, their dissipation peak being out of range for our rheometer. For simplification, especially in the legends of the figures in this chapter, we represent P(AAm-co-VIm)-M²⁺ dual crosslink gels as M²⁺, and the P(AAm-tPy)-Zn²⁺ gel as terpy-Zn²⁺. Thus, the characteristic relaxation times of these gels are in the following order:

$$(\text{fast}) \text{VIm-Zn}^{2+} \leq \text{VIm-Cu}^{2+} < \text{VIm-Ni}^{2+} < \text{terpy-Zn}^{2+} (\text{slow})$$

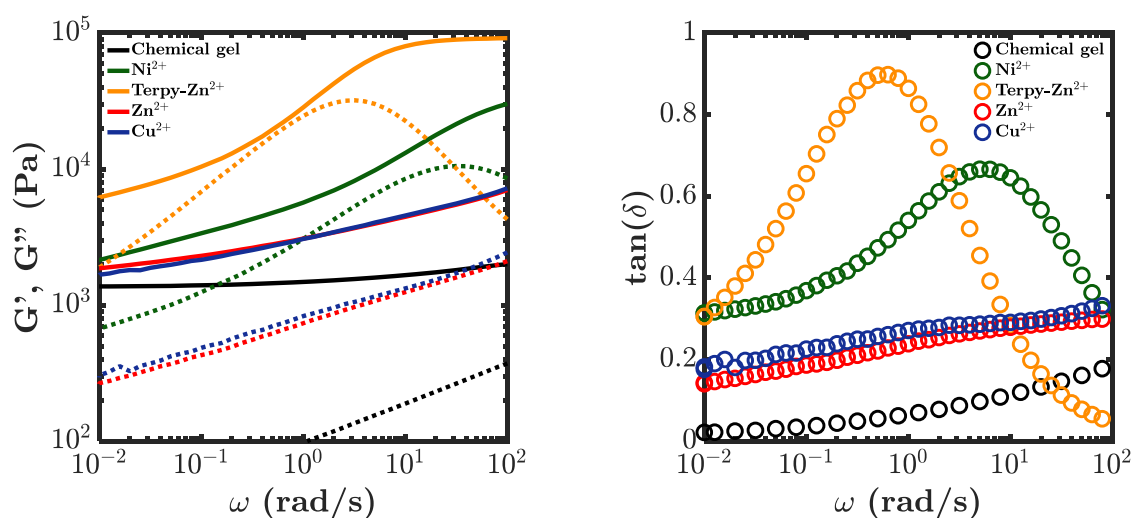


Figure 6.1: Storage and loss moduli (left), and loss factor $\tan(\delta)$ (right) versus frequency, of the 4 different dual-crosslink hydrogels along with the reference P(AAm-co-VIm) chemical gel.

It is interesting to note that the peak in $\tan(\delta)$ of the terpy- Zn^{2+} dual-crosslink hydrogel is higher than the peak of the VIm- Ni^{2+} dual-crosslink hydrogel. It is linked to the clear increase in the plateau value of G' we observe for the terpy- Zn^{2+} dual-crosslink hydrogel that we attributed to an increase in the number of elastically active physical crosslinks relative to that of the chemical crosslinks.

From these data of $\tan(\delta)$, we created a relaxation time master curve, by normalizing the frequency with the characteristic time of the dissipation peak. For the VIm- Ni^{2+} hydrogel and the terpy- Zn^{2+} hydrogel, we have determined the relaxation time in the previous chapters. For the VIm- Zn^{2+} or VIm- Cu^{2+} hydrogels, the characteristic time was not rheologically determined. Here, we make a strong assumption of a universal behavior and of the existence of a master curve; we manually horizontally shifted the loss factor $\tan(\delta)$ curves to that of the VIm- Ni^{2+} hydrogel. At the overlapping normalized frequency range, the superposition was reasonable. The resulting curves are presented in Figure 6.2. The characteristic relaxation times are summarized in Table 6.1

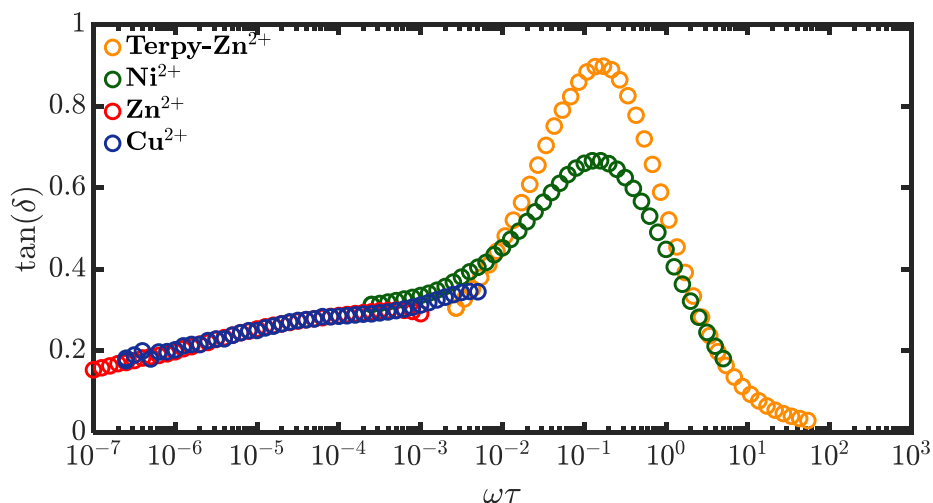


Figure 6.2: Superposition of the data from Figure 6.1, showing $\tan(\delta)$ versus the frequency shifted by the lifetime of the physical bond.

We can see that our different dual-crosslink hydrogels allow us to study a broad range of shifted frequencies (or Deborah numbers here). At high frequencies ($\omega\tau > 1$), the dissipation decreases drastically, the loss factor $\tan(\delta)$ reaching almost 0 at $\omega\tau = 50$. On the contrary, at low Deborah numbers, the dissipation decreases but the value of the loss factor does not even reach 0.1 even at $\omega\tau = 10^{-7}$, due to the second dynamic mode.

We also applied this superposition to the moduli, and the obtained master curves are shown in Figure 6.3. Though for this superposition a vertical shift was needed to obtain a good superposition, its influence is little since the values of the vertical shift factors were close to 1. The VIm- Ni^{2+} hydrogel was used as a reference for this superposition, the shift factors used for the other hydrogels are listed in Table 6.1. The superposition is quite good up to a Deborah number $\omega\tau > 10^{-1}$, where we observe a clear difference in behavior between the terpy- Zn^{2+} and the VIm- Ni^{2+} . It seems that these two hydrogels show a different behavior only at the faster dynamic, linked again to the number of elastically active physical bonds present in the dual-crosslink hydrogel.

The lifetimes measured from rheology are quite close from what we could find in the literature [1-3] (which usually gives k_{diss} the dissociation constant of the complex, which is simply $1/\tau$).

6. One bond to rule them all

Table 6.1: Measured and computed lifetimes τ of the physical bond, from rheology experiments, along with the vertical shift coefficient b and the lifetimes found in the literature. *At 11°C for a Zn-NH3 complex

Physical bond	τ_{lit} (s)	τ (s)	b
terpy-Zn ²⁺	0.79	0.27	0.56
VIm-Ni ²⁺	0.11	0.025	1
VIm-Cu ²⁺	-	2.5×10^{-5}	0.48
VIm-Zn ²⁺	6.2×10^{-5} *	5×10^{-6}	0.36

The vertical shift factor represents here the difference in the number of elastically active physical bonds present in the network. This would imply, for example, that at high frequency the terpy-Zn²⁺ dual-crosslink hydrogel possesses 3 times more elastically active physical crosslinks than the VIm-Ni²⁺ dual-crosslink hydrogel. Of course, this assumes that the horizontal shift is correct. Any uncertainty in the horizontal shift will mechanically lead to an uncertainty in the vertical one

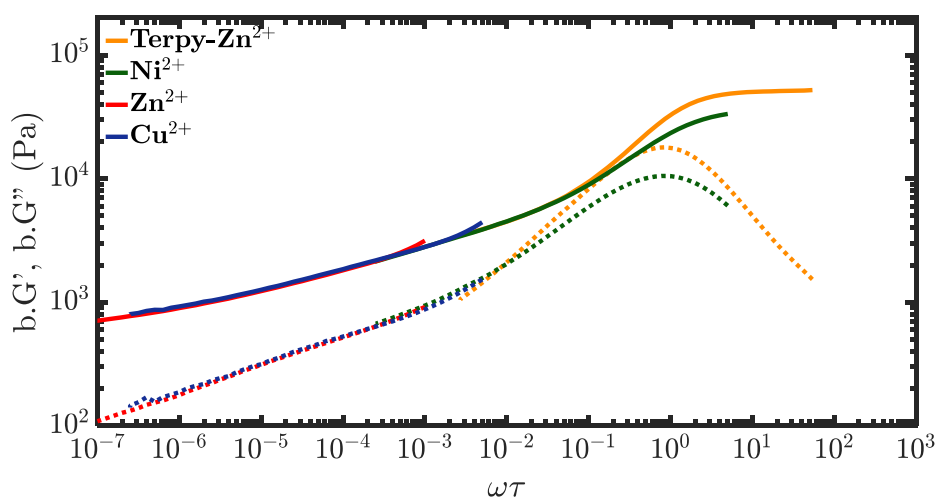


Figure 6.3 Superposition of the data from Figure 6.1, showing shifted G' and G'' versus the frequency shifted by the lifetime of the physical bond.

6.2. Large deformations

6.2.1. Tensile tests

Figure 6.4 shows the stress-strain curves obtained for each dual-crosslink hydrogel at the same stretch rate $\dot{\lambda} = 0.3 \text{ s}^{-1}$. On these curves, we see clearly the difference of behavior between each hydrogel. The hydrogels with fast dynamics (with Zn²⁺ or Cu²⁺ ions complexing with imidazole ligands) have a low Young's modulus, close to that of the bare chemical gel. By slowing down the dynamics of the hydrogel, this modulus increases (Ni²⁺ or terpy-Zn²⁺). In the case of the slowest hydrogel (bond with longer lifetime), the stretch at break is considerably reduced. The right graph from Figure 6.4 shows the reduced stress versus the inverse of the stretch. All dual-crosslink hydrogels present the same general behavior, with a decreasing slope with increasing λ , followed by a strain-hardening at higher stretches (apart from the tPy-Zn²⁺, which breaks before reaching any strain-hardening).

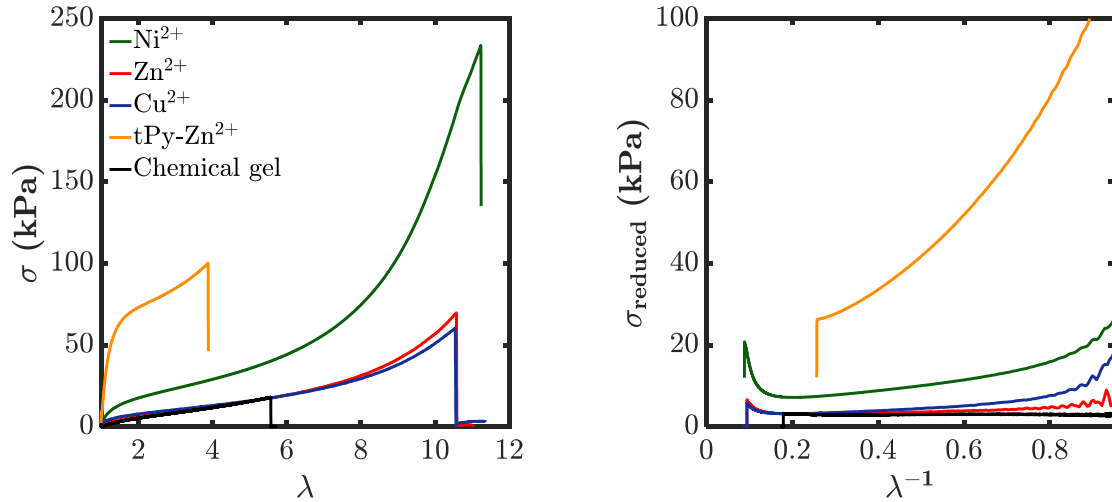


Figure 6.4: Left: Stress – strain curves of the 4 different dual-crosslink hydrogels, along with the reference chemical gel (black), at the same stretch-rate $\dot{\lambda} = 0,3 \text{ s}^{-1}$. Right: Mooney plots of the data from the left.

The moduli and stretch at break of these curves are plotted in Figure 6.5, versus the stretch-rate normalized by the relaxation time of the hydrogel measured in rheology (Weissenberg number). The superposition is not very satisfactory. This result suggests that the dynamics of the dual crosslink gels at large deformations may be different from those in small strain. Indeed, when applying a force on such a transient bond, it is probable that the lifetime of this bond decreases and the effect of the force could depend on the strength of the bond (thus the lifetime).

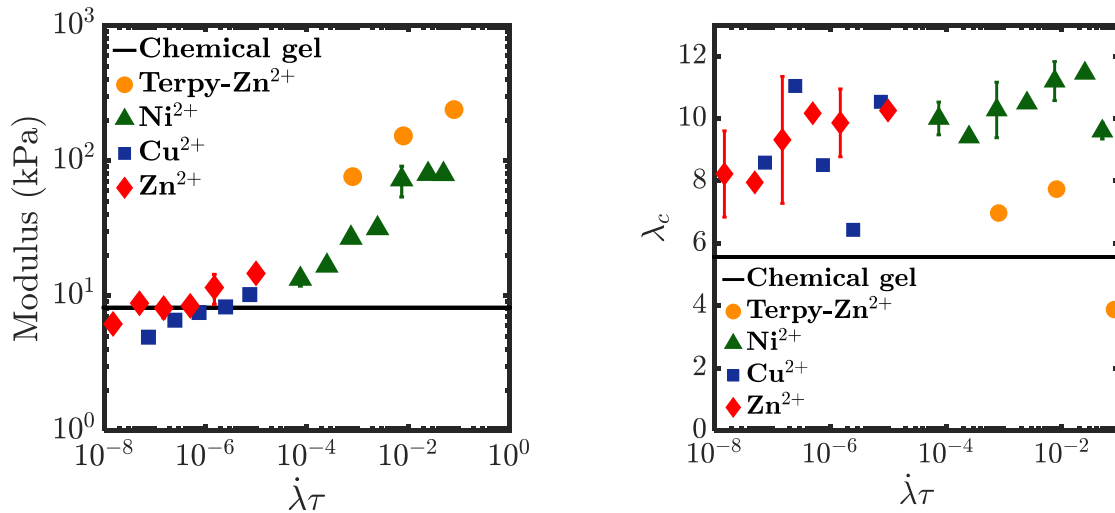


Figure 6.5: Left: Young's modulus versus the stretch-rate shifted by the relaxation time of the dual-crosslink hydrogel obtained from the rheology experiments, listed in Table 6.1. Right: stretch-at-break versus the stretch-rate shifted by the relaxation time of the dual-crosslink hydrogel obtained from the rheology experiments, listed in Table 6.1

If we hypothesize that another universality of the dynamics is active for the large deformations that allows us to superpose the curves for the different dual crosslink gels, we can estimate the characteristic times of our dual-crosslink hydrogels in large deformations by manually shifting the data in Figure 6.5 (left) to obtain the best master curve. The value of the shift factor from the VIIm-Ni²⁺ dual-crosslink

6. One bond to rule them all

hydrogel determined by rheology was used as reference. With this arbitrary adjustment, better master curves are obtained for the modulus and stretch at break, as shown in Figure 6.6. The values of the shift factors $a_{M^{2+},tensile}$ obtained in this way are presented in Table 6.2. The evolution of the modulus is quite easy to understand: the faster the material is stretched, the higher the modulus. At very low Weissenberg numbers, $\lambda a_{M^{2+},tensile} < 10^{-4}$, the bonds are too fast compared to the observation time of the experiment and they do not influence the modulus. When reaching a Weissenberg number around 10^{-4} , the modulus starts to increase. The difference in modulus between the terpy-Zn²⁺ hydrogel and the others is consistent with what we have previously observed in rheology experiments. We observe a slow increase of the stretch at break with $\lambda a_{M^{2+},tensile}$ until reaching about 3×10^{-2} , where it starts to decrease very quickly. The maximal stretches reached by the terpy-Zn²⁺ dual-crosslink hydrogel are lower than those of the VIm-Ni²⁺ dual-crosslink hydrogel at the same Weissenberg number.

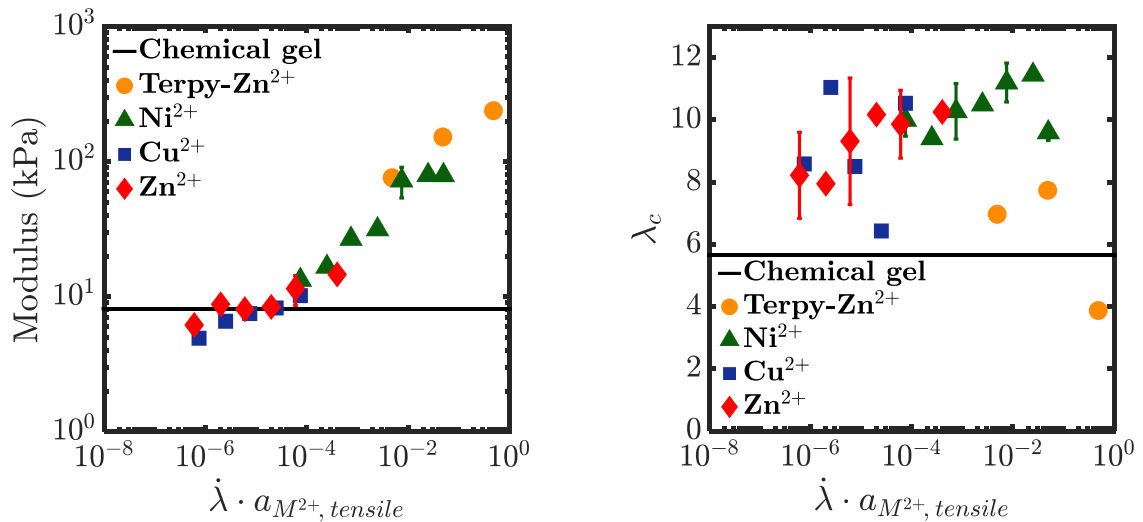


Figure 6.6 Left: Young's modulus versus the stretch-rate, shifted by the arbitrary shift factors from Table 6.2. Right: stretch-at-break versus the shifted by the arbitrary shift factors from Table 6.2. In both cases, the black line represents the mean results for the chemical gel.

Table 6.2: Shift factors $a_{M^{2+}}$ obtained from the elastic modulus data

Physical bond	$a_{M^{2+},tensile}$ (s)
Terpy-Zn ²⁺	1.62
Ni ²⁺	2.5×10^{-2}
Cu ²⁺	2.5×10^{-4}
Zn ²⁺	2×10^{-4}

In order to further evaluate the accuracy of the horizontal shift, we studied the different characteristics of the dual crosslink gels at large deformations, the reduced stress and onset of strain-hardening. These two parameters measured and discussed in the previous chapters, are plotted as a function of the same shifted stretch-rates in Figure 6.7 and reasonable master curves are obtained. The reduced stress at the onset of strain-hardening shows a similar behavior as the modulus, since the modulus corresponds to the number of the physical bonds/chains which are closed at $t = 0$ and which survive the initial deformation, while f_{min}^* corresponds to the number of physical bonds/chains which survive and are stretched in a non-Gaussian manner. The influence of the physical bonds started to be apparent from a Weissenberg number of about 10^{-3} , 10 times higher than the threshold observed for the Young's modulus. It should be noted that the point at high Weissenberg number for the terpy-Zn²⁺ dual-crosslink

hydrogel is the point of breaking, since the material does not display a strain-hardening behavior before breaking.

The stretch at the onset of strain hardening, λ_{SH} , shows also an acceptable superposition, revealing two regimes. (1) For $\dot{\lambda} a_{M^{2+},tensile} < 2 \times 10^{-3}$, an increase in λ_{SH} was observed, from $\lambda_{SH} = 3$ (which is the value of λ_{SH} for the bare chemical gel) up to $\lambda_{SH} = 6$. In this regime, however, the experimental error can be large, especially for the VIm-Cu²⁺ gel. As previously demonstrated, the strain-hardening at these low stretch-rates is independent on the stretch-rate. The higher values of λ_{SH} measured in the dual-crosslink network, than in the bare chemical gel at those low stretch-rates can be explained by the capability of the physical bond to homogenize the stresses inside the network. This delays the stretch at which a percolating network of polymer chains in their strain-hardening regime is reached. (2) For $\dot{\lambda} a_{M^{2+},tensile} > 2 \times 10^{-3}$, λ_{SH} decreases with Weissenberg number. At these stretch-rates, the influence of the physical bonds start to be seen on the moduli f_{min}^* . The number of physical bonds/chains that survive the stretching and are stretched in a non-Gaussian manner increases, increasing f_{min}^* . Following a usual law [4], λ_{SH} decreases in $\sqrt{f_{min}^*}$.

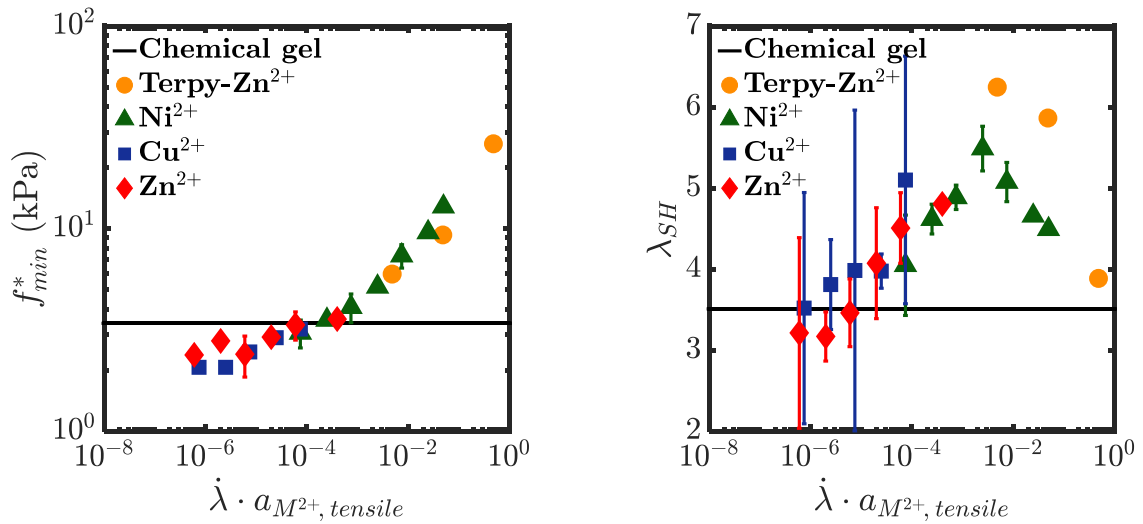


Figure 6.7: Left: Reduced stress at the onset of strain hardening versus the Weissenberg number with $a_{M^{2+},tensile}$ values from Table 6.2. Right: Stretch at the onset of strain-hardening versus the Weissenberg number. Note: the fast point of the terpy-Zn²⁺ dual-crosslink hydrogel corresponds to the point of breakage of the material.

The stress at break reached by the dual-crosslink hydrogels (shown in Figure 6.8) is always higher than the stress at break reached by the bare chemical gel. It increases slowly at Weissenberg numbers below 10^{-3} and then shows a steep increase, linked to the increased number of elastically active physical bonds. These values, for the terpy-Zn²⁺ dual-crosslink hydrogel are much smaller than for the other dual-crosslink hydrogels.

An interesting representation on the fracture data of this dual-crosslink hydrogel is plotted in Figure 6.8b, where the stress at break of the different hydrogels is plotted versus the stretch at break. The data takes a sort of bell shape, such as found by Bueche and Halpin in elastomers [5,6], suggesting that the fracture properties are dependent only on $\dot{\lambda}$. This conclusion is less obvious for the terpy-Zn²⁺ dual-crosslink hydrogel. The material becomes brittle, fragile, and Bueche-Halpin representation is not suited for this behavior.

6. One bond to rule them all

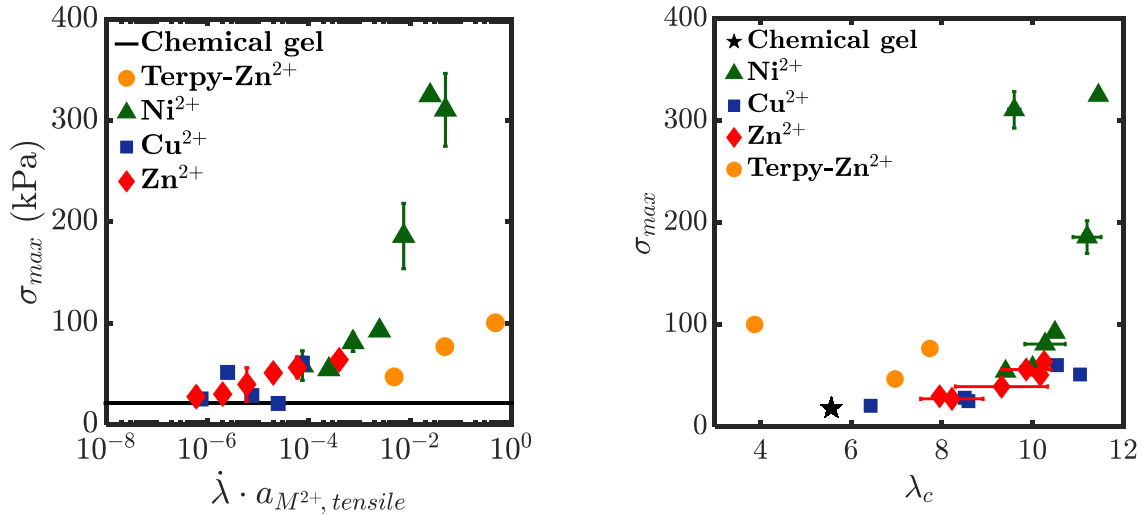


Figure 6.8: Left: Stress at break of the different hydrogel, versus the Weissenberg number. Right: Stress at break versus stretch at break, for the different hydrogels considered.

At low Weissenberg numbers, $\dot{\lambda}a_{M^{2+}, tensile} < 10^{-4}$, the physical bonds are invisible. The observation time being much longer than the lifetime of the physical bonds, there is no creation of new elastically active polymer chains, no physical network being added to the chemical network. The Young's modulus is the same as that of the bare chemical gel. f^*_{min} behaves in the same way, and the strain-hardening behavior depends only on the stretch since no physical bonds are involved. We also believe that the long-lived clusters of physical bonds might influence this strain-hardening: there are too few of them to increase the Young's modulus, but their influence on the creation of a percolating network of chains in their non-linear entropic regime will be critical. By acting as high-functionality crosslinking points, they will increase the level of strain-hardening.

However, *the stretch at break is still much higher than that of the bare chemical gel*. We were expecting the stretch at break to be equal to the stretch at break of the chemical gel when the physical bonds are invisible (at $\dot{\lambda}a_{M^{2+}, tensile} < 10^{-4}$). As mentioned before, it seems that the physical bonds prevent the nucleation of a macroscopic crack inside the material, by delaying the onset of the correlated bond scission of polymer chains. When the stretch reaches the critical stretch λ_c of the chemical gel (around 5), polymer chains start breaking inside the network. In a purely elastic network such as the bare chemical gel, this provokes the correlated breaking of chains, nucleating a fracture that will propagate immediately. In the dissipative dual-crosslink hydrogel, the correlated breaking of polymer chains happens at higher stretches, which delays the complete fracture of the material.

Upon increasing the Weissenberg number ($\dot{\lambda}a_{M^{2+}, tensile} \geq 10^{-4}$), the observation time decreases. Consequently, the lifetime of the physical bond becomes relevant: the number of active physical bonds when beginning the stretching increases. The number of active crosslinks and loaded elastic polymer chains in the network increases consequently. This causes an increase in the Young's modulus. During stretching, some physical bonds break. This causes the linear time-dependent relaxation we have detailed previously, where the breaking of physical bonds creates stress relaxations in the network. While stretching, some polymer chains reach a strain-hardening regime. Once this family of chains create a percolating network, the stress increases again. With the increase in the number of physical bonds, the onset of this strain-hardening changes. More physical bonds means shorter polymer chains,

which decreases the onset stretch of strain-hardening; it also provokes an increase in the intensity of strain-hardening. This strain-hardening follows always the same law, only its onset parameters changes.

At even higher Weissenberg numbers, typically above 10^{-1} , the physical bonds behave as permanent bonds during the deformation. The observation time is much shorter than the lifetime of the physical bonds. Most of them are active, and the number of polymer chains increases dramatically. Since those bonds cannot act as sacrificial bonds and do not dissipate energy, the stretch at break of the material decreases drastically – becoming even lower than the stretch at break of the bare chemical gel. The strain-hardening regime cannot be reached in that situation, since the dual-crosslink hydrogel breaks before reaching this regime. The terpy- Zn^{2+} dual-crosslink hydrogels we study at high Weissenberg number show some differences in absolute values with the imidazole-based dual-crosslink hydrogels, because of their much higher number of physical crosslinks.

The PVA-borax dual-crosslink hydrogels previously studied in our laboratory, and modeled by Hui and coworkers [7-13] show a behavior with the same characteristics as the dual-crosslink hydrogels developed in this study, with slow dynamics. Upon stretching, at the stretch-rates considered in the study, the physical bonds are active. The PVA-borax dual-crosslink hydrogels show the linear and time-dependent relaxation behavior that our metal-ligand dual-crosslink hydrogels show. Upon reaching a certain stretch, the network should reach a strain-hardening behavior where entropic elasticity follows the Langevin function. This regime, however, is not observed for the higher stretch-rates [12]: just as happens in the metal-ligand dual crosslink hydrogel, when the Weissenberg number is too high, the physical bonds act as permanent bonds and fracture becomes localized. The stretch at break of the network decreases, become lower even than the stretch of onset of the strain-hardening behavior. The material cannot exhibit this strain-hardening behavior at high stretch-rates compared to the relaxation frequency of the physical bond. This behavior was observed in solutions of unentangled ionomers [14], with a clear transition from a soft-ductile to a hard-brittle behavior. When the material becomes brittle, it reaches lower maximal strains and the strain-hardening behavior disappears.

6.2.2. Cyclic

Using the same shift-factors $a_{M^{2+},tensile}$ estimated in the previous section (Table 6.2), we also normalized the data from the uniaxial tensile cycle tests with cycles up to a maximal stretch $\lambda_{max} = 3$. The values of the stored and dissipated energies are plotted as a function of the Weissenberg number in Figure 6.9. Again, we found a good superposition of the results for the four dual crosslink hydrogels. The stored energy is constant at low Weissenberg numbers, and increases for $\dot{\lambda}a_{M^{2+},tensile} \geq 10^{-3}$. The dissipated energy is almost zero at 10^{-6} , and increases very slightly until $\dot{\lambda}a_{M^{2+},tensile} = 10^{-4}$. After this value, it increases clearly with the Weissenberg number, reaching 37 kJ/m^3 at $\dot{\lambda}a_{M^{2+},tensile} = 10^{-2}$. The threshold of increase of energy dissipation is 10^{-4} , which is the Weissenberg number where the elastic moduli started increasing.

6. One bond to rule them all

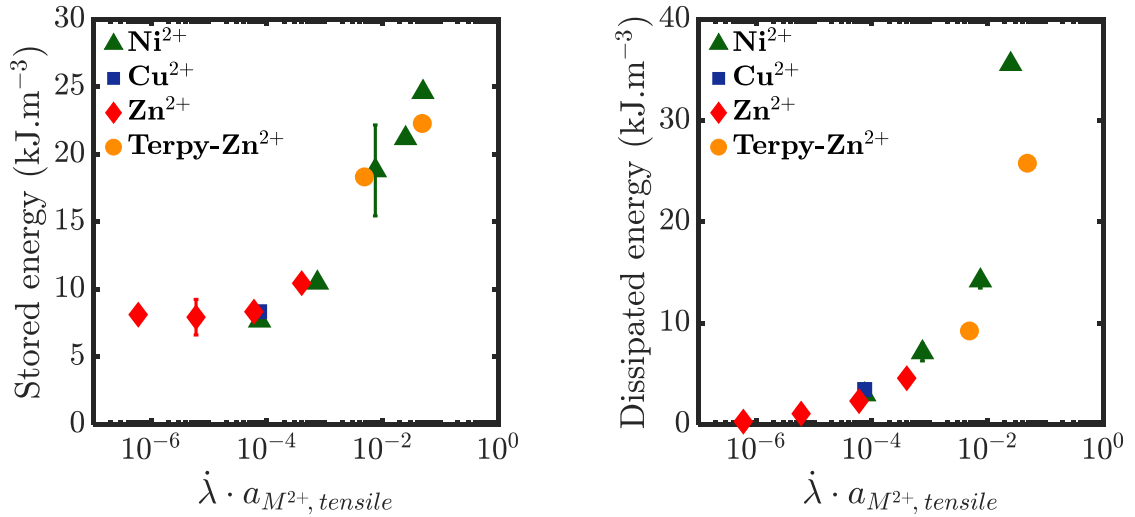


Figure 6.9: Left: Stored energy versus the Weissenberg number (with $a_{M^{2+}, tensile}$ values from Table 6.2), for cycles at $\lambda_{max} = 3$. Right: Dissipated energy versus the Weissenberg number (with $a_{M^{2+}, tensile}$ values from Table 6.2), for cycles at $\lambda_{max} = 3$.

Figure 6.10 shows the total mechanical energy brought into the system (sum of the stored and dissipated energies), along with the fraction of energy input that is dissipated as a function of the Weissenberg number. The total mechanical energy followed unsurprisingly the same behavior as the stored and dissipated energies. The hysteresis seems to evolve logarithmically with $\lambda a_{M^{2+}, tensile}$.

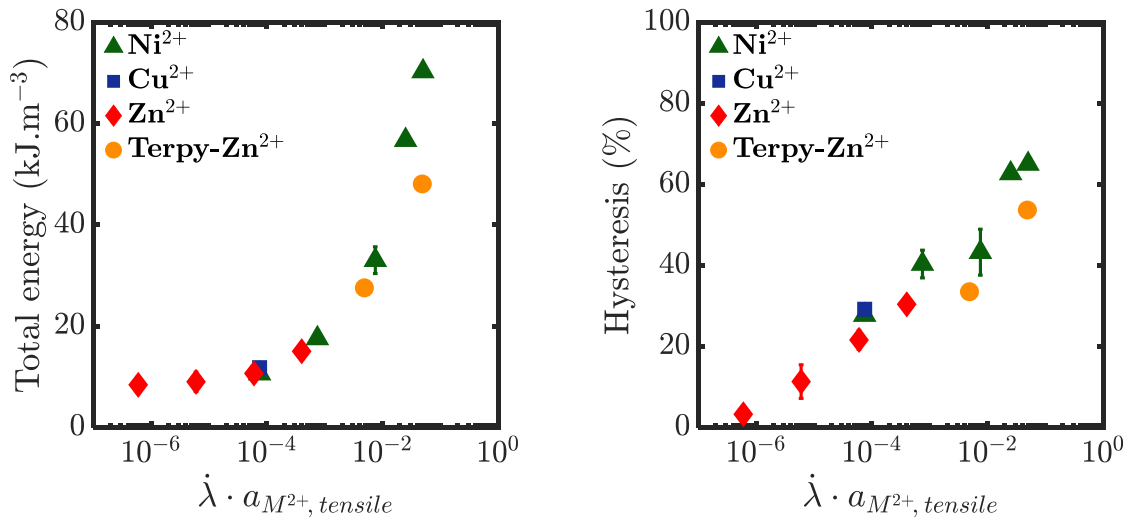


Figure 6.10: Left: Total mechanical energy versus the Weissenberg number (with $a_{M^{2+}, tensile}$ values from Table 6.2), for cycles at $\lambda_{max} = 3$. Right: Percentage of energy dissipated versus the Weissenberg number (with $a_{M^{2+}, tensile}$ values from Table 6.2), for cycles at $\lambda_{max} = 3$.

The large strain energy dissipation follows the same dynamics as the parameters observed in continuous tensile tests. At $\lambda\tau \approx 10^{-4}$, the physical bonds start to have a mechanical influence on the network. Young's modulus increases as the physical crosslinks contribute to the elasticity, and so does the energy dissipated by the physical network.

It is interesting to note that the energy dissipation is not equal to zero before this threshold value. The dissipation mechanisms existing at low Weissenberg numbers may be linked to the existence of clusters

of physical crosslinks, the lifetime of which is much longer than that of the individual physical bonds. At those values, they certainly induce some energy dissipation inside the material. Since the energy dissipation is negligible at $We = 10^{-6}$, we can estimate that those aggregates have a lifetime 10^5 longer than the physical crosslink, which is much more than what we estimated in the Chapter 2 with DLS and rheology experiments.

Figure 6.11 shows the same hysteresis data from the previous chapters, that we had obtained at different stretches and stretch-rates, plotted versus $\lambda/(\lambda a_{M^{2+}}) = t/a_{M^{2+},tensile}$ – the time needed to reach the desired stretch shifted by the lifetime of the physical bond. This time is representative of the so-called ‘observation time’. The large strain hysteresis shows a clear peak of 75% at a normalized time of 10. We can see some influence of the stretch on the hysteresis, especially at comparatively long times. The hysteresis is higher at low stretches ($\lambda = 3$), but apart from those particular points, the superposition is particularly good (using the shift factors from Table 6.2, obtained from different experiments).

If we consider that the peak in large strain dissipation should be around the lifetime of the physical bond, then this result implies that we underestimated our reference shift factor $\tau_{Ni^{2+}}$ by a factor of 10. It is also clear that this large strain dissipation occurs even at very long times or low stretch-rates: 5 decades away from the peak in dissipation, the hysteresis is still of 15 to 20%.

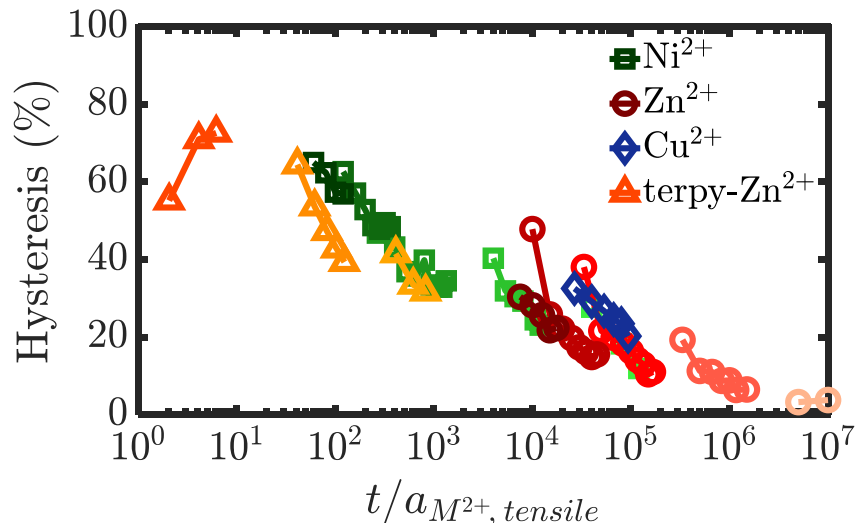


Figure 6.11: Hysteresis (in percentages) versus the time to reach the maximal stretch, shifted by the lifetime of the physical bond from Table 6.2, for the different dual-crosslink hydrogels. Darker colors represent the higher stretch-rates.

At low Weissenberg number, below 10^{-4} , the observation time is much longer than the characteristic lifetime of the physical bond. The number of active physical bonds in the network is negligible, and the mechanical behavior of the hydrogel is close to the one of the bare chemical gel. However, this behavior is observed only at very low Weissenberg numbers, at least 6 decades below the lifetime of the physical bond we considered here (we used the imidazole- Ni^{2+} bond as a reference). With increasing Weissenberg number (or decreasing observation time) up to between 10^{-5} , an energy dissipation appears. At these Weissenberg numbers, we have seen no evidence of an activity of the physical crosslinks (no increase in the elastic modulus, no influence of stretch-rate on the strain-hardening of the material). We link this

6. One bond to rule them all

energy dissipation to the characteristic frequency of the clusters of physical crosslinks, much lower than that of the physical bond alone.

Increasing the Weissenberg number further, the energy dissipation keeps increasing: with decreasing observation time, we increase the number of active physical bonds. Those active bonds break during stretching and the consequent relaxation of polymer chains will dissipate energy. The intensity of this dissipation is dependent on the initial number of active physical bonds. The physical bonds that reform during stretching are also able to dissipate energy [8].

Upon reaching short observation times compared to the lifetime of the physical bonds (or high Weissenberg number), the physical bonds start behaving as permanent bonds: over the course of the experiment, they are not able to break and dissipate energy. The overall energy dissipation drops, which is what we observe at high speed on the very slow dual-crosslink hydrogel (Figure 6.11). The peak of energy dissipation seems to be reached at times a decade superior to the lifetime of the physical bond we consider here, which might imply an overestimation of the bond lifetime on our part.

6.3. General remarks on the results in large deformations

Even in this master curve representation, the terpy-Zn²⁺ dual-crosslink hydrogel shows some differences in values with the other dual-crosslink hydrogels. Its modulus is much higher and its stretch and stress at break are much lower. Its energy dissipation is also slightly different from the VIm-M²⁺ hydrogels. However, the variations of those values with Weissenberg number are in line with those of the other dual-crosslink hydrogels. The difference in absolute values is certainly linked to the difference in number of elastically active physical crosslinks. We have seen in Chapter 2 that the VIm-Ni²⁺ dual-crosslink hydrogels bears around 20 mmol/L of elastically efficient physical crosslinks. The terpy-Zn²⁺ dual-crosslink hydrogel, from what we can see on the rheology curves, might have 3 times more.

It is interesting to note that the influence of the physical bonds begins at observation times longer than the characteristic time by a factor of 10³, or even 10⁴ in some cases. Our reference was $\tau_{Ni^{2+}}$ obtained from rheology. This observation implies either that the influence of the physical crosslinks is visible over a very wide range of decades of Weissenberg number, or that we observe the secondary dynamic of our dual-crosslink networks. We believe this last argument to be the right explanation. We have indeed shown the existence of clusters of physical crosslinks in the dual-crosslink hydrogels. These clusters have a slow dynamic, which influences the dynamics of the network at low Weissenberg numbers. There is a low number of those clusters, by definition, so their influence on the Young's modulus might not be important. However, their influence on the stress levels reached inside the network is much higher: even a low number of slow-dynamic bonds will drastically increase the stress, which might explain the increase in the maximal stress we observe even at low Weissenberg numbers. A cluster being in essence a high-functionality crosslink, it will increase the number of chains in their non-linear entropic regime and the consequent level of strain-hardening observed.

Overall, the horizontal shifts we applied to our large deformations data is quite validated. The shift factors we found in the superposition of Young's modulus apply perfectly well to all the other parameters we measure (strain-hardening onset, energy dissipation,...). This superposition works well at all the Weissenberg numbers considered here.

The stretch at break does not follow exactly the same dynamics as the other mechanical properties presented here. It decreases only after 2×10^{-2} , whereas the effect of the physical bonds on the strain-hardening is seen at 10^{-3} . This difference might be a sign of the different dynamics in play when considering the breaking of a dual-crosslink hydrogel, compared to the Young's modulus or the strain-hardening for example. Our hypothesis that the physical bonds prevent the nucleation of the fracture implies that the stretch at break is controlled by the failure of chemical bonds, which follows a different dynamics from the stretch-rate. Which in turn leads us to the study of the fracture properties of those dual-crosslink hydrogels.

6.4. Fracture

We have shown that the fracture properties of the dual-crosslink hydrogels evolve with the applied stretch-rate and the dynamics of the material. In this part, we will renormalize the fracture properties, with the Weissenberg number, in order to obtain an understanding of the behavior of a dual-crosslink hydrogel over a wide range of stretch-rates.

6.4.1. Single edge notch

The superposition with the Weissenberg number can be made for the data we obtained from single edge notch experiments. We first tried, in Figure 6.12, to realize this superposition on the fracture energy Γ with the lifetimes measured in rheology (listed in Table 6.1). This superposition is clearly not satisfactory. The dynamics of the fracture are very different from the dynamics we find in linear rheology, which is not a surprise. Just as for the parameters obtained from large deformations, we can still try to realize a horizontal shift.

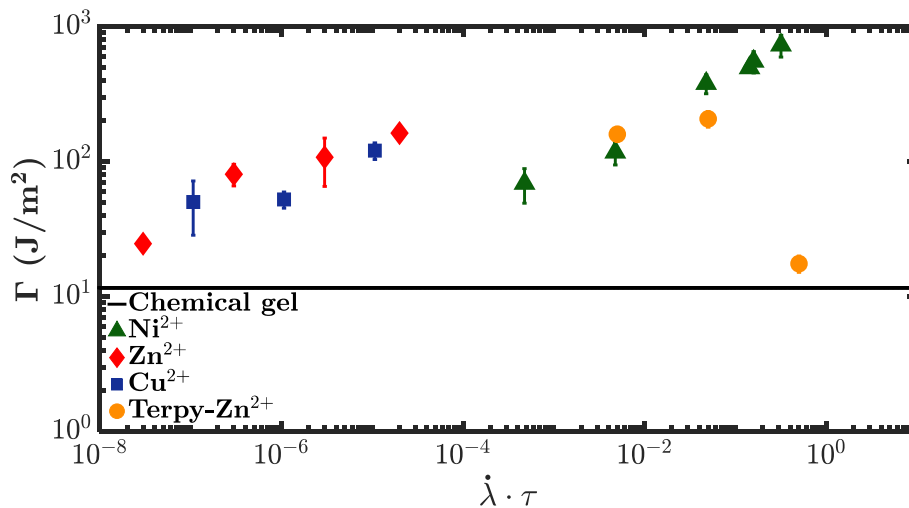


Figure 6.12: Fracture energy Γ of each dual-crosslink hydrogels, versus the stretch-rate shifted by the lifetime of the physical bonds measured in rheology (from Table 6.1).

The new horizontal shift factors that we obtained by shifting the values of Γ are listed in Table 6.3. They are different from the shift factors obtained in Section 6.2 of this chapter. The lifetime of the Im-Ni²⁺ physical bond, $\tau_{Ni^{2+}} = 0.025$ s, was used again as a reference.

6. One bond to rule them all

Table 6.3: Shift factors $a_{M^{2+},fracture}$ computed from single-edge notch fracture tests

Physical bond	$a_{M^{2+},fracture}$ (s)
Terpy-Zn ²⁺	1.35
Ni ²⁺	2.5×10^{-2}
Cu ²⁺	5×10^{-3}
Zn ²⁺	3.3×10^{-3}

As shown in Figure 6.13, master curves of the fracture energy Γ and the local fracture energy Γ_{local} for the different dual-crosslink hydrogels were obtained (Γ_{local} for the VIm-Cu²⁺ dual-crosslink hydrogel was not computed). As shown in the figure, the master curves obtained are reasonable and, for both representations of the fracture energy, the global trend is the same: the energies increased with the Weissenberg number, giving a peak around $\dot{\lambda}a_{M^{2+},fracture} = 10^{-2}-10^{-1}$. The fracture energy increases slowly from $20 J/m^2$ at $\dot{\lambda}a_{M^{2+},fracture} = 10^{-5}$ up to $800 J/m^2$ at 5×10^{-2} , and then decreased sharply to reach almost the value of Γ of the chemical gel. For the local fracture energy, the value at the peak was about $300 J/m^2$. Here the differences between the VIm-M²⁺ gels and the terpy-Zn²⁺ gel were small, presumably because the low values of the critical stretch were compensated by the high value of the stress (or modulus).

It is noteworthy that, even at observation times 10^5 longer than the lifetime of the physical bond (or stretch-rates 10^{-5} slower than the characteristic opening frequency of the bond), the fracture energy and the critical stretch are still higher than those of the bare chemical gel ($25 J/m^2$ and $\lambda_c = 2.5$, when the chemical gel has a fracture energy of $12 J/m^2$ and a critical stretch $\lambda_c = 1.8$). We believe this can be explained by the phenomenon of fracture nucleation delay we presented earlier. In a perfectly elastic hydrogel, the breaking of a polymer chain at the tip of the crack provokes the correlated fracture of the neighboring chains, which leads to the catastrophic propagation of the fracture. In this visco-elastic material, the energy that is transferred from the bond to its neighbors when it breaks may be dissipated and diluted in a larger zone in the network. This delays the breaking of the neighboring chains and the initiation of crack propagation.

As shown in Figure 6.14 the master curve for the critical stretch λ_c was obtained for the three VIm-M²⁺ dual crosslink gels, while the data for the Terpy-Zn²⁺ gel did not superpose well. The values of λ_c for the terpy-Zn²⁺ gels were lower than those for the VIm-M²⁺ dual crosslink gels. Still, one can see two trends in terms of Weissenberg number dependence. At $\dot{\lambda}a_{M^{2+},fracture} \leq 10^{-2}$, λ_c increased with the Weissenberg number from 2.5 to 6. At high Weissenberg numbers, above 10^{-2} , it then decreased. At the highest Weissenberg number, λ_c for the terpy-Zn²⁺ gel was found even smaller than that for the bare chemical gel. The same set of shift factors was used to shift the data for the crack velocity, and the obtained mastercurve is shown in Figure 6.14. The data for the terpy-Zn²⁺ gel did not superpose. Even for the VIm-M²⁺ superposition was not great. The dual-crosslink hydrogels show a crack velocity constantly increasing with Weissenberg number, until reaching a plateau at around 200 mm/s for $\dot{\lambda}a_{M^{2+},fracture} > 10^{-2}$.

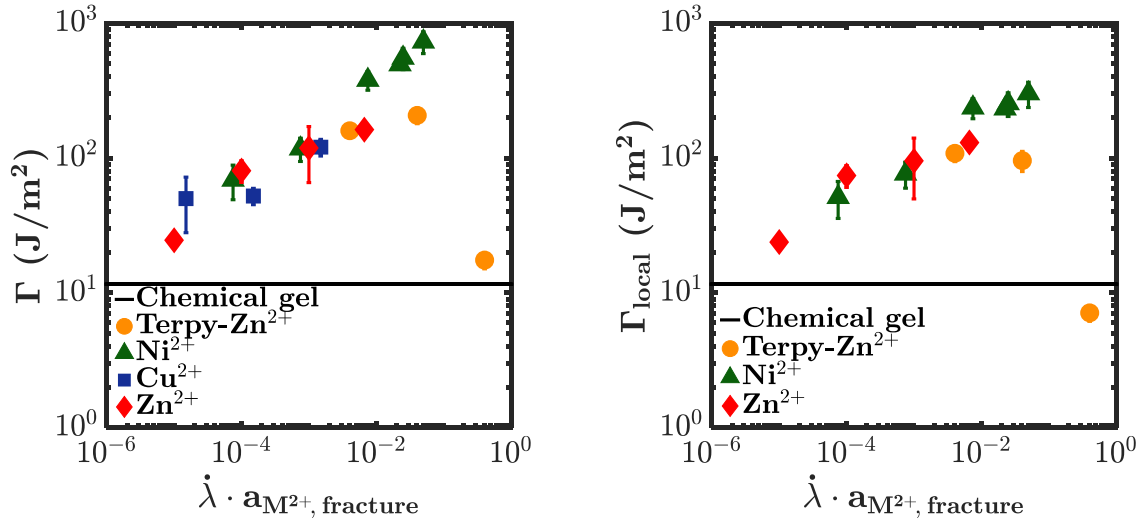


Figure 6.13: Fracture energy Γ (left) and local fracture energy Γ_{local} (right) versus the stretch-rate shifted by the shift-factors from Table 6.3.

The observed differences between the VIm- M^{2+} hydrogels and the terpy- Zn^{2+} gel should arise from the difference in the structure in the chemical gels. As we have seen, the terpyridine hydrogel is more homogeneously crosslinked than its imidazole counterpart, which might influence its fragility. A systematic study in fracture properties in comparison with the chemical gel would be necessary, which we were not able to complete because of the cost (in time and work) of the fabrication of the terpyridine monomer.

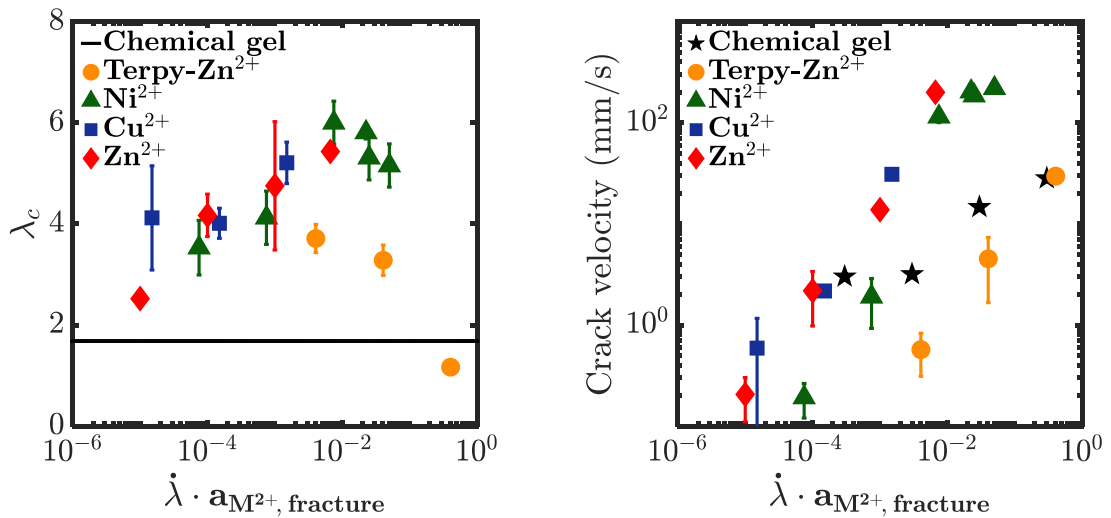


Figure 6.14 Left: Critical stretch at which the propagation of the crack begins, versus the Weissenberg number with shift factors $a_{M^{2+}, fracture}$ from Table 6.3. Right: Velocity of the fracture propagation, versus the Weissenberg number with shift factors $a_{M^{2+}, fracture}$ from Table 6.3.

The dynamics we observed on Figure 6.13 and Figure 6.14 raise an interesting question. The peak of fracture energy is located at relatively low Weissenberg numbers: we could have expected it to be closer to a Weissenberg number of 1, implying that when the inverse of the stretch-rate is close to the lifetime of the physical bond, the material is the toughest. Here, there is a factor 100 between those two values. There can be two explanations for this: (1) as we have noted in Figure 6.11, we might have

6. One bond to rule them all

underestimated our reference lifetime $\tau_{Ni^{2+}}$ by a factor of 10. This would move the peak closer to a Weissenberg number of 1. (2) The dynamics at play at the crack of the tip are not well represented by the stretch-rate applied to the bulk of the material. This second point seems more realistic, especially considering the extreme conditions in stretch, stress and stretch-rate at the tip of a crack before and during the propagation.

Since the crack propagation velocity can be a relevant parameter to evaluate the local dynamic at the crack tip, we plotted the local fracture energy vs the crack velocity shifted by the same shift factors, listed in Table 6.3 (Figure 6.15). Interestingly for the three dual crosslink gels, a master curve was obtained. The global trend was the same as that for the mastercurve plotted against the Weissenberg number, while the peak position is at 6. It should be noted that the shift factors we are using here were obtained from a stretch-rate superposition, making them homogeneous to a time. The abscissa in Figure 6.15 is then homogeneous to a length. However, for a lack of a better parameter to represent a propagation rate of the crack in the dual-crosslink hydrogels, this value will have to do. Moreover, the good superposition we obtain tends to justify our choice.

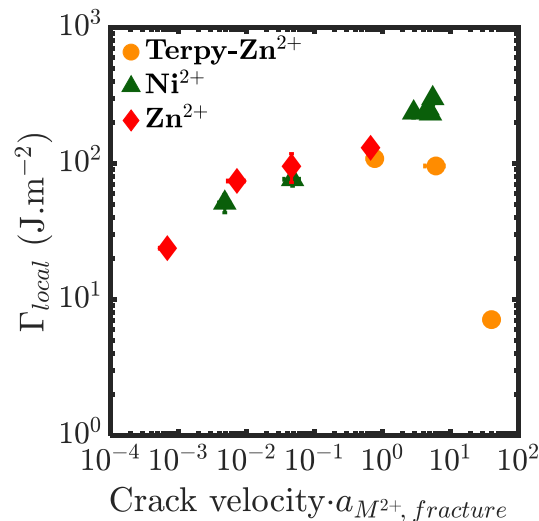


Figure 6.15: Local fracture energy versus the fracture velocity, shifted by the shift factors from Table 6.3.

The first step of the breaking of a network is the nucleation of a cluster of bond scission. When a polymer chain breaks, part of the stress it was bearing is transferred to its neighbors. If this increase in stress is too high, those chains will also break. This correlated fracture causes the nucleation of a crack, which will catastrophically propagate in the network. In the dual-crosslink hydrogel, this correlated breaking of polymer chains is delayed. When a chain breaks, the stress it was bearing is diluted in a large zone, and not just to the neighboring chemical chains. The nucleation of a crack happens at much larger deformations.

Once the fracture has nucleated, it must propagate. The energy needed to propagate a fracture was characterized as a function of the Weissenberg number. It shows a clear dependence on the dynamic of the material. At high Weissenberg numbers (above 10^{-1}), the observation time is much smaller than the lifetime of the physical bonds. A large number of physical bonds are active, and more importantly this number does not decrease over the experiment time. The network possesses a consequently large number

of active polymer chains and stores a lot of energy upon deformation. The propagation of a fracture in such a material happens at low stretches, needs little energy to happen, and is quite fast – the material exhibits brittle properties.

At low Weissenberg numbers (below 10^{-4}), the physical bonds are not active. The number of polymer chains in the dual-crosslink hydrogel is not increased compared to the chemical hydrogel. The number of active physical bonds is close to 0, apart from around the crack tip. In this region, stretches and stretch-rates are higher than in the rest of the material, which might activate some physical bonds. Moreover, the same mechanism of delay of the correlated breaking of polymer chains is still able to take place. The energy needed to propagate the crack is then higher than that of the chemical hydrogel, the dual-crosslink network is more stretchable, and the crack propagates slowly. Which explains why, even when the bulk of the material shows no dissipation of energy, the fracture properties are still enhanced.

At $\dot{\lambda} a_{M^{2+}, fracture}$ in the order of a few 10^{-2} , a high number of the physical bonds are elastically active. More particularly, those physical bonds can dissipate energy, by breaking and reforming on the polymer chains. The stresses at the tip of the crack can be diluted in a large zone, avoiding critical damage at the tip that would provoke the propagation of the crack. We can hypothesize that, the larger this dissipation zone, the tougher the material.

The toughness of our dual-crosslink hydrogels clearly follow a common evolution, dictated by the dynamic of the physical bond we introduce. It is interesting to note, however, that not all the parameters we compute here follow the exact same dynamics. In particular, when increasing the stretch-rate, the critical stretch λ_c starts decreasing before the fracture energy Γ_{local} decreases. This behavior was also seen in a similar study realized on the PVA-borax hydrogel [11]. However, in that case, the difference in dynamic was between λ_c and Γ , and not Γ_{local} .

6.4.2. Delayed fracture of pure shear samples

We had realized delayed fracture experiments, by stretching a notched sample in pure shear geometry up to a defined stretch λ_{max} . The idea of these experiments was to understand the influence of the physical crosslinks on a crack propagation happening at lower velocities. By imposing a certain stretch, we imposed a certain energy release rate \mathcal{G} to the crack, which would in turn provoke a certain crack velocity dependent on the dynamic of the material. We will now compare those experiments realized on two dual-crosslink hydrogels, VIm-Ni²⁺ and VIm-Zn²⁺, in order to find again a unified behavior.

Figure 6.16 shows the main results of the delayed fracture experiments, for both VIm-Ni²⁺ and VIm-Zn²⁺ dual-crosslink hydrogels. The materials, notched in a pure shear geometry, were stretched at $\dot{\lambda} = 0.3 \text{ s}^{-1}$ up to different λ_{max} . We have shown that the main parameter in this experiment is not the stretch, but the energy \mathcal{G} we apply to the material in stretching it up to λ_{max} . The time before the onset of propagation (on the left) shows clearly three families of samples:

- at $\mathcal{G} < 70 \text{ J.m}^{-2}$, the crack does not propagate immediately when the relaxation begins: there is a delay time, around 100 seconds, which decreases when increasing \mathcal{G} ;
- at $70 \text{ J.m}^{-2} < \mathcal{G} < 300 \text{ J.m}^{-2}$, the crack propagates immediately when the stretching stops and the relaxation begins;
- at $\mathcal{G} \geq 300 \text{ J.m}^{-2}$, two situations arise: in the case of the Zn²⁺ dual-crosslink hydrogel, the fracture propagates immediately, during the deformation. In the case of the Ni²⁺ dual-crosslink

6. One bond to rule them all

hydrogel, the crack also starts to propagate but quickly deviates vertically, showing an anisotropy of the network. It then starts propagating horizontally after 10 seconds.

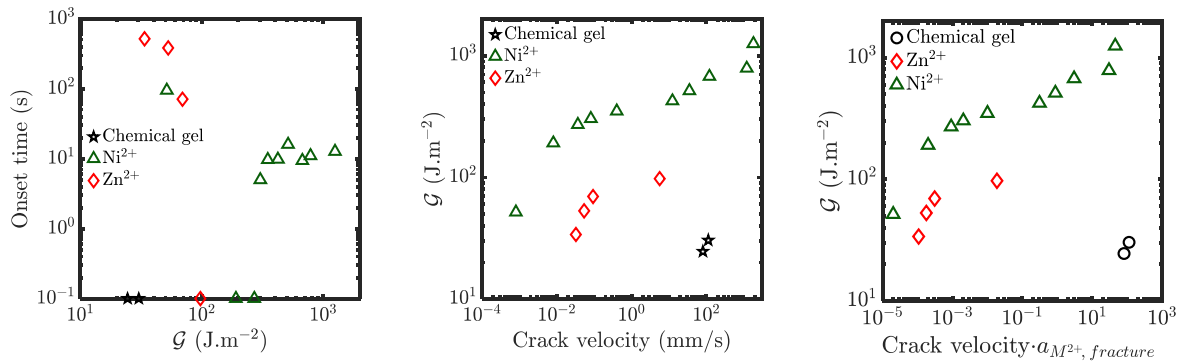


Figure 6.16: Left: Onset of crack propagation versus strain energy release rate, for both Ni²⁺ (green) and Zn²⁺ (red) dual-crosslink hydrogels. Center: Energy release rate versus crack velocity for the same hydrogels. Right: Energy release rate versus crack velocity shifted using the shift factors from Table 6.3.

- (1) The first group of samples, with a delay time before the beginning of the propagation, shows clearly the influence of the physical bonds on the network. At the same G , the propagation begins immediately in the bare chemical network. Here, the physical bonds at the tip of the crack dilute the stresses, hence diluting the damage; they also, as mentioned in other circumstances, prevent the correlated breaking of polymer chains in this region, which leads to a delay in the crack propagation.
- (2) Upon increasing G , we decrease this onset time to 0: when the crack stops, the physical bonds relax enough so that the polymer chains are critically stretched, and the crack propagates immediately.
- (3) The last group of samples, at $G \geq 300 \text{ J.m}^{-2}$, is actually showing only one behavior: the crack starts propagating at $G = 300 \text{ J.m}^{-2}$. The only difference between the Zn²⁺ and Ni²⁺ dual-crosslink hydrogel is their dynamics. Both networks are anisotropic at large deformations. The Ni²⁺ dual-crosslink hydrogel, exhibiting slower dynamics, has an anisotropy much more ‘permanent’ than the Zn²⁺ dual-crosslink hydrogel at this stretch-rate. This anisotropy provokes the deviation of the crack.

This last hypothesis is further demonstrated by the observations realized in the previous chapter, on the terpy-Zn²⁺ hydrogel, which exhibits such a crack deviation at ‘intermediate’ stretch rates compared to its lifetime. At higher stretch-rate, this deviation disappears.

The anisotropy of the network, which provokes this crack deviation, exists then only at a specific Weissenberg number. At lower Weissenberg, the bonds are too fast compared to the observation time and the network does not show an anisotropy (or an anisotropy lasting enough to influence the crack propagation). At high Weissenberg, we have seen the material become brittle: the stretch at which the crack propagates is then much lower than the stretch at which we observe this deviation. The material never becomes anisotropic enough to show a crack deviation. This last point induces a questioning on the influence of crack blunting. It has been stated that, for a crack to propagate in a highly blunted material, a new crack needs to nucleate [4]. The “crack tip” is so open that the high stresses it supposedly

bears have been delocalized over a large zone. The new crack created, in our very blunted Ni^{2+} dual-crosslink hydrogel stretched at $\lambda \geq 2.4$, starts to propagate horizontally and then quickly deviates vertically, facing an anisotropy in the network. When the crack tip is not blunted enough, this deviation does not appear. This explanation is challenged by the fact that this deviation was not observed on a PVA-Borax system, the dynamics of which are quite similar to that of the terpy- Zn^{2+} dual-crosslink hydrogel. The great differences in the organization of the physical bonds in this type of dual-crosslink hydrogel might explain this difference: in the PVA-Borax system, any monomer can create physical bonds with the borax ions.

The graphs on the center and right of Figure 6.16 show the energy release rate versus the crack velocity (or the crack velocity shifted by the lifetime). The energy release rate in the Zn^{2+} dual-crosslink hydrogel is much lower than that of the Ni^{2+} dual-crosslink hydrogel at the same crack velocity. Once shifted by the shift factors used in fracture, listed in Table 6.3, the curves do not superpose. This difference is certainly linked to the difference between the static experiment realized here, where the polymer chains at the crack tip are only stretched by the propagation of the crack, and the dynamic experiment realized on single-edge notch samples, where the polymer chains at the crack tip undergo large stretch-rates from the deformation and the crack propagation.

The two dual-crosslink hydrogels studied here show overall some qualitative differences in behavior, which prevent us from extracting a unified law of behavior. The stick-slip behavior of the Zn^{2+} dual-crosslink hydrogel stems from the fast dynamics of this dual-crosslink hydrogel. When a crack propagates, it is able to relax the stresses at the tip of the crack fast enough to stop the propagation, which is not the case for the Ni^{2+} dual-crosslink hydrogel. This second material on the other hand, shows much slower dynamics. When put under stretch, it acquires an anisotropy that is long-lived enough to force the crack to deviate.

6.5. On the dynamic behavior of the dual-crosslink network

We have managed to create a dynamic network, with a characteristic frequency that we are able to tune quite easily. We have shown that the properties of such a network all follow the same qualitative evolution with the Weissenberg number, whether in small deformations, large deformations or fracture. As the observation times decrease, the number of active physical bonds increases. Therefore, with increasing Weissenberg number (or in Deborah number in linear rheology) we increase the number of chains present in the network by increasing the number of active physical bonds. The material elastic properties increase logically with the number density of active chains (G' in rheology, Young's modulus in large deformations). With the increase in active physical bonds, follows of course an increase in the energy dissipated by the network: during the deformations, those physical bonds will break, and it is this breaking (and the subsequent relaxation of the polymer chain) that dissipates energy. The more active physical bonds there are in the network, the more physical bonds can break and the more energy the network can dissipate. Again, this dissipation of energy follows clearly a dynamic that is dependent only on the characteristic lifetime of this physical bond.

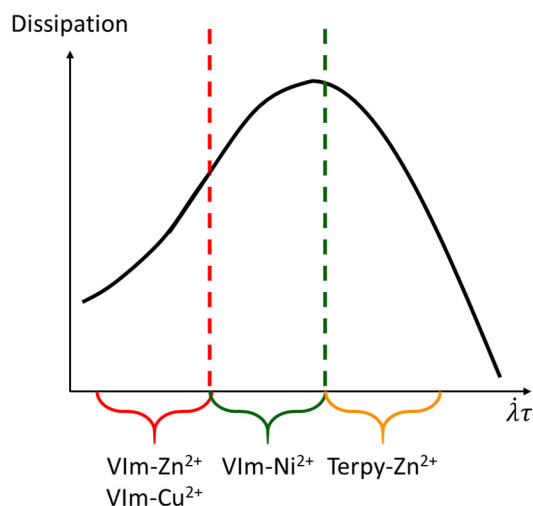


Figure 6.17: Schematic representation of the energy dissipation versus the Weissenberg number, as we have demonstrated for our different dual-crosslink hydrogels.

When reaching very large deformations, some polymer chains start showing a non-linear strain-hardening behavior, where the entropic elasticity follows a Langevin function, thus increasing their influence on the stiffness of the material. They start bearing more and more stress. This increase in stiffness is in competition with the decreasing number of active chains in the network, which tends to decrease the stresses the network bears. The strain-hardening behavior will become dominant on the network properties at a certain stretch that is dependent on the stretch-rate applied to the material: at low Weissenberg number, typically below 10^{-4} , this onset happens at large deformations. When the physical bonds start showing a mechanical influence on the network, this stretch onset decreases.

The fracture of the dual-crosslink hydrogels involves molecular phenomena that are more complex, described in the previous section (6.4). Still, the properties of fracture resistance of the material are completely dependent on its dynamics. The increase in stiffness with the Weissenberg number that we observed for the material is accompanied by an increase in its toughness, up until a Weissenberg number of 10^{-2} , above which the lifetime of the physical bonds becomes too long compared to the observation time, and the material quickly becomes brittle. Some interesting considerations were made at low stretch-rates, where the physical bonds prevent the correlated breaking of polymer chains and protect the network, even when the observation time is much longer than the lifetime of the physical bond.

However, some important comments (that we have not really detailed previously) can be made on the shift factors we determined in the different experiments. Those shift factors are listed in Table 6.4, along with the lifetimes measured in rheology. The lifetime of the Imidazole- Ni^{2+} bond was used as a reference for each experiment. The lifetimes of the physical bonds in rheology are much shorter than those computed in tensile or fracture tests. The shift factors we determined in tensile tests show a broader range of dynamics than those measured in fracture tests, by an order of a decade.

Table 6.4: Lifetimes τ of the different physical bonds, in the different experiments realized (Small deformations in linear rheology, large deformations in tensile tests and fracture properties)

	$\tau_{rheology}$	$a_{M^{2+},tensile}$	$a_{M^{2+},fracture}$
terpy-Zn ²⁺	0.27	1.62	1.35
Ni ²⁺	2.5×10^{-2}	2.5×10^{-2}	2.5×10^{-2}
Cu ²⁺	2.5×10^{-5}	2.5×10^{-4}	5×10^{-3}
Zn ²⁺	5×10^{-6}	2×10^{-4}	3.3×10^{-3}

The first conclusion we can draw from this is that the lifetime measured in linear rheology may not be relevant to experiments in large deformations. This is an important conclusion that can be rationalized. It has been demonstrated [15-19] that applying a force on a transient bond can reduce (or increase, but it is less common) its lifetime. An energetic consideration can help us understand this phenomenon. To open, the physical bond needs to overcome an energy barrier, as shown in Figure 6.18. The force applied on the physical bond raises the energy of the bound state, which decreases the energy barrier height to overcome in order to open. Force destabilizes the bond and reduces its lifetime. On a side note, some bonds have shown a “catch-slip” behavior [18], where applied force (below a certain force level) raises the energy of the bound state and the energy of the transition state. This second energy being raised faster, it increases the energy barrier height and increases the lifetime of the bond.

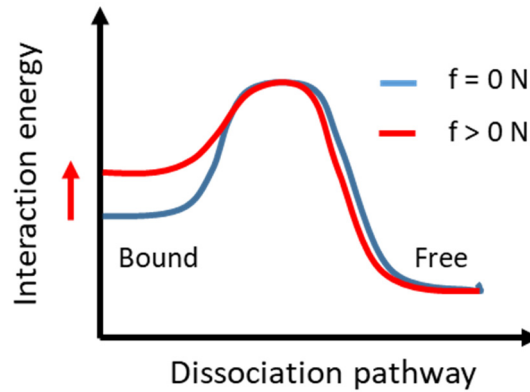


Figure 6.18: Destabilization of a transient bond: hypothetical energy barriers with (red) and without (blue) applied force.

The fracture properties also seem to follow a different dynamic behavior than that of the tensile tests: characteristic times of Zn²⁺ for example are increased by a factor 16 in fracture, compared to tensile tests. This could be explained by considering that the stretch-rates and stress-levels are not the same at the tip of the crack than in the bulk of the material. This change in lifetimes could then be caused simply by a change in stretch-rates, or the greater stress applied on the bond.

It should be noted that these changes we observe between rheology and large deformations directly imply that the reference shift factor we used for our large deformations experiment is not good. It must be affected by the large stresses and stretches of these experiments, and hence the range of Weissenberg numbers we observe in large deformations is not to be considered as an absolute value. Table 6.5 lists the lifetimes and shift factors obtained in the different experiments, normalized by this reference we used. The relative lifetimes from rheology span 5 orders of magnitude from 10^{-4} to 10. The shift factors from tensile tests span only 4 decades, from 10^{-2} to 10^2 . This fact might imply that not all the physical

6. One bond to rule them all

bonds are affected in the same way by the application of large stresses. In fracture, the shift-factors are more closely packed, from 10^{-1} to 50.

Table 6.5: Ratio of lifetimes over the reference lifetime of the Imidazole- Ni^{2+} bond, in the different types of experiments realized.

M^{2+}/Ni^{2+}	Rheology	Tensile tests	Fracture
Terpy- Zn^{2+}	10,8	64,8	54
Ni^{2+}	1	1	1
Cu^{2+}	10^{-3}	1×10^{-2}	0,2
Zn^{2+}	2×10^{-4}	8×10^{-3}	0,13

The dynamics at play in a propagation of a crack are clearly different from the dynamics of the bulk of the material, revealed by the tensile tests. We have shown in Chapter 2 and 4 the existence of clusters of physical bonds in our dual-crosslink hydrogels. Those clusters are long-lived and induce energy dissipation even at very low stretch-rate, but they might also have an influence on the fracture properties of the network. It is possible that, from a fast-dynamic driven behavior in linear rheology and small reversible deformations, we shift to a slow-dynamic driven behavior. This idea stems from our observations in large deformations, where the dynamics seem to be slower than in linear rheology. We showed for example that the peak of energy dissipation is located at times a decade higher than what we expected. In small deformations, the small number of clusters will have no influence on the properties of the materials. On the contrary, at large deformations, the small number of long-lived clusters can influence strongly the stress the material bears, creating a percolating network of highly stretched polymer chains. These clusters are moreover related to the physical bonds and hence, their lifetimes are dependent on the applied stress [19]. When increasing the stretch, the lifetime of the physical bonds decrease and so does the lifetimes of the clusters. At the tip of the crack, where the stresses are extreme, the physical bonds might become too fast and we might be seeing only the influence of the clusters. This could explain why the dynamics we observe in fracture for the faster bonds are much closer to the reference dynamic.

References

1. Hammes, G. G. & Steinfeld, J. I. Relaxation Spectra of Some Nickel(II) and Cobalt(II) Complexes. *Journal of the American Chemical Society* 84, 4639–4643 (1962).
2. Holyer, R. H., Hubbard, C. D., Kettle, S. F. A. & Wilkins, R. G. The Kinetics of Replacement Reactions of Complexes of the Transition Metals with 2,2',2''-Terpyridine. *Inorg. Chem.* 5, 622–625 (1966).
3. Rorabacher, D. B. The Kinetics of Formation and Dissociation of the Monoammine Complexes of the Divalent, First-Row, Transition Metal Ions. *Inorganic Chemistry* 5, 1891–1899 (1966).
4. Creton, C. & Ciccotti, M. Fracture and adhesion of soft materials: a review. *Reports on Progress in Physics* 79, 046601 (2016).
5. Halpin, J. C. Fracture of Amorphous Polymeric Solids: Time to Break. 10.
6. Halpin, J. C. & Bueche, F. Fracture of Amorphous Polymeric Solids: Reinforcement. 9.
7. Guo, J. et al. Fracture mechanics of a self-healing hydrogel with covalent and physical crosslinks: A numerical study. *Journal of the Mechanics and Physics of Solids* (2018) doi:10.1016/j.jmps.2018.03.009.
8. Guo, J., Long, R., Mayumi, K. & Hui, C.-Y. Mechanics of a Dual Cross-Link Gel with Dynamic Bonds: Steady State Kinetics and Large Deformation Effects. *Macromolecules* 49, 3497–3507 (2016).
9. Long, R., Mayumi, K., Creton, C., Narita, T. & Hui, C.-Y. Time Dependent Behavior of a Dual Cross-Link Self-Healing Gel: Theory and Experiments. *Macromolecules* 47, 7243–7250 (2014).
10. Long, R., Mayumi, K., Creton, C., Narita, T. & Hui, C.-Y. Rheology of a dual crosslink self-healing gel: Theory and measurement using parallel-plate torsional rheometry. *Journal of Rheology* 59, 643–665 (2015).
11. Mayumi, K., Guo, J., Narita, T., Hui, C. Y. & Creton, C. Fracture of dual crosslink gels with permanent and transient crosslinks. *Extreme Mechanics Letters* 6, 52–59 (2016).
12. Mayumi, K., Marcellan, A., Ducouret, G., Creton, C. & Narita, T. Stress–Strain Relationship of Highly Stretchable Dual Cross-Link Gels: Separability of Strain and Time Effect. *ACS Macro Lett.* 2, 1065–1068 (2013).
13. Zhao, J. Structure et propriétés des hydrogels à réticulation chimique et physique. (PSL Research University, 2018).
14. Shabbir, A. et al. Nonlinear shear and uniaxial extensional rheology of polyether-ester-sulfonate copolymer ionomer melts. *Journal of Rheology* 61, 1279–1289 (2017).
15. Marshall, B. T. et al. Direct observation of catch bonds involving cell-adhesion molecules. *Nature* 423, 190–193 (2003).
16. Li, N., Lü, S., Zhang, Y. & Long, M. Mechanokinetics of receptor–ligand interactions in cell adhesion. *Acta Mechanica Sinica* 31, 248–258 (2015).
17. Pereverzev, Y. V. & Prezhdov, O. V. Force-induced deformations and stability of biological bonds. *Physical Review E* 73, (2006).
18. Sarangapani, K. K. et al. Low Force Decelerates L-selectin Dissociation from P-selectin Glycoprotein Ligand-1 and Endoglycan. 9.
19. Novikova, E. A. & Storm, C. Evolving roles and dynamics for catch and slip bonds during adhesion cluster maturation. arXiv:1908.08934 [cond-mat, physics:physics, q-bio] (2019).

6. One bond to rule them all

Chapter 7

Mapping the damage in dual-crosslink hydrogels with mechanophores

7. Mapping the damage in dual-crosslink hydrogels with mechanophores

Table of contents

7.1. Mechanophores in hydrogels.....	210
7.2. A hydrosoluble dioxetane derivative to obtain time-resolved fracture information	213
7.2.1. Synthesis of the mechanophore and the hydrogel	214
7.2.2. Results and discussion.....	215
7.3. Anthracene Diels-Alder adduct as a crosslinker	216
7.3.1. Synthesis of the mechanophore	217
7.3.2. Synthesis of the chemical network with mechanophore	218
7.3.3. Mechanical properties of the dual-crosslinked hydrogel with mechanophores.....	220
7.3.4. Imaging the fracture front.....	221
7.4. Conclusion and perspectives.....	229
References	26

7. Mapping the damage in dual-crosslink hydrogels with mechanophores

The previous chapters have highlighted the existence of two mechanisms of increased resistance to fracture in our dual-crosslink hydrogels:

- The prevention of the correlated rupture of polymer chains, which inhibits the nucleation of a crack and delays the beginning of the propagation;
- The dissipation of energy at the crack tip during crack propagation, which homogenizes the stresses in this region and slows propagation.

We have assumed that the first mechanism is independent of the speed at which we load our samples, and influences the fracture resistance of the dual-crosslink hydrogels even at very low Weissenberg numbers (toughening the Zn^{2+} dual-crosslink hydrogel for example). The second mechanism should create a damage zone around the crack tip, and should depend on the stretch-rate by the characteristic size and the number of broken bonds in this region.

Complementary to the fracture experiments from which the assumptions come, it is necessary to perform further fracture experiments with spatial resolutions. In order to map the local damage before and during crack propagation, here we used confocal microscopy to observe the fluorescence from mechanophores used as cross linkers in the network, which have already been presented in the introduction of this manuscript. It is a challenge to use these mechanophore molecules in hydrogels, due to the very low solubility of common mechanophore molecules as well as to the low signal/noise ratio of emitted fluorescence in water. To integrate a mechanophore in the chemical network, some adaptations must be made.

In this chapter, we will demonstrate the results for two types of mechanophore molecules that have been tested in the laboratory for elastomers. First, we will detail the synthesis of a hydrosoluble variant of the dioxetane successfully used in multiple network elastomers [1,2]. This mechanophore should produce a photon when broken. The use of this mechanophore in water being inconclusive, I will then present the polymerization of a chemical gel with a π -extended anthracene, previously used in elastomers [3,4]. With this hydrogel, some promising results were obtained. We will discuss some qualitative results of images obtained with a confocal microscope.

7.1. Mechanophores in hydrogels

There are some examples in the literature of mechanophores incorporated in hydrogels. Zhang et al. [5] synthesized fluorescent polymersomes, based on a copolymer with hydrophilic and hydrophobic blocks. In the hydrophobic block was introduced a fluorophore that exhibits an aggregation-induced emission [6,7], tetraphenylethylene. This copolymer was then placed in a solution of varying water content, and its organization was studied with the fluorescence. They showed the appearance of polymersomes, which became fluorescent at high volume fraction in water. This fluorescence was induced by the phase-separation of the block copolymer in the membrane of the polymersome. Upon increasing volume fraction of water, the amount of organic solvent decreases. When the amount of organic solvent becomes too low (typically under 50% in their experiments), the hydrophobic blocks coalesce into solvent-free domains, which start showing fluorescence. Before that, the polymersomes are already formed, but the hydrophobic phases contain organic solvent, which limits the aggregation-induced emission of TPE.

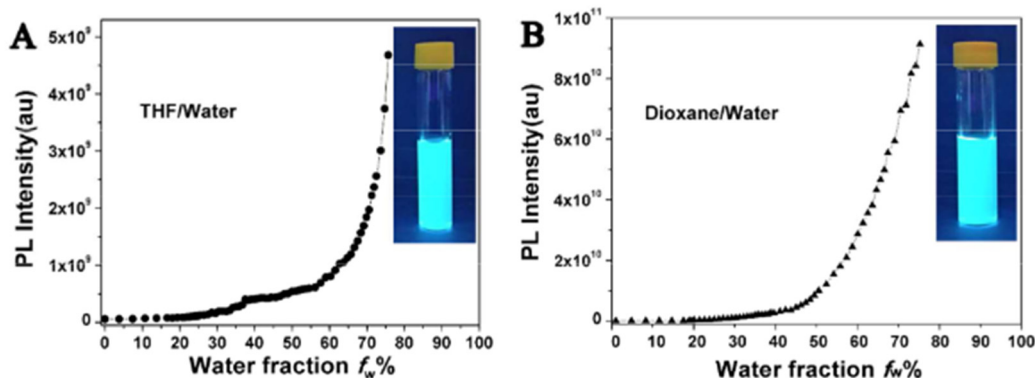


Figure 7.1: Evolution of fluorescence intensity as a function of water content during the polymersome formation. (A) THF/H₂O mixture. (B) Dioxane/H₂O mixture. Excitation wavelength is 382 nm. The photoluminescence (PL) intensity is the average intensity collected from the wavelength 473nm to 479nm. The two photographs in the insets correspond to the polymersome dispersions in pure water after dialysis against water when excited by UV light of 365 nm. Figure reprinted from [5].

Hu et al. [8] also used this aggregation-induced emission in bi-phased hydrogels. They incorporated ‘TVPA’, a fluorophore exhibiting aggregation-induced emission, in a hydrogel network of poly(*N*-isopropyl acrylamide) (PNIPAM) grafted with poly(*N,N*-dimethylacrylamide) (PDMA). This hydrogel shows a phase transition at $T > 32$ °C linked to the LCST of the PNIPAM [9]. At low temperature, the PNIPAM chains are water-soluble and the TVPA has a dark, red color; at high temperature, the PNIPAM chains collapse in dense hydrophilic regions and the TVPA exhibits a bright blue emission. This allows them to map the organization of the network in the hydrogel at different temperatures, with the objective to prove that the high resistance to fracture of these materials [9] at high temperatures is linked to multiple crack bifurcations caused by the presence of the dense PNIPAM regions in the network.

7. Mapping the damage in dual-crosslink hydrogels with mechanophores

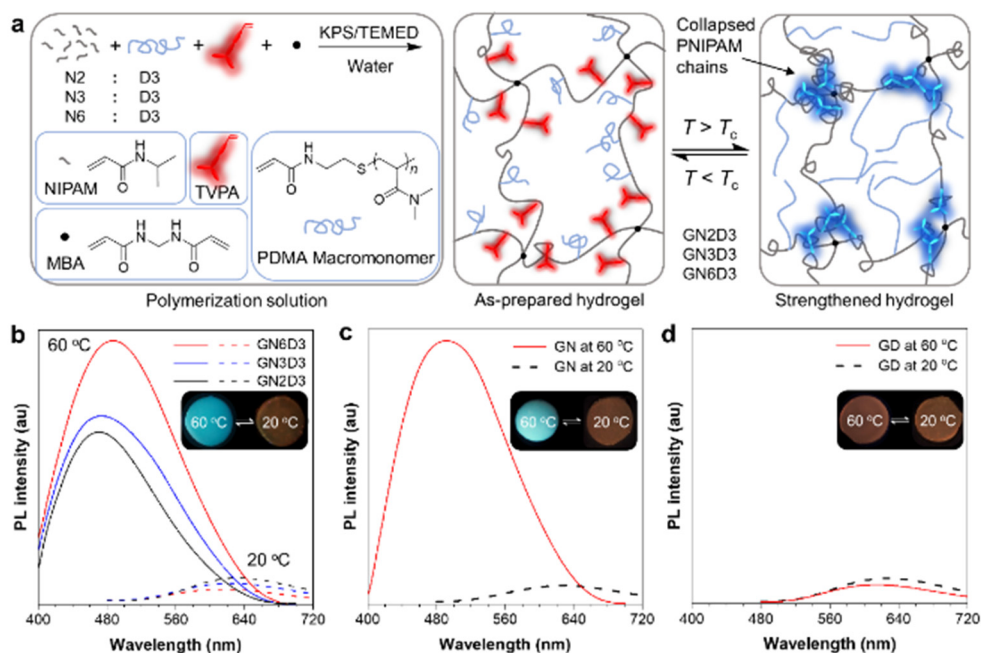


Figure 7.2: Schematic illustration of design principle and visualization of hydrophilicity-hydrophobicity transformation. **a**, TVPA was incorporated into the crosslinked NIPAM polymer network during the free radical polymerization of NIPAM, TVPA and PDMA macromonomers with MBA crosslinkers. The collapse of the resulting PNIPAM network is induced above its lower critical solution temperature (LCST, T_c) and the emission of the incorporated TVPA is expected to be enhanced and blue-shifted in the crowded and hydrophobic PNIPAM domains. Three hydrogels (GN2D3, GN3D3, GN6D3) were prepared with different weight fractions of NIPAM and PDMA. **b–d**, Emission spectra of TVPA incorporated GN2D3, GN3D3, GN6D3 (**b**), GD (**c**) and GN (**d**) hydrogels at 20 °C and 60 °C excited at 380 nm. Inset: fluorescent photos of hydrogels at 20 °C and 60 °C under 365 nm UV light. *Figure reprinted from [8]*

Another very interesting idea was developed by Matsuda et al [10]. In a double-network hydrogel, they diffused a molecule (ANS, 8-anilino-1-naphthalenesulfonic acid) that is not fluorescent in water. They combined this with their technique of ‘self-growing hydrogels’ [11]: when a chain breaks in such a material, the radicals created initiate a new polymerization with monomers in the solution. In this study, they used NIPAM monomers. The chains newly created at the localization of the bond breakage possess then an LCST. Upon heating the material, these chains collapse around the ANS, which becomes fluorescent. This particularly smart method gave great results on their double-networks (see Figure 7.3). They found a damage zone around the front of the crack of the order of 0.5 mm in the case of a cut sample (which is in the same order of magnitude of what J. Slootman found in her PhD [4] studying multiple network elastomers).

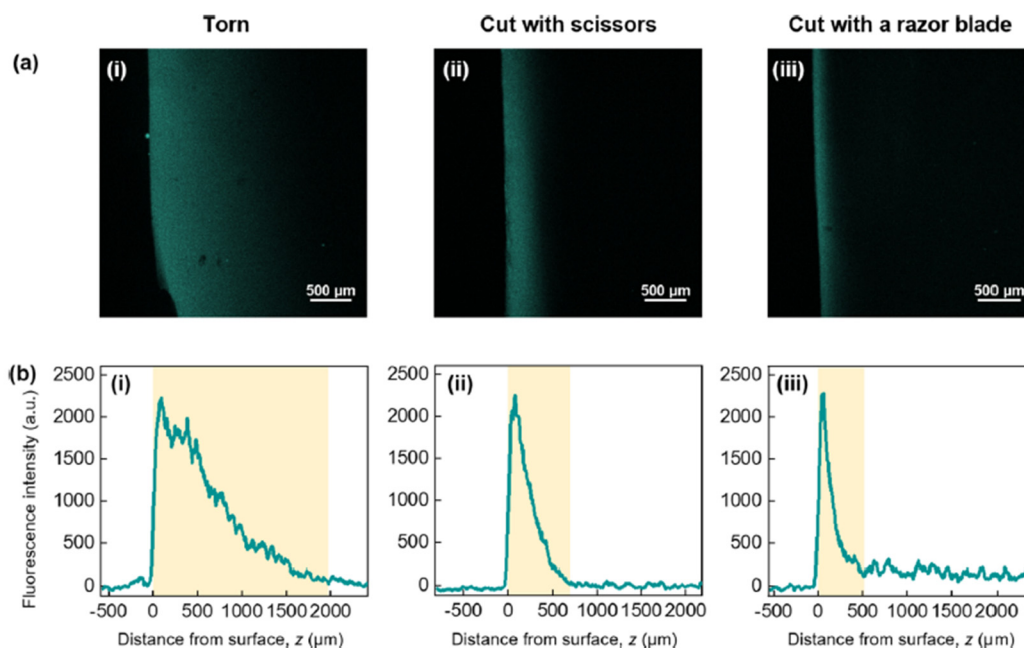


Figure 7.3: (a) Fluorescence images and (b) line profiles of fluorescence intensity $I(z)$ of the DN gels from the fractured surface to bulk. The DN gel was ruptured using different methods including being (i) fractured by tearing a trouser-shaped sample, (ii) cut using scissors, and (iii) cut using a microtome razor blade. Yellow highlighted regions in (b) roughly denote the damage zone. The same experimental condition was used for these three individual experiments. The profiles in (b) are the moving-averaged data. Figure reprinted from [10].

Those methods allow an interesting study of the phenomena involved in the propagation of a crack in a material. They lack however a time component: all the observations were realized post-mortem, and not during the propagation of the crack. In the next part, we will study a mechanophore that is expected to allow us to perform a dynamic study.

7.2. A hydrosoluble dioxetane derivative to obtain time-resolved fracture information

The molecule of bis(adamantyl) 1,2-dioxetane contains a four-membered ring, which is able to decompose into two carbonyl (ketones) moieties. One of those two moieties is in a singlet electronically excited state (20 ns of scission). A blue light (around 420 nm) is emitted during the relaxation of this excited moiety to the ground state. The molecule and its associate chemiluminescent reaction are represented in Figure 7.4 (A). Bis(adamantyl) 1,2-dioxetane is currently the only auto-luminescent system known [12]. Kopecky and Mumford [13] first synthesized and isolated it in 1969. Light emission while sonicating solutions of linear polymers or straining of polymer networks containing dioxetane cross-linkers gave evidence of bond scissions [14].

This molecule has already been widely used to map the damage in polymer networks [15]. Clough et al. [16] integrated the molecule as a crosslinker in a PDMS elastomer filled with silica nanoparticles, to highlight the contribution of chemical bond breakage to the irreversible strain-softening observed in this material, known as Mullins effect. Ducrot et al. [Erreur ! Source du renvoi introuvable.] incorporated this bis(adamantyl) dioxetane as a crosslinker in multiple network elastomers, to investigate the necking phenomenon observed at high stretches.

7. Mapping the damage in dual-crosslink hydrogels with mechanophores

The results for this last study (Figure 7.4) were particularly interesting, showing clearly that the reinforcing mechanism in the multiple-network elastomers they studied was linked to the breaking of a first sacrificial network, which provoked a characteristic necking phenomenon.

Here we will explore the possibility to integrate this molecule as a crosslinker in the chemical network of the hydrogel, in order to understand the damage process in the nucleation and propagation of a fracture.

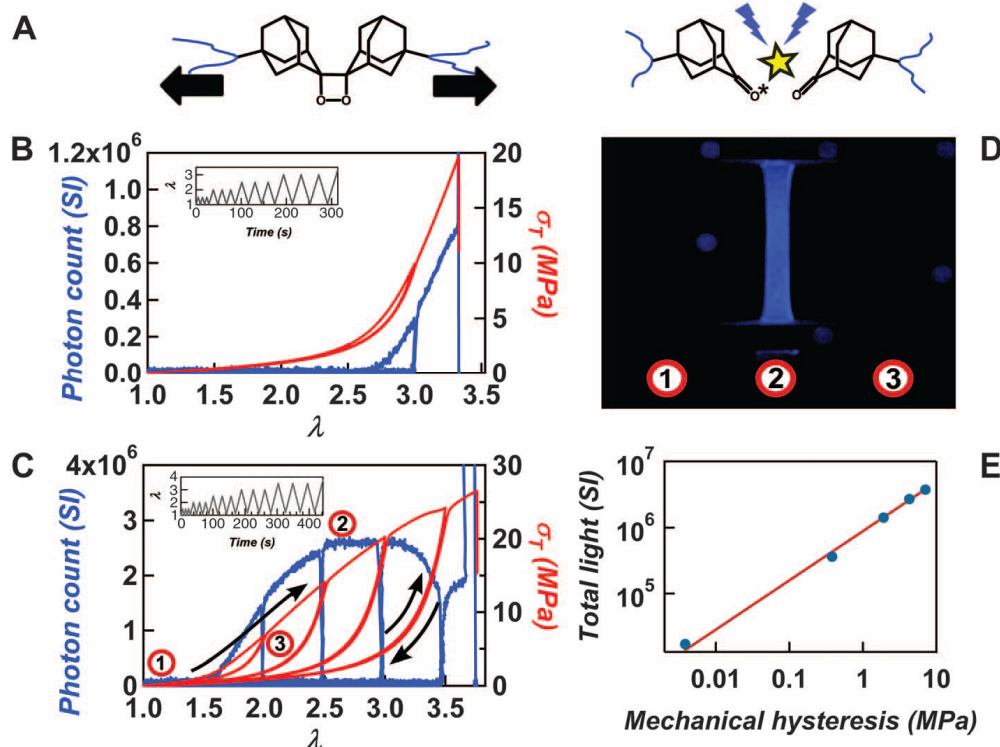


Figure 7.4: (A) Schematic of the chemoluminescence process, bond breakage of the dioxetane cross-linker, and light emission. (B) Step-cycle test for a single sample of the double network showing mechanical stress-strain curves (red) and light emission curves measured with image analysis (blue) for the same sample. A slight amount of bond breakage is observed at high strain. (C) Step-cycle test for a single sample of the triple network showing light emission (in blue) and stress (in red). Light emission is zero during unloading and reloading, until l of the n th cycle exceeds the maximum value of l of the $(n - 1)$ cycle. (D) Image of the luminescence of TN under loading at various steps of the experiment [reported in (C)]: (1) near the beginning of the test, (2) on the first loading at $l \sim 2.6$, and (3) on reloading at $l \sim 1.7$. (E) Cumulative light emitted during the cycles as a function of the mechanical hysteresis in TN. The mechanical hysteresis is defined as sum of the integrals under load-unload cycles, and the total light is the sum of the emitted light for that level of mechanical hysteresis. The total light varies as the mechanical hysteresis to the power 0.75. Figure reprinted from [1].

7.2.1. Synthesis of the mechanophore and the hydrogel

To integrate this mechanophore in the network, Chen et al. [14] grafted acrylate functions at each end of the molecule. They consequently used it as a chemical crosslinker in their network. We intended to follow the same method in our dual-crosslink hydrogels. However, the standard acrylated bis-adamantyl dioxetane is an organic molecule, insoluble in water. Which makes it impossible to use it in our standard synthesis (presented in Chapter 2). To circumvent this problem, Gabriel E. Sanoja developed, in our lab, a technique to graft, a hydrosoluble poly(ethylene glycol) chain before each acrylate function. With a

long enough chain, the molecule becomes sufficiently hydrosoluble to be used in the standard synthesis of the chemical hydrogel.

The total synthesis path of the molecule is presented here:

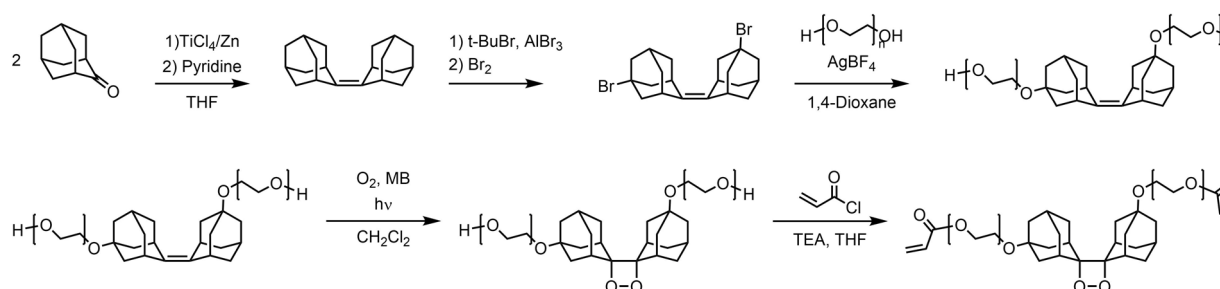


Figure 7.5: Synthesis path of the hydrosoluble dioxetane

The molecule obtained was used as a crosslinker in the polymerization. However, we confirmed its lower reactivity than that of MBA. In order to obtain a network having the same rheological properties as the standard chemical gel, only part of the MBA will be replaced by the mechanophore crosslinker. The polymerization process was then the same as that for our standard chemical gel shown in Chapter 2, and the quantities are listed in Table 7.1. To enhance the intensity of emission from the excited moiety, an energy acceptor was introduced in the material: acriflavine, used at a concentration of around 3 mmol/L.

Table 7.1: Formulation of the chemical network containing the dioxetane mechanophore. *weight percentage of water in the hydrogel.

	Molar mass (g/mol)	Specific gravity (g/mL)	Objective (mol %)	Concentration (mol/L)
AAm	71.1	-	90%	1.8
VIm	94.1	1.039	10%	0.2
MBA	154.2	-	0.12%	0.0024
Mechanophore	-	-	0.03%	0.0006
KPS	270.3	-	0.3%	0.006
TEMED	116.2	0.775	1%	0.02
Water	-	-	85.11%*	-

7.2.2. Results and discussion

Compression tests were realized on a sample of chemical hydrogel such as presented just before. The light emission from the sample was observed with an Andor iXon Ultra 897 EMCCD camera, specifically designed to capture low photon emissions. The experiments were realized in a dark room, to avoid any parasite light. On these hydrogels, we could not observe any significant light emission. Two reasons could be found for this absence:

- the mechanophore is not integrated in the network, or does not emit photons in water;
- the bond breakage inside the material is low, and the light emitted is not enough to be detected.

This camera being able to detect a few photons, the first option seemed to be the most realistic one. To confirm that, we realized the same experiments on a double network hydrogel, such as synthesized by Gong et al. [17], with a first network of poly(2-acrylamido-2-methylpropanesulfonic acid), with 4 mol% of crosslinking agents (composed of 80% MBA and 20% hydrosoluble bis(adamantyl) dioxetane), and a second network of polyacrylamide, crosslinked with 0.1 mol% of MBA. In fact, at large deformation, the first network is irreversibly broken, thus the amount of the damage is expected to be much higher.

7. Mapping the damage in dual-crosslink hydrogels with mechanophores

The compression experiments showed this time what we interpreted as a signal of bond breakage, shown in Figure 7.6.

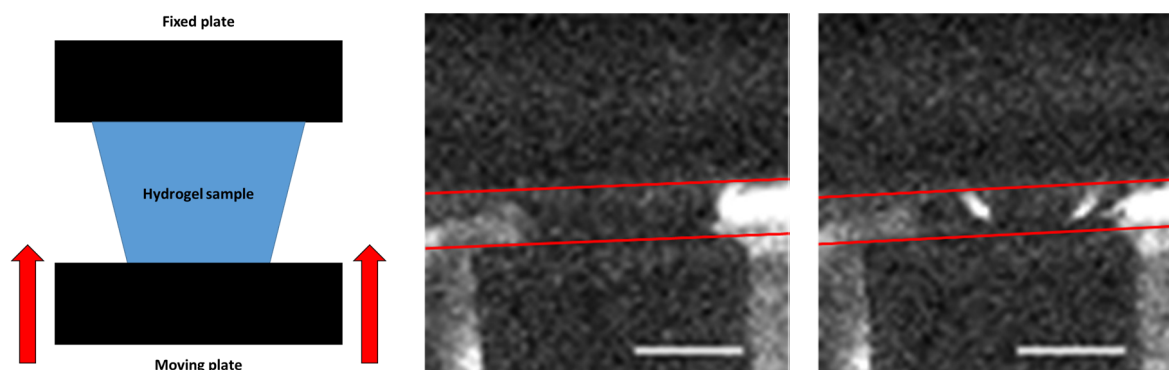


Figure 7.6: *Left:* Schematic representation of the compression experiment. *Center:* Double network hydrogel with acriflavine compressed between two plates (red lines), before fracture. *Right:* Same sample while breaking, showing signal. Scale bar is 2 mm.

With this success, we then tried to realize stretch experiments on the Ni^{2+} or Zn^{2+} dual-crosslink hydrogels. It is noteworthy that the Ni^{2+} ions, when complexed by water, absorb light at around 400 nm and might then decrease the signal received from the excited moiety of broken dioxetane. Zn^{2+} ions, however, do not absorb at this wavelength (see Annexes). We used a notched sample of Zn^{2+} dual-crosslink hydrogel, with the chemical network presented in Table 7.1 and acriflavine as a FRET agent, and stretched it until complete propagation of the fracture. Sadly, no light emission from the material was observed during this experiment. Our interpretation is that the bond breaking in this hydrogel is very low or concentrated in a small zone around the crack. We tried to observe light emission in a relatively broad zone of the material, implying a need to be quite far from the sample (around 50 cm). This decreases the amount of photons detected by the EMCCD camera. Moreover, a discussion with Yulan Chen led us to conclude that the presence of a solvent in the material drastically decreases the amount of photons detected by the EMCCD camera when a sample breaks (maybe linked to aggregation-induced quenching [6,18]).

The use of this (otherwise particularly interesting) mechanophore requires a more carefully controlled chemistry, and a better knowledge of where to look for the bond breakage.

7.3. Anthracene Diels-Alder adduct as a crosslinker

The π -extended anthracene mechanophore, developed by R. Göstl and R. Sijbesma [19], allows an easier analysis of bond breakage. Upon applying force on this mechanophore, a retro Diels-Alder reaction is triggered, releasing a 9π -extended anthracene as a fluorophore. This mechanophore was incorporated in different polyacrylate networks, and its fluorescence was activated by compression or ultrasounds. This mechanophore molecule is preferred for an easier study of the crack propagation compared to the dioxetane mechanophore, since its fluorescence remains active after the propagation of the crack.

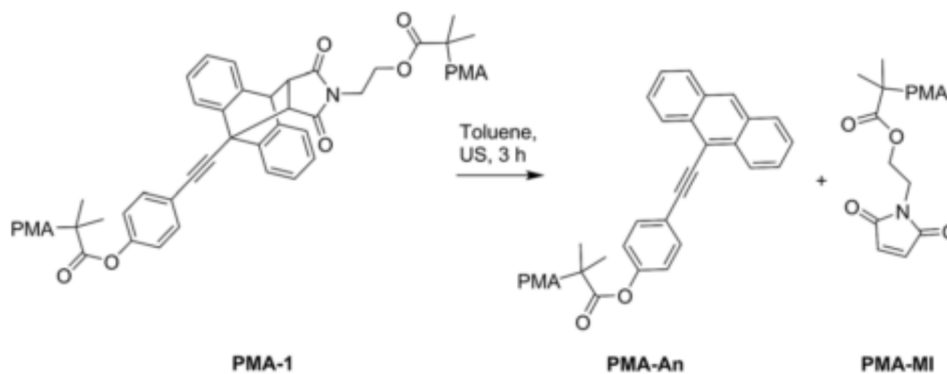


Figure 7.7: Mechanically induced retro Diels-Alder reaction on π -extended anthracene mechanophore. *Figure reprinted from [19]*

The results of the spectroscopy show a high quantum yield for the mechanophore, and a particularly good stability at ambient conditions of temperature and dioxygen. This mechanophore appears as an ideal probe for bond scission and post-mortem observations.

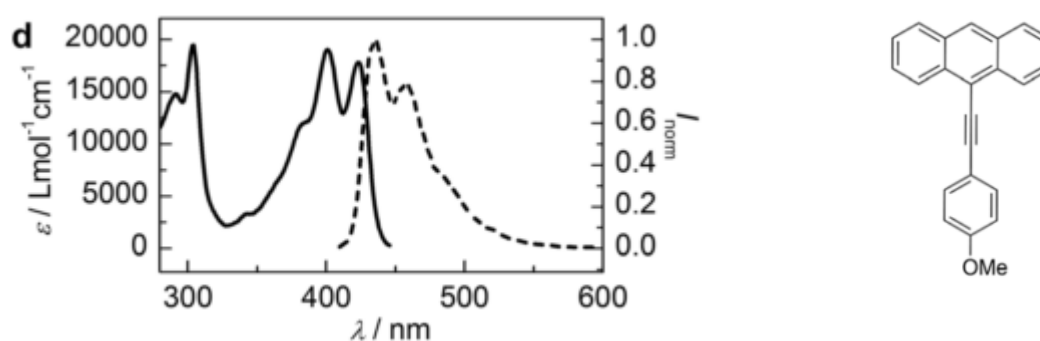


Figure 7.8: *Left:* UV-visible absorption (full line) and normalized fluorescence (dotted line) spectra of the π -extended anthracene. *Right:* reference fluorescent π -extended anthracene. *Figure reprinted from [19]*

J. Slotman et al. introduced this mechanophore as a crosslinker in a single network of poly(methylacrylate) or poly(ethylacrylate), demonstrating that bond scission accounts for a large part of energy dissipation at the crack tip of a visco-elastic material [3,4].

Stratigaki et al. [20] successfully introduced this mechanophore in a chemically crosslinked hydrogel. The observations give similar insights into the fracture of a hydrogel than what Matsuda et al. [10] developed, while it has certain advantages such as facility of use. Indeed, the technique developed by Matsuda et al. requires the breaking of the hydrogel under an inert argon (or N_2) atmosphere, so that the radicals created by bond breakage can initiate a free radical polymerization with the NIPAM monomers present in the feed. Here, simple bond breakage induces the fluorescence of the molecule.

7.3.1. Synthesis of the mechanophore

In our laboratory, J. Slotman and G.E. Sanoja synthesized the crosslinker, following the procedure presented in Figure 7.9.

7. Mapping the damage in dual-crosslink hydrogels with mechanophores

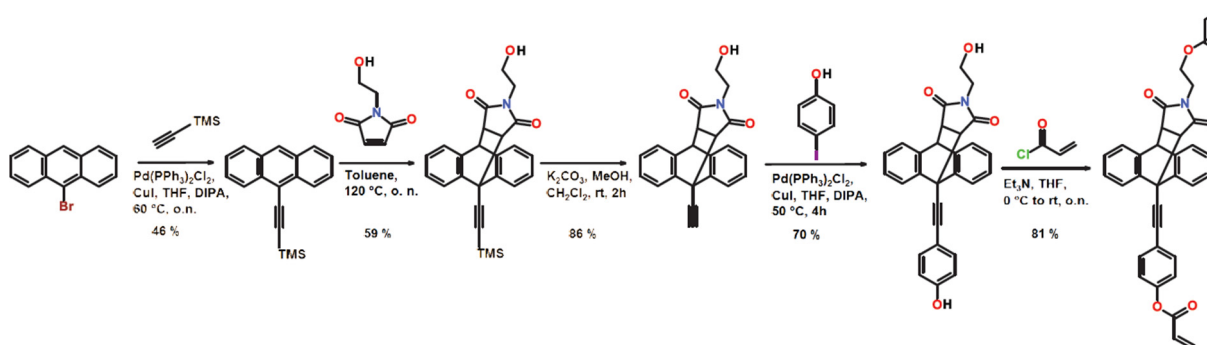


Figure 7.9: Synthesis path of the Diels-Alder adduct of π -extended anthracene, used as a crosslinker. Figure reprinted from [4]

7.3.2. Synthesis of the chemical network with mechanophore

The problem with this mechanophore is the same as for the dioxetane: it is insoluble in water. To solve this issue, Stratigaki et al. had the idea to realize the synthesis of the network in an organic solvent (dioxane in this case). They dried the obtained organogel and finally swelled it in the desired amount of water.

We applied this approach to our P(AAm-co-VIm) hydrogel, using the same synthesis as presented in Chapter 2 (part 1), replacing the water by the same volume of dioxane. The obtained gel was opaque (see Figure 7.10), implying a phase separation inside the gel.

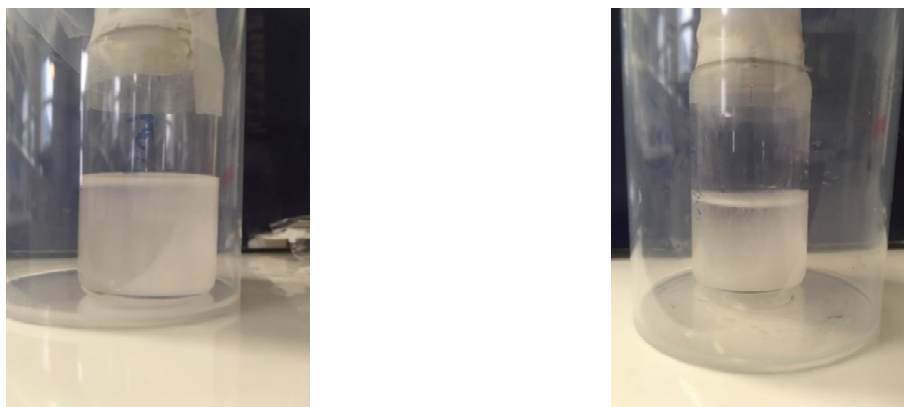


Figure 7.10: Formulation presented in Chapter II, with dioxane (left) or DMF (right) instead of water.

This is due to the very low solubility of polyacrylamide in dioxane, or in any organic solvent as the following experiments demonstrated (Figure 7.10 showing another example obtained replacing water by DMF). To achieve the integration of mechanophore in the network, we envisaged two solutions:

- Replacing the acrylamide monomer by a monomer such as dimethylacrylamide, the polymer of which is soluble in organic solvents;
- Realizing the synthesis in a hybrid solvent, using a mixture of water and organic solvent.

We chose the second method which was easier to implement, with less modifications of the chemical gel structure. The mixture of solvents should help solubilize the mechanophore (whose concentration is very low), while keeping the solubility of polyacrylamide in the solvent.

After multiple tests, a mixture of 50%DMF/50%water gave the best results. I obtained a transparent hydrogel, slightly less crosslinked than the reference chemical hydrogel but still close in properties.

The complete formulation is presented in Table 7.2. In order to obtain mechanical properties as close as possible to the reference chemical gel, we had to increase the amount of crosslinker in the network.

Again, the mechanophore represents 20% of the total concentration in crosslinker. The couple KPS/TEMED did not work efficiently in the hybrid solvent; I replaced it by VA-044 (presented in Chapter 5). This also avoided any undesirable interaction between the very oxidative KPS and the mechanophore.

Table 7.2 Formulation of the chemical network containing the π -extended anthracene mechanophore.
*weight percentage of solvent in the hydrogel.

	Molar mass (g/mol)	Specific gravity (g/mL)	Objective (mol %)	Concentration (mol/L)
AAm	71.1	-	90%	1.8
VIm	94.1	1.039	10%	0.2
MBA	154.2	-	0.2%	0.004
Mechanophore	-	-	0.05%	0.001
VA-044	270.3	-	0.3%	0.006
Water	-	-	42.5%*	-
DMF	-	-	42.5%*	-

The rheology of the obtained chemical gel is shown in Figure 7.11. Both moduli were found slightly higher than those for the gel synthesized in water, the behavior being acceptably similar. The mechanical response in tension of both chemical hydrogels is also presented in the same figure. The elastic modulus was the same for each gel. Interestingly the maximal stretch was greatly increased for the gel synthesized in the hybrid solvent. This might imply a better homogeneity in the chemical network, potentially linked to the change in initiator.

This increase in stretch at break will of course modify the properties in fracture of the subsequent dual-crosslink hydrogel. However, the trend in visco-elasticity and fracture properties should follow the same dynamics as the “classical” dual-crosslinked hydrogel, since the chemical crosslinks should not have any influence on the dynamics of the physical crosslinks (as shown in Chapter 2 part 3, and in [21]).

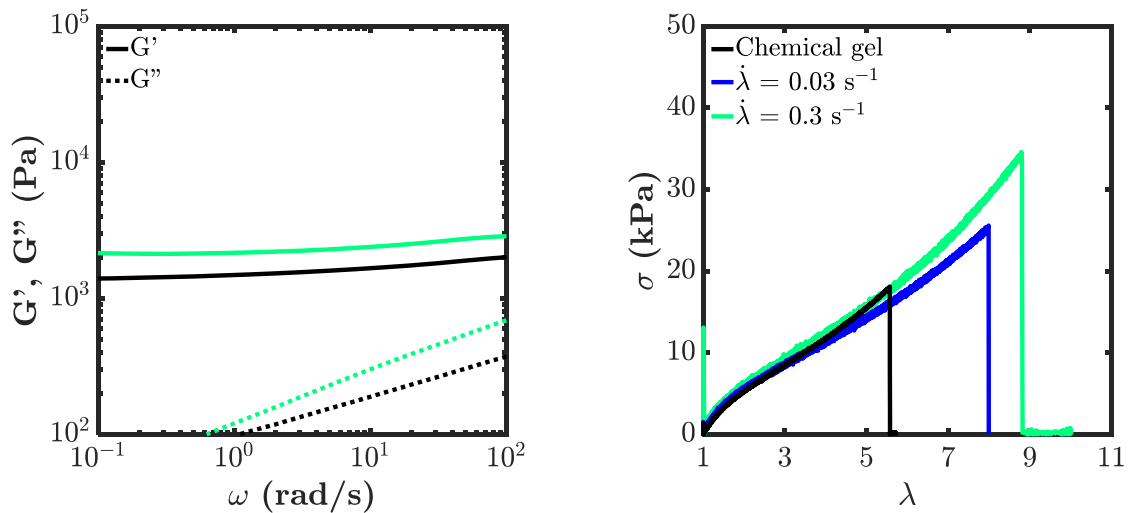


Figure 7.11: Left: elastic and loss moduli vs frequency, for the reference chemical gel (black) and the chemical gel synthesized in a hybrid solvent (green). Right: Stress-strain curve of a tensile test, for the reference chemical gel (black) and the chemical gel synthesized in a hybrid solvent (blue and green).

7.3.3. Mechanical properties of the dual-crosslinked hydrogel with mechanophores

The tensile properties of the P(AAm-co-VIm) dual-crosslinked hydrogel with Ni^{2+} ions are shown in Figure 7.12, along with the properties of the “classical” dual-crosslink hydrogel with Ni^{2+} ions without mechanophore.

The chemical hydrogel with mechanophore was more extensible than the reference with no mechanophore (stretch at break of 9 instead of 5.5). This increased extensibility was observable on the dual-crosslinked hydrogel with mechanophore, whose extensibility improved up to $\lambda = 13$ at $\dot{\lambda} = 0.3 \text{ s}^{-1}$, instead of 11 for the dual-crosslink hydrogel without mechanophore. This difference of 2 in maximal stretch is observable in all the stretch-rates studied here. Apart from that increase in maximal stretch, both dual-crosslink gels exhibited a very similar behavior at $\dot{\lambda} = 2 \text{ s}^{-1}$. At lower stretch-rates, the gel with mechanophore is less stiff than the standard one, with a less pronounced strain-hardening. The dual-crosslink hydrogel with mechanophores seems more homogeneous than the one obtained from the reference formula. This more homogeneous population of chain lengths might then provoke this clearer transition between non strain-hardening and strain-hardening regimes.

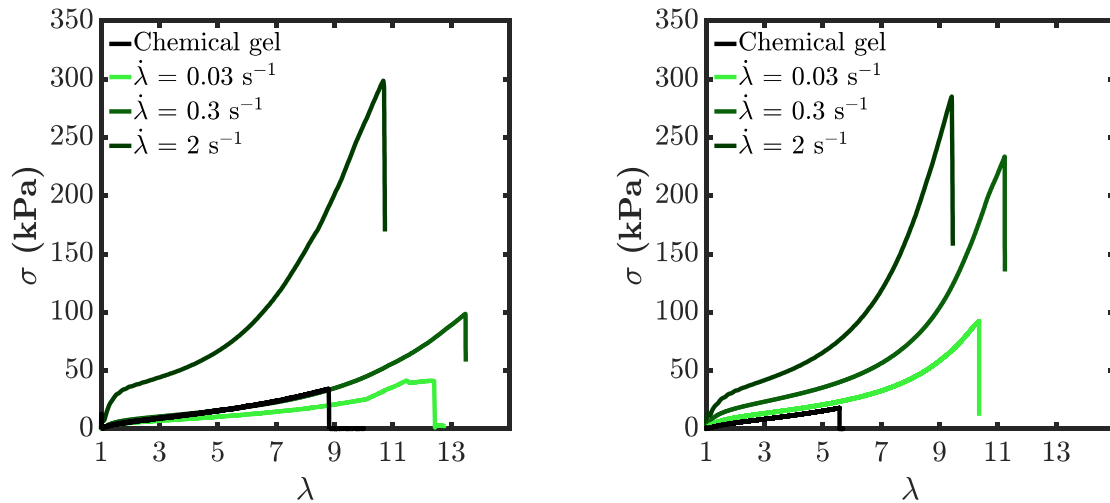


Figure 7.12: Stress-stretch curves for a Ni^{2+} dual-crosslinked gel with (left) and without (right) mechanophore crosslinker, at different stretch-rates, along with the stress-stretch curve of the corresponding reference chemical gel (black).

Figure 7.13 shows the results of tensile tests on notched samples of M^{2+} dual-crosslink hydrogels with and without mechanophores. The critical stretch at which the crack starts to propagate from the notch and the corresponding value of fracture energy Γ are plotted. At all the stretch rates tested, the extensibility of the Ni^{2+} dual-crosslink hydrogel was found higher than that of the gel without mechanophore. However, we did not find this difference with the gels of Zn^{2+} . The fracture energies of both dual-crosslink hydrogels with and without mechanophore were found almost identical (only two stretch-rates were studied with this Zn^{2+} dual-crosslink hydrogel, $\dot{\lambda} = 0.003 \text{ s}^{-1}$ and $\dot{\lambda} = 2 \text{ s}^{-1}$).

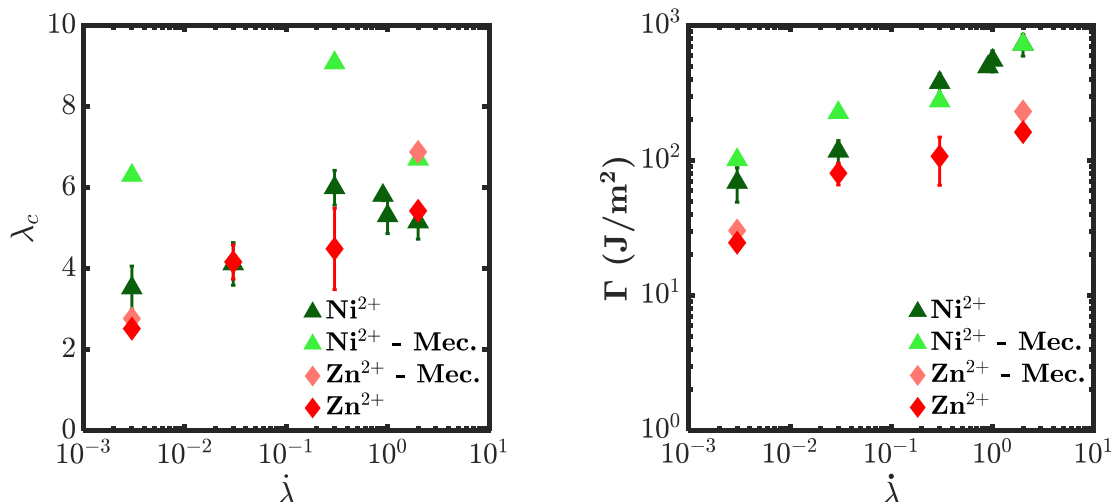


Figure 7.13: Critical stretch (left) and energy (right) at which a fracture propagates in the sample, for dual-crosslink gels with (labelled ‘Mec.’) and without mechanophore as crosslinker.

Figure 7.14 shows the velocity of the crack propagation in the sample. Here, we see some clear differences between the Ni^{2+} dual-crosslink hydrogels with and without mechanophore. The dual crosslink gels with mechanophore showed a slower crack propagation velocity, for both Ni^{2+} and Zn^{2+} .

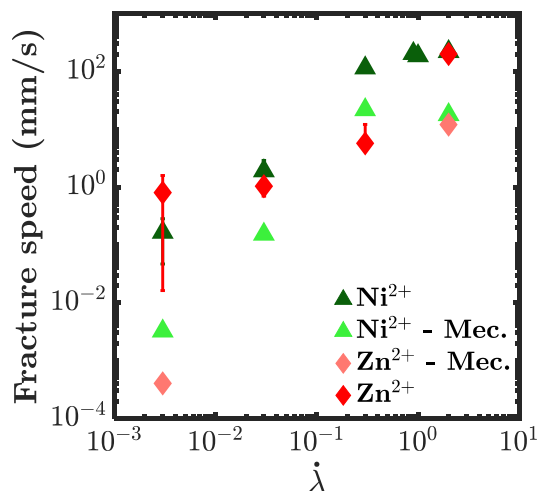


Figure 7.14: Crack propagation velocity versus the stretch-rate.

In summary, the synthesis of the dual crosslink gels with mechanophores in the DMF:H₂O mixed solvent results in some changes in the chemical network structure, compared to the synthesis in water previously studied, probably due to the different initiator used. However, the evolution with stretch-rate of the fracture properties of both types of hydrogels is practically identical, only the absolute value changes. This important result implies that the dynamic was not modified by the change in synthesis. The dynamics of these dual-crosslink networks with mechanophores are the same as the ones studied in the previous chapters, and we will use the lifetimes we found in fracture experiments in the previous chapter.

7.3.4. Imaging the fracture front

a. Tensile tests on notched samples

Tensile tests were performed on notched samples of M^{2+} dual-crosslink hydrogels with mechanophores. Figure 7.15 shows a schematic representation of this experiment. After stretching to rupture, the region

7. Mapping the damage in dual-crosslink hydrogels with mechanophores

near the crack front, or the created interface, of the sample was then imaged under a confocal microscope (the region of interest is also shown in Figure 7.15).

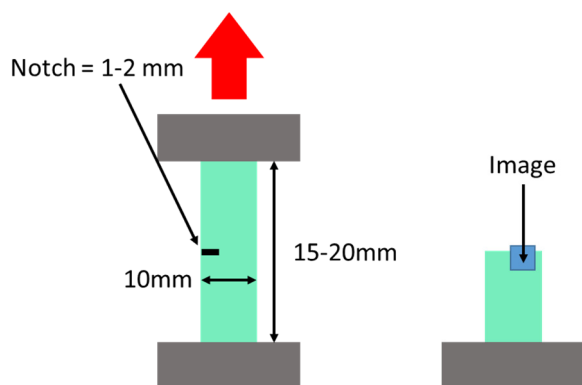


Figure 7.15: *Left:* Schematic representation of a single-edge notch fracture experiment; the red arrow represents the stretching direction. *Right:* Zone where images are taken in the confocal microscope.

Figure 7.16 shows the results of these fracture experiments (fracture stretch, fracture energy and propagation velocity) versus the Weissenberg number. This number was here computed using the shift factors found in the previous chapter for the fracture of dual-crosslink hydrogels with Ni^{2+} or Zn^{2+} ions. The superposition of these points was good, despite the limited number of data points (especially for the Zn^{2+} dual-crosslink hydrogel).

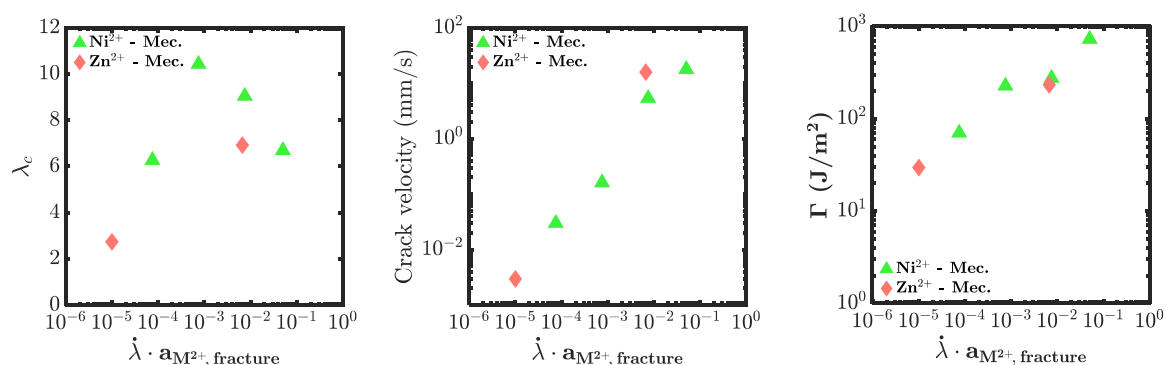


Figure 7.16: Critical stretch, fracture velocity and fracture energy vs $\dot{\lambda}$, shifted by the values of τ for fracture found in Chapter 6.

b. Confocal imaging – Method

The crack front was imaged under a confocal microscope. The observations are always made as presented in Figure 7.15, in a plane orthogonal to the crack plane. The confocal microscope sends a laser light at 405 nm, which activates the fluorescence of the π -extended mechanophore. The laser beam is focused through an objective lens and directed at the sample (see Figure 7.17). The excited fluorochrome molecule reemits light at a different wavelength. The detector records signal between 450 and 500 nm, allowing for a maximal detection of the fluorescence of the activated mechanophore.

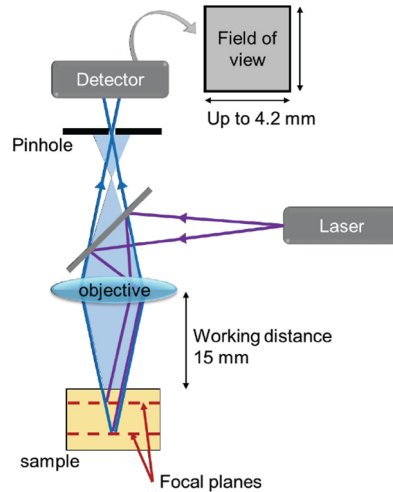


Figure 7.17: Schematic representation of a laser scanning confocal microscope (or macroscope) working principle.

Two different confocal microscopes were used during this project:

- a Nikon AZ-100/C2+ Laser Scanning Confocal Macroscope, with an AZ Plan Fluor 5x (focal length of 15 mm). Magnifications from 1x to 8x were available, by increments of 0.1x;
- a Leica Laser Scanning Confocal Microscope SP8, with magnifications of 10x, 20x, 40x and 63x (with working distances ranging from 11mm to 140 μm).

The macroscope allows for a larger field of view and a longer working distance, while it gives a lower resolution than the microscope. The results shown here were obtained on the microscope, since (as we will see) the size of the damage in the hydrogel is very small.

The images were made at a depth of 100 μm under the surface of the material, to avoid the artifacts created by dust particles. In order to keep the hydrogel hydrated, the samples were placed in their solution (MCl_2/NaCl) during imaging.

A typical image (here, the surface of the material) is presented in Figure 7.18. The blue part on the bottom is the material and the black part with no signal is out of the sample. The illumination seen on this image is the standard level of illumination in the material. This illumination is not homogeneous on the sample here, which is linked to the width of the field of view in this image. We can also see some brighter spots, which are attributed to dust particles stuck on the surface of the material.

7. Mapping the damage in dual-crosslink hydrogels with mechanophores

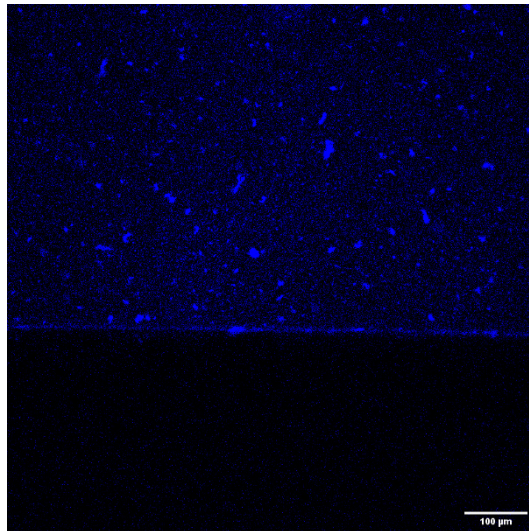
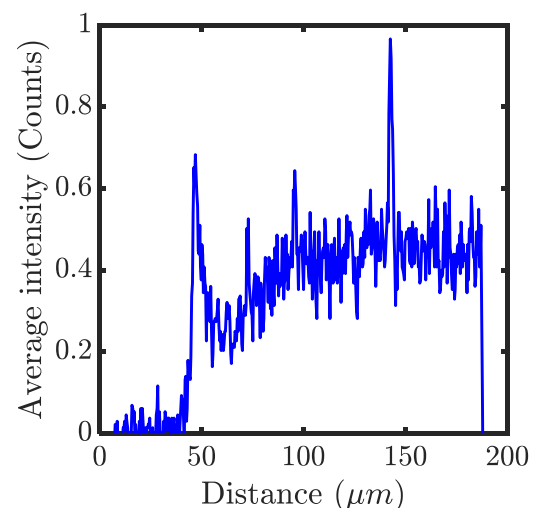
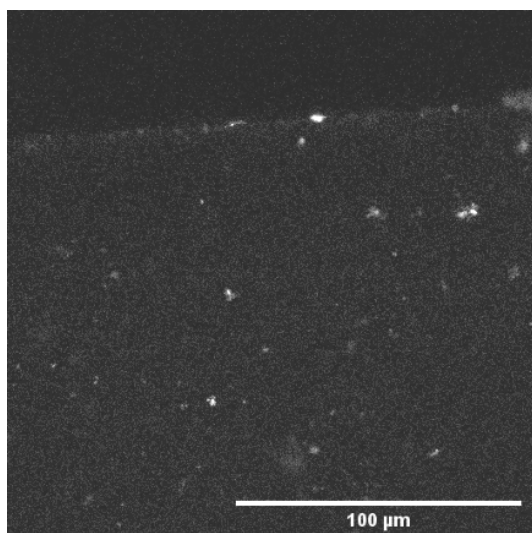


Figure 7.18: Image of a fracture front – surface of the material. Scale bar is 100 μm .

c. Results and discussion

The samples previously tested were imaged under the confocal microscope, with a 63x objective. The results for a Ni^{2+} dual-crosslink hydrogel at different stretch-rates are shown in Figure 7.19. We can notice that light intensity from the sample was homogeneous, except for (1) many bright spots randomly distributed all over the sample, which we attribute again to the auto-fluorescence from particles or dust contaminating the samples during preparation, and (2) the crack front exhibiting a clear bright line. This result suggests that there is some damage localized very close to the crack plane. The image obtained for $\dot{\lambda} = 2 \text{ s}^{-1}$ shows also artifacts at the interface, attributed to bubbles.

The curves on the right represent the average intensity found on a line perpendicular to the crack front. This average was computed on a region with no artifacts such as dust particles or bubbles. The results confirm a fluorescence on the front of the crack. The breaking of bonds when the fracture propagates is then very localized around the crack tip, in a damage zone no wider than a few micrometers.



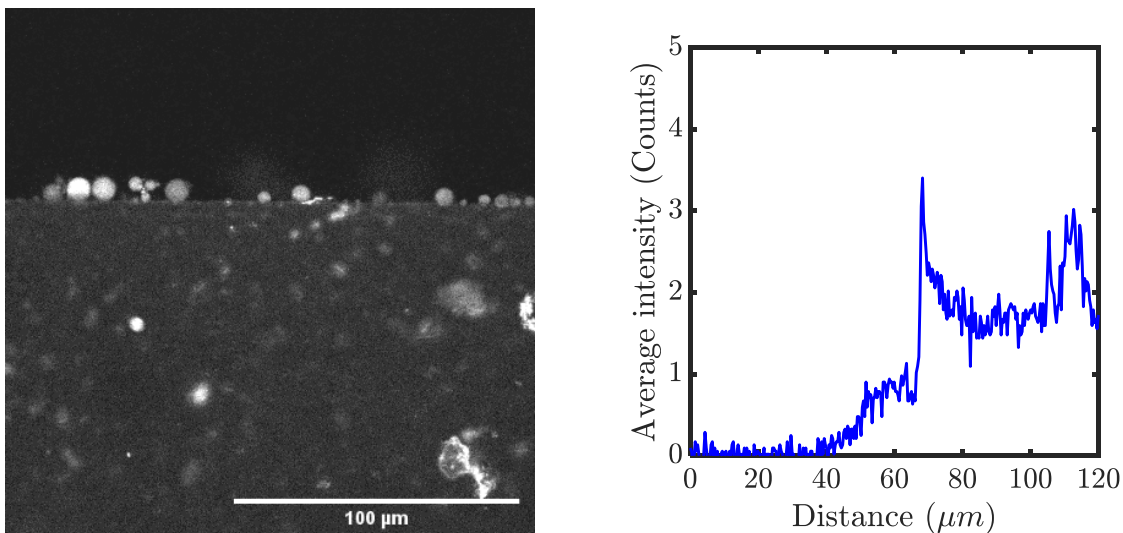
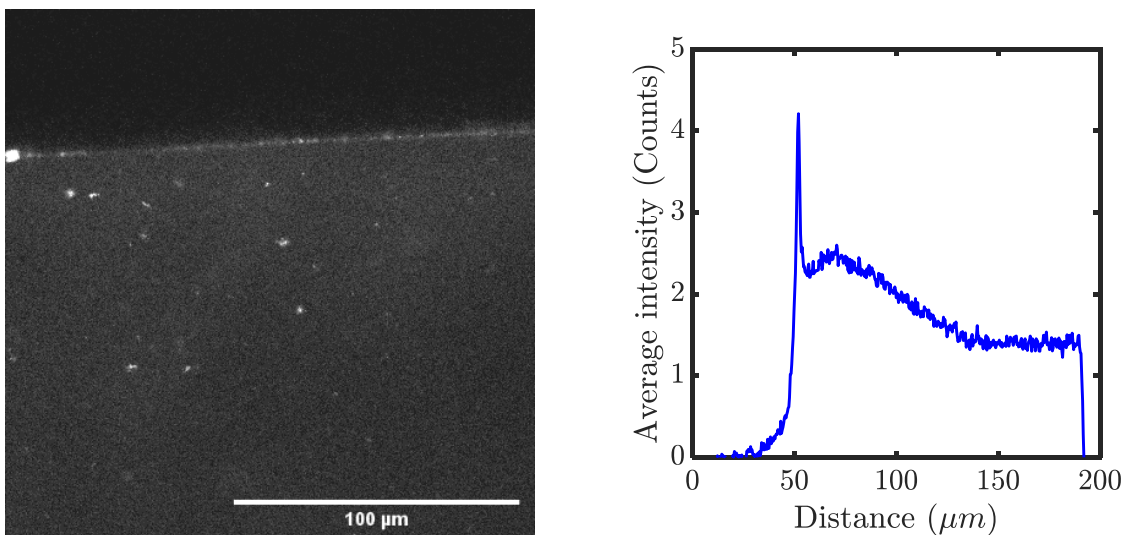


Figure 7.19: Left: Fracture front of a Ni^{2+} dual-crosslink hydrogel stretched at $\dot{\lambda} = 0.03 \text{ s}^{-1}$ (top) and 2 s^{-1} (bottom). Right: Averaged fluorescence intensity vs distance, from the images on the left.

The same imaging was realized on samples of Zn^{2+} dual-crosslink hydrogel at two different stretch-rates. The images are clearer here, with less dust particles. The laser intensity used to image those samples was lower than that used for the Ni^{2+} dual-crosslink hydrogels. This can be explained by the fact that Ni^{2+} absorbs light at around 400 nm, hence absorbing the excitation laser light. A higher intensity is needed to reach the fluorescent molecule, whose concentration is at best 100 times lower than the free Ni^{2+} in solution. Since Zn^{2+} in water does not absorb at 405 nm, images with a high signal-to-noise ratio were obtained for the dual-crosslink hydrogels. The averaged intensities show clearly an activation close to the crack front, just as for the Ni^{2+} dual-crosslink hydrogel.



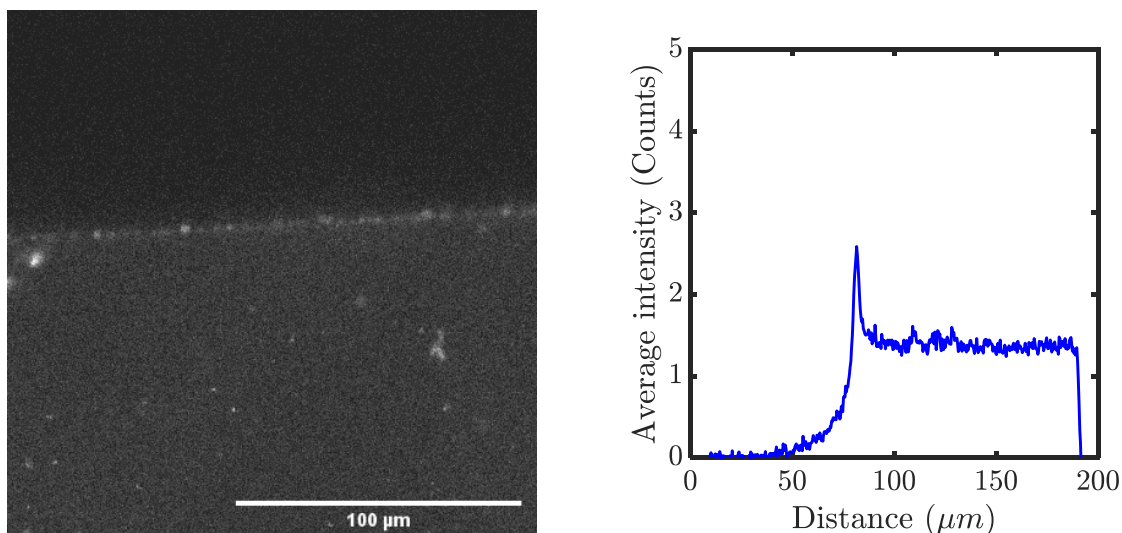


Figure 7.20: Left: Fracture front of a Zn^{2+} dual-crosslink hydrogel stretched at $\dot{\lambda} = 0.003 \text{ s}^{-1}$ (top) and 2 s^{-1} (bottom). Right: Averaged fluorescence intensity vs distance, from the images on the left.

The intensities between the two hydrogels cannot be compared, since the laser intensity used was different. While we compared the length of the damage zone which was estimated as schematically presented in Figure 7.21.

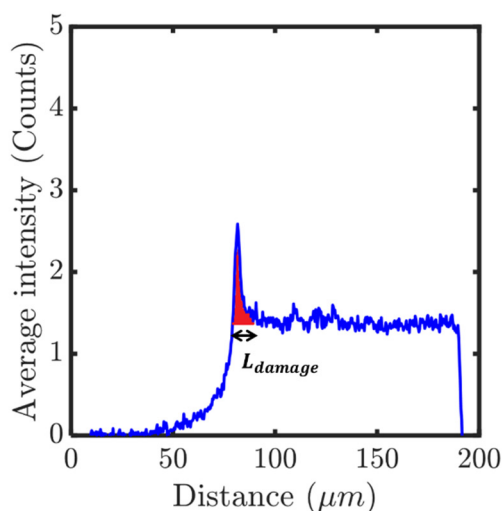


Figure 7.21: Measure of the size of the damage zone

In order to correlate the damage zone size with the dynamics of the dual crosslink gels, in Figure 7.22 this characteristic length of damage was plotted against the Weissenberg number (using the shift factors of the fracture tests shown in Chapter 6 and the Ni^{2+} as reference). This length showed a peak around $\dot{\lambda}\tau \sim 10^{-3} - 10^{-2}$, increasing from 4 to 9 μm , and then decreasing again to 5 μm at higher stretches. It is interesting to note that this width of damage follows the stretch at which the fracture starts to propagate (plotted again in Figure 7.22 for comparison purposes). This result implies that bond breakage during the propagation of a fracture is linked to the level of stretch at which the chains are when the fracture propagates.

The peak of damage zone width does not correspond to a peak in fracture energy, suggesting that the fracture energy does not directly control the size of the bond breakage zone in the propagation of a crack.

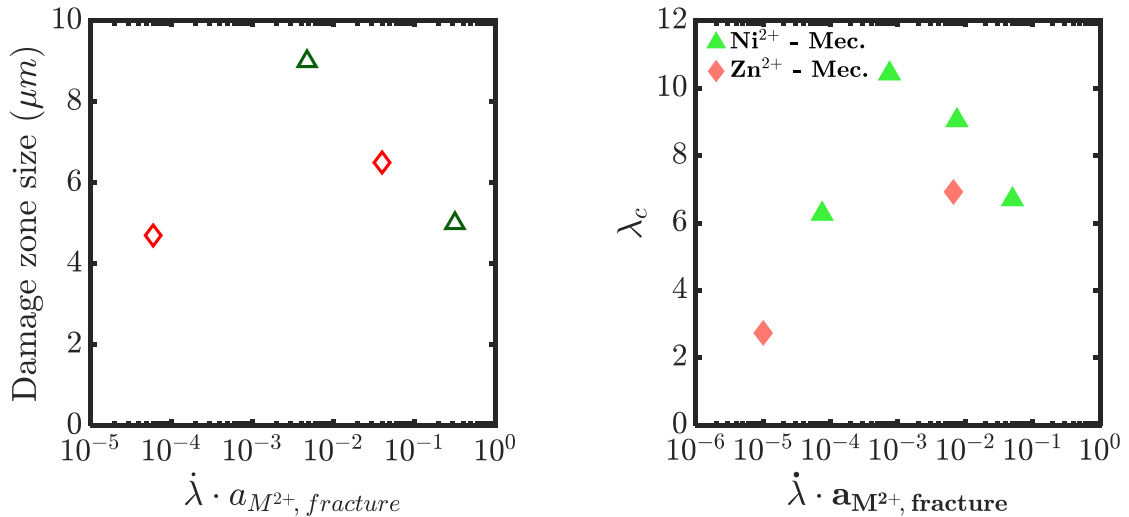
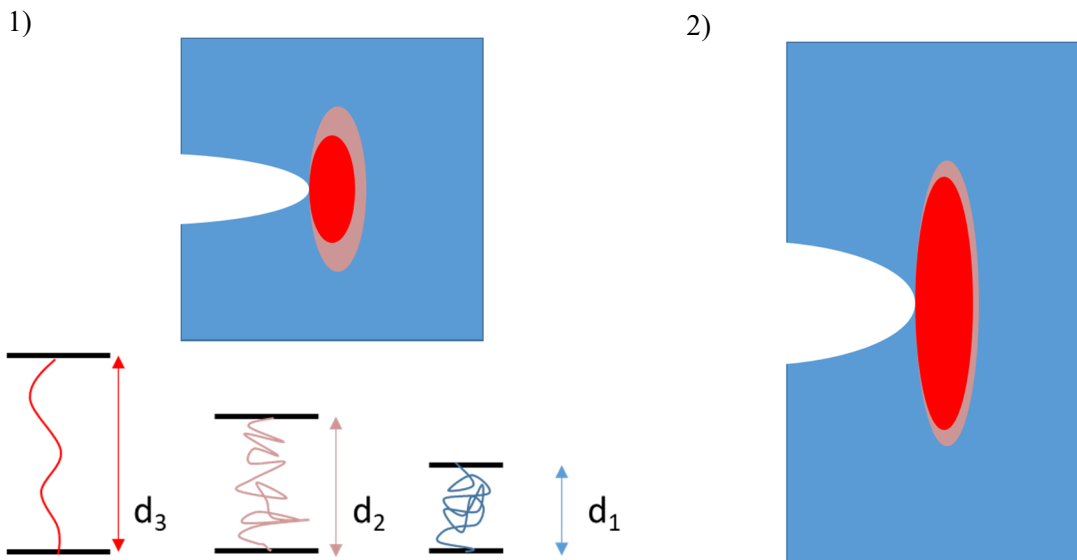


Figure 7.22: *Left:* Size of the damage zone measured on confocal images from Figure 7.19 and Figure 7.20, versus the Weissenberg number of the experiment. *Right:* Critical stretch at which the fracture starts to propagate in a notched sample of dual-crosslink hydrogel, versus the Weissenberg number of the experiment. The values of τ are taken from the previous chapter.

At a Weissenberg number of $\dot{\lambda}\tau = 4 \times 10^{-3}$, when a crack starts to propagate, the stretch is quite high (around 10). The polymer chains are highly stretched. When λ_c is reached and the first polymer chains break, their charge is transferred to their neighbors. Those neighbors are consequently stretched further, until they break.

At a lower (or higher) Weissenberg number, the polymer chains are less stretched when the crack starts to propagate. So, when the first polymer chain breaks and transfers its charge to its neighbors, those neighbors must first be stretched up to the same stretch as in the case where $\dot{\lambda}\tau = 4 \times 10^{-3}$, and then be stretched until they break. This decreases the ease with which polymer chains are broken, and hence the size of the damage zone.

This can also be explained in terms of probability of fracture. The probability of breaking of a polymer chain increases with the stretch of this chain. In a material that is more stretched, particularly at the crack tip where stretches are much higher, the probability of observing bond breakage will be much higher, which explains the difference in the size of the damage zone we observe here.



7. Mapping the damage in dual-crosslink hydrogels with mechanophores

Figure 7.23: Schematic representation of the evolution of the chain extension at the crack tip at low stretch (1) and high stretch (2).

The energy dissipation does not control the length of the damage zone, but the critical stretch does. These results are similar to what J. Sloodman found on single network elastomers [3,4].

The study of the damage zone around a crack and its evolution with the parameters of the crack propagation has been studied in the literature, by different techniques than this one. Studies realized by Yu et al. [22] and Foyart et al. [23] on double-network hydrogels show a dependence of the length of the damage zone on the crack velocity. In both studies, the length of the damage zone either increased [22] or decreased [23] following the crack velocity. Foyart and coworkers attributed this change in behavior to the variation in the nature of the material studied (they were studying double self-assembled networks, while Yu and coworkers studied the double networks of Gong et al. [17]). Yu and coworkers also showed, in their double networks, a close relationship between the size of the damage zone and the fracture energy of the material.

We do not observe the same relationships here. As shown in Figure 7.24, the size of the damage zone follows quite well the stretch at which the crack propagates. The fracture energy does not seem to have any influence on this length, which can be rationalized by reminding that this fracture energy takes into account the viscoelastic energy dissipation, which is lifetime-dependent. The length we are observing is a characteristic of the covalent bond damage zone, and not necessarily the visco-elasticity.

The evolution of the width of damage zone with the crack velocity shows an increase up to 0.1 mm/s, then a decrease at higher velocities. This bell-shaped curve is also found when shifting this velocity with the lifetime of the physical bonds involved in each experiment.

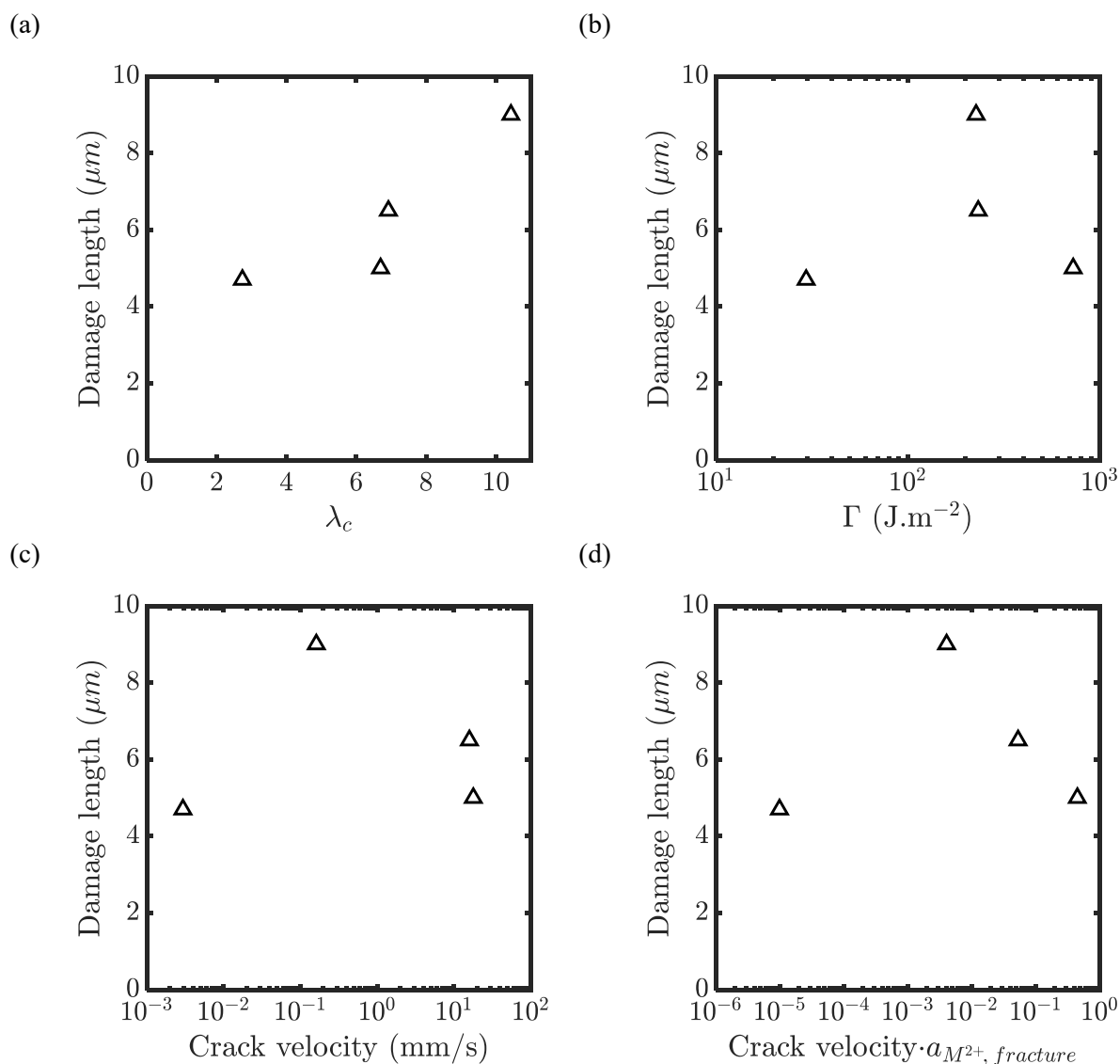


Figure 7.24: Damage zone width in μm , versus (a) the critical stretch λ_c , (b) the fracture energy Γ , (c) the crack velocity and (d) the shifted crack velocity

7.4. Conclusion and perspectives

Our objective in this chapter was to use mechanophores, in order to better characterize the bond scission mechanisms during the propagation of a crack in our dual-crosslink hydrogels. These results could then have been linked to our previous macroscopic results, to obtain a better understanding of how the physical bonds act to toughen the chemical network, delay the onset of fracture and change the propagation of the crack.

Our first trial, with the dioxetane derivative, was not a success. Many reasons might be invoked (chemistry was not perfectly controlled, optical set-up could be enhanced), but we believe now that the main reason for this (half) failure was the fact that we did not know exactly what to look for in those dual-crosslink hydrogels. With the knowledge we have now, that bond scission happens in a very localized region around the crack, we could maybe obtain better results.

We have successfully introduced, in the dual-crosslink hydrogel, a 9π -extended anthracene DA adduct crosslinker. This molecule, which becomes fluorescent once broken, was introduced as a chemical crosslinker. We have realized single edge notch tests on two dual-crosslink hydrogels (with Zn^{2+} and

7. Mapping the damage in dual-crosslink hydrogels with mechanophores

Ni²⁺ ions) containing this mechanophore. The results showed us a damage zone close to the crack tip, between 4 and 10 μm wide, where bond scission is detected. The size of this zone changed with the stretch-rate, following the exact same behavior as the critical stretch at which the fracture starts to propagate. The characteristic length of covalent bond scission around the crack tip is then controlled by the stretch at which the crack propagates.

The literature available on the size of a damage zone in hydrogels mentions a clear influence of the crack velocity on the length of the damage zone, whether an increase or a decrease. In our case, this length starts by increasing with the crack velocity, and then decreases after a certain value. The relationship between both parameters is however not clear. The influence of the bond scission on the fracture energy has also yet to be revealed in those dual-crosslink hydrogels – in the same manner as has been done on the double networks [4].

These experiments show great promise to the understanding of the bond breaking at the tip of a crack before and during propagation. However, more experiments are needed to improve this understanding:

- More experiments with this same set-up (single-edge notch tests) would confirm the first observations we have made here;
- A closer study of the tip of the crack would be interesting. As mentioned in the previous chapters, we suppose that the physical bonds delay the onset of the propagation by preventing the correlated fracture of polymer chains at the crack tip. The fracture of the chains remains uncorrelated until a certain fracture energy is available for the crack to propagate. The intensity of the uncorrelated breaking might vary with the Weissenberg number of the experiment;
- To differentiate the influences of the stretch and crack velocity on the damage zone, we could realize delayed-fracture experiments on dual-crosslink hydrogels with mechanophores. As seen clearly in the Zn²⁺ dual-crosslink hydrogels for example, the crack velocity changes during the propagation, realized at a fixed stretch λ . This would allow us to see how the damage evolves with both parameters;
- A calibration of the light intensity versus the number of broken bonds would also be interesting. In their investigations on elastomers, Slootman et al. [3,4] used a solution of linear polymers, in which they infused an activated version of the 9 π -extended anthracene at different concentrations, giving them a clear calibration curve. This is impossible here, since this activated calibration molecule is again insoluble in water. We could however obtain such a curve by heating our mechanophore-containing polymer. Indeed, heat has been used as an activation switch for our anthracene mechanophore. By drying and heating hydrogels with different mechanophore contents, and re-swelling them afterwards so that the observation media remains the same, we could create a calibration curve. This would allow us to study also the concentration of bond breakage along the crack, and its evolution with the Weissenberg number.

References

1. Ducrot, E., Chen, Y., Bulters, M., Sijbesma, R. P. & Creton, C. Toughening Elastomers with Sacrificial Bonds and Watching Them Break. *Science* 344, 186–189 (2014).
2. Millereau, P. et al. Mechanics of elastomeric molecular composites. *PNAS* 115, 9110–9115 (2018).
3. Slootman, J. et al. Quantifying and mapping covalent bond scission during elastomer fracture, arXiv.
4. Slootman, J. Quantitative detection of damage in soft materials using mechano-fluorescence. (2019).
5. Zhang, N. et al. Fluorescent Polymersomes with Aggregation-Induced Emission. *ACS Nano* 12, 4025–4035 (2018).
6. Mei, J., Leung, N. L. C., Kwok, R. T. K., Lam, J. W. Y. & Tang, B. Z. Aggregation-Induced Emission: Together We Shine, United We Soar! *Chem. Rev.* 115, 11718–11940 (2015).
7. Hu, R. et al. Twisted Intramolecular Charge Transfer and Aggregation-Induced Emission of BODIPY Derivatives. *J. Phys. Chem. C* 113, 15845–15853 (2009).
8. Hu, Y. et al. Making Hydrogels Stronger through Hydrophilicity-Hydrophobicity Transformation, Thermoresponsive Morphomechanics and Crack Multifurcation. <https://chemrxiv.org/> (2020)
9. Guo, H. et al. Thermoresponsive Toughening in LCST-Type Hydrogels with Opposite Topology: From Structure to Fracture Properties. *Macromolecules* 49, 4295–4306 (2016).
10. Matsuda, T., Kawakami, R., Nakajima, T. & Gong, J. P. Crack Tip Field of a Double-Network Gel: Visualization of Covalent Bond Scission through Mechanoradical Polymerization. *Macromolecules* [acs.macromol.0c01485](https://doi.org/10.1021/acs.macromol.0c01485) (2020) doi:10.1021/acs.macromol.0c01485.
11. Matsuda, T., Kawakami, R., Namba, R., Nakajima, T. & Gong, J. P. Mechanoresponsive self-growing hydrogels inspired by muscle training. *Science* 363, 504–508 (2019).
12. Yuan, Y., Yuan, W. & Chen, Y. Recent advances in mechanoluminescent polymers. *Sci. China Mater.* 59, 507–520 (2016).
13. Kopecky, K. R. & Mumford, C. Luminescence in the thermal decomposition of 3,3,4-trimethyl-1,2-dioxetane. *Can. J. Chem.* 47, 709–711 (1969).
14. Chen, Y. et al. Mechanically induced chemiluminescence from polymers incorporating a 1,2-dioxetane unit in the main chain. *Nature Chemistry* 4, 559–562 (2012).
15. Chen, Y. & Sijbesma, R. P. Dioxetanes as Mechanoluminescent Probes in Thermoplastic Elastomers. *Macromolecules* 47, 3797–3805 (2014).
16. Clough, J. M., Creton, C., Craig, S. L. & Sijbesma, R. P. Covalent Bond Scission in the Mullins Effect of a Filled Elastomer: Real-Time Visualization with Mechanoluminescence. *Advanced Functional Materials* 26, 9063–9074 (2016).
17. Gong, J. P., Katsuyama, Y., Kurokawa, T. & Osada, Y. Double-Network Hydrogels with Extremely High Mechanical Strength. *Adv. Mater.* 15, 1155–1158 (2003).
18. Förster, T. & Kasper, K. Ein Konzentrationsumschlag der Fluoreszenz des Pyrens. *Zeitschrift für Elektrochemie, Berichte der Bunsengesellschaft für physikalische Chemie* 59, 976–980 (1955).
19. Göstl, R. & Sijbesma, R. P. π -extended anthracenes as sensitive probes for mechanical stress. *Chem. Sci.* 7, 370–375 (2016).
20. Stratigaki, M. et al. Fractography of poly(N -isopropylacrylamide) hydrogel networks crosslinked with mechanofluorophores using confocal laser scanning microscopy. *Polymer Chemistry* (2019) doi:10.1039/C9PY00819E.
21. Zhao, J., Mayumi, K., Creton, C. & Narita, T. Rheological properties of tough hydrogels based on an associating polymer with permanent and transient crosslinks: Effects of crosslinking density. *Journal of Rheology* 61, 1371–1383 (2017).

7. Mapping the damage in dual-crosslink hydrogels with mechanophores

22. Yu, Q. M., Tanaka, Y., Furukawa, H., Kurokawa, T. & Gong, J. P. Direct Observation of Damage Zone around Crack Tips in Double-Network Gels. *Macromolecules* 42, 3852–3855 (2009).
23. Foyart, G., Liguore, C., Mora, S. & Ramos, L. Rearrangement Zone around a Crack Tip in a Double Self-Assembled Transient Network. *ACS Macro Lett.* 5, 1080–1083 (2016).

General Conclusion

General Conclusion

Previous works on dual-crosslink hydrogels had shown the importance of the lifetime of the transient bond introduced in the network on the mechanical properties of the material. Work on a PVA-borax dual-crosslink hydrogel, with a slow dynamics, had shown an embrittlement of the material with increasing stretch-rate, while work on a metal-ligand dual-crosslink hydrogel, with faster dynamics, had shown the opposite behavior. A unified vision of the evolution of these properties of fracture resistance of these hydrogels with dynamic bonds with the stretch-rate was tentatively established, with no clear success.

In this project, we extended the work on this metal-ligand dual-crosslink hydrogels in several different ways and opened new promising paths of analysis.

Preparation of dual-crosslink hydrogels with easily tunable dynamics and controlled microstructure

In order to prepare comparable dual-crosslink hydrogels, we developed a protocol to ensure that the only differences in the materials we study are linked to the lifetime of the transient bond introduced. To do so, we first synthesized a chemically crosslinked hydrogel, with ligand moieties on the polymer chain. The chemical hydrogel was then placed in a solution of metal ions, which diffuse inside the network and complex with the ligands, thus physically crosslinking the polymer chains. The lifetime of the transient bond depends only on the metal-ligand complexes considered. We have successfully used complexes of imidazole with Nickel(II), Zinc(II) and Copper(II) ions, along with complexes of terpyridine and Zinc(II) ions. Complexes of terpyridine with Nickel(II) ions gave materials too brittle to be handled and tested properly, while complexes of imidazole and Mercury(II) ions did not create physical crosslinks inside our network, the ions binding with only one ligand.

The four coordination complexes we used gave dual-crosslink hydrogels with quite different dynamics, which could be scaled as:



Absorption isotherms realized on the 4 different dual-crosslink hydrogels showed different metal uptakes during the infusion of the chemical network by metal ions. While VIm-Ni^{2+} and VIm-Cu^{2+} dual-crosslink hydrogels followed the same absorption profile, with a maximal number of bis-complexes of $[\text{NiIm}_2]^{2+}$ estimated at around 45 mmol/L (along with 45 mmol/L of mono-complexes of $[\text{NiIm}]^{2+}$), the Terpy-Zn^{2+} dual-crosslink hydrogel showed evidence of a higher number of physical crosslinks, closer to 100 mmol/L.

The dynamics of the dual-crosslink hydrogels with VIm-Ni^{2+} crosslinks were studied in detail, by linear rheology and dynamic light scattering experiments. Two different dynamics were clearly seen in this network. A first, fast dynamic was attributed to the lifetime of the physical bonds introduced in the network. The second (and slower) dynamic mode was linked to clusters of physical bonds, the presence of which was proved by realizing small-angle X-ray scattering experiments. Those clusters were also found in a VIm-Zn^{2+} dual-crosslink hydrogel in higher numbers than in the VIm-Ni^{2+} dual-crosslink hydrogel. This difference in number density is explained by an energetic consideration. VIm-Zn^{2+} complexes have a low enthalpy of formation, which makes the increase in entropy linked to the clustering of physical bonds dominant; on the contrary, VIm-Ni^{2+} exhibit a higher enthalpy of formation, which decreases the relative importance of the clustering of physical bonds, and makes those bonds

more randomly distributed along the network. In both dual-crosslink hydrogels, we could extract from the SAXS experiments two length-scales, 3 nm and 16 nm, which corresponded respectively to the correlation length of the polymer chains measured in DLS and to the mesh size of the chemical network extracted from rheology. The physical bonds are organized in two families, one of clusters close to the chemical crosslinks, and one of randomly distributed bonds.

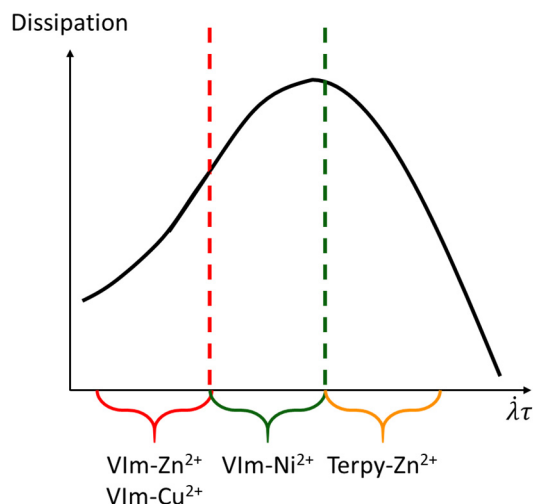


Figure 1: Schematic energy dissipation versus the Weissenberg number, for the different dual-crosslink hydrogels.

A unified behavior of the metal-ligand dual-crosslink hydrogel, controlled by this metal-ligand dynamic

We have compared the behavior of each dual-crosslink hydrogel in large deformations, using the VIm-Ni²⁺ dual-crosslink hydrogel as a reference.

This reference dual-crosslink hydrogel showed a clear increase of stretch at break compared to the bare chemical gel. Its mechanical properties in large deformations (elastic modulus, energy dissipation...) increased clearly with the deformation rate applied to the material. Its fracture resistance properties followed the same trend.

Following our observations on the lifetimes of the physical bonds, the VIm-Zn²⁺ and VIm-Cu²⁺ dual-crosslink hydrogels showed properties characteristic of a softer material, with lower moduli and fracture energy, and a less pronounced strain-hardening behavior. All those parameters still increased with the stretch-rate. At the other end of the dynamics spectra, the terpy-Zn²⁺ dual-crosslink hydrogel showed a clear embrittlement with increasing stretch-rate; the elastic modulus increased with the stretch rate, while the stretch at break and fracture energy decreased.

Each of the parameters we determined from our experiments could be superposed in a master curve when plotted versus the shifted stretch-rate. In linear rheology, the inverse of the frequency at which the loss modulus shows a peak was taken as shift factor, and was taken as directly representative of the lifetime of the physical bond. In large deformations, the shift factor was determined empirically to obtain the best master curve. These shift factors should then be representative of the type of dynamics in the dual-crosslink hydrogel that dominate the behavior in large deformations. Such an empirical way to build master curves cannot provide a characteristic time in absolute terms. However it gives information

General Conclusion

on the rate dependence of the leading dynamic process that controls the behavior. In fracture experiments, another set of shift factors was empirically determined, based on superposing the critical stretch at which a pre-existing crack starts to propagate. In both cases a reasonable master curve, and hence a generic behavior, was observed. However the difference between the shift factors observed in large deformations and those in fracture experiments was significant. The range of dynamics reached in fracture was shrunk by at least a decade compared to what was achievable in tensile tests. This particular observation might be linked to a shift in the origin of the most relevant dynamic of the dual-crosslink hydrogels in fracture. At the high stretches and stresses considered at the tip of a crack, the physical bonds will become much too fast. Their influence might then become invisible, and the behavior of the crack would be influenced by the clusters of physical bonds, which lifetime is also decreased by the stresses applied to the material.

These master curves allowed us to establish how the behavior of a dual-crosslink hydrogel evolves with the stretch-rate.

Low Weissenberg number ($\leq 10^{-4}$ in tensile tests, $\leq 10^{-3}$ in fracture)

At low normalized stretch-rates, or Weissenberg number, the observation time of the experiment is much longer than the exchange time of the physical crosslink. The physical bonds are mechanically invisible upon loading the sample. The Young's modulus is close to that of the bare chemical gel, since few or no stretched polymer chain is added by the existence of physical crosslinks. The strain-hardening behavior is related only to the chemical network, and does not vary with the stretch-rate.

The energy dissipated in this situation should be negligible. However, this is not the case. Even at those low Weissenberg numbers, at least 10% of the energy brought to the network was dissipated. This dissipation was linked to the existence of clusters of physical crosslinks. Those clusters have no influence on the Young's modulus, for they are too low in number.

The fracture properties of the dual-crosslink hydrogel are however greatly enhanced compared to those of the bare chemical gel. The stretch-at-break is doubled, just as the onset of propagation of a crack and the fracture energy. These observations lead us to hypothesize another mechanism of protection of the chemical network:

- (1) When a chemical bond breaks in the network, it relaxes fast to its random coil conformation. This movement stretches the neighboring chains (Figure 2, 1.A), at a rate which is unknown but certainly fast and uncorrelated to the stretch-rate imposed to the material;
- (2) In the bare chemical hydrogel, this leads to the breaking of the neighboring chains (Figure 2, 1.B). This correlated breaking of chains will nucleate a crack in the material, which will propagate catastrophically;
- (3) In the dual-crosslink hydrogel, the physical bonds maybe invisible during loading but are still present and are visible during the fast relaxation of the broken chain (Figure 2, 2.A). They are able to dissipate the energy transferred by this broken covalent chain, by homogenizing the stresses in the network, hence protecting the neighboring covalent bonds. The correlated breaking of the polymer chains is delayed, and the network breaks at higher stretches.

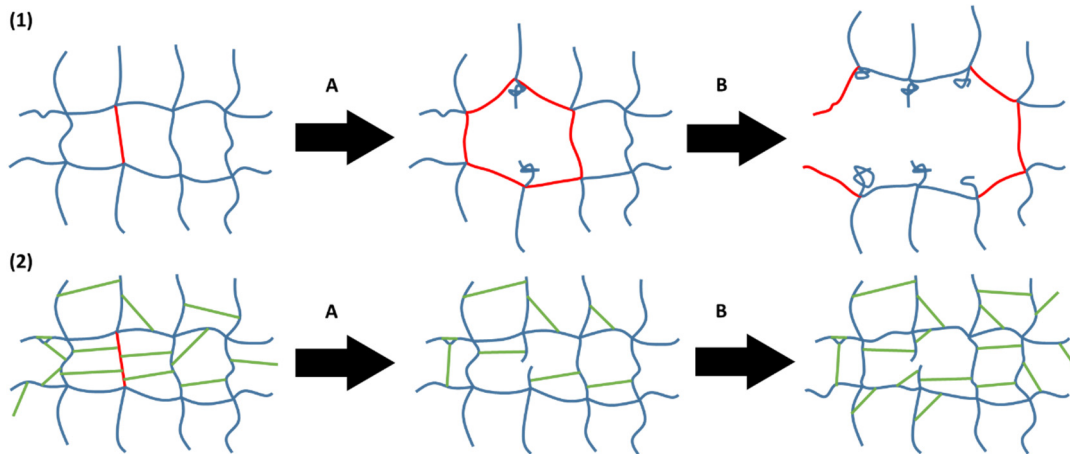


Figure 2: Schematic representation of the prevention of correlated bond breaking. The chemical network is represented in blue, and the physical bonds in green. The red chains are chains under high stress, close to breaking.

This mechanism (very schematically shown on Figure 2) protects the chemical network even when the stretch-rate is too low to induce energy dissipation inside the material during loading.

Intermediate Weissenberg number ($10^{-4} < W_e < 10^{-2}$ in tensile tests, $10^{-3} < W_e < 10^{-2}$ in fracture)

With increasing Weissenberg number, the number density of physical bonds surviving and active during the stretching increases. The elastic modulus, determined by the concentration of deformed polymer chains in the network, increases accordingly. The minimal reduced stress f_{min}^* reached by the material, representative of the onset of strain-hardening, increases. The stretch of onset of strain-hardening decreases, following a law in $(f_{min}^*)^{-1/2}$.

The evolution of this strain-hardening behavior is the result of a competition between two mechanisms: the number of chains decreases during stretching, following a linear and time-dependent relaxation, but their individual contribution increases and the stress observed in the material increases drastically. With increasing Weissenberg number, the number of chains in their nonlinear extension regime increases, and the intensity of the strain-hardening increases consequently.

The energy dissipation inside the material, linked to the number of bonds breaking during the stretching, follows the same increase (the more chains carry energy upon stretching at the beginning of the experiment, the more bonds can break). The fracture properties increase with this increase in the number of active physical bonds. The local fracture energy reaches a value of 300 J/m^2 and the crack propagation velocity reaches 200 mm/s .

These changes are related to the increase in number of active physical crosslinks for increasing strain rates (Young's modulus, on set and intensity of strain-hardening behavior) or the subsequent increase in energy dissipation (fracture properties) which homogenizes the stresses and stretches in the material, and therefore avoids the concentrations of defects and creation of defects.

High Weissenberg number ($\geq 10^{-2}$ in tensile tests and in fracture)

Upon higher increase of the Weissenberg number, the observation time of the experiment becomes equivalent or even lower than that of the physical bonds. Those start to behave almost as permanent

General Conclusion

crosslinks. The properties of the dual-crosslink hydrogel evolve consequently, showing a clear transition from soft and ductile to hard and brittle.

Young's modulus keeps increasing, since the number of active bonds increases. The dissipated energy seems to reach a plateau, and even decrease at lower observation times, evidencing clearly the "permanent" behavior of the physical crosslinks, and the stiffening of the dual-crosslink hydrogel.

The fracture properties show a particularly clear transition to brittleness. The stretch at break, whether of the notched or unnotched sample, drops drastically from the plateau value reached at intermediary Weissenberg numbers. This drop is followed by a decrease of the local fracture energy, from the plateau of 300 to 8 J/m^2 . The velocity of the crack propagation stays at a plateau around 200 mm/s .

At the highest Weissenberg number tested, the dual-crosslink hydrogel breaks before even reaching its strain-hardening regime, becoming more brittle than the bare chemical gel.

At these Weissenberg numbers, the dual-crosslink hydrogel does not dissipate energy and becomes brittle.

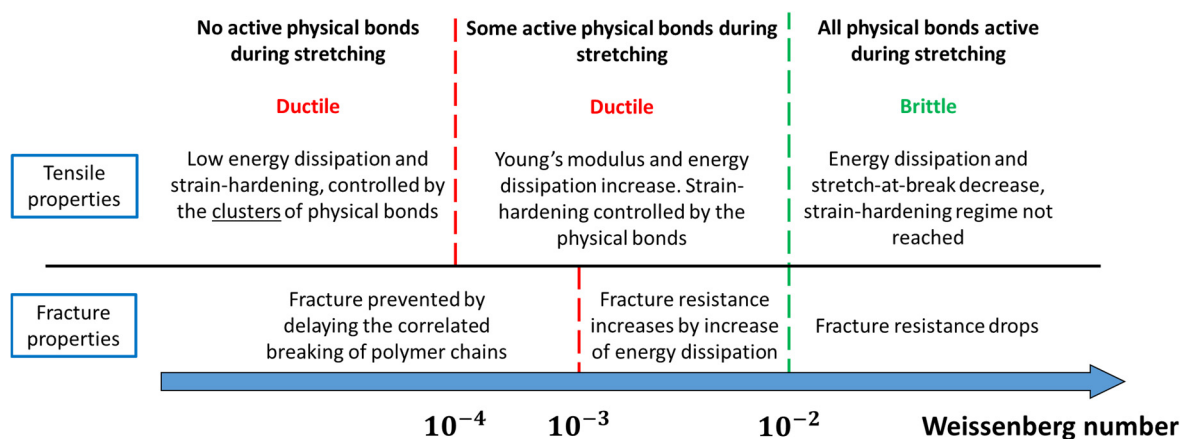


Figure 3: Schematic view of the evolution of the behavior of a dual-crosslink chemical gel with the Weissenberg number.

Influence of the micro-structure at large deformations

Overall, we believe to have demonstrated a large influence of the clusters of physical bonds on the behavior in large deformations and fracture of our dual-crosslink hydrogels. While their influence on the elastic modulus is low, a small number of long-lived crosslinks will have a large influence on the intensity of the strain-hardening levels reached, by acting as high-functionality crosslinking points. When increasing the stresses applied to those physical bonds, their lifetime decreases exponentially. Thus, we could expect the lifetime of the clusters to decrease accordingly. At the tip of a crack, where the stresses are high, their lifetime will become of the order of magnitude of the observation time, thus influencing the fracture properties of the material. The dynamics we observe at the tip of the crack might be related to these clusters, explaining why the dynamics we observe are more closely packed.

Observation and characterization of the propagation of a crack at fixed stretch

These dual-crosslink hydrogels showed an interesting rate-dependent toughening. To understand better the molecular mechanisms at play during fracture, we realized some additional experiments to characterize the propagation of a crack in these materials, from the initiation of the propagation to the propagation itself.

Two materials were studied, the fast VIm-Zn²⁺ and the intermediate VIm-Ni²⁺. When we applied a defined energy release rate \mathcal{G} on notched sample of those hydrogels, we could see four clearly different propagation behaviors, all determined by the energy \mathcal{G} that we imposed.

At $\mathcal{G} < 20 \text{ J/m}^2$

In the bare chemical gel or in the dual-crosslink hydrogels, the crack did not propagate.

At low imposed $\mathcal{G} < 70 \text{ J/m}^2$

The crack did not propagate immediately, but after a delay time decreasing with \mathcal{G} (from 1000 s at $\mathcal{G} = 20 \text{ J/m}^2$ to 80 s at 60 J/m^2). The network at the tip of the crack will show a first relaxation, followed by the slow propagation of the crack. This propagation depends on the dynamic of the bond:

- (1) With slow dynamics (VIm-Ni²⁺), the crack propagates slowly and continuously until the complete breaking of the hydrogel.
- (2) With fast dynamics (VIm-Zn²⁺), the crack propagation shows a stick-slip behavior. The relaxation of the physical bonds at the tip of the crack is fast enough to actually stop the crack. The crack tip will then show another relaxation, and a subsequent propagation. The stresses at the tip of the crack relax much faster in such a dual-crosslink hydrogel than in the VIm-Ni²⁺, and the effect of that relaxation on the speed of the crack is much more important.

At $70 \text{ J/m}^2 \leq \mathcal{G} < 280 \text{ J/m}^2$

The crack propagates immediately in both dual-crosslink hydrogels. The propagation speed increases with applied \mathcal{G} , for both dual-crosslink hydrogels studied. The propagation speed is always lower for the VIm-Zn²⁺ dual-crosslink hydrogel however, thanks to its ability to relax stresses faster than the VIm-Ni²⁺ dual-crosslink hydrogel.

At $\mathcal{G} \geq 280 \text{ J/m}^2$

At these high levels of stretch, the behavior changes with the dual-crosslink hydrogel considered.

- (1) In the VIm-Zn²⁺ dual-crosslink hydrogel, the crack propagates immediately upon reaching this level of released energy;
- (2) In the VIm-Ni²⁺ dual-crosslink hydrogel, the anisotropy induced by the deformation of the material has more influence, because of the long life of the physical bond and the clusters of those. The crack starts to propagate at 280 J/m^2 , but will then immediately deviate by 90°. After an onset time of about 10 s, it propagates fast in the direction perpendicular to the loading direction.

This deviation of the crack is believed to depend on the Weissenberg number considered during the experiment: the VIm-Zn²⁺ dual-crosslink hydrogel is stretched at low Weissenberg number, while the

General Conclusion

VIm-Ni²⁺ dual-crosslink hydrogel is stretched at high Weissenberg number. When reaching 280 J/m², the VIm-Ni²⁺ dual-crosslink hydrogel shows an orientation, an anisotropy in the loading direction, which is much more long-lived than in the VIm-Zn²⁺ dual-crosslink hydrogel. In the latter, it is easy for the crack to propagate in the direction perpendicular to the loading direction.

In this experiment, the energy brought to the crack could not be plotted in a master curve versus the velocity of the crack shifted by the shift factors found in previous fracture experiments. These differences come from the differences observed in anisotropy and stick-slip behaviors, linked to the differences in dynamics of both dual-crosslink hydrogels.

We have also visualized bond breakage during the propagation of a crack, by introducing mechanophores as chemical crosslinkers in the material. Our first attempt at using a hydrosoluble dioxetane derivative did not bring the results expected. We believe the presence of a solvent to be a cause of decrease of the intensity of the light emitted when this mechanophore breaks. We then turned our attention to an anthracene derivative, with which we could directly map the damage around the tip of the crack, and study it on post-mortem observations. The integration of this molecule in the network required a change in the synthesis of the hydrogel, using a solvent mix between water and an organic solvent. The resulting hydrogels demonstrated a behavior close to the behavior of our reference chemical gel. We could then study two dual-crosslinks hydrogels containing this mechanophore. The results showed a very localized damage zone around the crack tip with a width of the order of a few micrometers, evolving clearly with the Weissenberg number. This damage zone followed the state of stretch of the material when the crack propagates: the higher the stretch, the larger the damage zone. The toughness of the material does not influence directly the size of this damage zone. Now the next step would be to quantify the bond scission in this region, to try and link it to the material toughness.

Future works and open questions

We believe to have characterized quite well the evolution of the behavior of the dual-crosslink hydrogel with the stretch-rate. Now, in order to increase our understanding of this behavior, and definitely prove its link to the number of physical bonds, we would need to develop a molecular analytical model to fit or predict these data. Such a model was developed for the PVA-borax dual-crosslink hydrogel, and might be applied to our metal-ligand dual-crosslink hydrogel with some modifications. In particular, the model applied on the PVA-Borax dual-crosslink hydrogel hypothesizes that the stress does not influence the lifetime of the physical bond, which is not the case in our system. We should have provided here enough data to have a strong basis for such an improved model.

The main experimental perspectives are linked to the use of mechanophores in the network. This technique gives us access to multiple molecular information on the propagation of a crack that would otherwise be inaccessible. In particular, it would allow us:

- To realize a closer study of the crack tip before initiation. In this place, we should observe a large proportion of uncorrelated breaking of polymer chains, potentially dependent on the stretch-rate, which would prove the ability of the physical bonds to delay the correlated breaking of the chains;
- To differentiate the influences of the stretch and the crack velocity on the damage zone, by realizing delayed-fracture experiments on dual-crosslink hydrogels with mechanophores. As seen clearly in the VIm-Zn²⁺ dual-crosslink hydrogels for example, the crack velocity changes during the propagation, realized at a fixed deformation λ . This would allow us to see how the damage evolves with both parameters;
- To develop a refined set-up, to observe the propagation of the crack in real time under the confocal micro- or macroscope. This set-up that we have used is limited for now by the field of view we can access: these dual-crosslink hydrogels are particularly stretchable, and the region of interest around the crack tip is larger than this field of view.

All these experiments will need to be coupled with an accurate calibration of the fluorescence intensity by the number of broken bonds in the network, to increase the information accessible.

This methodology could bring a much sharper understanding of the molecular mechanisms in play during the propagation of a crack in a ductile and dynamic hydrogel.

Annexes

I. Titration methods

I.I. UV-Visible titration of Ni^{2+} and Cu^{2+}

In order to measure the concentration in Ni^{2+} or Cu^{2+} ions of the solution, we use a UV-spectrophotometer, to measure the concentration of the related complex $[\text{M}(\text{H}_2\text{O})_6]^{2+}$. The complex $[\text{Ni}(\text{H}_2\text{O})_6]^{2+}$ is green, absorbing light at around 400 nm; $[\text{Cu}(\text{H}_2\text{O})_6]^{2+}$ is blue, absorbing around 800nm.

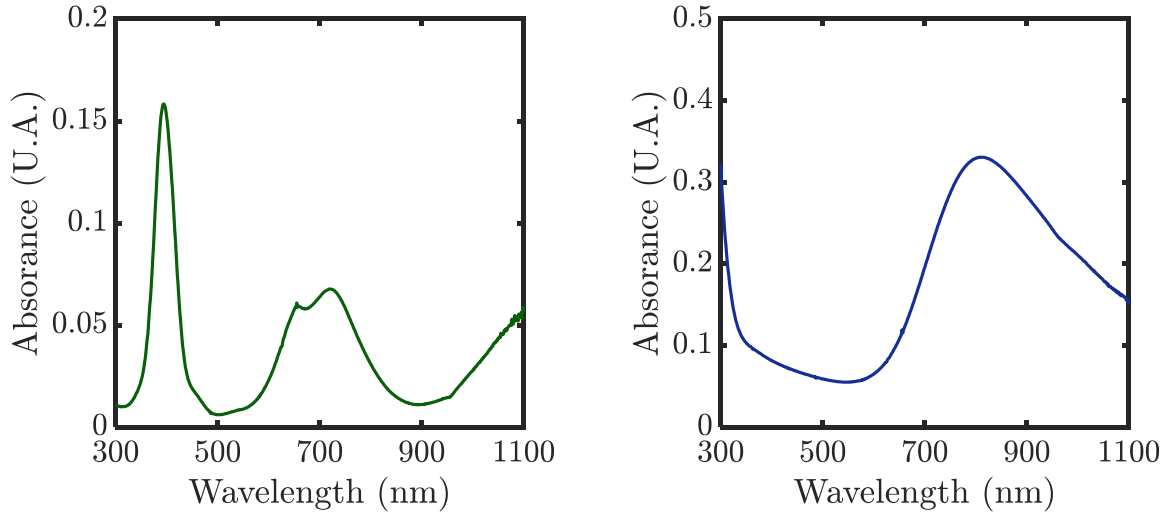


Figure I.1: Left: Absorbance of Ni^{2+} ions in water versus the wavelength. Right: Absorbance of Cu^{2+} ions in water versus the wavelength.

We can then measure the initial concentration in the solution, the concentration at time t , and deduce from the difference (knowing the volumes of the solution and of the hydrogel) the amount of Ni^{2+} ions absorbed by the hydrogel.

$$[\text{M}^{2+}]_{gel} = \frac{V_{0,solution} \cdot [\text{M}^{2+}]_{0,solution} - V_{solution}(t) \cdot [\text{M}^{2+}]_{solution}(t)}{V_{gel}(t)} \quad \text{Eq. I.1}$$

Eq. I.1 gives the concentration of nickel ions inside the dual-crosslinked gel. Note that in the hydrogel, there is an equilibrium between bound M^{2+} ions on the polymer chains and free M^{2+} ions in the gel solution. The concentration of these last ones is the same as the concentration of free M^{2+} ions in the diffusing solution. Considering this, we can compute the effective concentration of bound M^{2+} ions, given by Eq. I.2, were we consider:

- The concentration of free nickel ions in the hydrogel is equal to the concentration of nickel ions in the diffusing solution;
- The volume of water inside the gel is equal to the volume of the gel (in other words, the polymer has no volume).

This second hypothesis is extreme. It will however give a value of bonded Ni^{2+} ions that is slightly underestimating the real value.

$$[\text{M}^{2+}]_{coord} = \frac{V_{0,solution} \cdot [\text{M}^{2+}]_{0,solution} - (V_{solution}(t) + V_{gel}(t)) \cdot [\text{M}^{2+}]_{solution}(t)}{V_{gel}(t)} \quad \text{Eq. I.2}$$

I.II. Titration of Zn^{2+} by conductimetry

Zn^{2+} ions do not create colored complexes in aqueous solution, so UV-visible spectrophotometry is not of interest here. In order to measure the concentration of Zn^{2+} ions in the solution, a titration by conductimetry was realized. In a conductivity meter, we titrated the diffusing solution by a solution of NaOH at an accurately known concentration. This titration provokes two successive evolutions of the conductivity.

First, the Zn^{2+} ions are precipitated in zinc oxide particles by the hydroxides we introduce:



During this first part of the titration, we are subtracting from the solution one Zn^{2+} ion and, for each of those subtracted ions, adding two Na^{+} ions. The molar ionic conductivities of those species are:

$$\lambda_{Zn^{2+}} = 10.56 \text{ mS} \cdot \text{m}^{-2} \cdot \text{mol}^{-1}$$

$$\lambda_{Na^{+}} = 5.008 \text{ mS} \cdot \text{m}^{-2} \cdot \text{mol}^{-1}$$

Since we incorporate 2 Na^{+} for each Zn^{2+} we retrieve, the conductivity of the solution should only slightly decrease while Zn^{2+} ions precipitate ($2\lambda_{Na^{+}} - \lambda_{Zn^{2+}} = -0.4 \text{ mS} \cdot \text{m}^{-2} \cdot \text{mol}^{-1}$).

Once all the metal ions have precipitated, the measured conductivity of the solution should increase quickly, since we will only be adding Na^{+} and OH^{-} ions. This will give us two lines with very different slopes, and the intersection of those two lines will give us the equivalent volume of the titration and the concentration of Zn^{2+} ions in the diffusing solution. Using the formula Eq. I.2, we will obtain the concentration of bound Zn^{2+} in the hydrogel.

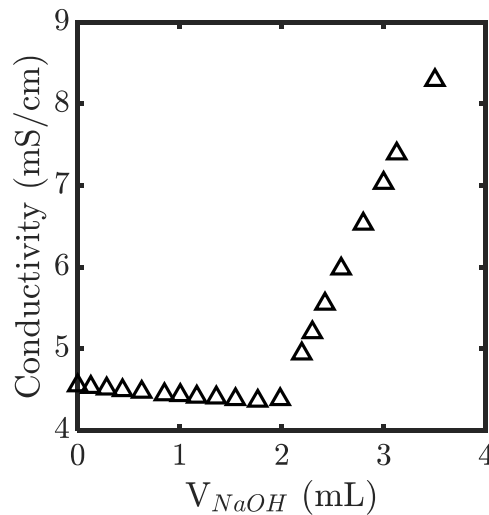


Figure I.2: Example of titration of a Zn^{2+} solution by NaOH. Conductivity of the solution, versus the volume of NaOH added to the solution.

Note: during the titration the volume of the solution will change, which will also influence the conductivity value. To avoid that issue, we have chosen the concentration of the titrating solution so that the total added volume is less than 10% of the titrated solution. We have also considered values of “corrected” conductivity, $k_{corrected} = k * V(t)/V(0)$ with k the measured conductivity and $V(t)$ the volume of the titrated solution at instant t of the titration.

I.III. Colorimetric titration of Hg^{2+}

The absorption of Hg^{2+} was measured by a complexation titration, with a color indicator.

First, the Hg^{2+} ions are complexed by an accurately measured excess of disodium ethylene diamine tetra acetic salt (Na_2EDTA). The un-complexed EDTA is then titrated by a solution of ZnCl_2 in presence of Eriochrome Black T (a complexometric indicator) in a pH 10 buffer.

Before the titration by ZnCl_2 , there are complexes of $[\text{HgEDTA}]$ and free EDTA molecules in solution. The Eriochrome Black T gives a blue color. Upon addition of ZnCl_2 , the Zn^{2+} ions will create coordination complexes with the remaining EDTA. Once all the EDTA is complexed, Zn^{2+} will form a complex with the Eriochrome Black T, and give a pink color. This will be the sign of the end of the titration.



Figure I.3: Titration of an Hg^{2+} solution by a ZnCl_2 solution, in presence of Eriochrome Black T and EDTA. Left: Color of the solution before the equivalence point, where EDTA complexes Zn^{2+} ions and Eriochrome Black T is free in solution.. Right: Color of the solution just after the equivalence point, where Eriochrome Black T complexes the Zn^{2+} ions in excess.

The exact protocol is detailed below:

- Dilute 1mL of the diffusing solution, containing Hg^{2+} ions, in 9mL of water;
- Add 10mL of a $\text{NaHCO}_3/\text{Na}_2\text{CO}_3$ buffer at $\text{pH} \approx 10$;
- Add to this an accurate volume of EDTA solution, the concentration of which is accurately known;
- Incorporate a few μg of Eriochrome Black T (the solution should become blue);
- Titrate by a ZnCl_2 solution, until the solution becomes pink.

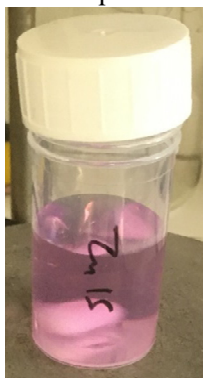
With the equivalent volume of the titration, taken at the color change, we can compute the concentration of free EDTA in solution and thus, access the concentration of Hg^{2+} ions in the initial solution, which leads us to the concentration of bound ions inside the P(AAm-co-VIm) hydrogel.

I.IV. Colorimetric titration of Zn^{2+}

The titration method used was similar as the one used to titrate Hg^{2+} ions, a colorimetric titration. This time, the Zn^{2+} diffusing solution is directly titrated by an EDTA solution in the presence of Eriochrome Black T, in a buffer at $\text{pH} \approx 10$. Before the titration, Eriochrome Black T is in a coordination complex

with EDTA and has a pink color. After the equivalence of the titration, it becomes blue. The change in color allows finding the equivalent volume and the concentration in Zn^{2+} ions of the diffusing solution.

Before equivalence



After equivalence



Figure I.4: Titration of a Zn^{2+} solution by an EDTA solution, in presence of Eriochrome Black T. Left: Color of the solution before the equivalence point, where Eriochrome Black T complexes Zn^{2+} ions. Right: Color of the solution just after the equivalence point, where EDTA complexes Zn^{2+} ions and Eriochrome Black T is free in solution.

The exact protocol is detailed below:

- Dilute 1mL of the diffusing solution, containing Zn^{2+} ions, in 9mL of water;
- Add 10mL of a $NaHCO_3/Na_2CO_3$ buffer at $pH \approx 10$;
- Incorporate a few μg of Eriochrome Black T (the solution should become pink);
- Titrate by an EDTA solution, until the solution becomes blue.

This method should slightly overestimate the concentration in Zn^{2+} ions of the solution, thus underestimating the concentration in ions of the hydrogel.

II. Tensile tests

Tensile tests were realized on Instron tensile machines, models 5565, 5965 or 3343. To avoid the drying of the hydrogel samples during the tests, the longer experiments (more than 1 minute) were realized in a cell containing paraffin oil. Hydrogel samples were mechanically clamped. A 10 N load cell was used to measure the force, and the displacement was taken as the displacement of the crosshead.

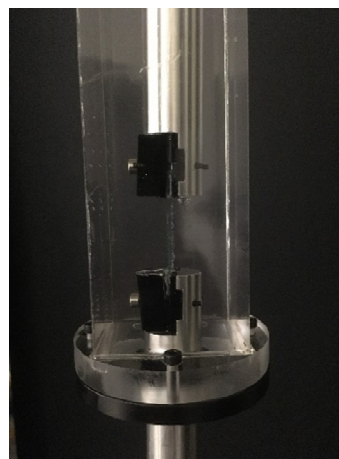


Figure II.1: Left: Instron 5965, with the oil cell in place. Right: Mechanical clamps and oil cell with the hydrogel sample in place, ready for the experiment.

III. Supplementary information on cyclic experiments at high stretch-rate

III.I. Ni^{2+} Dual-crosslink hydrogel with $[\text{Ni}^{2+}] = 100 \text{ mmol/L}$, stretched at $\dot{\lambda} = 0.3 \text{ s}^{-1}$ up to $\lambda = 3$ and $\lambda = 6$.

The same experiments as in section 3.2.2 were realized on a Ni^{2+} dual-crosslink hydrogel with $[\text{Ni}^{2+}] = 100 \text{ mmol/L}$, at a stretch-rate of $\dot{\lambda} = 0.3 \text{ s}^{-1}$ (10 times faster than the experiments presented in section 3.2.2). The results are shown in Figure III.1 and Figure III.2.

Just as we saw in section 3.2.2, the modulus decreased with the number of cycles. It reached a value around 35 kPa for $\lambda_{max} = 3$ and 25 kPa for $\lambda_{max} = 6$. This difference might be linked to the large softening we see in this dual-crosslink hydrogel at $\dot{\lambda} = 0.3 \text{ s}^{-1}$. The residual stretch increased to 0.5 for $\lambda_{max} = 3$ and 0.9 for $\lambda_{max} = 6$.

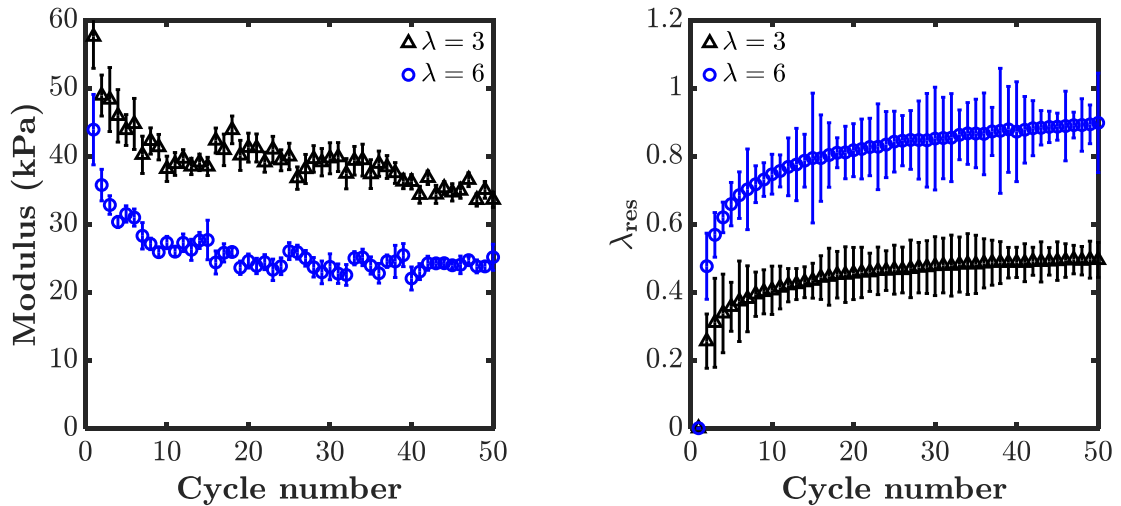


Figure III.1: Left: Modulus of the Ni^{2+} dual-crosslink hydrogel versus the number of cycles applied. Right: Residual stretch of the Ni^{2+} dual-crosslink hydrogel versus the number of cycles applied.

The energy stored and dissipated evolves just as it did for $\dot{\lambda} = 0.03 \text{ s}^{-1}$ (section 3.2.2). Their decrease was seen up to 10 cycles, instead of 5 for the previous stretch-rate. As previously, the hysteresis decreased only between the first and second cycle.

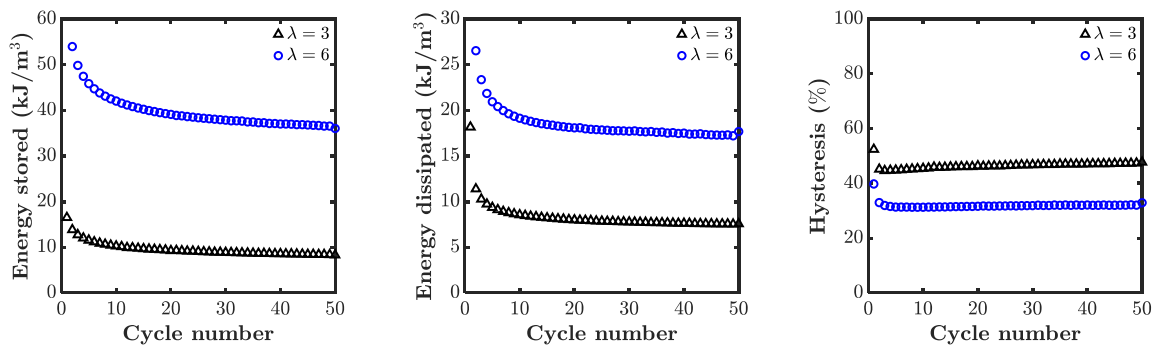


Figure III.2: Left: Energy stored by the Ni^{2+} dual-crosslink hydrogel versus the number of cycles applied. Center: Energy dissipated by the Ni^{2+} dual-crosslink hydrogel versus the number of cycles.. Right: Hysteresis between loading and unloading of the Ni^{2+} dual-crosslink hydrogel versus the number of cycles applied.

III.II. Zn^{2+} Dual-crosslink hydrogel with $[\text{Zn}^{2+}] = 100 \text{ mmol/L}$, stretched at $\dot{\lambda} = 0.3 \text{ s}^{-1}$ up to $\lambda = 3$ and $\lambda = 6$.

The same experiments as in section 4.5.2 were realized on a Zn^{2+} dual-crosslink hydrogel with $[\text{Zn}^{2+}] = 100 \text{ mmol/L}$, at a stretch-rate of $\dot{\lambda} = 0.3 \text{ s}^{-1}$ (10 times faster than the experiments presented in section 4.5.2). The results are shown in Figure III.3 and Figure III.4.

Contrary to what we saw in section 4.5.2, where the modulus did not change with the number of cycles, here the modulus decreased with the number of cycles. It reached a value around 8 kPa for both λ_{max} . This difference between the two experiments indicates a beginning of the influence of the physical crosslinks on the mechanical properties of the network.

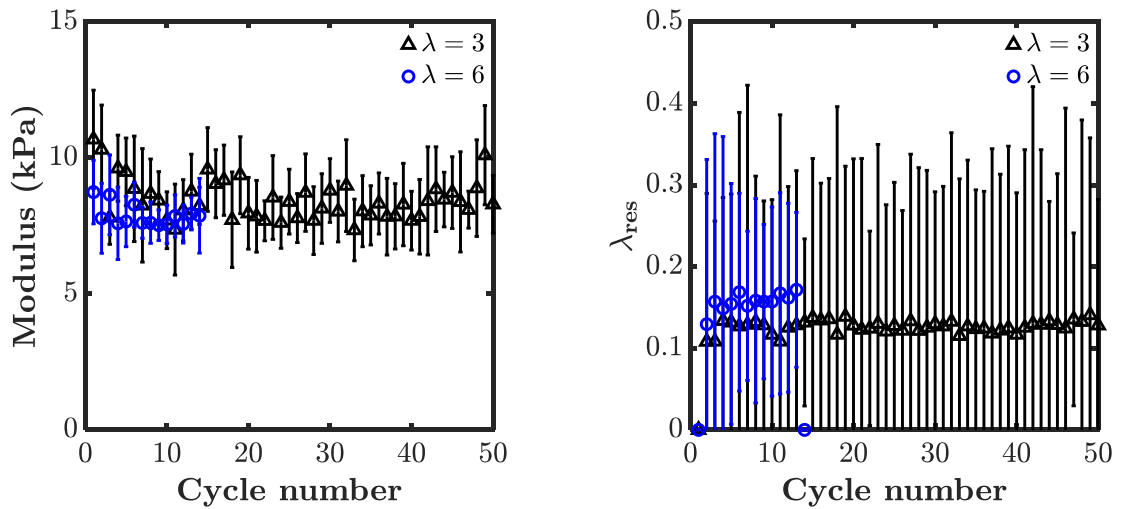


Figure III.3: Left: Modulus of the Zn^{2+} dual-crosslink hydrogel versus the number of cycles applied. Right: Residual stretch of the Zn^{2+} dual-crosslink hydrogel versus the number of cycles applied.

The sample stretched up to $\lambda_{max} = 6$ broke after 15 cycles. This might be linked to a high damage in the material, leading to the nucleation and propagation of a fracture. More probably, it is linked to a defect in the material that became critical upon high stretching.

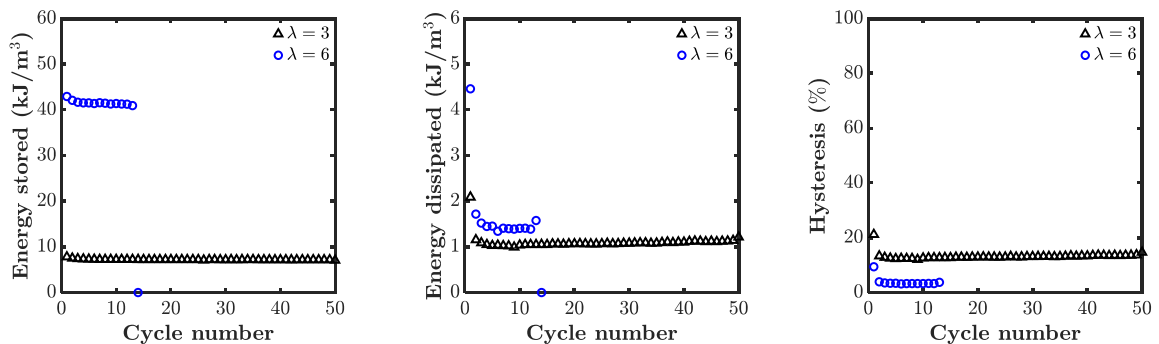


Figure III.4: Left: Energy stored by the Zn^{2+} dual-crosslink hydrogel versus the number of cycles applied. Center: Energy dissipated by the Zn^{2+} dual-crosslink hydrogel versus the number of cycles. Right: Hysteresis between loading and unloading of the Zn^{2+} dual-crosslink hydrogel versus the number of cycles applied.

The energy stored and dissipated evolves just as it did for $\dot{\lambda} = 0.03 \text{ s}^{-1}$ (section 3.2.2). Their decrease was seen up to 5 cycles, just as for the previous stretch-rate. As previously, the hysteresis decreased only between the first and second cycle.

IV. Chemical hydrogel with terpyridine moieties

The chemical hydrogel realized with terpyridine moieties showed interesting properties. When put in contact with any object made of iron, it chelates iron from the object, creating this characteristic violet color (see picture on Figure IV.1). This effect disappeared when the hydrogel was loaded with Zn^{2+} ions.



Figure IV.1: Picture of a chemical hydrogel with terpyridine instead of imidazole, synthesized following the formula from section 5.2. Violet “ring” shows the presence of complexes of terpyridine and Fe^{2+} ions, which appeared when the hydrogel was put in contact with an iron punch.

RÉSUMÉ

Les matériaux mous tels que les hydrogels ont de nombreuses applications intéressantes, mais leur utilisation est limitée par leur fragilité mécanique. Nous avons produit des hydrogels résistants, avec des points de réticulation permanents (réticulations chimiques) et temporaires (constitués de complexes de coordination). Nous avons d'abord étudié leur microstructure et leur dynamique, en mettant en évidence l'existence de deux dynamiques dans le réseau (une rapide liée au complexe métal-imidazole, et une lente liée à des agrégats de complexes). Nous avons ensuite montré que ces réseaux sont bien plus résistants et déformables qu'un réseau classique, grâce à la dissipation d'énergie introduite par ces liaisons physiques temporaires. Nous avons fait varier cette dynamique en changeant l'ion métallique utilisé pour l'accélérer, ou en changeant le ligand utilisé pour la ralentir. Comme le réseau chimique en lui-même ne change pas, nous avons pu étudier le même matériau sur une large gamme de vitesses de déformations relatives, aussi appelée nombre de Weissenberg. Nous avons étudié l'évolution de la dissipation d'énergie dans ce réseau en fonction de ce nombre. En comparant cette évolution de dissipation d'énergie et l'évolution des propriétés de résistance à la fracture du matériau, nous avons montré que l'étude de la dissipation d'énergie dans le volume du réseau ne permet pas de comprendre la dissipation d'énergie en tête de fracture, lorsque cette fracture se propage dans le matériau. Afin de mieux caractériser ce mécanisme de dissipation en tête de fracture, nous avons utilisé une méthode permettant de visualiser la rupture chimique grâce à une activation de fluorescence par rupture de liaison. Les premiers résultats de cette méthode montrent une forte influence de la déformation sur l'ampleur de l'endommagement dans le réseau, et promettent de très intéressantes futures découvertes.

MOTS CLÉS

Fracture, Hydrogels, Polymères, Renforcement mécanique, viscoélasticité, fluorescence

ABSTRACT

Hydrogels have many potential applications, while their usage is limited by their mechanical fragility. We have developed tough hydrogels, based on polyacrylamide with permanent (chemical) and temporary (physical) crosslinks, the latter being coordination complexes between a ligand on the chains and a metallic ion. We have first studied their dynamics and microstructure, evidencing the existence of two dynamics in the hydrogel (fast one related to the lifetime of the nickel-imidazole complex, and slow one related to the lifetime of aggregates of such complexes). We showed that those networks have improved fracture resistance and stretchability compared to the purely chemical network, thanks to the energy dissipation induced by the physical bond breaking. To better understand the influence of the dynamic of the bond on the mechanical behaviors of the network, we varied them by changing the metallic ion to accelerate it or the ligand to slow it down. The chemical network being the same in all those materials, we were able to study the same hydrogel on a wide range of relative deformation rates, or Weissenberg number. We have studied the evolution of energy dissipation with this number and, by comparing this dissipation with the fracture resistance properties of the hydrogel, we have shown that bulk energy dissipation alone is not enough to explain the energy dissipation at the tip of a propagating crack. To characterize this dissipation at the crack tip, we have used a method of visualization of bond breakage by fluorescence activation. The first results with this method show a strong influence of the stretch (and not the stretch-rate) on the width of the damage zone along the crack, and give great promises for future discoveries on this subject.

KEYWORDS

Fracture, Hydrogels, Polymers, Mechanical reinforcement, viscoelasticity, fluorescence